NANOCELLULOSE AS AN ENHANCED OIL RECOVERY AGENT FOR CARBONATE RESERVOIRS

A THESIS SUBMITTED TO
THE GRADUATE SCHOOL OF NATURAL AND APPLIED SCIENCES
OF
MIDDLE EAST TECHNICAL UNIVERSITY

BY

CANDAN ÜNAL KIZILIRMAK

IN PARTIAL FULFILLMENT OF THE REQUIREMENTS
FOR
THE DEGREE OF DOCTOR OF PHILOSOPHY
IN
PETROLEUM AND NATURAL GAS ENGINEERING

SEPTEMBER 2023

Approval of the thesis:

NANOCELLULOSE AS AN ENHANCED OIL RECOVERY AGENT FOR CARBONATE RESERVOIRS

submitted by **CANDAN ÜNAL KIZILIRMAK** in partial fulfillment of the requirements for the degree of **Doctor of Philosophy** i**n Petroleum and Natural Gas Engineering, Middle East Technical University** by,

Prof. Dr. Halil Kalıpçılar
Dean, Graduate School of **Natural and Applied Sciences** _____

Assoc. Prof. Dr. İsmail Durgut
Head of the Department, **Petroleum and Natural Gas Eng.** _____

Prof. Dr. Serhat Akın
Supervisor, **Petroleum and Natural Gas Eng., METU** _____

Examining Committee Members:

Prof. Dr. Hasan Öztürk
Mining Eng., METU _____

Prof. Dr. Serhat Akın
Petroleum and Natural Gas Eng., METU _____

Assoc. Prof. Dr. Çağlar Sınayuç
Petroleum and Natural Gas Eng., METU _____

Assoc. Prof. Dr. Murat Çınar
Petroleum and Natural Gas Eng., ITU _____

Asst. Prof. Dr. İbrahim Metin Mıhçakan
Petroleum and Natural Gas Eng., ITU _____

Date: 08.09.2023

I hereby declare that all information in this document has been obtained and presented in accordance with academic rules and ethical conduct. I also declare that, as required by these rules and conduct, I have fully cited and referenced all material and results that are not original to this work.

Name Last name : Candan ÜNAL

Kızılırmak

Signature :

ABSTRACT

NANOCELLULOSE AS AN ENHANCED OIL RECOVERY AGENT FOR CARBONATE RESERVOIRS

Ünal Kızılırmak, Candan
Doctor of Philosophy, Petroleum and Natural Gas Engineering
Supervisor : Prof. Dr. Serhat Akın

September 2023, 195 pages

Almost one third of the oil cannot be recovered from the reservoir. Along with being a solution to recover that amount of oil, enhanced oil recovery (EOR) techniques have become vital in the life span of a mature field due to decrease in oil field explorations in the last decade. There are several conventional enhanced oil recovery (EOR) methods, such as gas injection, thermal methods, and chemical injection methods including alkaline, surfactant flooding, and polymer flooding. In addition to these conventional techniques, novel and more environmentally friendly EOR models should be developed due to environmental concerns. There are several green agents and biopolymers contributing to additional oil recovery. This study introduces nanocellulose as one of these green agents to develop an alternative EOR technique for carbonate reservoirs. Being a sustainable material due to its biodegradable nature, availability and cost-effectiveness (abundant in the nature), and their convenience for a wide range of pore sizes make nanocellulose a favorable candidate for EOR. The injection of nanocrystalline cellulose as an EOR method for carbonate reservoirs is a new concept for the oil industry. This study presents an in-depth analysis of nanocellulose as an enhanced oil recovery agent for carbonate reservoirs, focusing on its potential to improve oil recovery, with a particular emphasis on its successful

mechanism of wettability alteration, elucidated through laboratory-scale studies. Thus, this research investigated nanocellulose through material characterization studies including viscosity tests, solubility tests, and wettability tests to interpret better its oil recovery mechanism and convenience for carbonate reservoirs. The findings indicated that nanocellulose exhibits greater compatibility with low-salinity water, particularly when the water has a salinity level below 10,000 ppm of NaCl concentration. Contact angle measurements were employed to quantify the alterations in wettability towards a more water-wet state. The results revealed significant wettability modifications induced by nanocellulose, decreasing contact angle between rock surface and oil droplet from 135.1° to 67.3°, leading to improved oil mobilization and displacement within the carbonate matrix. Besides, several core flooding experiments were performed with carbonate core plug samples to mimic its possible applications in the field. The main objective of coreflood tests was to assess the effectiveness and stability of nanocellulose in improving oil recovery, considering variations in nanocellulose concentration (0.5 wt%, 1 wt%, and 2 wt%) and the API gravity of oil samples (16, 22, and 36). Results indicate that nanocellulose injection in carbonate reservoirs exhibits a significant increase in oil recovery efficiency with an additional oil recovery of up to 28.2%. As a sustainable and effective enhanced oil recovery agent, nanocellulose holds great potential for commercial applications in the oil and gas industry, offering an innovative approach to maximize oil production from carbonate reservoirs.

Keywords: Enhanced oil recovery, Nanocellulose, Carbonate reservoirs, Coreflood experiments

ÖZ

NANOSELÜLOZUN KARBONAT REZERVUARLARINDA GELİŞTİRİLMİŞ PETROL KURTARIM ARACI OLARAK KULLANIMI

Ünal Kızılırmak, Candan
Doktora, Petrol ve Doğal Gaz Mühendisliği
Tez Yöneticisi: Prof. Dr. Serhat akın

Eylül 2023, 195 sayfa

Rezervuardaki petrolün yaklaşık üçte biri çoğunlukla üretilemiyor. Üretilemeden rezervuarda bırakılan bu petrolün kurtarımına katkı sağlamanın yanı sıra, geliştirilmiş petrol kurtarım yöntemleri son zamanlarda yeni petrol sahası keşiflerinin azalmasıyla daha da hayati bir önem kazanmıştır. Gaz enjeksiyonu, termal yöntemler ve kimyasal yöntemler (alkali enjeksiyonu, sürfaktant enjeksiyonu ve polimer enjeksiyonu) gibi çeşitli konvansiyonel geliştirilmiş petrol kurtarım metodları bulunmaktadır. Çevreyi korumaya yönelik kaygılar da dikkate alındığında, bu yöntemlere ek olarak daha çevre dostu ve yenilikçi yöntemler geliştirilmelidir. İlave petrol kurtarımına katkıda bulunan çeşitli çevreci ve biyopolimer cinsi malzemeler bulunmaktadır. Bu çalışmada, nanoselüloz karbonat rezervuarları için bu çevreci malzemelerden biri olarak sunulmuştur. Biyolojik olarak çevreye zarar vermeden bozunup çözünebildiği, sürdürülebilir olması, doğada bolca bulunması sebebiyle halihazırda kolay ulaşılabilir olması sebebiyle ekonomik olması ve nano boyutta oldukları için çok geniş bir gözenek sıkalasına sahip rezervuarlarda uygulanabilir olması nanoselülozu geliştirilmiş petrol kurtarımı metodu olarak iyi bir aday yapmaktadır. Nanokristal yapıdaki nanoselülozun karbonat kayaçlardan ilave petrol üretebilmek için kullanımı petrol endüstrisi için oldukça yeni bir konsept.

Bu sebeple, bu çalışmada, vizkozite analizleri, çözünürlük testleri, ıslanımlılık testleri gibi malzeme karakterizasyonu adı altında gerçekleştirilen alt çalışmalar ile nanoselülozun özelliklerinin karbonat kayaçlar için uygunluğunun daha iyi anlaşılması ve geliştirilmiş petrol kurtarımı olarak kullanımındaki temel mekanizma araştırılmıştır. Çalışmalar neticesinde, nanoselüloz düşük tuzluluktaki sularda, özellikle 10,000 ppm NaCl konsentrasyonunda daha düşük tuzluluktaki sularda, daha iyi uyumluluk göstermiştir. Yapılan temas açısı çalışmasıyla da nanoselülozun ıslanımlılığa etkisi nicel olarak belirlenmek istemiştir. Temas açısı çalışmalarına göre, nanoselüloz ile kayaç ve petrol arasındaki temas açısı 135.1°'den 67.3°'ye düşmektedir. Ayrıca, tapalarda gerçekleştirilen çeşitli karot öteleme testleriyle de rezervuar koşulları temsil edilerek olası bir uygulamada nanoselülozun ilave petrol kurtarımına katkısı test edilmiştir. Bu akış testlerinde çeşitli nanoselüloz konsentrasyonlarının ve farklı API gravitesine sahip petrollerin, nanoselüloz ile petrol kurtarımına etkisini tespit etmek hedeflenmiştir. Akış testlerinden alınan başarılı sonuçlar nanoselülozun rezervuar kayaca zarar vermeden ilave petrol kurtarımına katkıda bulunduğunu ve %28.2' ye kadar ilave petrol kurtarımı sağlayabildiğini göstermektedir. Sonuç olarak bu çalışmanın genel amacı, nanoselülozun karbonat rezervuarlarında bir potansiyel geliştirilmiş petrol kurtarımı ajanı olarak etkinliğini çeşitli yönleriyle analiz etmektir.

Anahtar Kelimeler: Geliştirilmiş petrol kurtarımı, Nanoselüloz, Karbonat rezervuarları, Öteleme testleri

To my lovely grandmother Şahsenem, still living in our hearts,

To the one and only, my beloved daughter İpek,

ACKNOWLEDGEMENTS

I would like to express my deepest gratitude to my advisor, Prof. Dr. Serhat Akın, for his mentorship, support, and invaluable insights throughout the journey of this research.

I extend my thanks to my thesis committee members, Assoc. Prof. Dr. Çağlar Sınayuç and Prof. Dr. Hasan Öztürk, for their constructive feedback and valuable suggestions, which have significantly contributed to the improvement of this work.

I am immensely grateful to Turkish Petroleum, especially the R&D Center, for providing the necessary resources and facilities that made this research possible. I extend my heartfelt thanks to my colleagues, Can Ercan, Adem Çuhadar, Arzu Aktosun, Suzan Müge Yetim, Sevim Yavuz Bayram, Yinal Neşes Huvaj. In addition to their technical support, their continuous encouragement and belief in the importance of this study have been a great source of motivation.

Lastly, but certainly not least, I owe a debt of gratitude to my family. To my husband İbrahim, for his unwavering support, patience, and understanding during the countless hours dedicated to this research. To my daughter İpek, for being a constant source of joy and inspiration, motivating me to strive for excellence. To my mom Suna, dad İlter, grandmother Şahsenem, grandfather İlhan, and mother-in-law Elif. Their love, encouragement, and prayers have been my pillar of strength, pushing me never to give up and persevere through challenges.

This research would not have been possible without the collective support and encouragement of all those mentioned above. I am truly fortunate and grateful to have such wonderful people in my life.

TABLE OF CONTENTS

ABSTRACT vii

ÖZ ix

ACKNOWLEDGEMENTS xii

TABLE OF CONTENTS xiii

LIST OF TABLES xvii

LIST OF FIGURES xix

CHAPTERS

1 INTRODUCTION 1

2 LITERATURE REVIEW 5

2.1 Enhanced Oil Recovery Methods 6

2.1.1 Thermal Enhanced Oil Recovery 6

2.1.2 Gas Injection 9

2.1.3 Chemical Enhanced Oil Recovery 11

2.2 Conformance Control Methods 12

2.2.1 Mechanical Methods 12

2.2.2 Chemical Methods 13

2.3 Nanoparticles and Their Use in Oil Industry 14

2.4 Nanocellulose 20

2.4.1 Cellulose Nanocrystal (CNC) 22

2.4.2 Cellulose Nanofibril (CNF) 23

2.4.3 Bacterial Nanocellulose (BNC) 23
2.5 Application of Nanocellulose in Oil Industry 24
2.5.1 Application of Nanocellulose in Drilling Fluids 24
2.5.2 Application of Nanocellulose in Enhancing Oil Recovery 26
3 STATEMENT OF PROBLEM 29
4 MATERIAL CHARACTERIZATION 31
4.1 Nanocellulose Powder Samples 31
4.1.1 CNF in Powder Form 32
4.1.2 CNC in Powder Form 34
4.2 Aqueous Suspension of Nanocrystalline Cellulose (NCC) 36
4.3 Solubility Bottle Tests 38
4.3.1 Effect of Salinity 39
4.3.2 Effect of Nanocellulose Concentration 40
4.3.3 Effect of Temperature 41
4.4 Viscosity Bottle Tests 42
4.5 Particle Size Analyses 46
4.5.1 Particle Size Distribution Measurements 47
4.5.2 Zeta Potential Measurements 53
4.6 Interfacial Tension (IFT) Measurements 56
4.7 Wettability Study 59
4.8 Contact Angle Measurements 62
5 COREFLOOD OIL ERCOVERY TESTS 67
5.1 Material and Methods 67
5.1.1 Nanocellulose Suspension 67

5.1.2 Synthetic Formation Water 68
5.1.3 Dead Oil 69
5.2 Rock Sample Properties and Preparation of Coreflood Tests 70
5.2.1 Core Plug Cleaning 71
5.2.2 Routine Core Analyses 72
5.2.3 Mercury Injection Capillary Pressure (MICP) Analysis 77
5.2.4 Core Plug Saturation 80
5.3 Coreflood Experimental Setup 81
5.4 Coreflood Test Procedure 85
5.5 Further Analysis on Core Plug Samples 87
5.5.1 X-Ray Diffraction (XRD) Analysis 87
5.5.2 SEM/EDS Analyses 88
5.5.3 Thin Section Analysis 89
6 RESULTS AND DISCUSSION 91
6.1 Oil Recovery Coreflood Test Results 91
6.1.1 Coreflood Test #1 91
6.1.2 Coreflood Test #2 96
6.1.3 Coreflood Test #3 102
6.1.4 Coreflood Test #4 107
6.1.5 Coreflood Test #5 112
6.1.6 Coreflood Test #6 116
6.1.7 Coreflood Test #7 121
6.2 XRD Analysis Results 126
6.3 SEM/EDS Analysis Results 129

6.3.1 Results for Before Nanocellulose Oil Recovery Tests 129
6.3.2 Results for After Nanocellulose Oil Recovery Tests 133
6.4 Thin Section Analysis 140
6.4.1 Thin Section Analysis for Plug #211 140
6.4.2 Thin Section Analysis for Plug #347 142
6.5 Discussion 145
7 CONCLUSIONS AND RECOMMENDATIONS 163
REFERENCES 167
APPENDICES
A. XRD Results of End Trim Samples 191
CURRICULUM VITAE 195

LIST OF TABLES

TABLES

Table 4.1: General properties of powder CNF (Nanocellulose (n.d.)) 33
Table 4.2: General properties of powder CNC (Nanocellulose (n.d.)) 35
Table 4.3: General properties of NCC (Nanocellulose (n.d.)) 37
Table 5.1: Properties of nanocellulose dispersion 67
Table 5.2: Properties of synthetic water sample used in the coreflood tests 68
Table 5.3: Properties of oil samples used in the coreflood tests 69
Table 5.4: SARA fractions of oil samples 69
Table 5.5: GC analysis results of oil samples used in coreflood tests 70
Table 5.6: Routine core analysis results 74
Table 5.7: RQI and RZI values for plug samples used in coreflood tests..... 76
Table 5.8: Pore throat size classification (Nelson, 2009) 80
Table 6.1: Test conditions for test #1 with plug #210 91
Table 6.2: Differential pressure values for water injection to plug #210 92
Table 6.3: Saturation results for test #1 96
Table 6.4: Oil recovery test results for plug #210 96
Table 6.5: Test conditions for test #2 with plug #211 96
Table 6.6: Saturation results for test #2 101
Table 6.7: Oil recovery test results for plug #211 101
Table 6.8: Test conditions for test #3 with plug #347 102
Table 6.9: Differential pressure value for water injection to plug #347 102
Table 6.10: Saturation results for test #3 106
Table 6.11: Oil recovery test results for plug #347..... 106
Table 6.12: Test conditions for test #4 with plug #346 107
Table 6.13: Saturation results for test #4 112
Table 6.14: Oil recovery test results for plug #346..... 112
Table 6.15: Test conditions for test #5 with plug #213 112
Table 6.16: Differential pressure values for water injection to plug #213 113

Table 6.17: Differential pressure values for water injection to plug #213 after 1 wt% nanocellulose soaking 116
Table 6.18: Saturation results for test #5 116
Table 6.19: Oil recovery test results for plug #213 116
Table 6.20: Test conditions for test #6 with plug #207 117
Table 6.21: Saturation results for test #6 121
Table 6.22: Oil recovery test results for plug #207 121
Table 6.23: Test conditions for test #7 with plug #209 121
Table 6.24: Saturation results for test #7 126
Table 6.25: Oil recovery test results for plug #209 126
Table 6.26: XRD analysis results for core plug samples #211, #347, and #346 ... 128
Table 6.27: Test conditions and fluid properties for oil recovery coreflood tests . 146
Table 6.28: Basic core properties of each core plug sample 147
Table 6.29: Summary of oil recovery coreflood tests results 149

LIST OF FIGURES

FIGURES

Figure 2.1: Thermal EOR Classification 7
Figure 2.2: Chemical structure of cellulose (Mishra, 2018) 20
Figure 2.3: Cellulose nanocrystals (CNC) extraction (Phanthong et al., 2018)..... 22
Figure 2.4: Cellulose nanofibril (CNF) extraction (Phanthong et al., 2018) 23
Figure 4.1: Stereo Microscope 31
Figure 4.2: CNF view under stereo microscope (left view with no magnification, right view with 115x magnification)..... 32
Figure 4.3: TEM image of CNFs (Nanocellulose (n.d.)) 33
Figure 4.4: Stereo microscope views of CNF mixed with water (115x magnification) 34
Figure 4.5: CNC (dry powder) views under stereo microscope with 115x magnification 34
Figure 4.6: TEM image of CNCs (Nanocellulose (n.d.)) 35
Figure 4.7: Stereo microscope views of CNC mixed with water (115x magnification) 36
Figure 4.8: Aqueous suspension of nanocrystalline cellulose (NCC), 6%wt 37
Figure 4.9: SEM image of NCC (Nanocellulose (n.d.)) 38
Figure 4.10: Solubility bottle tests for 1 wt% nanocellulose prepared by using water with varying salinities (room temperature)..... 39
Figure 4.11: 1 wt% nanocellulose prepared by using water with 65,000 ppm NaCl (room temperature) 40
Figure 4.12: Solubility bottle tests for 2 wt% nanocellulose prepared by using water with varying salinities (room temperature)..... 40
Figure 4.13: Solubility bottle tests for 1 wt% nanocellulose prepared by using water with varying salinities (after 6 hours at 65 °C)..... 41
Figure 4.14: Solubility bottle tests for 2 wt% nanocellulose prepared by using water with varying salinities (after 6 hours at 65 °C)..... 41

Figure 4.15: 1 wt% and 2 wt% nanocellulose solutions in the oven at 65 °C.....43
Figure 4.16: Anton Paar rheometer 44
Figure 4.17: Nanocellulose after viscosity measurement.....44
Figure 4.18: Shear viscosity curves for 1 wt% nanocellulose aged at 65°C up to 24 hours 45
Figure 4.19: Shear viscosity curves for 2 wt% nanocellulose aged at 65°C up to 24 hours 46
Figure 4.20: Varying concentrations of nanocellulose solution (0.5 wt%, 1 wt% and 2 wt%) for size distribution and zeta potential measurements (a) prepared with fresh water b) prepared with 10,000 ppm NaCl water c) prepared with 30,000 ppm NaCl water.....47
Figure 4.21: Schematic view of Mastersizer2000 (Particle Size and Zeta Potential Measurement Laboratory, Central Laboratory, n.d.).....47
Figure 4.22: Particle size distribution for 0.5 wt% nanocellulose solution prepared by using fresh water.....48
Figure 4.23: Particle size distribution for 1 wt% nanocellulose solution prepared by using fresh water.....49
Figure 4.24: Particle size distribution for 2 wt% nanocellulose solution prepared by using fresh water.....49
Figure 4.25: Particle size distribution for 0.5 wt% nanocellulose solution prepared by using water with 10,000 ppm NaCl.....50
Figure 4.26: Particle size distribution for 1 wt% nanocellulose solution prepared by using water with 10,000 ppm NaCl.....50
Figure 4.27: Particle size distribution for 2 wt% nanocellulose solution prepared by using water with 10,000 ppm NaCl.....51
Figure 4.28: Particle size distribution for 0.5 wt% nanocellulose solution prepared by using water with 30,000 ppm NaCl.....51
Figure 4.29: Particle size distribution for 1 wt% nanocellulose solution prepared by using water with 30,000 ppm NaCl.....52

Figure 4.30: Particle size distribution for 2 wt% nanocellulose solution prepared by using water with 30,000 ppm NaCl 52
Figure 4.31: Zeta potential of 0.5 wt% nanocellulose solution prepared by using fresh water..... 54
Figure 4.32: Zeta potential of 1 wt% nanocellulose solution prepared by using fresh water..... 55
Figure 4.33: Zeta potential of 2 wt% nanocellulose solution prepared by using fresh water..... 55
Figure 4.34: Zeta Potentials of solutions prepared by using water with 10,000 ppm NaCl and varying nanocellulose concentrations (a) 0.5 wt% nanocellulose, b) 1 wt% nanocellulose, c) 2 wt% nanocellulose)..... 56
Figure 4.35: Zeta Potentials of solutions prepared by using water with 30,000 ppm NaCl and varying nanocellulose concentrations (a) 0.5 wt% nanocellulose, b) 1 wt% nanocellulose, c) 2 wt% nanocellulose)..... 56
Figure 4.36: IFT test system 57
Figure 4.37: Oil droplet on the tip of the needle inside 1 wt% nanocellulose solution..... 58
Figure 4.38: Nanocellulose within the system after dismantling..... 58
Figure 4.39: Wettability restoration process of plug end trim (a) aging in the oil, b) placing plug end trim in formation water, c) plug end trim after taken from formation water)..... 60
Figure 4.40: Contact angle before nanocellulose soaking, original wettability condition of the rock 61
Figure 4.41: Testing effect of nanocellulose on the wettability of plug end trim (a) aging in the 1 wt% nanocellulose solution prepared with fresh water, b) placing plug end trim in formation water)..... 61
Figure 4.42: Contact angle after aging with 1 wt% nanocellulose 62
Figure 4.43: Contact angle measurement with 20,000 ppm NaCl synthetic brine solution (representing before treatment with nanocellulose)..... 64

Figure 4.44: Contact angle measurement with 1 wt% nanocellulose solution (representing after treatment with nanocellulose) 65
Figure 5.1: Preparation of diluted nanocellulose (stirrer on the left, sonic bath on the right) 68
Figure 5.2: Soxhlet extraction (left), temperature-controlled oven (right) 71
Figure 5.3: Helium porosimeter test system 72
Figure 5.4: Air permeameter test system 73
Figure 5.5: Porosity-permeability x-plot for core plug samples 74
Figure 5.6: RQI vs normalized porosity for the plug samples used in coreflood tests 77
Figure 5.7: Micromeritics Autopore IV 78
Figure 5.8: Pore throat size distribution curves of plug samples used in coreflood tests 80
Figure 5.9: Vacuum saturator (left), plug samples in formation water (right) 81
Figure 5.10: Schematic drawing of coreflood setup 82
Figure 5.11: Coreflood System, CFS-1 Setup 83
Figure 5.12: Coreflood System, CFS700 Setup 85
Figure 6.1: Oil injection before aging for plug #210 93
Figure 6.2: Water injection after aging of plug #210 94
Figure 6.3: 2 wt% nanocellulose injection to plug #210 95
Figure 6.4: Water injection after 2 wt% nanocellulose soaking, plug #210 95
Figure 6.5: Water injection for saturating core plug #211 97
Figure 6.6: Oil injection before aging for plug #211 98
Figure 6.7: Water injection after aging of plug #211 99
Figure 6.8: 2 wt% nanocellulose injection to plug #211 100
Figure 6.9: Water injection after 2 wt% nanocellulose soaking, plug #211 101
Figure 6.10: Oil injection before aging for plug #347 103
Figure 6.11: Water injection after aging of plug #347 104
Figure 6.12: 2 wt% nanocellulose injection to plug #347 105
Figure 6.13: Water injection after 2 wt% nanocellulose soaking, plug #347 106

Figure 6.14: Water injection for saturating core plug #346 108
Figure 6.15: Oil injection before aging for plug #346 108
Figure 6.16: Oil injection after aging for plug #346 109
Figure 6.17: Water injection after aging of plug #346 110
Figure 6.18: 1 wt% nanocellulose injection to plug #346 111
Figure 6.19: Water injection after 1 wt% nanocellulose soaking, plug #346 111
Figure 6.20: Oil injection before aging for plug #213 113
Figure 6.21: Water injection after aging for plug #213 114
Figure 6.22: 1 wt% nanocellulose injection to plug #213 115
Figure 6.23: Water injection for saturating core plug #207 117
Figure 6.24: Oil injection before aging for plug #207 118
Figure 6.25: Oil injection after aging for plug #207 119
Figure 6.26: 0.5 wt% nanocellulose injection to plug #207 120
Figure 6.27: Water injection after 0.5 wt% nanocellulose soaking, plug #207 120
Figure 6.28: Water injection for saturating core plug #209 122
Figure 6.29: Oil injection before aging for plug #209 123
Figure 6.30: Water injection after aging of plug #209 124
Figure 6.31: 0.5 wt% nanocellulose injection to plug #209 125
Figure 6.32: Water injection after 0.5 wt% nanocellulose soaking, plug #209 125
Figure 6.33: End trim samples of core plug 211, 347 and 346 before and after oil recovery coreflood tests 127
Figure 6.34: Sample used for before nanocellulose oil recovery test (core plug #347) 130
Figure 6.35: SEM image-1 of core sample #347 before coreflood tests 130
Figure 6.36: EDS results for the points (01, 02 and 03) mentioned in Figure 6.35 131
Figure 6.37: SEM image-2 of core sample #347 before coreflood tests 132
Figure 6.38: EDS results for the points (01, 02 and 03) mentioned in 6.37 133
Figure 6.39: Samples used for after oil recovery test with 2 wt% nanocellulose (core plug #347) 134

Figure 6.40: SEM image-1 of core sample #347 (sample in the left in Figure 6.39) after oil recovery test with 2 wt% nanocellulose.....134
Figure 6.41: EDS results for the points (01, 02 and 03) mentioned in Figure 6.40 135
Figure 6.42: SEM image-2 of core sample #347 (sample in the left in Figure 6.39) after oil recovery test with 2 wt% nanocellulose.....136
Figure 6.43: EDS results for the points (01, 02 and 03) mentioned in Figure 6.42 136
Figure 6.44: SEM image-1 of core sample #347 (sample in the right in Figure 6.39) after oil recovery test with 2 wt% nanocellulose.....137
Figure 6.45: EDS results for the point (01) mentioned in Figure 6.44.....137
Figure 6.46: SEM image-2 of core sample #347 (sample in the right in Figure 6.39) after oil recovery test with 2 wt% nanocellulose.....138
Figure 6.47: EDS results for the point (01) mentioned in Figure 6.46.....138
Figure 6.48: SEM image-3 of core sample #347 (sample in the right in Figure 6.39) after oil recovery test with 2 wt% nanocellulose.....139
Figure 6.49: EDS results for the points (01, 02 and 03) mentioned in Figure 6.48 139
Figure 6.50: Skeletal packstone with porosity, plug #211 before coreflood tests.141
Figure 6.51: Microscope image for plug #211 after coreflood tests with nanocellulose followed by waterflood.....142
Figure 6.52: Image-1-Skeletal packstone with stylolites and vuggy porosity, plug #347 before coreflood tests 143
Figure 6.53: Image-2- Calcispherulid-bearing benthic foraminiferal skeletal pacsktone with moldic and vuggy porosity, plug #347 before coreflood tests 143
Figure 6.54: Image-3- Skeletal rudstone with fracture porosity and vuggy porosity, plug #347 before coreflood tests 144
Figure 6.55: Plug #347 after coreflood tests with nanocellulose flood followed by waterflood.....145

Figure 6.56: Nanoparticles organized within wedge-shaped films, resulting in a gradient of structural disjoining pressure at the wedge vertex (Wasan et al., 2011) 151
Figure 6.57: Wettability alteration mechanism by disjoining pressure (a-first oil-wet condition of the pore system, b-injection of nanocellulose into system, c-subsequent injection of water after nanocellulose) 153
Figure 6.58:Transient log-jamming process (El-Diasty and Ragab, 2013) 154
Figure 6.59: Additional oil recovery comparison for coreflood tests 1 and 2 155
Figure 6.60: Additional oil recovery comparison for coreflood tests 1, 2 and 3 .. 156
Figure 6.61: Additional oil recovery comparison for coreflood tests 3 and 4 157
Figure 6.62: Additional oil recovery comparison for coreflood tests 4 and 5 158
Figure 6.63: Additional oil recovery comparison for coreflood tests 5 and 6 159
Figure 6.64: Additional oil recovery comparison for coreflood tests 6 and 7 161

CHAPTER 1

INTRODUCTION

The economic growth followed by the industrial improvements and increasing population all over the world are the main indicators of increase in global energy demand. Crude oil and hyrocarbon gases are the primary energy sources to meet that demand. However, the oil and gas production is carried out along with enormous amounts of reservoir water production. Such water production, along with oil, might be indispensible to some extent at the beginning of the production stage of wells. The origin and type of produced water should be determined. If water is produced at a rate above the economic limit of water/oil ratio and does not contribute the production of oil, or commingled flow of oil and water takes places above the economic limit, excess water production becomes a problem for the life of a reservoir.

In addition to excess water production, oil fields can readily complete their productive life by reaching residual oil saturation levels. Some fields might start a declining trend in oil production at the very beginning of their production history. At this point, enhanced oil recovery (EOR) methods come to stage to offer solutions to that problem. There are several EOR methods including thermal methods and chemical injections. Various techniques or processes that aim to increase oil recovery by changing physicochemical properties of the reservoir rock and/or the fluids.

Nano technology is widely used in various industries, including oil and gas, by offering effective solutions to oilfield and reservoir related problems. Thanks to their particle size (3-100 nm) and low viscosity, nano particles have been becoming more favorable as an easily injected agent. Nano particles are used for enhancing oil recovery through their unique properties that make them effective agents in improving the efficiency of traditional oil extraction methods. One of the key

properties of nano particles that contribute to oil recovery is their large surface area. Nano particles have an extremely high surface area-to-volume ratio that provide abundant active sites for interactions with oil and reservoir rock surface. This property enhances their adsorption capacity and allows them to displace and mobilize trapped oil effectively. Another important property of nano particles is enhanced mobility. Nano particles exhibit excellent mobility control of oil displacement in porous reservoir formations, even in low-permeability formations like carbonate reservoirs. Their small size allows them to penetrate deep into the reservoir matrix, reaching and mobilizing oil in areas that are difficult to access by conventional methods. Additionally, nano particles' properties can be tailored and optimized to suit specific reservoir conditions and recovery mechanisms. By altering factors like particle size and surface charge, their performance can be fine-tuned for various oil recovery scenarios. Some nano particles possess inherent wettability-altering capabilities, allowing them to change the wetting characteristics of the reservoir rock surface. This property can enhance oil displacement and increase the sweep efficiency during the recovery process. Furthermore, nano particles can maintain their stability and effectiveness under high-pressure, high-temperature, and high-salinity conditions typically encountered in oil reservoirs. Many nano particles used in enhanced oil recovery, such as nanocellulose, are derived from renewable and biodegradable sources, making them environmentally friendly and sustainable alternatives to traditional chemical agents.

In this research, nanocellulose is introduced as an alternative green enhanced oil recovery agent. Nanocellulose, owing to its biodegradable nature, abundant availability, and cost-effectiveness, emerges as a favorable candidate for EOR. Its versatility in pore sizes further supports its application potential. In this research, nanocellulose was thoroughly characterized through viscosity, solubility, and wettability tests to unravel its oil recovery mechanism and suitability for carbonate reservoirs. Additionally, core flooding experiments with carbonate core plug samples were conducted to simulate field applications. The promising results from

the core flooding experiments signify the potential of nanocellulose to contribute significantly to additional oil production.

The thesis is structured as follows:

- Chapter 2 comprises a literature review, discussing existing EOR methods for carbonate reservoirs, the use of nano particles in the oil industry, and the applications of nanocellulose in the oil industry.
- Chapter 3 presents the statement of the problem addressed in the research.
- Chapter 4 focuses on the material characterization of nanocellulose.
- Chapter 5 details the procedure and technical aspects of the coreflood tests conducted.
- Chapter 6 presents the results and discussions derived from the research.
- Chapter 7 provides a summary of conclusions drawn from the research and offers recommendations for future studies.

CHAPTER 2

LITERATURE REVIEW

As the population of the world increases incrementally, the need for energy also shows a drastic increase. Although there are several sources of energy for meeting that energy demand, the fossil fuels and especially oil and gas, are still at the top of this list as the largest contributor to the primary energy demand.

The number of new hydrocarbon discoveries is declining, and production from mature fields is decreasing. At that point, enhanced oil recovery (EOR) comes to the stage as a well-accepted technique in terms of contributing to global hydrocarbon production worldwide. EOR benefits companies by increasing the recovery factor, extending the lifespan of the fields, and maximizing the reserves by helping the recovery of additional volumes. EOR is a significant tool for aiding to match the growing energy demand by maintaining production, thus it raises the returns on former investments.

To better understand the feasibility of EOR applications, it is better first to understand production stages of a conventional oil field. It is split into three stages: primary production, secondary production and tertiary recovery, also named as enhanced oil recovery (EOR). Primary oil production is the production of oil via the natural energy of the reservoir system. Primary oil production also includes utilization of artificial lift systems, such as pumps. Secondary recovery aims pressure maintenance in the reservoir by injecting water to displace oil and drive it to a production wellbore or by injecting gas in the gas cap. Utilization of secondary oil recovery techniques can recover only about 30% of the oil in the reservoir and leave up to 70% of the oil in the ground (McGlade et al., 2018). Tertiary recovery, also known as EOR, is the key option for further increase in oil production. Despite mostly being costly to employ on the field, it is much easier to produce oil from already recovered oil fields through various EOR methods, which claim prospects

for producing up to 60 percent, or more, of the original oil in place (The US Department of Energy, n.d.).

2.1 Enhanced Oil Recovery Methods

EOR provides physicochemical alteration of reservoir rock or fluids to contribute to contribute additional recovery, distinguishing EOR from secondary recovery mechanisms. To illustrate, EOR based steam or gas injections aim to have thermal or compositional transformation of either reservoir rock or fluid while waterflooding and gas injection through secondary recovery are employed to push oil to the production wells. EOR techniques are classified into three major subcategories: thermal processes, high pressure gas injection processes, and chemical processes.

2.1.1 Thermal Enhanced Oil Recovery

Thermal EOR methods are feasible to apply for heavy and viscous oil. The main mechanism of thermal EOR is the introduction of heat/thermal energy into the reservoir (Butler, 1991). Increase in the reservoir temperature results in decrease in the viscosity of the oil dramatically, thus, mobility of the oil in the reservoir is improved due to thinning of the pil by heat introduction. Heavy oil refers to oils with gravity values lower than 20°API, and a reservoir viscosity range of 50–5,000 cP (Albulkadir et al., 2017). Thermal EOR technology involves hot water injection, steam flooding, in situ combustion and electrical heating. Classification of thermal EOR methods can be seen in Figure 2.1.

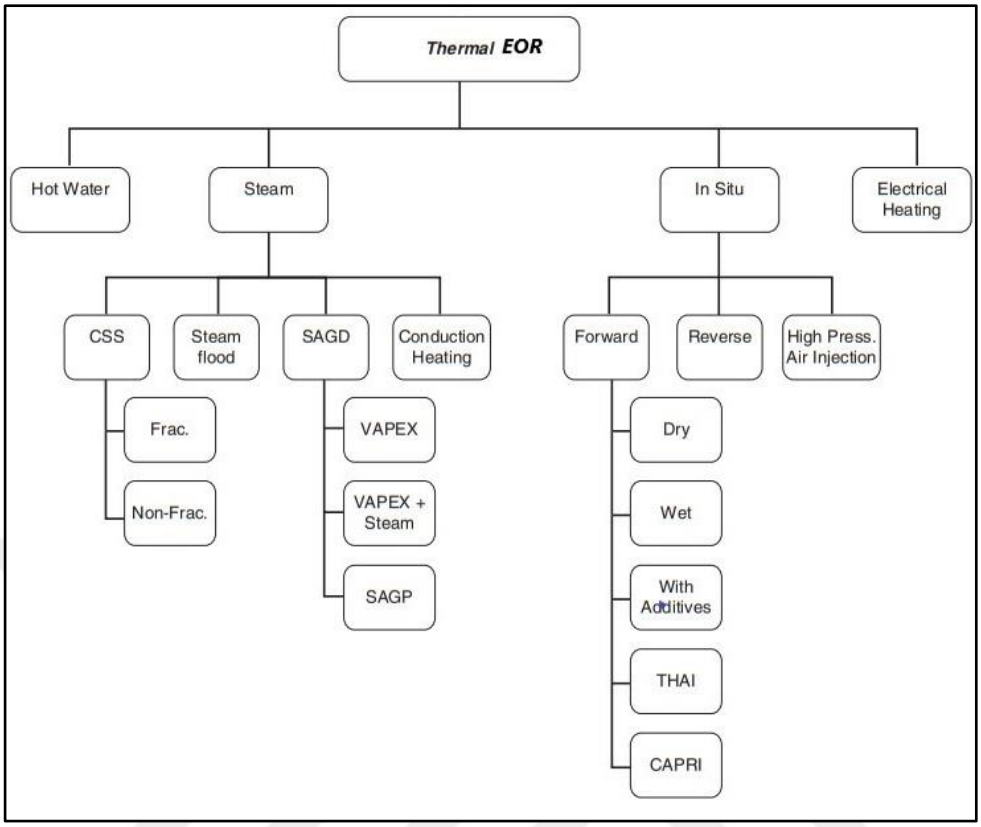

Figure 2.1: Thermal EOR Classification

Hot water injection is very similar to conventional water flooding. Hot water injection consists of heating water on the surface and injected into the reservoir via injection wells. Heat decreases the oil's viscosity and ease the oil flow in addition to the displacing mechanism of waterflooding to the production wells. Mobility of oil increases more compared to mobility of water as a result of temperature increase (Edmondson, 1965; Tang & Morrow, 1997; Alajmi et al., 2009).

Steam injection is the most common method including steam flooding, cyclic steam injection/stimulation (CSS) and steam assisted gravity drainage (SAGD). Steam flooding applies heat to the reservoir by injecting steam into the formation. The main mechanism is the reduction of oil viscosity, and hence improvement of oil mobility. Steam flooding is favorable mainly for shallow reservoirs.

In steam injection, steam is continuously injected from generally one or multiple injection wells, and oil is produced from the production wells (Farouq Ali & Melday,

1979; Farouq Ali, 1982). The steam chamber formed through the injection of steam from injection wells displaces the oil into the production well by decreasing oil viscosity (Lake & Walsh, 2008). Reservoir pressure and depth are the limiting factors for the application of steam injection (Kovscek, 2012). Cyclic steam injection, also known as steam huff and puff or cyclic steam injection, introduces wet saturated steam into the reservoir at high temperature and pressure. The well is shut in for a few days or several weeks to let the steam has enough soaking time to heat the oil in the reservoir and reduce viscosity. Then, oil production takes place due to lower viscosity of the oil after soaking process (Owens & Suter, 1965; Lake & Walsh, 2008). As the reservoir temperature decreases, the oil production also decreases, resulting in employing cycles repetitively (Alvarez & Han, 2013).

Steam assisted gravity drainage (SAGD) is an advanced steam injection technique which is more favorable in heavy oil and tar sands (with gravity values less than or equal to 10° API). Butler (1985) developed SAGD in order to obtain in situ recovery from the bitumen of Alberta. The technique relies on gravity segregation of steam through a pair of parallel horizontal wells in the reservoir. Top well serves as the injection well, and the bottom horizontal well is utilized as the production well. Steam is injected through upper horizontal well. Steam rises to the top of the formation and creates a steam chamber, which reduces the viscosity. Oil with reduced viscosity starts moving down by gravity, and it is produced by lower horizontal well. Expansion and spread of steam chamber laterally is provided by continuous injection of steam. The key point of a successful SAGD application is having high vertical permeability (Thomas, 2008).

In situ combustion (ISC), erroneously known as fire flooding, relies on the injection of air or oxygen to generate heat by burning some portion of the oil and produce combustion gases internally. In the combustion zone, very high temperature levels are reached in the range of 450-600°C, which causes a higher viscosity reduction downstream of the combustion front. As the combustion takes place, in the reservoir, in situ, there are no heat losses along surface lines or wellbore, which makes ISC more efficient than steam injection in terms of thermal efficiency (Chu, 1977; Chu

1982). There are several different applications of ISC: forward combustion, reverse combustion, and high pressure air injection. ISC can be applied as forward or reverse based on the propagation direction of combustion front and injected gas. If the ignition takes place near the injection well, it is called forward combustion. Unlike forward combustion, ignition occurs near the production well in reverse combustion. Low temperature oxidation of oil in place without ignition is known as high pressure air injection, more favorable for light oil reservoirs (Thomas, 2008).

Reduction of viscosity by heat can be gained by various other methods, including, downhole combustors (Al-Mashrafi et al., 2021), electromagnetic heating (Bera & Babadagli, 2015), microwave heating in the reservoir (Sahni et al., 2000; Jalalalhosseini, 2015) and downhole electric resistance heaters (Rangel-German et al., 2004).

2.1.2 Gas Injection

Gas injection is one of the non-thermal EOR methods best appropriate for light oils with low viscosity values. It might be either miscible or immiscible depending on the target of EOR and reservoir conditions.

Miscible gas flooding is based on mixing of gas completely with oil either at first contact or multiple contacts. Mixing of gas and crude oil in the reservoir takes place at or above the minimum miscibility pressure (MMP). Nitrogen and natural gas or the combination of these gases can be utilized for the injection process due the fact that their MMP values are similar to each other. The primary methods for miscible flooding include the miscible slug process, enriched gas drive, vaporizing gas drive, and high-pressure gas injection (utilizing CO_2 or N_2). These techniques have been discussed in studies by Fath and Pouranfard (2014) and Nwidee et al. (2016). The process referred to as "enriched gas drive" involves the continuous injection of a gas (which can be natural gas, flue gas, or nitrogen) that contains higher concentrations of C2-C4 fractions. Under increased pressures, these fractions begin to condense

within the crude oil, forming a transition zone. Achieving miscibility requires multiple interactions between the injected gas and the reservoir oil. This mechanism is best suited for deep reservoirs (deeper than 6000 ft) due to high pressure requirements (Thomas, 2008). In vaporizing gas drive, C_2-C_6 fractions of oil vaporize under high pressure (10-15 MPa) and generate a transition zone. Miscibility is reached after multiple contacts. The process is limited to the reservoirs with oil having enough C_2-C_6 fractions (Benmekki & Mansoori, 1986; Stalkup, 1987). High pressure gas injection includes the injection of CO_2 and N_2. In CO_2 injection, intermediate fractions of oil are vaporized into CO_2 phase. Through gas injection, gas phase is enriched by lighter carbon fractures resulting in a denser gas phase. Miscible zone is developed by the condensation of heavier gas into the reservoir oil. As a result, viscosity and density reduction take place. Due to the miscibility between CO_2 and crude oil, interfacial tension between the two phases is reduced to zero, forming a single phase fluid moving towards producers (Holm, 1959; Fath & Pouranfard, 2014; Saraperded et al., 2014). Due to cost related concerns and readily availability from natural sources, CO_2 injection is favorable for both sandstone and carbonate reservoirs (Dino et al., 2007; Holtz, 2008; Moritis, 2008). Similar to the miscible CO_2 injection mechanism, N_2 injection also has miscibility mechanism. MMP values for N_2 injection is much higher when compared to that for miscible CO_2 injection. Cantarell N_2 flood project in Mexico is known as one of the largest field application of miscible N_2 injection with high production levels (Sebastian & Lawrence, 1992; Sanchez et al., 2005).

Immiscible gas flooding involves the gas injection into the reservoir below MMP, at which gas and oil cannot become miscible. Immiscible gas flooding process end up with lower recovery values than miscible flooding mechanism. Oil recovery achieved by immiscible flooding is mainly based on oil swelling, which increases the efficiency of macroscopic displacement (Oren et al., 1992; Taheri et al., 2013; Yousefi et al. 2019). Oklahoma City field in the US and Bahrain field in Bahrain are the first field applications of this method back in the 1930s accomplished by using lean hydrocarbon gas (Muskat, 1949; Cotter, 1962; Shehabi; 1979).

2.1.3 Chemical Enhanced Oil Recovery

Chemical EOR is mainly based on enhancing the water injection efficiency by using various mechanisms of chemicals depending on the reservoir. These mechanisms include but are not limited to reducing IFT, increasing viscosity for conformance control, improving sweep efficiency, and wettability alteration (Donaldson et al., 1989). Surfactant flooding, polymer flooding, and alkaline flooding are the mostly known conventional chemical EOR methods. (Samanta et al., 2012; Babu et al., 2015).

Surfactant flooding relies on the injection of surfactant solution right after waterflooding so that oil-water interfacial tension is reduced and reservoir rock wettability is altered. All this mechanism results in additional oil recovery. There are various types of surfactant: anionic, cationic, non-ionic, and zwitterionic surfactants (Gurgel et al., 2008).

Polymer flooding targets enhancing oil recovery by increasing sweep efficiency. Water soluble polymer solution, whose mobility is less than oil is injected into the reservoir. Viscous, less mobile phase polymer solution moves through higher permeable sections by reducing flow rate. Therefore, sweep efficiency is improved for the sections with lower permeability values (Clarke et al., 2016). Synthetic polymers (such as, polyacrylamide, PAM), hydrolysed polyacrylamide (HPAM), biopolymers (such as, xanthan gum) and superabsorbent polymer composite (SAPC) are improved for polymer flooding to improve mobility ratio and eliminate permeability contrasts (Wever et al., 2011; Abidina et al., 2012). Loss of polymer into the porous media and polymer degradation are the major possible drawbacks of the mechanism. Thus, it is better to apply polymer flooding at the very beginning of waterflood till water breakthrough (Chang, 1978).

Alkaline flooding mechanism is based on the reaction of injected alkaline fluid (such as sodium hydroxide, sodium orthosilicate or sodium carbonate) with oil (acid components), to develop in situ surfactants. As the result, reduction of oil-water

interfacial takes places and, hence, reservoir rock wettability is changed (Bortolotti et al., 2009). Alkaline, surfactant, and polymer (ASP) flooding is the combined method of all aforementioned chemical EOR processes to take advantage of each process, including IFT reduction, wettability alteration, and sweep efficiency improvement (Chen et al., 2013). Wettability alteration takes place in the case of using larger concentrations of alkaline solutions compared to the one in conventional alkaline flooding application (Froning & Leach, 1967).

There are various other methods of chemical EOR in addition to the ones defined above. Emulsion flooding (Mandal & Bera, 2015), inorganic nanoparticle flooding (Mohammadi et al., 2017), gel injection for conformance control (Demir et al., 2008; Aldhaheri et al., 2016), foam flooding (Kovscek & Radke, 1994; Sunmonu & Onyekonwu; 2013), micellar flooding as the combination of micellar slug and polymer slug (Gogarty & Tosch, 1968; Farouq Ali & Thomas, 1986), and microbial EOR (Kogler et al., 2017) can be also listed as promising methods in terms of using physicochemical alterations to improve oil recovery.

2.2 Conformance Control Methods

Excessive water production is one of the critical issues faced in oil and gas reservoirs. Oil fields under water drive or producing by waterflood are likely to produce water together with oil. Oil companies currently produce almost a barrel of oil along with three barrels of water from their mature fields (Bailey et al., 2000). There are several conformance control techniques to mitigate water-based problems which can be classified in two different types: mechanical and chemical methods.

2.2.1 Mechanical Methods

Mechanical techniques encompass a range of approaches, such as cementing, inserting sand plugs, utilizing packers, employing bridge plugs, applying mechanical patches, and implementing pattern flow control. In general, mechanical techniques

are limited to near wellbore applications and require the implementation of a specific completion tool. For example, dual completion systems are applied against water conning (Swisher & Wojtanowicz, 1995; Shirman, 2000; Seright, 2008) and hydro cyclones are used to isolate and separate water during the production stage (Meldrum, 1988). Packers are also used to seal the unwanted water sections. There are two major packers: expandable packers and non-expandable packers. Inflatable elements are the major parts of expandable packers aimed to enlarge in the wellbore and satisfy the isolation conditions. Most of the expandable packers do not provide permanent sealing; they are retrievable (Sun & Bai, 2017). Inflatable packers, bridge plugs, swell packers, straddle packers, inflatable cement retainers, and expandable tubulars are classified under expandable packers. Their expansion mechanism is triggered by several mechanisms. For example, mechanic expansion is the major mechanism for expanding bridge plugs and expandable tubulars (Al-Shahrani et al., 2007). The expansion of swell packers is achieved by being in contact with fluids in wells. Depositing either sand or cement into a well results in isolating the lower perforations. Another method for addressing channeling and blocking near-well fractures is to employ cement squeezing, which involves filling the affected areas (Sun & Bai, 2017).

2.2.2 Chemical Methods

Traditional mechanical approaches, including cementing, bridge plugs, and mechanical tubing patches, prove highly efficient when addressing less complex conformance issues and managing issues like wellbore water sealing, such as casing leaks and fluid flow behind the pipe (Seright et al., 2001). Plugging matrix or fractures in the reservoir are the main objectives of the chemical methods. Chemical methods include pumping chemical products into an injector or producer wells. Chemical methods consist of silicate solutions and gels (Grattoni et al., 2001; Fleury et al., 2017), resins (Seright et al., 2003), and polymer gels (Sydansk, 1990; Sydansk, 2007).

At the beginning, polymers were injected directly for water diversion. As large volumes of polymer were used in field applications, the method of using polymers deep in the reservoir was not cost effective. Philips Co. (Needham et al., 1974) initiated the first polymer gel application as a conformance control by using partially hydrolyzed polyacrylamides (HPAM) and aluminum citrate. The polymer gel system usually comprises a high-molecular weight polymer and a cross linker. Depending on their formulations, the triggering mechanism to make polymer molecules link together to form interconnected polymer molecules alters. These rigid, viscous gels completely or partially plug flow channels where water production is excess and provide a barrier to water flow. The mixture of polymer solution and crosslinking agent is known as gelant. Polymer gel treatment, also called as relative permeability modifier, is formed when the enough gelation time passes and polymer molecules crosslink to each other. Polymer gels can be classified into two groups: In situ crosslinked polymer gels and pre-formed gels. Utilizing in-situ crosslinked polymer gels is an effective approach for addressing casing leaks with flow limitations, flow issues occurring behind the pipe with constraints, two-dimensional coning through a hydraulic fracture from an aquifer, and natural fracture systems that connect to an aquifer. On the other hand, pre-formed gels are primarily employed to tackle faults or fractures intersecting deviated or horizontal wells, a single fracture causing channeling between wells, and natural fracture systems that facilitate channeling between wells. Treatments with in-situ crosslinked polymer gels are good solutions for casing leaks with flow restrictions, flow behind pipe with flow restrictions, two-dimensional coning through a hydraulic fracture from an aquifer, and natural fracture system leading to an aquifer.

2.3 Nanoparticles and Their Use in Oil Industry

Nanotechnology is the nanoscale integration of science, medicine, engineering, and technology. Moreover, it is mainly focused on the utilization of nanoparticles with a particle size varying from 1 nm to 100 nm. Due to the improvements in extraction

technology and their unique chemical, thermal, and mechanical properties, nanoparticles become more attractive and convenient for use in various industries (Bera & Belhaj, 2016). Nanotechnology has been brought to the upstream petroleum industry, including drilling, completion, fracturing, and EOR, as a cutting-edge approach (Hoelscher et al., 2012; Turkenburg et al., 2012). Nanoparticles are still being studied in the laboratory scale as a potential EOR method. Nanoparticles can be categorized into magnetic types (such as iron, cobalt, and their respective oxides), metallic types (including gold, silver, copper, and platinum), or metal oxide variants (consisting of oxides like aluminum, zinc, silicon, magnesium, zirconium, cerium, and titanium) as outlined by Nwidee et al. in 2018. A base fluid with nanoparticles suspended in it with an average size of less than 100 nm is known as a nanofluid (Wasan et al., 2011; El-Diasty & Ragab, 2013). In comparison to microscale suspensions, suspensions of nanoscaled materials exhibit higher stability against sedimentation due to the great amount of surface forces that prevent the particles from aggregating (Husein, 2017). The primary characteristics listed below have rendered nanoparticles and nanofluids potentially useful compounds or materials for use in the oil industry (Foroozesh & Kumar, 2020).

One crucial factor in achieving successful drilling operations is the reduction of formation damage, which can be accomplished by employing appropriate drilling fluid additives to establish an effective filter cake. This filter cake plays a crucial role in safeguarding formations against excessive filtrate invasion. Research has been conducted on various additives aimed at preventing mud filtrates from entering the formations in close proximity to the borehole. Recently, there has been a growing interest in a range of metallic oxide nanoparticles due to their unique characteristics, notably their small size and relatively high surface-area-to-volume ratio (Barry et al., 2015; Mahmoud et al., 2017; Mahmoud & Nasr-El-Din; 2018; Zhou et al., 2020).

Asphaltene molecules' tendency to self-associate results in the formation of large clusters and viscoelastic networks, significantly increasing the viscosity of heavy oil. Given this, research focused on improving heavy oils by removing asphaltenes is of

utmost importance. This objective can be achieved by employing magnetic nanoparticles (MNPs) since the attachment of asphaltenes to the nanoparticle surface will reduce their ability to form interactions with each other (Nassar et al., 2012; Betancur et al., 2016).

Through one or more of the mechanisms including wettability alteration, interfacial tension decrease, disjoining pressure, and stabilizing foams and/or emulsions under challenging conditions, the nanomaterials utilized in nano flooding assist in oil recovery.

Nanofluids have the capability to induce physical interactions with fluid-solid interfaces, thereby modifying the wetting properties of solid surfaces. As an example, the oil industry has endorsed the use of nanoparticles for altering surface wettability (Vafaei et al., 2006; Hendraningrat et al., 2013). Various nanofluids, such as SiO_2 and ZrO_2, showed a reduction in contact angles on carbonates. Similar studies on sandstones were also performed using TiO_2 and Al_2O_3, and it was shown that these substances brought about a substantial shift in the wetting characteristics of rock surfaces, transitioning them from being oil-wet to either intermediate-wet or water-wet conditions (Ehtesabi et al., 2013; Giraldo et al., 2013; Nowrouzi et al., 2020). By overcoming the available disjoining pressure, zirconia nanoparticles could alter the wettability of rocks. Additionally, as the concentration of nanoparticles in oil increases, the water becomes more viscous, which lowers the mobility ratio and improves oil recovery (Rezvani et al., 2017).

Nanoparticles have the capacity to move readily through porous materials over significant distances thanks to their small size. They can traverse pores without obstructing the pore throats since their particle size does not reach the magnitude required to block the pore throats within porous media, as noted by Ayatollahi et al. (2012) and Mcelfresh et al. (2012). Surface and interfacial features of nanoparticles that offer a variety of interactions between various reservoir phases, such as lowering the oil-water interfacial tension (IFT), further make it possible to improve oil recovery. Because of their significant specific surface area and surface energy,

nanoparticles, like in the case of surfactants, naturally adhere to the oil-water interface to decrease interfacial tension (IFT) (Zhu et al., 2006; Wang et al., 2008).

Nanoparticles can actively interact with fluid-fluid interfaces because of their high surface area to volume ratio and strong adsorption affinity (Ehtesabi et al., 2013). As a result, nanofluids may have lower interfacial tensions than base fluids (Ravera et al., 2006). Laboratory studies conducted by Torsater et al. (2012) and Hendraningrat et al. (2013) revealed that IFT between synthetic oil and brine was decreased after addition of nanoparticles into the brine.

Previous research has identified key mechanisms by which silica nanoparticles enhance oil recovery. These mechanisms include reducing the interfacial tension between oil and water and altering the rock's wettability towards a water-wet condition (Ayatollahi & Zerafat, 2012; Zallaghi et al., 2017). In a different study, Roustaei et al. (2012) employed hydrophilic-lipophilic polysilicon (HLP) and naturally wet polysilicon (NWP) in an experiment demonstrating that IFT was decreased from 26.3 mN/m to 2.55 mN/m and 1.75 mN/m, respectively.

To prolong the maintenance of high steam quality in the thermal recovery of extra heavy oil or bitumen, metallic nanoparticles with exceptional thermal characteristics (notably, their heat-carrying capacity) are employed. For instance, induction heating with magnetic nanoparticles (MNPs) is a possible substitute that can overcome conventional thermal techniques' drawbacks. Due to hysteresis loss and relaxation loss, MNPs will produce a self-heating effect when an alternating magnetic field is applied at a specific frequency, helping to heat heavy oil (Bhatia & Chacko, 2011).

Shokrlu and Babadagli (2010) investigated the effects of several nano- and micron-sized metals of iron, nickel, and copper and their varied oxides on the viscosity reduction of heavy oil in their laboratory trials. With nano-sized particles, the results showed a stronger viscosity reduction of oil samples, which was observed and attributed to their greater specific surface area (Taborda et al., 2017). Additionally, it was stated that the viscosity of heavy oil might be reduced by using a nano-nickel

catalyst (Li et al., 2007). Furthermore, Srinivasan and Shah (2014) investigated how the addition of nanofluids based on surfactants reduced the viscosity of heavy oil. The findings of mixing the produced nano-emulsions with heavy oil samples showed promising results. In another research, Pramana et al. (2010) also studied that that nano-ferrofluid heats up more rapidly through electromagnetic induction compared to graphite fluid and brine.

Numerous research papers have presented experimental findings that clearly demonstrate the positive impact of nanofluids on enhancing oil recovery. The extent of this enhancement depends on various nanofluid properties, including particle size, concentration, and material composition. Researchers have proposed several potential mechanisms for nanofluid-enhanced oil recovery. These mechanisms encompass alterations in wettability to promote water-wet conditions, reductions in interfacial surface tension (IFT) between oil and water, adjustments in disjoining pressure, increased viscosity of aqueous solutions, lowered oil viscosity, processes like climbing film and slug-like displacement, log-jamming where nanoparticles obstruct specific pores and redirect trapped oil to neighboring pores, combinations of multiple mechanisms, and unidentified mechanisms yet to be determined (Wasan et al., 2011; Torsater et al., 2012; Luo et al., 2016).

With the use of nanoparticles as viscosity modifiers, it is possible to make the injected fluid more viscous, which enhances the mobility ratio of the flood and results in a high sweep efficiency and more effective EOR (Murshed et al., 2008). Nanoparticles have the ability to transform an emulsion's rheological properties from a Newtonian fluid to a non-Newtonian fluid. When trapped oil is emulsified in situ, a non-Newtonian fluid with a higher viscosity forms, which may have a better sweep efficiency than the injected fluid (Malkin, 2013). The resulting fluid may have a piston-like mechanism that can more effectively displace the oil and defeat capillary forces.

Nanoparticles-assisted polymer (NAP) flood is the utilization of nanoparticles in conventional polymer flooding to benefit from nanoparticles as viscofiers.

According to Zeyghami et al. (2014), silica nanoparticles increase viscosity in sulfonated PAM solutions while having an increasing influence on hydrolyzed polyacrylamide (HPAM) at higher silica concentrations and a decreasing effect at lower silica concentrations. Based on the findings by Khalilinezhad et al. (2016), dispersed silica nanoparticles increase solution viscosity and oil recovery during a nanoparticles-aided polymer (NAP) flood by reducing polymer adsorption.

A nanoemulsion is a type of emulsion stabilized by nanoparticles that exhibits a remarkable capacity to overcome problems that are present in traditional emulsions stabilized by surfactants or colloidal solids. The exceptional thermal and mechanical durability, along with their inherent stiffness, enables nanoparticles to maintain stability even in demanding reservoir environments. In situations characterized by short stability durations, where substances like surfactants and polymers tend to break down, nanoparticles stand out. In comparison to microemulsions, nanoemulsions exhibit a broader range of applicability and can withstand extreme conditions, including high temperatures, pressures, shear forces, and salinity, ensuring their stability within reservoirs (Mandal et al., 2012).

Small size and shape of nanoparticles enable efficient transit or propagation through the porous media of the reservoir's micron-sized pores without clogging the pore throats. Nanoemulsions are also tiny enough to pass through pore throats without retaining much. They are appropriate for widespread field applications (Zhang et al., 2010). Apart from the utilization of nanoparticles for emulsion technology, foam stability is provided by nanoparticles even in the hot reservoir conditions. It was concluded by Yu et al. (2013) that oil recovery in both high and low permeability cores during waterflooding can be improved by nanoparticle stabilized CO_2 foam.

Nanoparticles are also employed to address the issue of conformance control, offering more efficient solutions. In the presence of external substances like surfactants and co-surfactants/alcohols, oil and water typically form emulsions. In such flooding scenarios, in-situ emulsion formation is quite common and contributes to enhanced oil recovery. The primary reasons behind emulsion flooding are the

lower interfacial tension (IFT) of the resulting emulsion and the ability of emulsion droplets to block the high-permeability zones of the reservoir, thus enabling injected fluids to access trapped oil by passing through the unswept zone (de Farias et al., 2012).

When nanoparticles adhere to the oil-water interface, their high desorption energy results in a more stable emulsion compared to surfactant-based emulsions, which have lower desorption energy due to surfactant molecules. These nanoparticle-based emulsions, often referred to as pickering emulsions, exhibit stability even in challenging reservoir conditions, including high shear rates, in contrast to surfactant-based emulsions (Sharma et al., 2015; Pandey et al., 2018; Zoppe et al., 2021).

2.4 Nanocellulose

Cellulose is a type of natural linear polymer with the chemical formula $(C_6H_{10}O_5)_n$, where n denotes the degree of polymerization (Figure 2.2). The most abundant biopolymer in the world, cellulose is crucial for the tissue structure of eukaryotic cells and plant cell walls (Cervin et al., 2013; Zoppe et al., 2021). It is made of beta glucose monomers that are connected by 1-4 glycosidic bonds and has a degree of polymerization between 10,000 and 15,000 (Poletto et al., 2013).

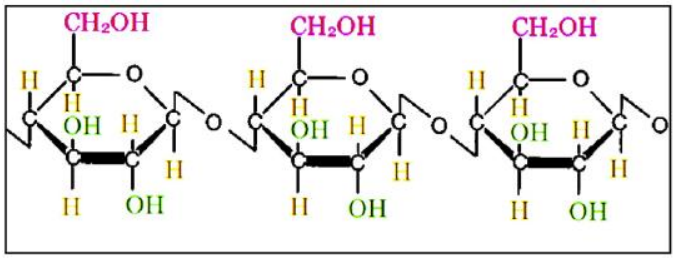

Figure 2.2: Chemical structure of cellulose (Mishra, 2018)

An essential technique for isolating nanocellulose from cellulosic materials is acid hydrolysis. This process takes advantage of the combination of structured and unstructured segments within cellulose chains, resulting in the preservation of the

structured portions while the unstructured regions are broken down by the acid. Sulfuric acid is the primary acid employed in acid hydrolysis (Moon et al., 2011; Lavoine et al., 2012). The key parameters that govern the properties of the produced nanocellulose are reaction time, temperature, and acid concentration. However, a significant drawback of acid hydrolysis is the generation of acidic wastewater during the washing phase required to neutralize the pH of the nanocellulose solution (Peng et al., 2011).

It is a naturally occurring polysaccharide obtained from various cellulosic sources, the most popular of which are cotton and wood. The amount and properties of cellulose might differ depending on the features of the sources (for example, wood contains between 40 and 50 percent cellulose, whereas cotton contains 90 percent cellulose) (Khazraji & Robert, 2013). The main properties of cellulose are hydrophilicity with a contact angle of 20^{o}-300^{o} and the absence of taste and odor (Mishra, 2018).

The term "nanocellulose" (NC) refers to cellulose fibrils or crystallites with at least one dimension in the nanoscale range (smaller than 100 nm), which can be produced by chemically or mechanically treating plant or wood cellulose (Isogai, 2013).

Nanocellulose is structurally distinct from conventional materials and have a variety of benefits over them, including low density, high crystallinity, high modulus, high strength, and superior modifiability (Zhu et al., 2021). Because of their hydrophilicity, which results from the abundance of hydroxyl groups on their surface, NCs can be dispersed in some strong polar solvents, particularly in water (Thomas et al., 2020).

Nanocellulose is appealing for applications in various industries due to its exceptional characteristics and biodegradability, such as nanocomposite materials, surface-modified materials, and transparent paper with unique functions (Abitbol et al., 2016). Nanocomposite materials containing nanocellulose are known for their distinctive characteristics, including remarkable mechanical and thermal strength, in

addition to their lightweight and transparent nature (Dufresne, 2012). Nanocellulose has a large surface area and is rich in hydroxyl groups, making it useful for surface modification (Moon et al., 2011).

Three forms of cellulose can be distinguished based on their varying lengths: cellulose nanocrystals (CNCs), cellulose nanofiber (CNF), and bacterial nanocellulose (BNC).

2.4.1 Cellulose Nanocrystal (CNC)

The rod-like nanocrystal configuration is referred to as a cellulose nanocrystal. The amorphous areas in the native cellulose are removed using the acid hydrolysis process. As illustrated in Figure 2.3, in order to create CNC, the amorphous components of cellulose are hydrolyzed using mineral acids, then the remaining acids and impurities are removed, and the crystals are separated by sonication (Dong et al., 1998; Brinchi et al., 2013). During the production of cellulose nanocrystals (CNC), also referred to as nanocrystalline cellulose or cellulose whiskers, the highly crystalline segment within native cellulose usually remains unaltered through the acid treatment process, resulting in the formation of a rod-shaped structure (Habibi et al., 2010).

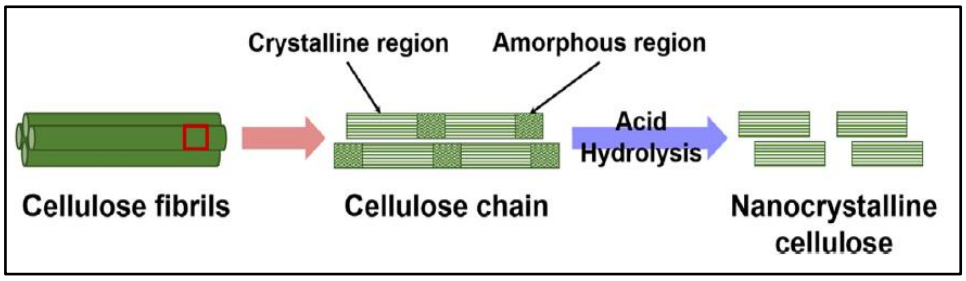

Figure 2.3: Cellulose nanocrystals (CNC) extraction (Phanthong et al., 2018)

The level of crystallinity in cellulose nanocrystals is comparatively high, ranging from 54 to 88%. The size of cellulose nanocrystals depends on the type of their source, but typically they have dimensions of 3–30 nm in diameter and 100–1 μm in

length (Lavoine et al., 2012). It demonstrates that nanocrystalline cellulose has all dimensions that fall within the nanometer size range.

2.4.2 Cellulose Nanofibril (CNF)

When wood pulp is subjected to mechanochemical treatment, it produces nanofibrillated cellulose (CNF), which is used to express fibrils with dimensions in the nanometric range. Individual nanofibrils and aggregated nanofibrils make up CNF (Turbak et al., 1982 & 1983; Liu et al., 2014). Its chemical makeup is entirely composed of cellulose and has both crystalline and amorphous regions (Dufresne, 2012). Figure 2.4 illustrates the schematic of nanofibrillated cellulose that can be separated from cellulose chains by the cleavage of fibrils along the force provided by a mechanical process (Moon et al., 2011).

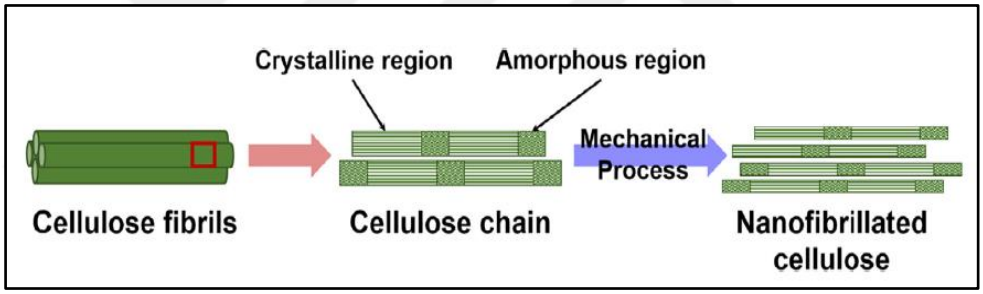

Figure 2.4: Cellulose nanofibril (CNF) extraction (Phanthong et al., 2018)

In contrast to nanocrystalline cellulose, nanofibrillated cellulose exhibits greater length, a higher aspect ratio (length to diameter), increased surface area, and a higher concentration of hydroxyl groups, all of which make it more receptive to surface modifications (Lavoine et al., 2012).

2.4.3 Bacterial Nanocellulose (BNC)

A special type of nanocellulose from nanocrystalline and nanofibrillated cellulose is bacterial nanocellulose (BNC). A top-down approach can be used to extract nanocrystalline and nanofibrillated celluloses from lignocellulosic biomass, but

bacterial nanocellulose is created by bacteria, primarily Gluconacetobacter xylinus, over the course of a few days to two weeks (Abitbol et al. ,2016; Jozala et al., 2016). The chemical composition of bacterial nanocellulose is identical to that of the other two varieties of nanocellulose. It assumes the form of twisted ribbons with average diameters ranging from 20 to 100 nm and micrometer-scale lengths, resulting in a significant surface area per unit. BNC stands out for its remarkably high degree of polymerization, reaching up to 8,000, as well as its outstanding mechanical strength, biocompatibility, and water-retention capability. Additionally, it possesses a fine and pure fiber network structure (Kamel, 2007).

2.5 Application of Nanocellulose in Oil Industry

Nanocellulose has a lot of potential as a new material for oil and gas production based on the superior colloidal and interfacial features discussed above. Traditional oilfield chemical reagents are facing enormous difficulties as oil demand and development intensity rises year after year. Limitations of traditional chemicals under tough oil reservoir environments, such as low adaptation, instability at high temperatures, reservoir damage, and formation pollution, call for immediate attention. To meet the accelerating demands of a market that is expanding quickly and the demands of future oilfield technology, it is essential to develop unique, high-performance, environmentally friendly, and non-damaging chemical reagents for oilfield applications.

2.5.1 Application of Nanocellulose in Drilling Fluids

Micro- and nanoparticles are being utilized more frequently in the production of oil and natural gas to increase drilling fluid efficiency and handle growing production issues. Rheology and fluid loss are two crucial performance indicators for drilling fluid that plays a significant role in the drilling process. The problem of maintaining the drilling fluid quality is brought on by the reservoir conditions, which are

gradually getting worse as the formation depth continues to increase (Wang et al., 2021). Nanocellulose can be used to withstand severe conditions because of its strong mechanical and thermal stability features. The rheology, fluid loss, and thermal stability of the drilling fluid can all be significantly enhanced by using nanocellulose (Liu et al., 2019a; Ramasamy & Amanullah, 2020; Wei et al., 2020).

Compared to traditional bulk cellulose, their highly organized structures offer much enhanced thermal and chemical stability. Due to the presence of hydroxyl groups on their surfaces, CNF and CNC are easily dissolved in water and produce fluids with shear-thinning rheology and thixotropy at low concentrations. Drilling and drill-in fluids may benefit from these two key characteristics of nanocellulose mentioned above (Hall et al., 2018). CNF with high performance water-based mud formulation and its derivatives were examined by Hall et al. (2017 & 2018). The performance of the slurry was investigated after several nanocellulose and derivatives, including CNF, carboxymethyl cellulose nanofibers (C-CNF), and TEMPO-oxidized cellulose nanofibers (TO-CNF), were employed to create the cement slurry. In contrast to xanthan gum, which disintegrated following heat treatment, CNF had superior thermal durability and could have preserved overall integrity even at higher temperatures.

The use of CNC as a rheology modifier in drilling fluids was investigated by Li et al. (2015). Microfibrillated cellulose (MFC) was hydrolyzed with sulfuric acid to produce the CNC that was employed in their investigation. Compared to bentonite mud with MFC, CNC-containing bentonite mud has better rheological and fluid loss qualities. The outcomes demonstrated that including CNC improved the rheological characteristics, thermal stability, water loss, and mud cake deposition of the water-based bentonite slurry.

Attention is being focused on nano-sized additives in cement slurry formulation for better cement characteristics. Chemical reactions can be considerably improved and increase hydration due to the high surface area present in nanoscale materials (Sanchez and Sobolev, 2010). Because it has been used in the cementing process to

enhance features such as rheological properties, durability, degree of hydration, yield stress, shear thinning, etc., nanocellulose is an excellent option to support cement sustainability. According to Ardanuy et al. (2012), CNF has an impact on the mechanical characteristics of cement composites. Moreover, cement slurry can be reinforced with cellulose nanocrystal particles. For the duration of the cement slurry's setting process, adding nanocellulose particles can insulate it hermetically (Petrus, 2015).

Investigations were also conducted into the use of CNF as a rheology modifier in oil well cement. It was found that, as anticipated, shear stresses rose when shear rate and CNF loading levels rose in the cement matrix of the oil well. Both the yield stress and the plastic viscosity exhibited this pattern (Sun et al., 2016).

2.5.2 Application of Nanocellulose in Enhancing Oil Recovery

Injecting a displacement fluid into reservoirs to release the residual oil in porous rocks is a traditional chemical EOR technique. Although polymer flooding improves sweep efficiency due to the fluid's high apparent viscosity, it also has issues with the reservoir's harsh conditions, low water/oil mobility ratio, and wettability of the rock surface. It is necessary to search for an effective and ecologically friendly replacement material used in EOR to address these technical obstacles. As a displacing fluid or interface stabilizer in EOR, nanocellulose has excellent potential (Wei et al., 2020; Zhu et al., 2021).

Wei et al. (2017) studied that emulsification, dragging, and wettability change are three mechanisms by which surface-functionalized CNFs boosted 3%–17% oil recovery over water flooding. The hydrophobic and hydrophilic groups were successfully grafted onto CNFs, greatly enhancing their interfacial activity and salt tolerance. Surface modification did, however, increase the material's cost (Wei et al., 2019).

One of the most crucial oil recovery methods used in the production of oil and gas fields is foam flooding. Before injection, foam might be produced either at the surface or in the reservoir's pore space. Sweep inhomogeneity brought on by layers with higher permeability than the surrounding formations or by gravity override are both mitigated by foam flooding (Sheng, 2013). The effectiveness of foam flooding to maximize oil recovery is directly dependent on the stability of the foam system. Through a synergistic interaction with the surfactants on the liquid film, nanocellulose raises the liquid-carrying capacity of the liquid film and enhances foam stability (Wang et al., 2021). At the gas-liquid interface, nanocellulose particles can be adsorbed, greatly enhancing the stability of the foam system (Wei et al., 2017; Liu et al., 2019). The cellulose nanofibers (L-CNFs) that Wei et al. (2019b) developed contain lignin and are green and biodegradable. They are utilized to maintain the liquid foam's interface so that oil production can be achieved. It was discovered through observation that the addition of L-CNF considerably increased the rates of foam drainage.

In terms of stabilizing emulsions, nanocellulose with exceptional stability has received a lot of interest. The emulsion generated by nanoparticles is particularly stable due to the ability of nanocellulose to be irreversibly absorbed at the oil–water interface (Kalashnikova et al., 2011). High aspect ratio and amphiphilic characteristics characterize nanocellulose. Therefore, depending on the hydrophobicity/hydrophilicity of the cellulose surface medium, a more hydrophobic crystal plane of nanocellulose or a more hydrophilic crystal plane of nanocellulose could be directed toward the surrounding medium. Due to its amphiphilic properties, nanocellulose has the potential to be used as an emulsion stabilizer (Medronho & Lindman, 2014; Nikfarjam et al., 2015; Dai et al., 2020).

Permeable channels in the reservoirs can be effectively obstructed through surfactant flooding, which can employ pre-prepared oil-in-water emulsions or induce in-situ emulsification. This process redirects water toward low-permeability zones, enhancing the efficiency of trapped oil recovery. Therefore, the stability of the oil-in-water (o/w) emulsion is pivotal in this flooding technique. Wei et al. (2019c)

showcased the stabilizing influence of CNF when added to an alkaline-induced o/w emulsion created through saponification, using high total acid number (TAN) crude oil in an alkaline solution.

In recent years, there has been a considerable focus on employing nanocellulose as a unique agent for displacing oil and enhancing oil recovery (Aadland et al., 2019). Li et al. (2017) proposed the use of nanocellulose in enhanced oil recovery, highlighting that the regenerated nanocellulose dispersion displayed notable resistance to salt and temperature, rendering it a promising material for improving oil recovery. Raza and Gates (2021) explored the oil displacement process using CNC fluids, revealing that CNC nanofluids have the potential to increase the viscosity of the aqueous phase and reduce the interfacial tension between oil and water. Moreover, as demonstrated by Molnes et al. in 2016, CNC dispersions in brine exhibited mobility and stability even under increasing ionic strength, making them potentially suitable as flooding fluids when injected into sandstone cores. Additionally, an investigation into CNC's injectability into highly porous sandstone cores, conducted by Molnes et al. in 2018, suggested that CNC has promise as an additive in injection water for enhanced oil recovery (EOR).

CHAPTER 3

STATEMENT OF PROBLEM

Enhanced Oil Recovery (EOR) techniques play a vital role in extracting trapped oil from carbonate reservoirs, which present unique challenges due to their complex and heterogeneous nature. Nanocellulose has emerged as a promising candidate for enhancing oil recovery in such reservoirs, offering potential advantages in improving sweep efficiency and displacing residual oil. However, the successful application of nanocellulose as an EOR agent necessitates a comprehensive understanding of its behavior within carbonate rock formations, particularly through lab-scale flow tests and thorough material characterization.

The primary problem to be addressed in this study is to investigate the effectiveness and mechanisms of nanocellulose as an EOR agent in carbonate rocks. By conducting lab-scale flow tests aimed to explore the flow behavior of nanocellulose dispersions through porous media, including adsorption, retention, and potential plugging effects, as well as the impact on wettability alteration.

Furthermore, the material characterization of nanocellulose is of utmost importance to comprehend its structural properties and interactions with the carbonate rock matrix. The investigation will explore the rheological properties and stability of nanocellulose dispersions under relevant reservoir conditions. Therefore, this study aims to address these knowledge gaps and challenges by conducting a comprehensive investigation of nanocellulose as an enhanced oil recovery agent for carbonate rocks.

By addressing these critical aspects through lab-scale flow tests and comprehensive material characterization of nanocellulose, this study seeks to contribute valuable insights into the feasibility and efficacy of nanocellulose as an enhanced oil recovery agent for carbonate rocks. The findings from this study will aid in optimizing EOR strategies and provide valuable guidance for future research and potential field

applications, ultimately advancing the field of enhanced oil recovery and contributing to sustainable oil recovery.

CHAPTER 4

MATERIAL CHARACTERIZATION

This chapter presents a comprehensive investigation of nanocellulose material characterization for its application in enhanced oil recovery (EOR). Various characterization techniques were employed to study the physical and chemical properties of nanocellulose, including solubility bottle tests, viscosity bottle tests, particle size analysis, interfacial tension (IFT) measurements, wettability studies, and contact angle measurements.

4.1 Nanocellulose Powder Samples

At the beginning of this research study, two major types of nanocellulose samples, namely, cellulose nanofibrils (CNF) and crystalline nanocellulose (CNC), were investigated. CNFs are produced with three different processes: mechanical treatment (grinding, milling), chemical treatment (TEMPO oxidation), and combination of both processes.

Figure 4.1: Stereo Microscope

CNF samples have both amorphous and crystalline structure in an individual fiber. On the other hand, CNCs are obtained from cellulose fibrils by acid hydrolysis. Acid removes the amorphous parts and crystalline regions are left in the structure. CNCs have about 90% crystallinity. Both CNF and CNC samples were analyzed by using stereo microscope (Figure 4.1), which reflects the light from the surface of an object not transmitting through it.

4.1.1 CNF in Powder Form

Images of powder form of CNF samples taken by using stereo microscope can be seen in Figure 4.2.

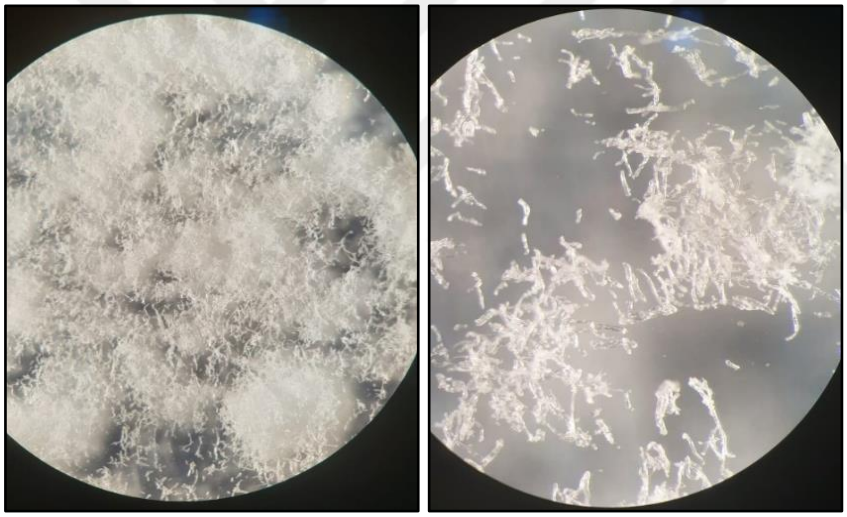

Figure 4.2: CNF view under stereo microscope (left view with no magnification, right view with 115x magnification)

Main functional group of CNFs is -OH. Transmission electron microscopy (TEM) image of powder form CNF can be seen in Figure 4.3.

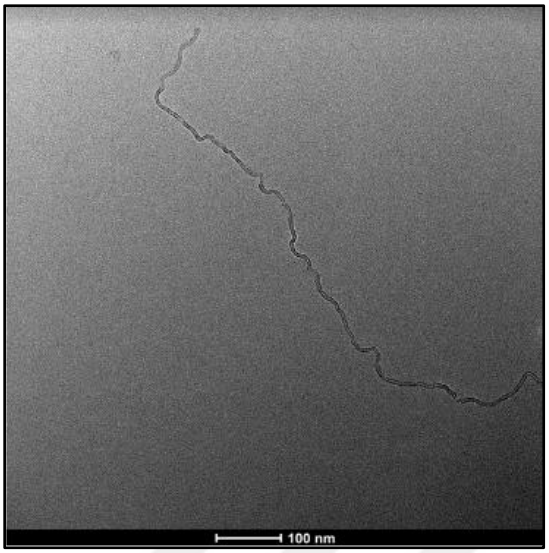

Figure 4.3: TEM image of CNFs (Nanocellulose (n.d.))

The major characteristics of powder form CNF, including average particle size, cellulose crystallinity, decomposition temperature and density, are listed in Table 4.1. All these properties were provided by the CNF manufacturing company.

Table 4.1: General properties of powder CNF (Nanocellulose (n.d.))

Appearance (form)	Dry powder (~4 wt% moisture)
Avg particle size	10-20 nm width, 2-3 μm length
Cellulose crystallinity (XRD)	92%
Decomposition temperature	329 °C
Density	1.50 g/cm^3

As stated in its Material Safety Data Sheet (MSDS) form, CNF has a hydrophilic character. It can be dispersed in water by using high-pressure homogenizer. Stereo microscope view of CNFs powder mixed with water can be seen in Figure 4.4. Although, CNF is hydrophilic, it is difficult to obtain a homogenous solution in which CNF still keeps its dimensions in nano size.

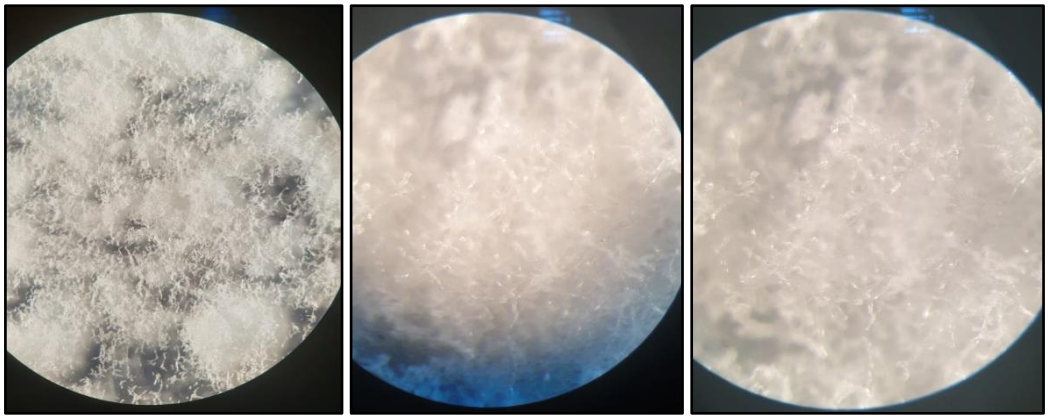

Figure 4.4: Stereo microscope views of CNF mixed with water (115x magnification)

4.1.2 CNC in Powder Form

Images of powder form of CNC samples taken by using stereo microscope can be seen in Figure 4.5.

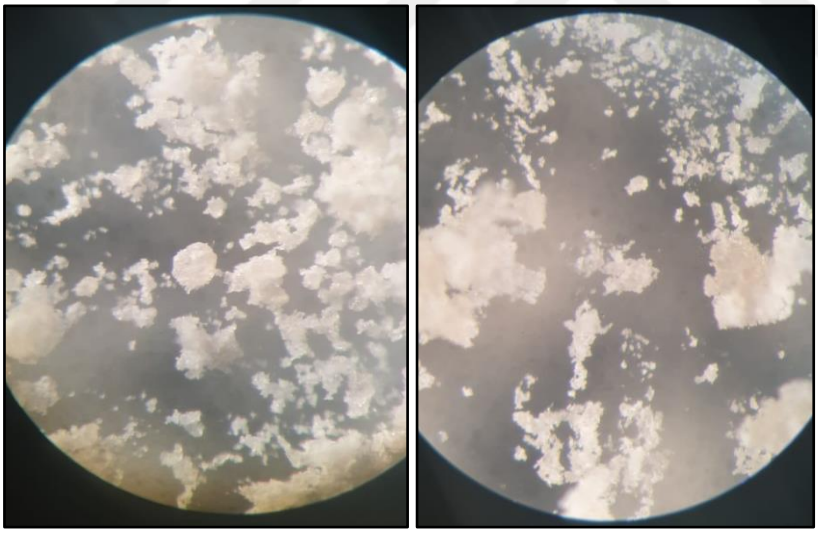

Figure 4.5: CNC (dry powder) views under stereo microscope with 115x magnification

Besides hydroxyl (OH) groups as main chemical group, CNC also has sulphate (half-ester) groups as a result of acid hydrolysis process. Transmission electron microscopy (TEM) image of powder form CNC can be seen in Figure 4.6.

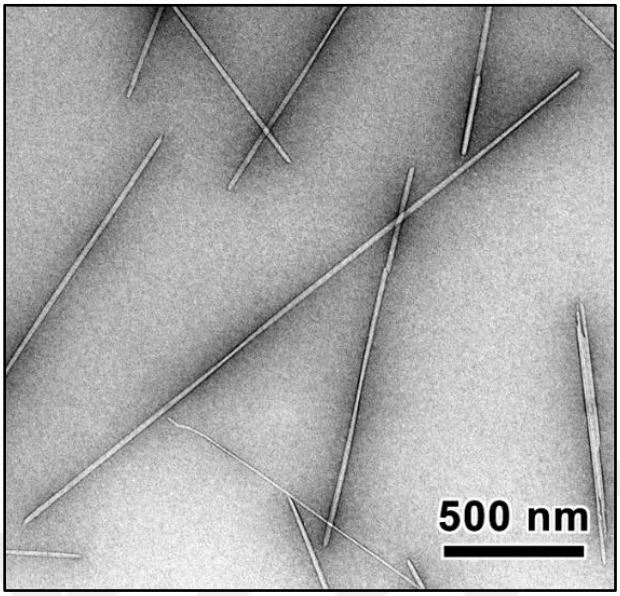

Figure 4.6: TEM image of CNCs (Nanocellulose (n.d.))

The major characteristics of powder form CNC, including average particle size, cellulose crystallinity, decomposition temperature and density, are listed in Table 4.2. All these properties were provided by the CNC manufacturing company.

Table 4.2: General properties of powder CNC (Nanocellulose (n.d.))

Appearance (form)	Dry powder (~4 wt% moisture)
Avg particle size	10-20 nm width, 300-900 nm length
Cellulose crystallinity (XRD)	92%
Decomposition temperature	349 ^{o}C
Density	1.49 g/cm^{3}

According to MSDS form of CNC, it also shows hydrophilic characteristics. Like in the case of CNF, high-pressure homogenizer can be used to disperse CNC in water. Stereo microscope view of CNCs powder mixed with water can be seen in Figure 4.7. Despite its hydrophilic behavior, dispersion of CNC is not that much simple as it may aggregate and form molecules larger than nanometer scale.

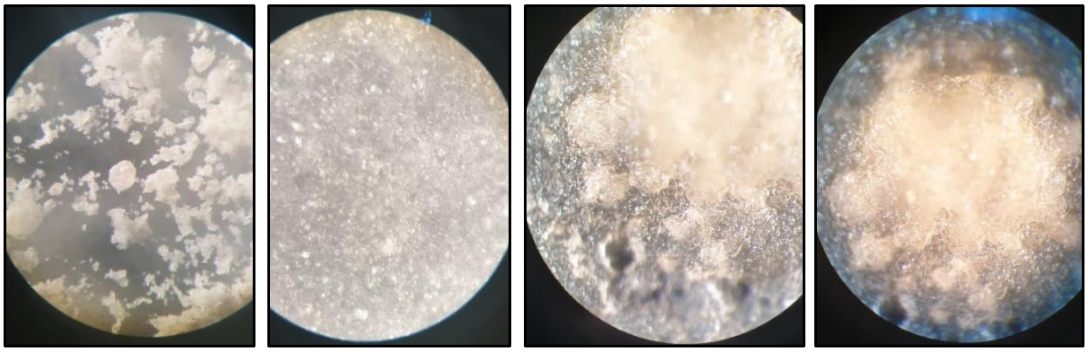

Figure 4.7: Stereo microscope views of CNC mixed with water (115x magnification)

Dispersion stability is also another issue for such nano materials. It can be easily observed in the stereo microscope views that powder CNC mixed with water is blur and, in a gel like form. It seems to have inhomogeneous structure with an agglomeration like texture.

4.2 Aqueous Suspension of Nanocrystalline Cellulose (NCC)

It is difficult to stabilize powder forms of nanocellulose in aqueous suspension by preparing solutions in the laboratory. Forming homogenous and stable dispersion of a nano material is vital in the case of core pore scale studies. The particles have a great tendency of agglomeration which may lead to plugging of pores due to higher particle size of coagulated nanocellulose particles. The use of already existing suspension ease the application by skipping the stabilization problem of powder samples. Thus, aqueous suspension of nanocrystalline cellulose (NCC), 6%wt (Figure 4.8) was decided to be utilized in the further flow tests.

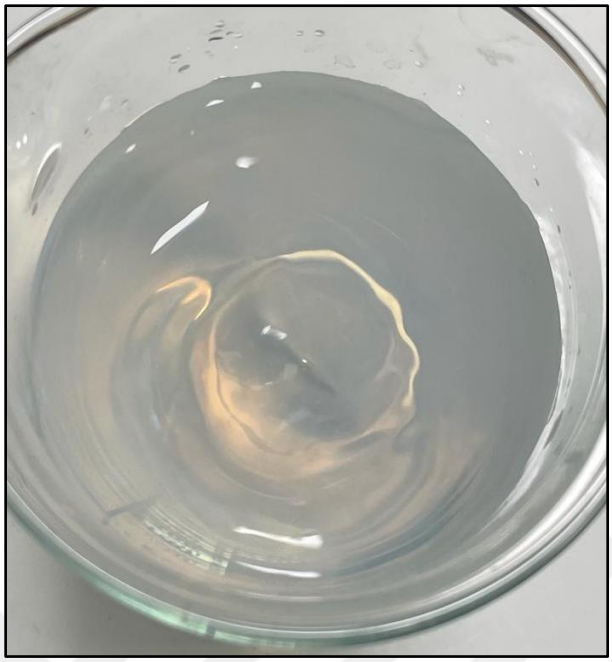

Figure 4.8: Aqueous suspension of nanocrystalline cellulose (NCC), 6%wt

The major characteristics of aqueous suspension of nanocrystalline cellulose, including particle diameter, cellulose crystallinity, pH and bulk density, are listed in Table 4.3 and SEM image of NCC can be seen in Figure 4.9. All these properties were provided by the manufacturing chemical company.

Table 4.3: General properties of NCC (Nanocellulose (n.d.))

Appearance (form)	Aqueous gel, 6 wt%
Particle diameter (crystallite)	2.4-4.6 nm
Cellulose crystallinity (XRD)	89%
pH	6-7
Bulk density	0.68 g/cm^3

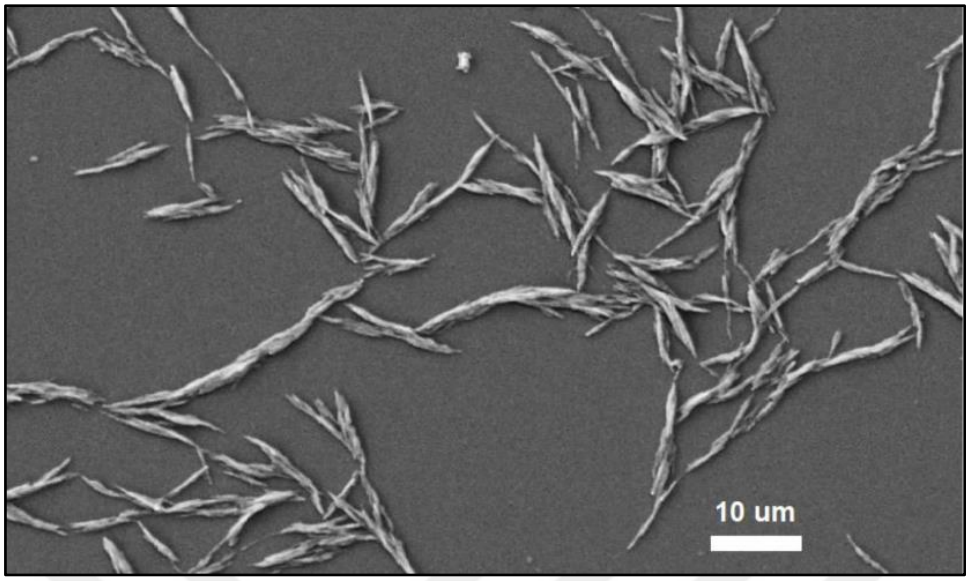

Figure 4.9: SEM image of NCC (Nanocellulose (n.d.))

As a result, NCC was decided to be used for further flow tests in this study as a green enhanced oil recovery agent. Therefore, it was essential to characterize its properties to comprehend its behavior during the tests and analyze the working mechanism of that material. The rest of the sub-chapters within the Material Characterization Chapter of this study refer to the analysis conducted with/on NCC. Different concentrations of NCC were obtained by diluting already available 6 wt% NCC sample by using water with a specified salinity value.

4.3 Solubility Bottle Tests

The solubility bottle tests were conducted to evaluate the solubility of nanocellulose in different water systems, providing crucial information about its compatibility with reservoir fluids and injection fluids. These tests helped assess the stability of nanocellulose in various reservoir conditions, including temperature and salinity variations. In order to see the effect of salinity, nanocellulose concentration and temperature, basic solubility bottle tests were performed. The nanocellulose base solution was placed in a glass tube and required amount of water was added. The tube was shaken to ensure mixing. Then, the bottle tubes were left for stabilization.

This procedure was repeated to evaluate the effects of different parameters on the solubility of nanocellulose.

4.3.1 Effect of Salinity

1 weight (wt) % nanocellulose solutions were prepared by using water with varying NaCl concentrations. Tap water and water with different salinities (1,000 ppm, 5,000 ppm, 10,000 ppm, 30,000 ppm and 65,000 ppm NaCl) were mixed with nanocellulose base solution to generate 1 wt% nanocellulose solution to analyze the effect of salinity. Bottles were kept at room temperature for some settling time to see the effect of salinity on nanocellulose solution (Figure 4.10).

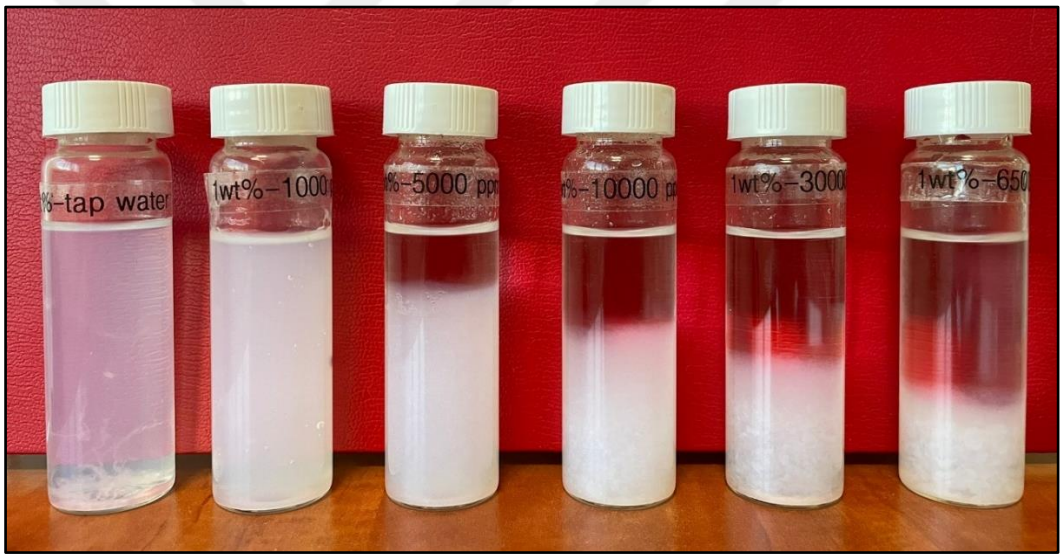

Figure 4.10: Solubility bottle tests for 1 wt% nanocellulose prepared by using water with varying salinities (room temperature)

The sample prepared with tap water (the least saline water in the test group) seems more homogenized with no suspended nanocellulose particles. Increasing salinity has a negative effect on the solubility of nanocellulose in water. It is obvious from the bottle tests that nanocellulose solution prepared with more saline water contains some suspended particles. Furthermore, particle agglomeration is visible by increasing NaCl concentration, especially salinity values higher than 10,000 ppm (Figure 4.11).

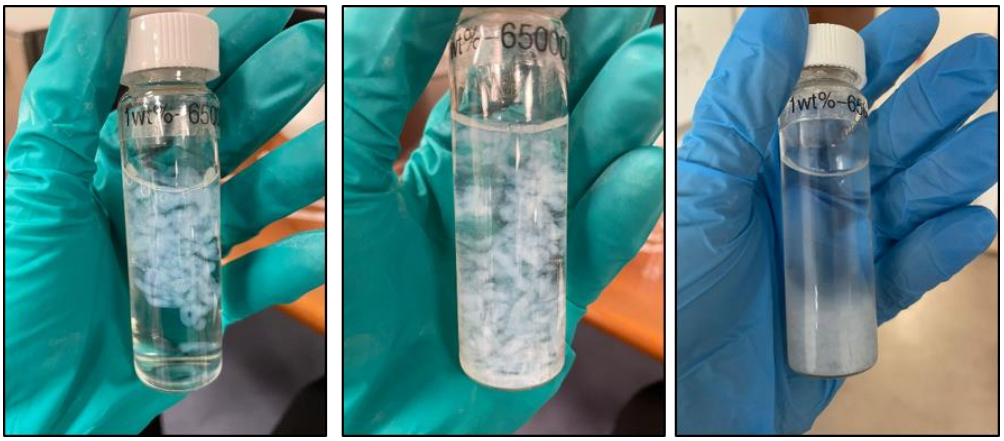

Figure 4.11: 1 wt% nanocellulose prepared by using water with 65,000 ppm NaCl (room temperature)

4.3.2 Effect of Nanocellulose Concentration

The same solubility bottle tests were conducted with 2 wt% nanocellulose solution to compare the effect of nanocellulose concentration on the solubility (Figure 4.12).

Figure 4.12: Solubility bottle tests for 2 wt% nanocellulose prepared by using water with varying salinities (room temperature)

Increasing nanocellulose concentration results in more visible suspended particles. The cloudy part of the solution with visible suspended samples seems to increase with increasing concentration.

4.3.3 Effect of Temperature

Another set of samples were also prepared by using water with varying salinity values and aforementioned nanocellulose concentrations (1 wt% and 2 wt%) and kept in the oven at 65 °C for more than 6 hours to see the effect of temperature on solubility (Figure 4.13 and Figure 4.14).

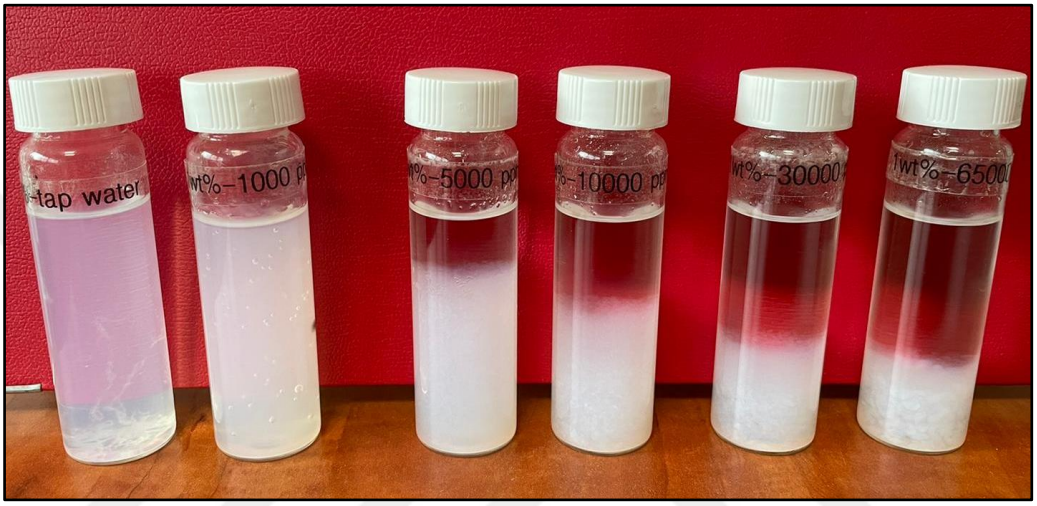

Figure 4.13: Solubility bottle tests for 1 wt% nanocellulose prepared by using water with varying salinities (after 6 hours at 65 °C)

Figure 4.14: Solubility bottle tests for 2 wt% nanocellulose prepared by using water with varying salinities (after 6 hours at 65 °C)

When the samples with same nanocellulose concentrations and water salinities at different temperatures (room temperature and 65 °C) are compared, it is evident that

there is almost no difference in their solubility. The height of the cloudy part of the bottles are almost same for both temperature values. As in the case of room temperature, the sample prepared with tap water is again the most homogenous one after waiting 6 hours at 65 °C. It might be concluded that high reservoir temperatures do not negatively affect the solubility of nanocellulose and that suspended particles are not expected to precipitate at elevated temperature. It might be better to prepare nanocellulose solutions by using less saline water for the stabilization of the nanocellulose particles.

4.4 Viscosity Bottle Tests

Another step for the characterization of nanocellulose is the viscosity bottle tests. Viscosity bottle tests were utilized to investigate the rheological behavior of nanocellulose solutions. By measuring the changes in viscosity under different shear rates and temperatures, the study gained insights into the stability and effectiveness of nanocellulose as an EOR agent over time and under shear forces commonly encountered during injection processes.

After concluding that less saline water used in the preparation of nanocellulose dispersion results in more homogenous solution, it is decided to conduct viscosity bottle tests with only fresh water, preferably tap water. In this way, solubility affect would be eliminated and misleading interpretation would be prevented by using readily homogenous dispersion.

In the context of viscosity bottle tests, the effect of concentration on the viscosity were tested for different time intervals at 65 °C. Two different concentrations of nanocellulose solution, 1 wt% and 2 wt%, were prepared by using fresh water. Solutions were placed in four glass tubes in order to measure viscosity for four different periods of time. The viscosities of nanocellulose solution in glass tubes were measured right after preparation at ambient conditions for both concentrations.

Then, the other glass tubes were placed in the oven with a set temperature of 65 °C (Figure 4.15).

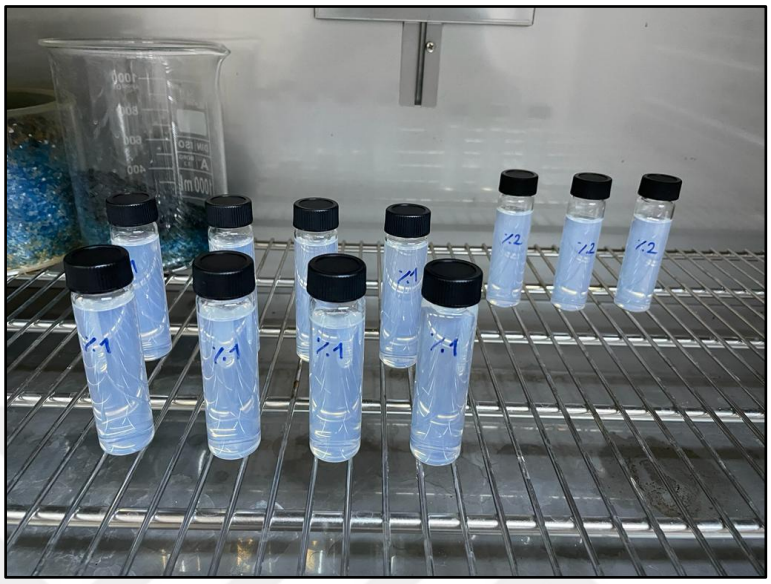

Figure 4.15: 1 wt% and 2 wt% nanocellulose solutions in the oven at 65 °C

Viscosity measurements were performed by using an Anton Paar rheometer (Figure 4.16). The rheometer used in the tests has a rotational system, based on the rotation of a cylindrical body immersed in a liquid, which experiences a viscous resistance force when a rotational speed is imposed on the system. The measuring bob is placed in the sample during the tests. The instrument provides viscosity data of a specific fluid with respect to varying shear rate at a certain temperature.

Figure 4.16: Anton Paar rheometer

After placing the glass tubes in the oven, the viscosities of 1 wt% and 2 wt% nanocellulose solution in glass tubes were measured after 6 hours, 8 hours, 12 hours and 24 hours of aging in the oven at 65 °C. The view of bob after measuring viscosity of nanocellulose solution can be seen in Figure 4.17.

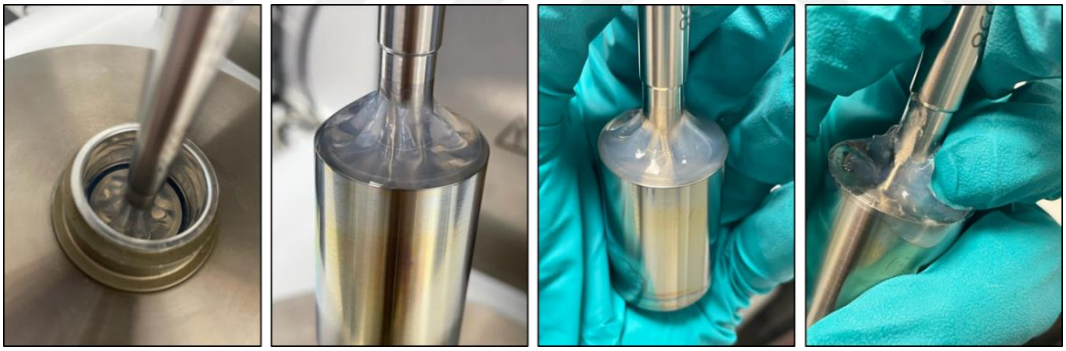

Figure 4.17: Nanocellulose after viscosity measurement

Shear viscosity curves for 1 wt% nanocellulose aged at 65°C can be seen in Figure 4.18. The curves show the viscosity change of 1 wt% nanocellulose by time at 65°C. Overall, the viscosity of nanocellulose increases by time gradually at a constant shear rate. Increasing shear rate results in a decline in the viscosity values for each period individually.

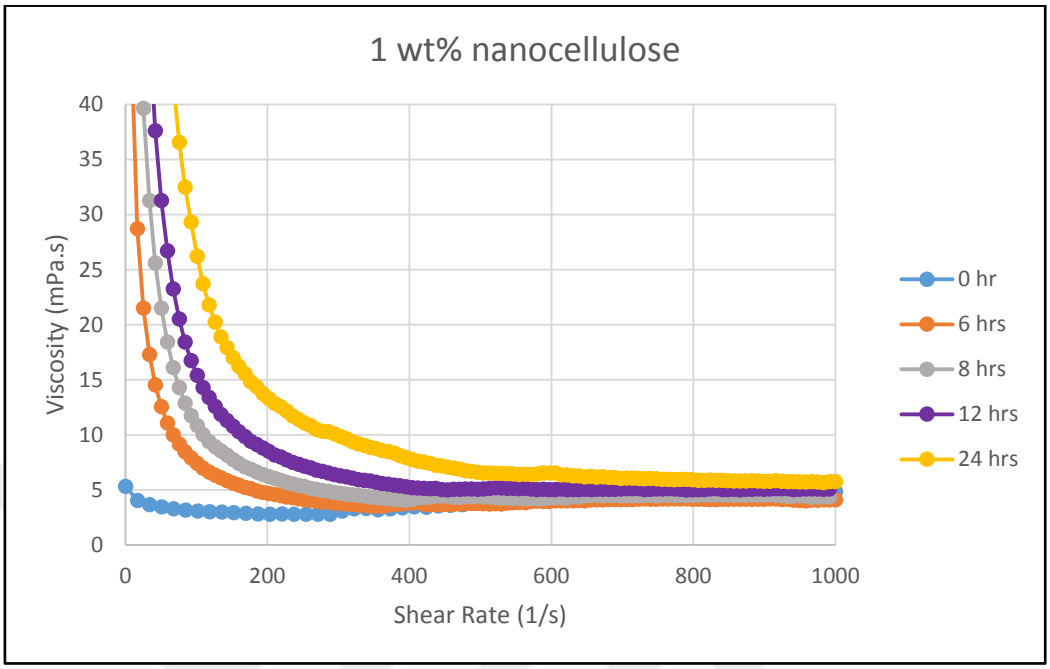

Figure 4.18: Shear viscosity curves for 1 wt% nanocellulose aged at 65°C up to 24 hours

Shear viscosity curves for 2 wt% nanocellulose aged at 65°C can be seen in Figure 4.19. The graphs provide information about the viscosity change of 2 wt% nanocellulose by time at 65°C similarly, the viscosity of nanocellulose increases by time gradually at a constant shear rate.

At a given shear rate and period, viscosity is higher in the case of 2 wt% nanocellulose concentration compared to 1 wt% nanocellulose concentration. Higher viscosity values might be advantageous for oil field applications in terms of residence time, which is preferred as longer as possible.

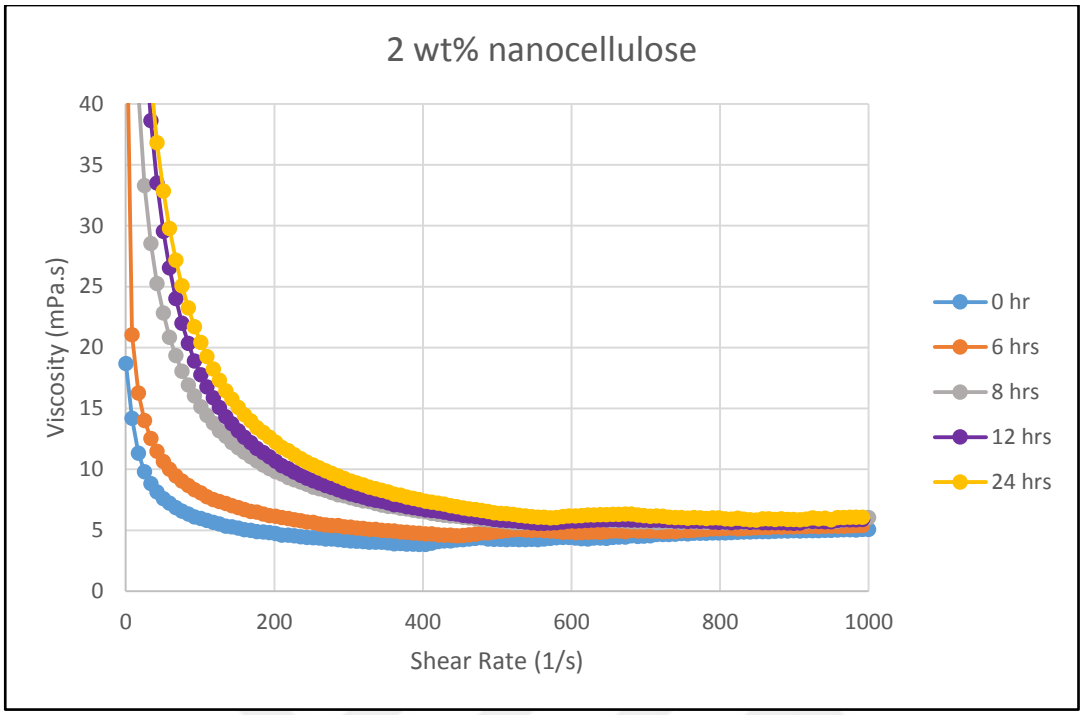

Figure 4.19: Shear viscosity curves for 2 wt% nanocellulose aged at 65°C up to 24 hours

4.5 Particle Size Analyses

Particle size analysis was studied to determine nanocellulose particle size distribution, which plays a significant role in its performance in reservoirs. Understanding particle size variations aided in optimizing nanocellulose injection strategies to target specific pore sizes within the reservoir matrix.

Samples with different nanocellulose concentrations (0.5 wt%, 1 wt% and 2 wt%) and water with varying salinities (fresh water, 10,000 ppm NaCl, and 30,000 ppm NaCl) were prepared for size distribution and zeta potential measurements. The main objective of this part of the study was to see the effect of nanocellulose concentration and salinity of water used in samples on the particle size and stability of nanocellulose. These samples can be seen in Figure 4.20.

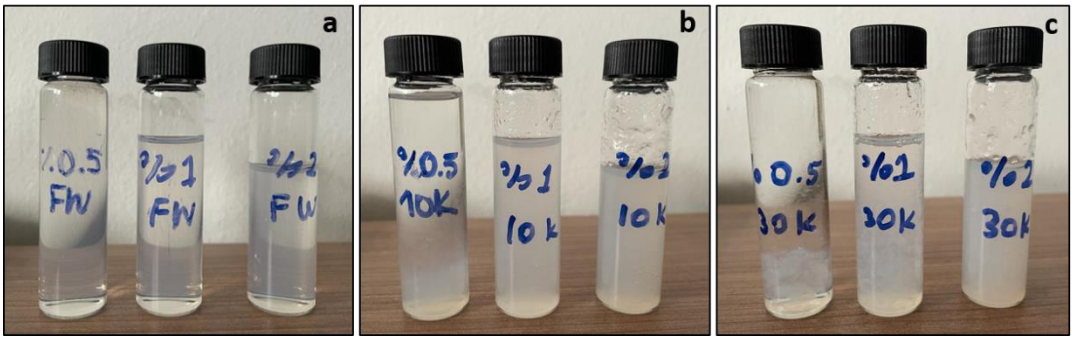

Figure 4.20: Varying concentrations of nanocellulose solution (0.5 wt%, 1 wt% and 2 wt%) for size distribution and zeta potential measurements (a) prepared with fresh water b) prepared with 10,000 ppm NaCl water c) prepared with 30,000 ppm NaCl water

4.5.1 Particle Size Distribution Measurements

Particle size distribution of samples with particles ranging from 0.02 to 2000 μm is obtained by using laser diffraction technique. This method is based on the diffraction of laser through the sample. Particles dispersed in a liquid medium can be used. There are two major light sources: blue and red-light sources. Red laser is used for detecting larger particles, while the blue laser is utilized for measuring smaller particles. Actually, particle size distribution is the transformation of diffraction patterns, which are measured by detectors, based on an optical model.

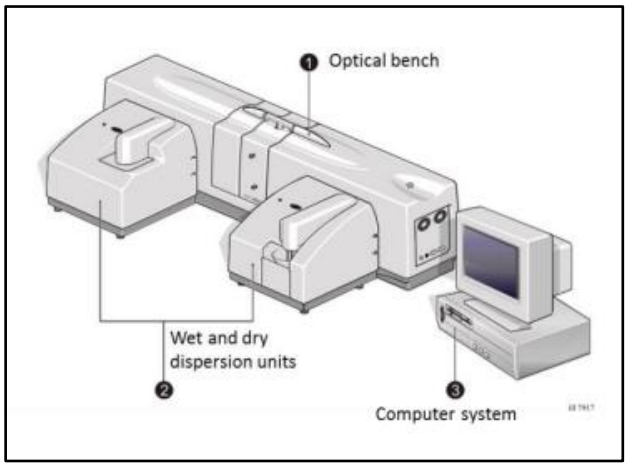

Figure 4.21: Schematic view of Mastersizer2000 (Particle Size and Zeta Potential Measurement Laboratory, Central Laboratory, n.d.)

Zetasizer, specifically Mastersizer2000 (Figure 4.21), was used to analyze the size distribution from 20 nm to 2 µm and zeta potential values of these particles (Figure 4.20). These analyses were conducted by METU Central Laboratory (MERLAB) at room temperature. Results are presented in the figures below (Figure 4.22, Figure 4.23, Figure 4.24, Figure 4.25, Figure 4.26, Figure 4.27, Figure 4.28, Figure 4.29, and Figure 4.30).

Figures include average particle size/diameter (Z-average) and polydispersity index (PDI). Z-average is the intensity weighted mean. The degree of uniformity of a size distribution of particles is defined by using polydispersity term. PDI, also known as heterogeneity index, ranges from 0.0 (representing a perfectly uniform sample in terms of particle size) to 1.0 (representing a polydisperse sample with numerous particle size populations). PDI values higher than 0.7 refer that the sample has a wide particle size distribution, while PDI values lower than 0.05 indicate monodisperse systems (Danaei et al., 2018).

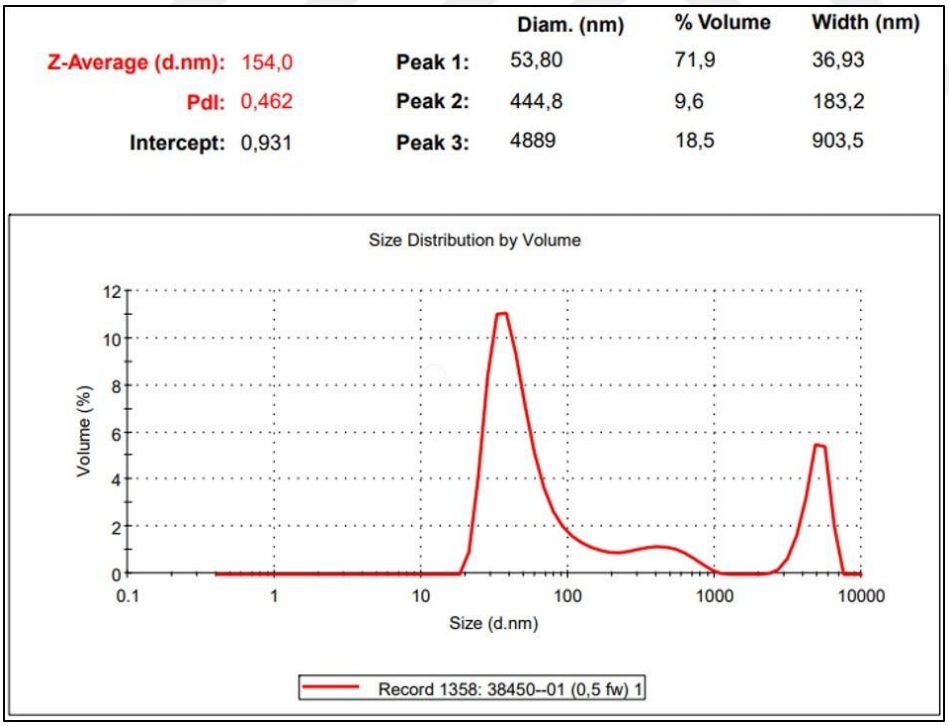

Figure 4.22: Particle size distribution for 0.5 wt% nanocellulose solution prepared by using fresh water

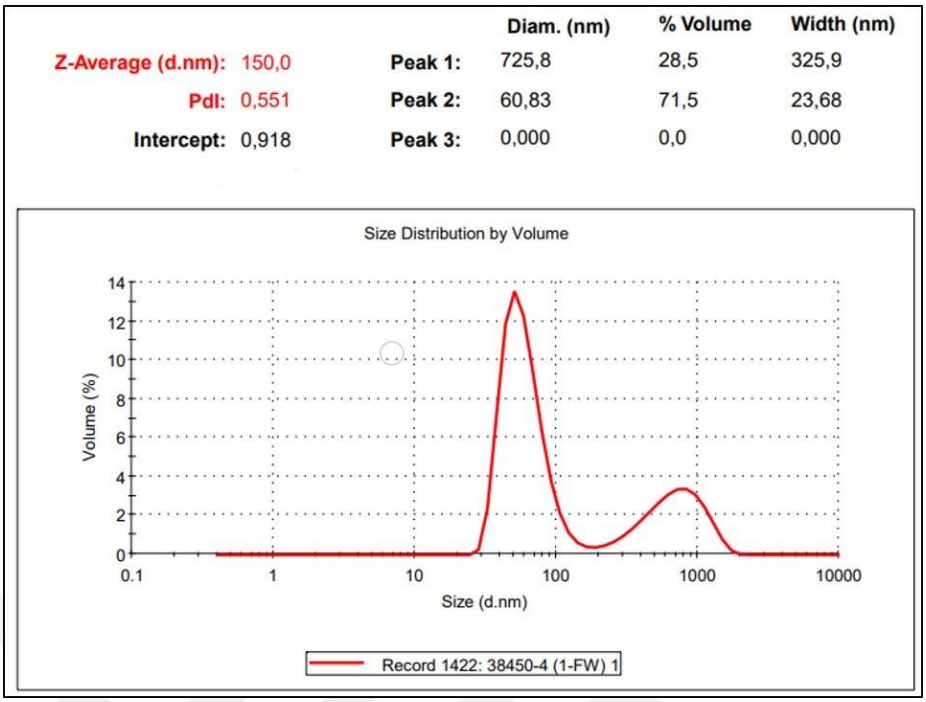

Figure 4.23: Particle size distribution for 1 wt% nanocellulose solution prepared by using fresh water

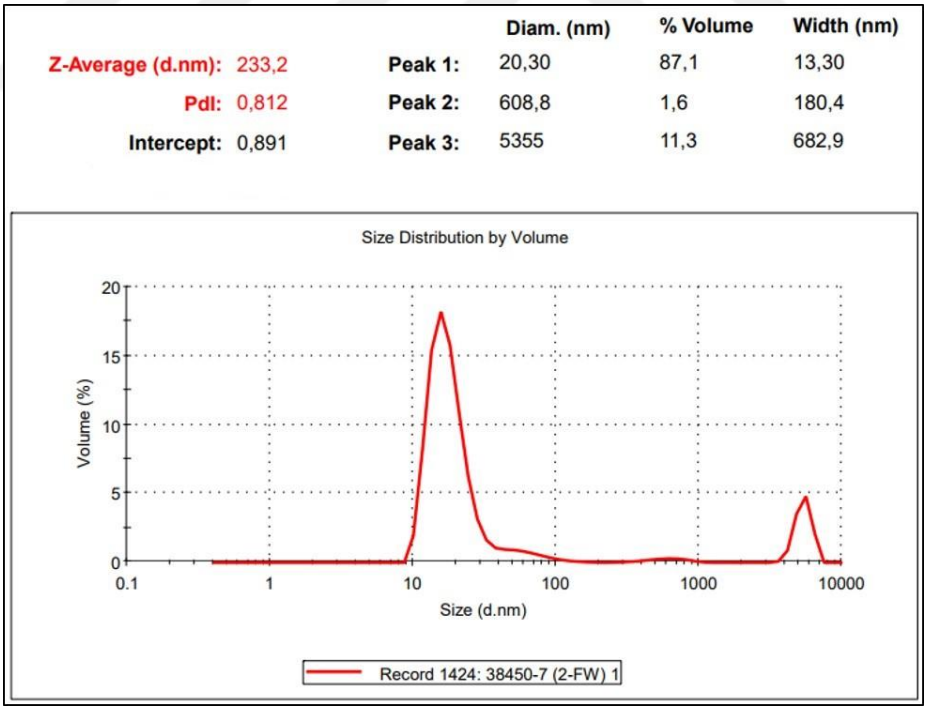

Figure 4.24: Particle size distribution for 2 wt% nanocellulose solution prepared by using fresh water

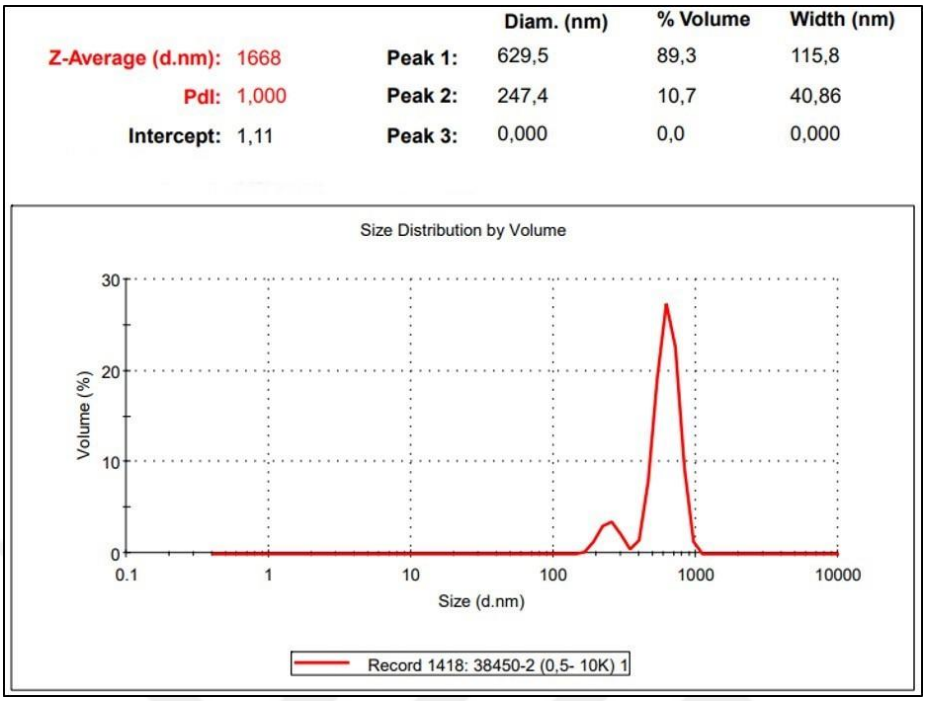

Figure 4.25: Particle size distribution for 0.5 wt% nanocellulose solution prepared by using water with 10,000 ppm NaCl

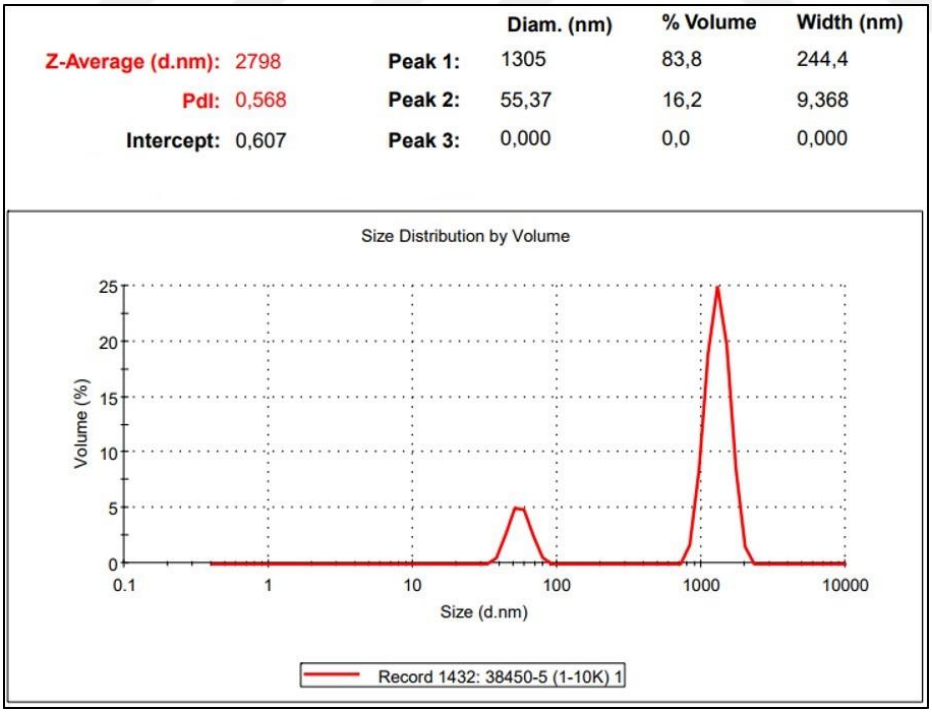

Figure 4.26: Particle size distribution for 1 wt% nanocellulose solution prepared by using water with 10,000 ppm NaCl

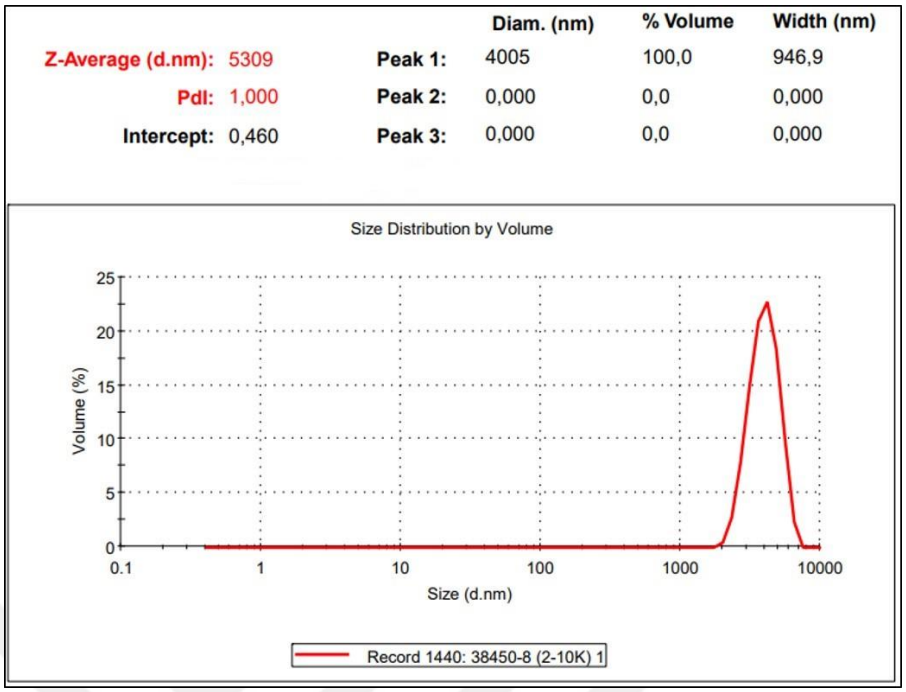

Figure 4.27: Particle size distribution for 2 wt% nanocellulose solution prepared by using water with 10,000 ppm NaCl

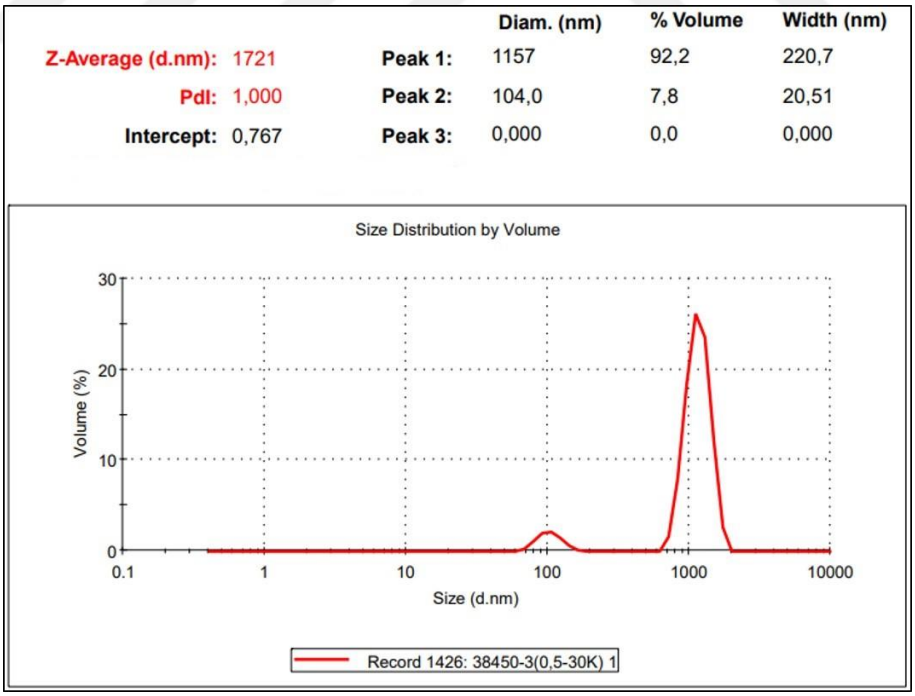

Figure 4.28: Particle size distribution for 0.5 wt% nanocellulose solution prepared by using water with 30,000 ppm NaCl

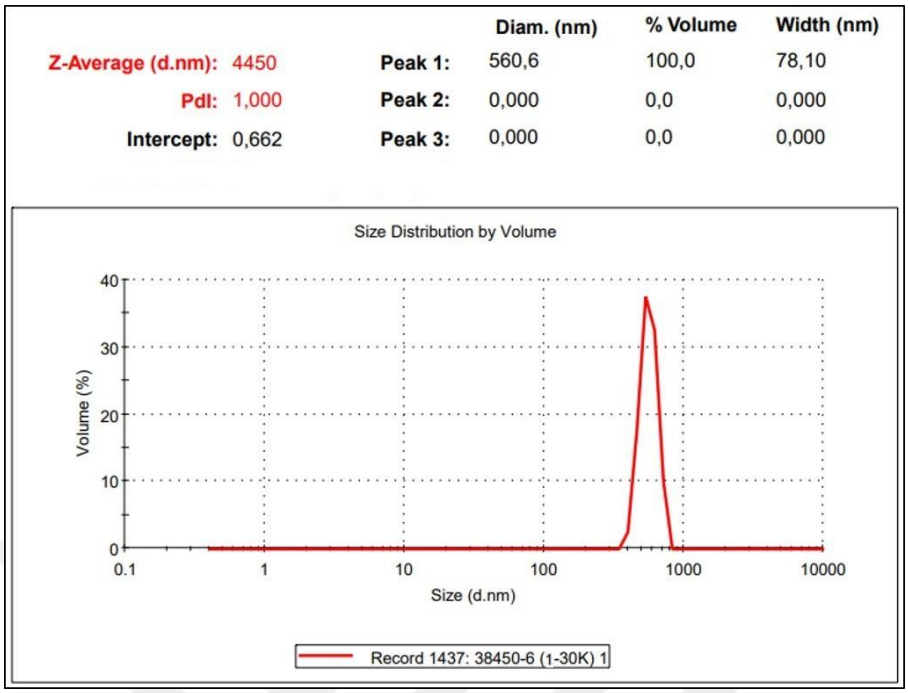

Figure 4.29: Particle size distribution for 1 wt% nanocellulose solution prepared by using water with 30,000 ppm NaCl

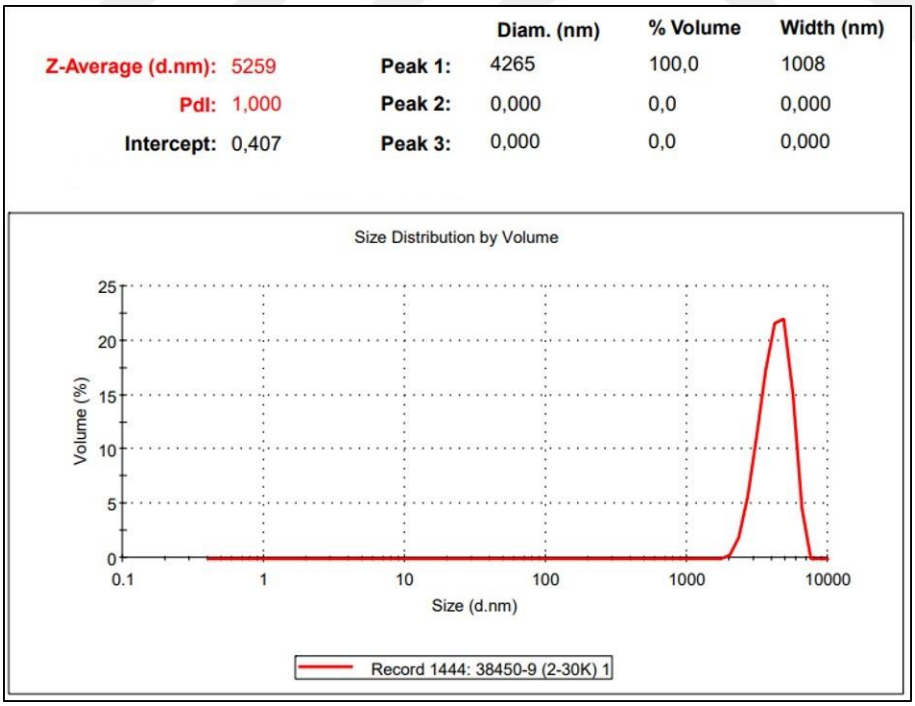

Figure 4.30: Particle size distribution for 2 wt% nanocellulose solution prepared by using water with 30,000 ppm NaCl

The particle size distribution graphs indicate that nanocellulose solutions prepared using fresh water exhibit greater uniformity, as evidenced by the lower Polydispersity Index (PDI) values. However, an increase in nanocellulose concentration has a detrimental impact on this uniformity, resulting in a shift towards heterogeneous solutions. Notably, the 2 wt% nanocellulose solution displays heterogeneity according to PDI values, whereas the 0.5 wt% and 1 wt% nanocellulose solutions maintain uniform solutions.

4.5.2 Zeta Potential Measurements

Zeta potential is a measure of the surface charge of a particle and measured by light scattering methods. Zeta potential is one of the major indicators for stability measurements. Opposite charged ions creates a layer, called as Stern layer, on the surface of nanoparticle. Diffuse layer comprising loosely associated ions, resides on the top of Stern layer as an outer layer. These two layers are called together as electrical double layer. As nanoparticles are placed in a liquid medium, a boundary is created naturally between ions in the bulk dispersant and ions in the diffuse layer (Raval et al., 2019). Electrical potential of this boundary plane is called as Zeta Potential of the particle, ranges from +100 mV to -100 mV.

The magnitude of zeta potential refers to the potential stability of the colloidal system. Higher zeta potential values point to high interparticle repulsion and stable suspension. The lower value of zeta potential is an indicator of a possible unstable suspension due to flocculation, aggregation, agglomeration of the particles. Nanoparticles with zeta potential values greater than +30 mV or smaller than -30 are indicated as stable suspensions with no aggregation. However, nanoparticles with zeta potential values within a range of -30 mV and +30 mV are considered as poor colloidal stability systems and highly likely to face flocculation, agglomeration, or aggregation (Metin et al., 2011).

Zeta potential measurements of aforementioned samples were conducted by METU Central Laboratory (MERLAB) at room temperature. Results are presented in the figures below (Figure 4.31, Figure 4.32, Figure 4.33, Figure 4.34, and Figure 4.35).

Zeta potential distribution curves for the solutions prepared by using water with 10,000 ppm NaCl and 30,000 ppm NaCl are not available due to higher conductivity of these samples (Figure 4.34 and Figure 4.35). Samples with higher conductivity values than the cutoff in the automatic mode are analyzed by Fast Field Reversal technique, which provides only a mean zeta potential, not a distribution. Since there is no zeta distribution, there is no standard deviation of the mean, and it can be detected as 0.00 mV.

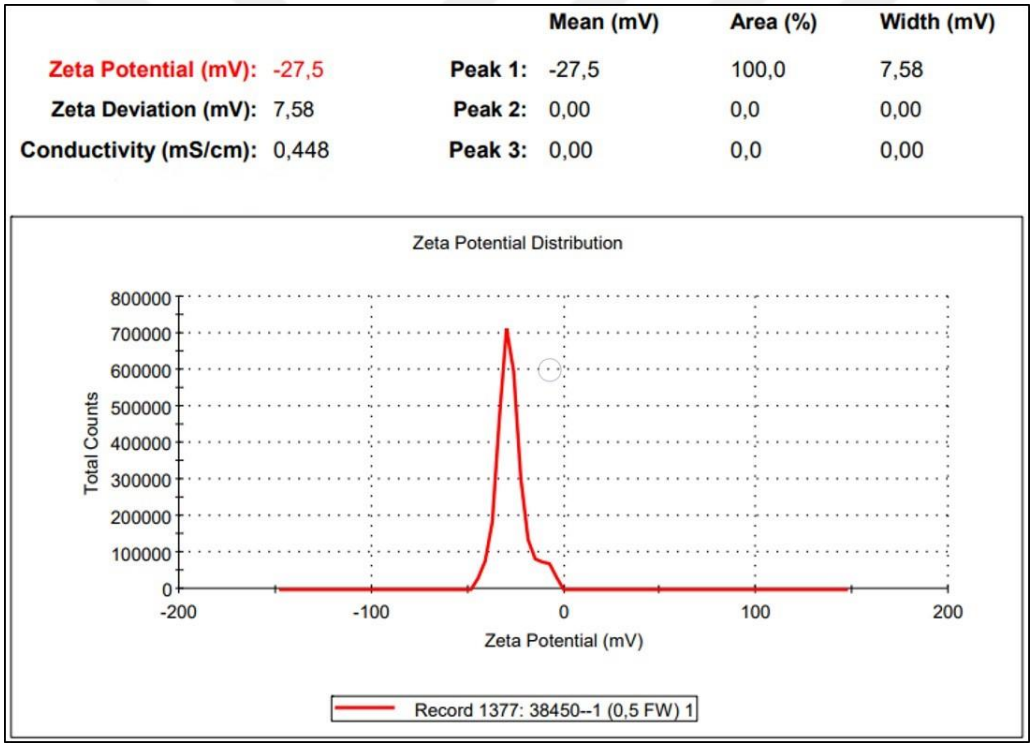

Figure 4.31: Zeta potential of 0.5 wt% nanocellulose solution prepared by using fresh water

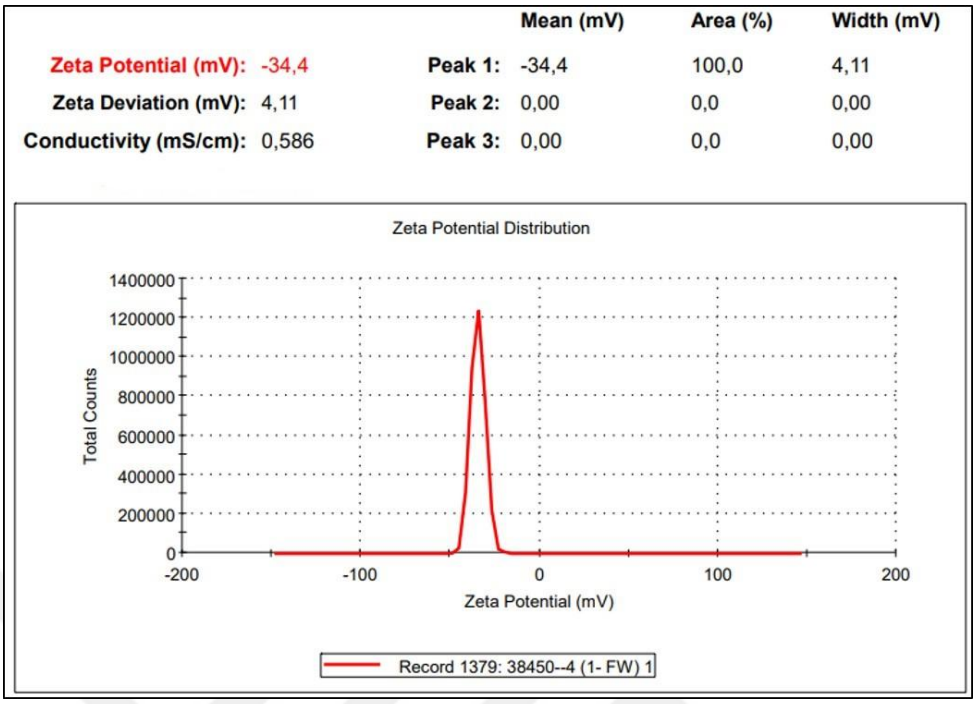

Figure 4.32: Zeta potential of 1 wt% nanocellulose solution prepared by using fresh water

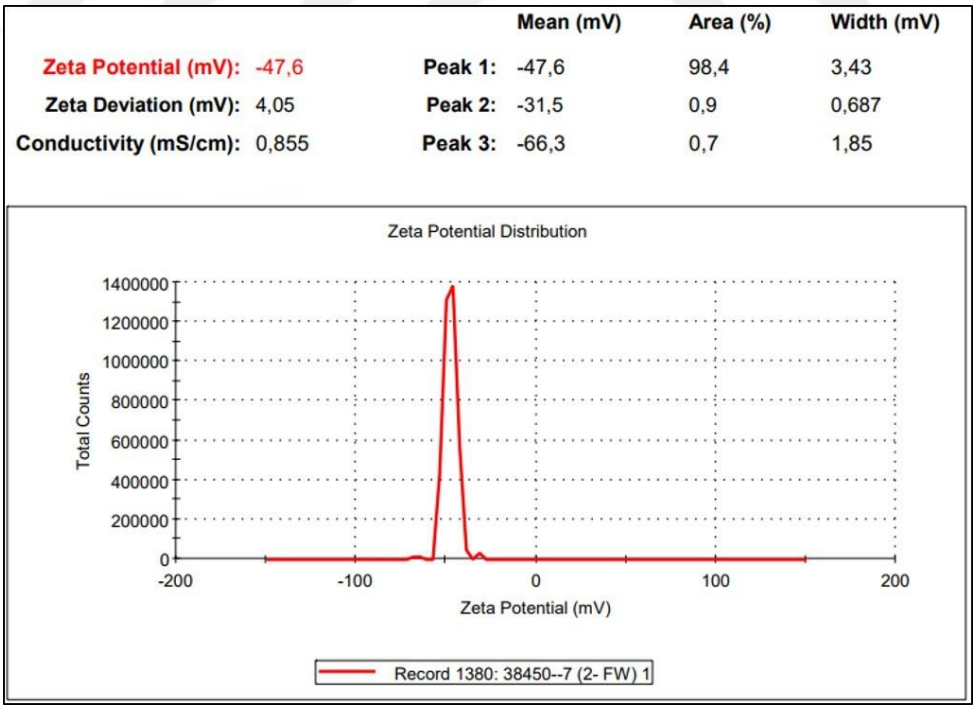

Figure 4.33: Zeta potential of 2 wt% nanocellulose solution prepared by using fresh water

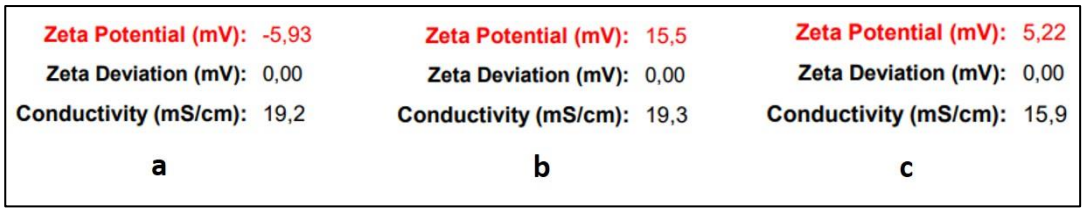

Figure 4.34: Zeta Potentials of solutions prepared by using water with 10,000 ppm NaCl and varying nanocellulose concentrations (a) 0.5 wt% nanocellulose, b) 1 wt% nanocellulose, c) 2 wt% nanocellulose)

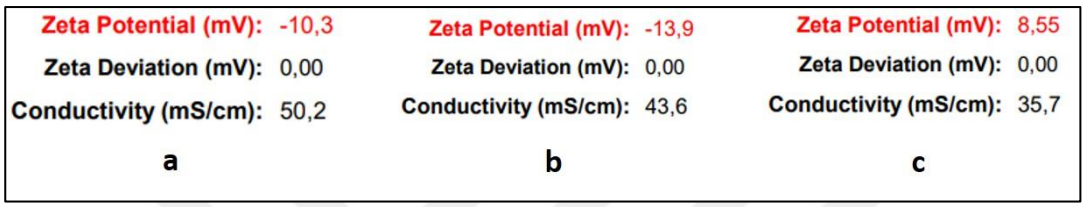

Figure 4.35: Zeta Potentials of solutions prepared by using water with 30,000 ppm NaCl and varying nanocellulose concentrations (a) 0.5 wt% nanocellulose, b) 1 wt% nanocellulose, c) 2 wt% nanocellulose)

According to zeta potential results of the samples, solutions prepared by using fresh water are more stable than the solutions prepared by using higher salinity water. It can be concluded that as the salinity of the water used in nanocellulose dispersion increases, the tendency to flocculation, agglomeration, or aggregation increases resulting in unstable solutions.

4.6 Interfacial Tension (IFT) Measurements

Interfacial tension is the force of attraction between the molecules at the interface of two immiscible fluids. Rock samples typically have complex pore structures of various pore sizes and shapes. When crude oil is present in the rock's pore space, an interface formed between the oil and the solid surfaces of the rock. The interfacial tension between the rock and crude oil determines the ability of the oil to flow through the rock's pores.

If the interfacial tension between the rock and crude oil is low, the two phases have a strong attraction or affinity for each other. This low interfacial tension allows the

oil to easily spread and flow through the rock's pores, resulting in better oil recovery during extraction processes. On the other hand, if the interfacial tension between the rock and crude oil is high, it indicates a weaker attraction between the two phases.

IFT test was performed with Vinci IFT700 system shown in Figure 4.36. In addition to contact angle between liquid-gas or liquid-liquid and solid system, test system is capable of providing surface tension and interfacial tension using the pendant drop method. It involves the formation of a pendant droplet of one liquid suspended from a capillary tube (needle), immersed in another liquid. A drop is produced from the capillary needle in a bulk fluid at reservoir conditions (up to 10,000 psi pressure and 175 °C). The complete shape of that drop is monitored with a high-resolution video lens system and analyzed with an advanced software. API gravity of oil used in the test was 36.

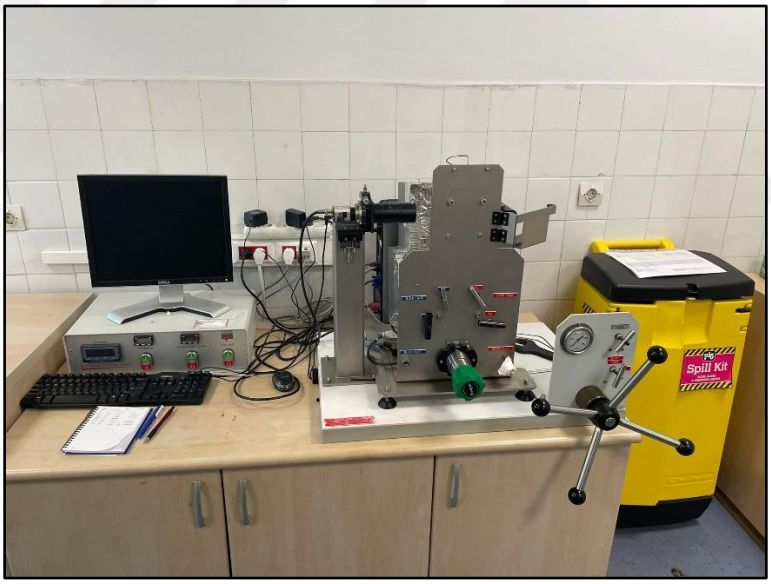

Figure 4.36: IFT test system

The tests were specifically designed to investigate the impact of nanocellulose concentration by conducting measurements at two different concentrations, namely 1 wt% and 2 wt%, at a temperature of 65 °C. However, it was observed that the test cell containing nanocellulose appeared blurry at this elevated temperature. Despite this issue, an oil droplet was introduced into the 1 wt% nanocellulose solution. It was

successfully captured on the tip of the needle in a well-defined shape, as shown in Figure 4.37. Unfortunately, it was not possible to generate an interfacial tension value due to the blurred appearance of the nanocellulose dispersion caused by image contrast difficulties arising from the high temperature conditions.

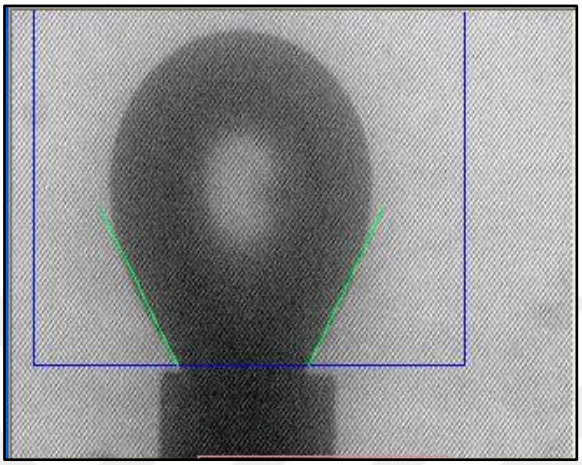

Figure 4.37: Oil droplet on the tip of the needle inside 1 wt% nanocellulose solution

Upon dismantling the system, the nanocellulose was observed to be in a gel-like form, as depicted in Figure 4.38. The higher temperature conditions likely induced this gel-like state, causing the nanocellulose to become more viscous and resulting in a blurred appearance. This change in physical properties made it challenging to carry out the intended measurements successfully. The gel-like nature of the nanocellulose at elevated temperatures contributed to the difficulty in accurately assessing and characterizing its behavior in the system.

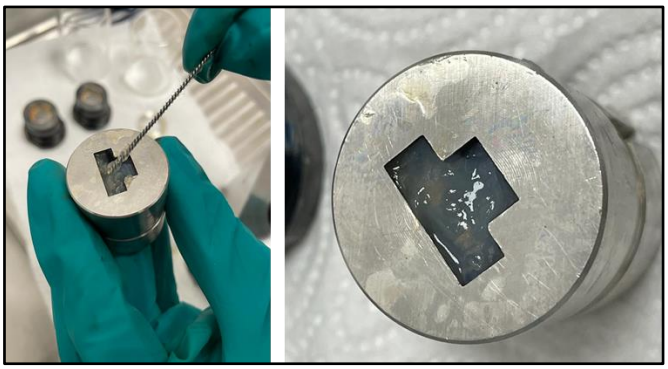

Figure 4.38: Nanocellulose within the system after dismantling

4.7 Wettability Study

Wettability is crucial for the optimization of oil recovery. It is the tendency of a solid to contact a particular fluid rather than another in the presence of a multiphase or two-phase fluid system. This tendency is explained by the balance of surface and interfacial forces. In reservoir rock system, it can be considered as the preference of reservoir rock to be covered with water, oil or gas. In other words, if the rock prefers to contact with water, it is called as water-wet reservoir rock. An oil-wet reservoir will favorably contact oil.

The degree of wettability of a reservoir rock (either water-wet or oil-wet) is mostly affected by adsorption of oil phase, mineralogy of the rock itself, and spreading capability of the oleic phase. Reservoir rock wettability is measured by contact angle, which is the angle between fluid-solid interface in a single fluid phase system. In a multifluid system, in the presence of two immiscible fluids, like oil and water, the contact angle is considered as angle measured through water. If contact angle is smaller than 90°, reservoir rock is defined as water-wet. The case of contact angle greater than 90° refers to an oil-wet system (Abdallah et al., 2007; Agbalaka et al.,2008).

Wettability studies played a vital role in understanding the interaction between nanocellulose and reservoir rock surfaces. Nanocellulose's ability to alter the wettability of the rock surface from oil-wet to water-wet was investigated, as this transformation is crucial for enhancing oil recovery by improving water imbibition and displacing oil.

This study aims to understand the effect of nanocellulose on wettability as an enhanced oil recovery agent. In this study, the wettability effect of nanocellulose was investigated with a basic test. The end trim of carbonate plug sample used in the core flooding experiments was used for this purpose.

The plug end trim was placed in a closed glass bottle filled with oil. It was left for aging in the oil at a temperature of 65 °C for four weeks to restore wettability with

the original one to represent reservoir rock. The oil used in the test was the same as the one used in enhanced oil recovery tests.

Then, the plug end trim was taken from the bottle and placed in another closed glass bottle filled with formation water. It was left in the formation water at a temperature of 65 °C for ten days (Figure 4.39).

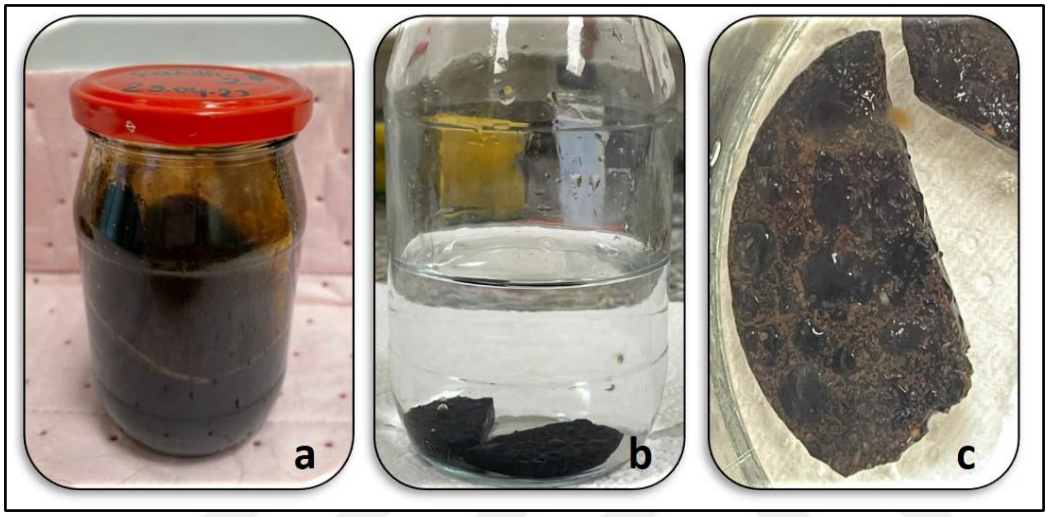

Figure 4.39: Wettability restoration process of plug end trim (a) aging in the oil, b) placing plug end trim in formation water, c) plug end trim after taken from formation water)

The release of oil droplets from the end trim was observed and photographed as seen in Figure 4.40. It can be seen from the figure that oil is highly spread on the plug end trim. As wettability is the tendency of a fluid to spread on a rock surface in the presence of another immiscible fluid, it can be inferred that the rock is strongly oil-wet with a contact angle greater than 90°.

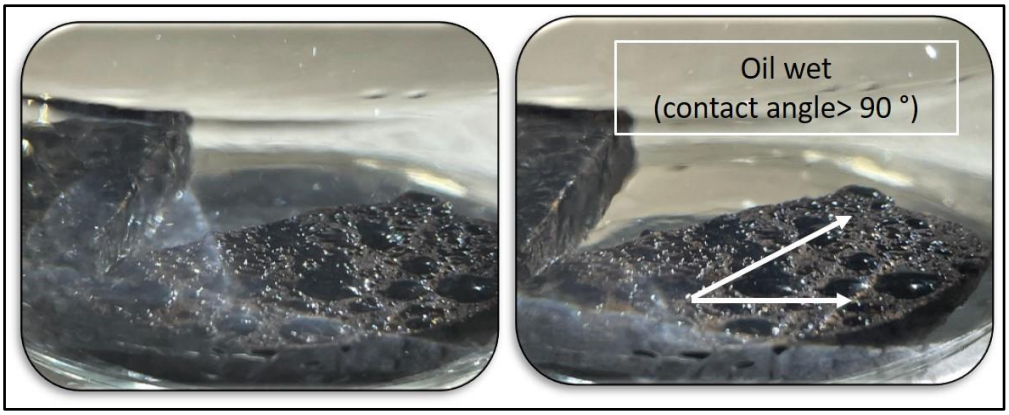

Figure 4.40: Contact angle before nanocellulose soaking, original wettability condition of the rock

Next, the same plug end trim was put into a closed glass bottle filled with 1 wt% nanocellulose solution prepared by using fresh water. It was left in the bottle with a temperature of 65 °C for three days.

Then, the plug end trim was taken from the bottle and placed in another closed glass bottle filled with formation water. It was left in the formation water at a temperature of 65 °C for ten days (Figure 4.41).

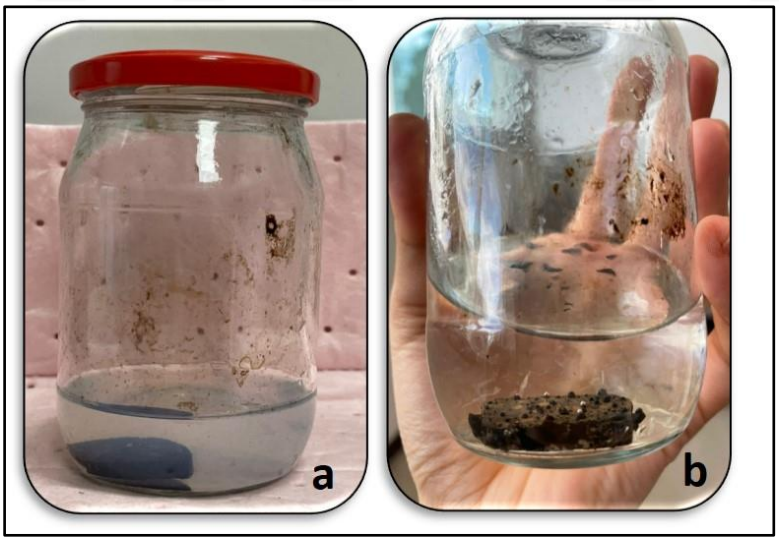

Figure 4.41: Testing effect of nanocellulose on the wettability of plug end trim (a) aging in the 1 wt% nanocellulose solution prepared with fresh water, b) placing plug end trim in formation water)

The release of oil droplets from the end trim was observed and photographed as seen in Figure 4.42. It is very clear that the oil droplets on the surface of plug end trim has a less tendency to spread with narrower shape. It can be obviously seen from the figure that oil is highly spread on the plug end trim. It can be defined that the rock is less oil-wet with a contact angle still greater than 90°, but closer to 90° when compared to the conditions before nanocellulose aging application.

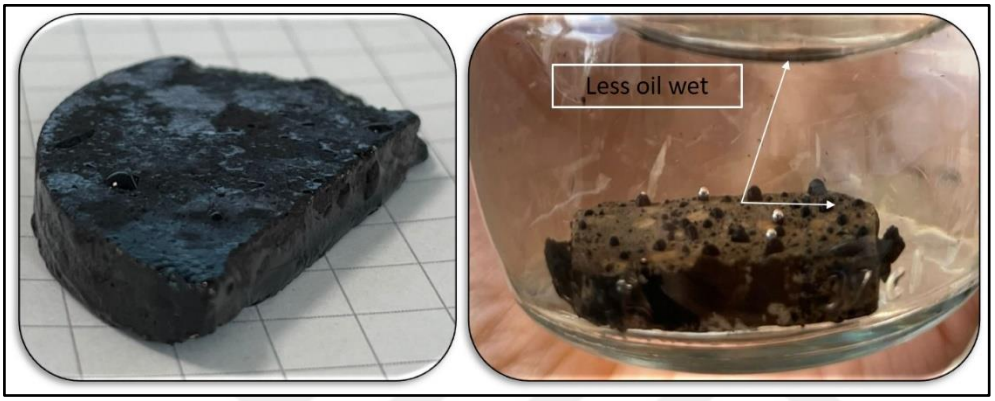

Figure 4.42: Contact angle after aging with 1 wt% nanocellulose

It can be concluded such that nanocellulose has a wettability alteration effect by shifting wettability mechanism to a less oil wet when compared to original wettability conditions. This wettability alteration tendency of nanocellulose might be a major explanation of the additional oil recovery mechanism of nanocellulose in the core flooding tests.

4.8 Contact Angle Measurements

Contact angle refers to the point where the interface of oil and water meets the surface of a rock. It is a useful tool for assessing changes in surface wettability, as it quantifies the shift in affinity of the rock surface from one fluid to another in a continuous manner.

Various methods have been developed to measure contact angle, with the sessile drop method being the most widely utilized in the petroleum industry. In this method, the flat surface of the rock sample, which is aged in the oil under reservoir

temperature, is horizontally suspended in water or another fluid, and a drop of oil is placed at the bottom of the rock sample. A photograph is taken to measure the contact angle accurately. In this system, a contact angle between 0° and 60°-75° is considered water-wet, while a contact angle between 180° and 105°-120° indicates an oil-wet system. A contact angle between 75° and 105° is classified as neutral-wet (Anderson, 1986).

Contact angle measurements further complemented the wettability studies by quantifying the contact angle between nanocellulose solutions and the rock surface. These measurements provided essential data on the surface energy and wettability alteration mechanisms induced by nanocellulose. In this study, the contact angles of the rock sample within synthetic formation water and 1 wt% nanocellulose were measured using the sessile drop method as described.

The core plug sample was trimmed into thin sections measuring approximately 2 mm. These sections were then meticulously polished to achieve a completely smooth surface. To eliminate any potential surface impurities, the prepared thin sections underwent a cleaning process using toluene and distilled water. Following the procedures outlined by Villard et al. (1993) and Manshad et al. (2017), the polished rock pieces with flat surfaces were aged with crude oil to achieve an oil-wet reservoir rock sample. During this step, thin section was fully immersed in the crude oil, whose API gravity was 36, for a duration of three weeks at atmospheric pressure and reservoir temperature (65 °C). After aging in the crude oil, the polished rock piece was exposed to formation brine (20,000 ppm NaCl synthetic brine solution) to test surface wettability. Oil droplet was sent to the rock piece's surface, which was immersed in synthetic formation brine. Contact angle measurements indicated an oil-wet rock (oil still adhered to the surface), as shown Figure 4.43.

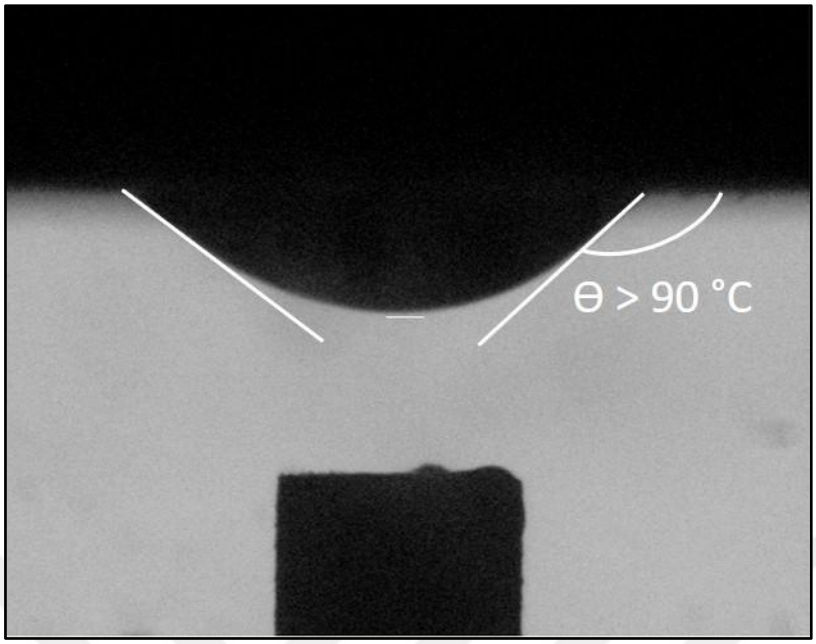

Figure 4.43: Contact angle measurement with 20,000 ppm NaCl synthetic brine solution (representing before treatment with nanocellulose)

In order to see the effect of nanocellulose, another thin section went through the same stages as in the initial scenario. Then, it was immersed in a solution containing 1 wt% nanocellulose, aiming to examine how nanocellulose affects changes in wettability. During this stage, aging took place at 65 °C for three days. Subsequently, a drop of oil with an API gravity of 36 was injected onto the rock surface in 1 wt% nanocellulose solution using a syringe needle, and the second and final contact angles were measured (Figure 4.44). The wettability of the carbonate core was qualitatively assessed by determining the contact angle of crude oil droplets on the surface of the prepared thin section at room temperature, both before and after the treatment with 1 wt% nanocellulose, which are 135.1° and 67.3°, respectively.

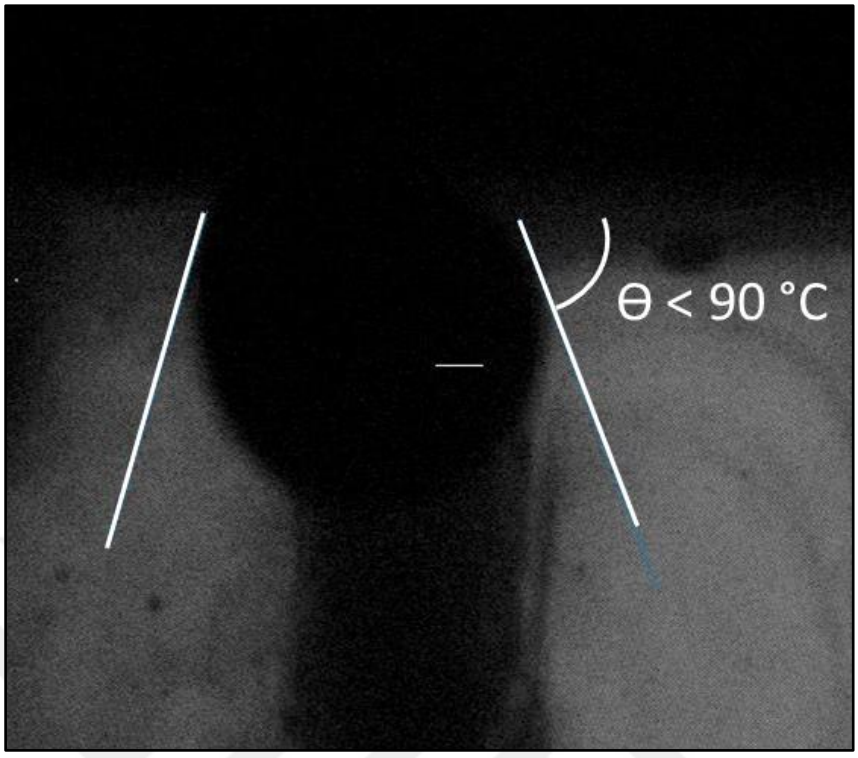

Figure 4.44: Contact angle measurement with 1 wt% nanocellulose solution (representing after treatment with nanocellulose)

Illustrated in Figure 4.43, the rock surface demonstrated a distinctly oil-wet state (contact angle > 90) after undergoing the aging process with crude oil. Figure 4.44 provides clear evidence that treatment with 1 wt% nanocellulose resulted in a significant decrease in the contact angle of the oil droplet on the surfaces compared to the initial state. This suggests a transition in surface wettability, changing from an oil-wet condition to an intermediate or water-wet state.

The contact angle serves as a quantitative technique for assessing how a surface interacts with various phases when multiple phases are present. As reported by Sagala et al. in 2020, an increase in nanofluid concentration corresponds to an increase in the contact angle, signifying a transition in core wettability from intermediate to a more strongly water-wetting state. It is worth noting that although higher concentrations lead to a greater degree of water-wettability, surpassing the optimal concentration may not necessarily result in higher oil recovery. Excessive concentrations can cause nanoparticles to form clusters or aggregates that may block

reservoir pores and hinder fluid flow. Hence, maintaining an optimal concentration is crucial for effective enhanced oil recovery (EOR) applications (Lu et al., 2017).

CHAPTER 5

COREFLOOD OIL ERCOVERY TESTS

Within the scope of this research, flow tests were conducted under reservoir conditions with core plug samples to test the efficiency of nanocellulose dispersion as an enhanced oil recovery agent. Materials and method, experimental set up and procedure are explained in detail in this chapter.

5.1 Material and Methods

5.1.1 Nanocellulose Suspension

Two different forms of nanocellulose were supplied by the chemical company: powder and dispersion forms. Aqueous suspension of cellulose nanocrystals (CNC) was used in all flow tests within the scope of this study. The basic properties of nanocellulose used in all oil recovery tests is given in Table 5.1.

Table 5.1: Properties of nanocellulose dispersion

Concentration (wt%)	Bulk Density (g/cm3)	Particle Diameter (crystallite) (nm)	pH
6% wt	0.68	2.4 - 4.6	6-7

6 wt% nanocellulose dispersion was diluted to the required specific concentration using tap water. Nanocellulose dispersion was directly put in the water and stirred with a magnetic stirrer at high speed for 15 min to obtain a homogenous diluted solution. Obtained diluted solution was put into a sonic bath for an hour, which is demonstrated in Figure 5.1.

Figure 5.1: Preparation of diluted nanocellulose (stirrer on the left, sonic bath on the right)

It is vital to follow all the Health and Safety (HSE) procedures while working with nanoparticles. Due to their particle size, inhaling and contacting this type of materials with the skin might cause damage to the lungs and skin. Therefore, disposable lab coats, two-layer lab gloves, and appropriate lab masks and glasses were used during the dilution process of nanocellulose.

5.1.2 Synthetic Formation Water

Synthetic formation water was prepared by using NaCl and deionized water for each coreflood test by mixing appropriate proportions to reach the designed salinity value. Synthetic water sample was used at saturating core plug samples and water flooding stages. Each synthetic brine sample was filtered with the millipore vacuum filter. The main properties of synthetic water used in coreflood tests are given in Table 5.2.

Table 5.2: Properties of synthetic water sample used in the coreflood tests

Density at 65 °C (g/cm^3)	Dynamic Viscosity at 65 °C (cP)	Total Salinity (NaCl) (ppm)
0.995	0.45	20,000

5.1.3 Dead Oil

Crude oil samples from three different Southeastern Turkish oil reservoirs were used in the coreflood tests. Properties of oil samples are listed in Table 5.3.

Table 5.3: Properties of oil samples used in the coreflood tests

Oil Name	API Gravity	Density at 65 °C (g/cm^3)	Dynamic Viscosity at 65 °C (cP)
R	16	0.928	202.4
C	22	0.877	14.9
S	36	0.810	2.3

5.1.3.1 SARA Analysis

SARA analysis method is used to categorize the components of crude oil based on their polarizability and polarity. It divides them into four fractions: saturates, aromatics, resins, and asphaltenes. The saturate fraction comprises nonpolar substances. Aromatics, which contain one or more aromatic rings, exhibit slightly higher polarizability. The remaining two fractions, resins and asphaltenes, contain polar substituents. The analysis is typically conducted using various separation techniques, such as column chromatography or solvent extraction, followed by quantification of the different fractions (Fan and Buckley, 2002).

SARA analysis of each oil sample was conducted and SARA fractions are listed in Table 5.4.

Table 5.4: SARA fractions of oil samples

Oil Name	Asphaltenes (%)	Saturates (%)	Aromatics (%)	Resins (%)
R	18.3	23.3	53.1	5.3
C	18.7	24.6	49.8	6.9
S	1.2	44.1	52.1	2.6

5.1.3.2 Gas Chromatography (GC) Analysis

Additionally, the results of the high-resolution gas chromatographic (GC) analysis of the three crude oil samples is presented in Table 5.5.

Table 5.5: GC analysis results of oil samples used in coreflood tests

Components	Mole %		
	Oil-R	Oil-C	Oil-S
N_2	0.0	0.0	0.0
CO_2	0.0	0.0	0.0
C_1	0.0	0.0	0.0
C_2	0.0	0.0	0.0
C_3	0.0	0.5	0.7
iC_4	0.0	0.2	1.6
nC_4	0.0	0.8	1.9
iC_5	0.0	1.2	0.0
nC_5	0.0	0.0	0.0
nC_6	0.2	0.3	1.3
nC_7	4.6	7.1	4.4
C_8	5.6	4.7	8.5
C_9	6.8	4.3	16.9
C_{10}	7.4	3.6	13.6
C_{11}	5.1	2.3	8.8
C_{12}	4.3	3.0	9.4
C_{13}	2.0	1.0	7.7
C_{14}	1.2	0.8	4.3
C_{15+}	62.8	70.3	20.9

5.2 Rock Sample Properties and Preparation of Coreflood Tests

Core plug samples taken from carbonate cores from the same reservoir formation were used in all coreflood experiments. This chapter will present the basic petrophysical properties of each core plug sample.

5.2.1 Core Plug Cleaning

First of all, plug samples were cleaned by extraction with hot toluene in Soxhlet extractors. Soxhlet extraction is designed for removal of hydrocarbons and water from core samples. The Soxhlet thimble is placed in a siphon tube and the system is placed on a heating mantle. The bottom flask is filled with the appropriate solvent, which is toluene in our case. As far as the toluene comes to its boiling point (110°C), it evaporates and travels up to the condenser, which is continuously circulated with cold water. When the toluene reaches the condenser, it condenses and gets through the plug samples. The hot toluene diffuses into the pores of core samples and removes hydrocarbons. Evaporation of water from core plug samples takes places when the temperature of toluene is circa 100°C or more. Toluene and oil (removed from the pores) siphon as they reach the reflux point. The cycle of heating flask, contains oil-toluene mixture, fresh toluene vapor production, condensation and extraction oil from the pores is repeated continually for many times until no further discoloration of solvent occurs.

Figure 5.2: Soxhlet extraction (left), temperature-controlled oven (right)

The core plugs may contain salts from formation water, some residual water, and some heavier components of residual oil by the end of Soxhlet extraction with toluene stage. Thus, the core plug samples were placed in methyl alcohol in a vacuum oven to eliminate the remaining contaminants. The cleaned core plugs samples were dried in a temperature-controlled oven at 70°C as part of the cleaning process.

Finally, the weight, diameter and length of the dried cylindrical core plug samples were measured and recorded to be used for routine core analyses calculations.

5.2.2 Routine Core Analyses

5.2.2.1 Porosity Measurement

Porosity measurements of core plug samples were conducted using a helium gas expansion porosimeter (Figure 5.3) based on Boyle's Law. Each plug sample was individually placed within the matrix cup connected to the porosimeter. If the core plug sample was too short, the matrix cup was filled with known bulk volume billets. Helium, maintained at a known pressure of 100 psig from a reference cell with a known volume, was introduced isothermally into the matrix cup. This allowed for the expansion of helium into the available pore spaces within the core plug sample, determining the grain volume utilized for calculating grain density and pore volume, ultimately resulting in the determination of the core plug sample's porosity. The shape of plug sample (a perfect cylinder) is vital for pore volume measurement. Therefore, helium porosimeter method does not provide very accurate results for plugs with irregular shapes or with vugs on their surfaces.

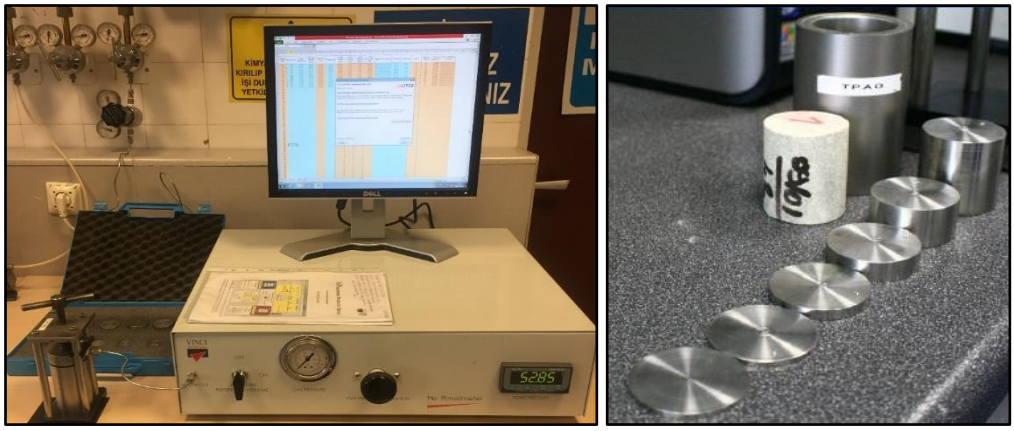

Figure 5.3: Helium porosimeter test system

5.2.2.2 Permeability Measurement

Permeability measurements were performed on the core plugs, which were placed within a Hassler-type core holder and confined under a pressure of 300 psig. The use of a steady-state gas permeameter (Figure 5.4) allows for precise determination of gas permeability in core-sized samples at room temperature and moderate confining pressures, employing the steady-state method. This method involves maintaining a constant flow rate across the sample.

Figure 5.4: Air permeameter test system

The constant flow rate of dry air passing through the core sample is observed, and the differential pressure across the plug sample is read from pressure gauge. These measurements, in conjunction with the core sample's length and cross-sectional area, are employed to compute air permeability by applying "Darcy's Law" for three different mean pressures, under the condition that the air flow is laminar. Finally, Klinkenberg permeability (kL) is calculated by plotting measured air permeability (k_{air}) vs. mean pressure applied. The porosity and permeability results are listed in Table 5.6 and Figure 5.5 displays the permeability-porosity relationships for selected plug samples, based on data obtained from Routine Core Analysis (RCA).

Table 5.6: Routine core analysis results

Plug Name	Length (mm)	Diameter (mm)	Pore Volume (cc)	Porosity (%)	kair (md)	kL (md)	Grain Density (g/cc)
210	69.75	37.67	20.3	26.1	218.7	198.7	2.70
211	71.3	37.67	21.8	27.1	211.7	191.7	2.70
347	65.9	37.7	13.5	18.2	55.6	49.0	2.69
346	65.8	37.7	14.1	19.3	101.4	80.0	2.69
213	70.65	37.6	18.8	24.0	136.1	124.2	2.70
207	65.38	37.31	19.3	26.9	244.5	224.5	2.69
209	68.67	37.8	22.7	29.0	151.7	139.4	2.70

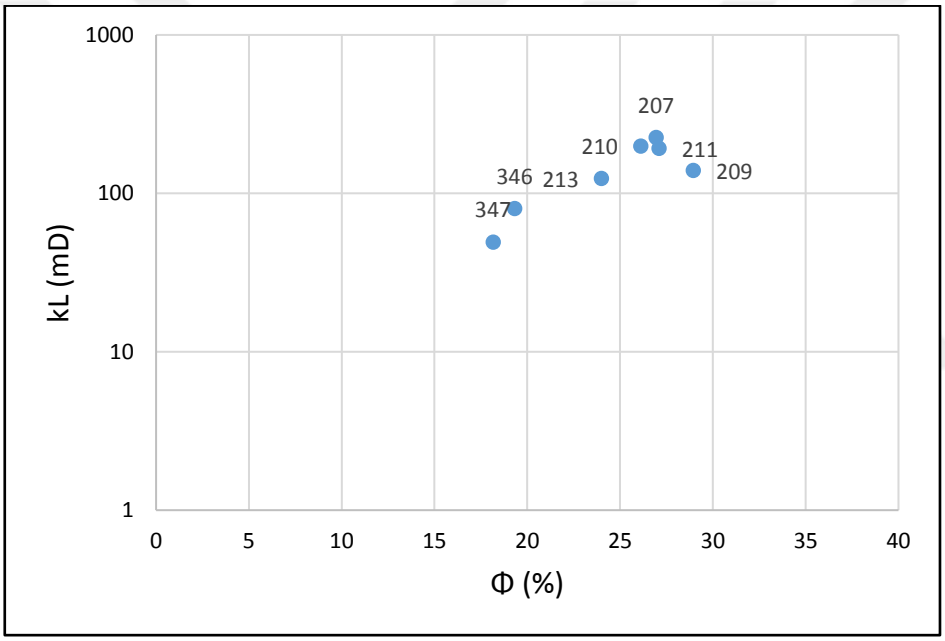

Figure 5.5: Porosity-permeability x-plot for core plug samples

5.2.2.3 Reservoir Quality Index (RQI) and Flow Zone Indicator (FZI) Calculations

Carbonate reservoirs are characterized by their heterogeneity, resulting from sedimentary deposition and diagenetic processes occurring after deposition. The characterization of carbonate rock reservoirs is essential in comprehending their storage and flow capacities (Martin et al., 1997).

A practical approach involves dividing the reservoir into different hydraulic flow units, which allows for effective reservoir zonation based on distinct petrophysical characteristics like porosity, permeability, pore throat, and cementation exponent. To achieve this, a sound methodology is proposed to identify and characterize hydraulic units within mappable geological units or facies for classification and differentiation of each zone. Flow unit evaluation is carried out using the flow zone indicator (FZI) and reservoir quality index (RQI) calculations (Martin et al., 1997).

The technique relies on a modified Kozeny-Carmen equation and the concept of mean hydraulic radius, which are represented as FZI (Amaefule et al., 1993; Orodu et al., 2009). The functions for RQI and FZI are as follows:

$$RQI = 0.0314\ x\ \sqrt{\frac{k}{\phi}} \qquad (1)$$

$$\phi_z = \frac{\phi}{1-\phi} \qquad (2)$$

$$FZI = \frac{RQI}{\phi_z} \qquad (3)$$

The parameter $\emptyset z$ represents the ratio of pore volume to grain volume, providing valuable information about the porosity of the reservoir. In a reservoir, different flow units exhibit distinct FZI values, reflecting the distribution of pore space geometry. By correlating the Reservoir Quality Index (RQI) and $\emptyset z$, geoscientists and reservoir engineers can gain comprehensive insights into the reservoir's heterogeneity and performance potential. Thus, in this study, FZI and RQI values were calculated using equations (1), (2), and (3) to assess the heterogeneity of plug samples. The calculated results of FZI and RQI values are presented in Table 5.7.

Table 5.7: RQI and RZI values for plug samples used in coreflood tests

Plug No	Porosity (%)	ka (md)	kL (md)	Grain Density (g/cc)	RQI (µm)	FZI (µm)
210	26.1	218.7	198.7	2.70	0.87	2.45
211	27.1	211.7	191.7	2.70	0.84	2.25
347	18.2	55.6	49.0	2.69	0.52	2.32
346	19.3	101.4	80.0	2.69	0.64	2.67
213	24.0	136.1	124.2	2.70	0.71	2.26
207	26.9	244.5	224.5	2.69	0.91	2.46
209	29.0	151.7	139.4	2.70	0.69	1.69

On a log-log plot of RQI versus normalized porosity (Figure 5.6), core samples with similar hydraulic characteristics and petrophysical properties will exhibit a unit slope straight line. This relationship allows for the identification of reservoir flow units that share common characteristics. The intercept of the unit slope with the y-axis, where the normalized porosity equals one, defines the FZI for that particular group of samples.

The graph in Figure 5.6 reveals that the plug samples exhibit a similar distribution of RQI values, indicating a degree of homogeneity among them. The concentration of data points within this limited range of FZI values indicates a high degree of similarity in hydraulic characteristics and petrophysical properties across the majority of the reservoir samples. Furthermore, the samples appear to align along the same FZI line, which suggests a potential similarity in reservoir characteristics and behavior. These findings provide valuable information about the reservoir's internal consistency and the potential for uniform oil recovery within the studied area. Understanding the heterogeneity of the plug samples based on FZI and RQI values is crucial for optimizing enhanced oil recovery strategies and maximizing hydrocarbon production from the reservoir. Plug samples #346 and #209 could be considered as potential outliers within the data set according to Figure 5.6.

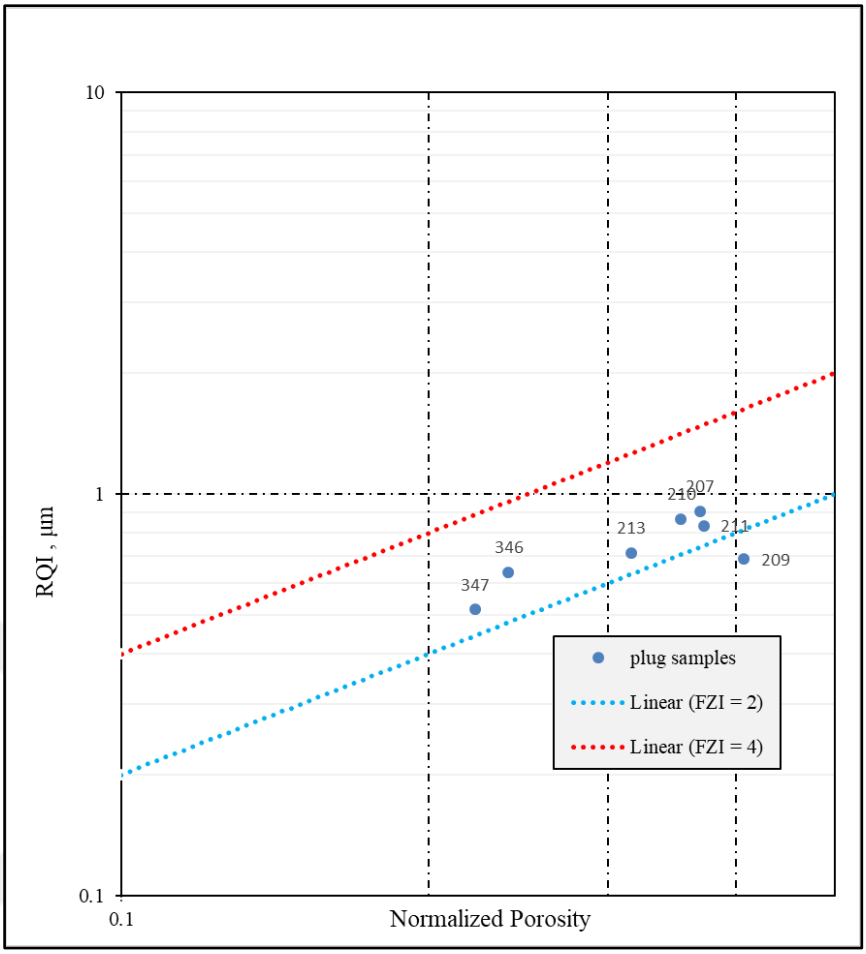

Figure 5.6: RQI vs normalized porosity for the plug samples used in coreflood tests

5.2.3 Mercury Injection Capillary Pressure (MICP) Analysis

Mercury injection capillary pressure (MICP) analysis is a method used to measure pore throat size in rocks. The process involves injecting mercury into a sample under controlled pressure. As the pressure increases, the mercury fills the larger pores and eventually enters the narrowest part of the pore network, typically the pore throats, the narrowest constrictions connecting adjacent pores. The pressure required to inject mercury into these small pore throats is recorded. By analyzing the pressure data, the size distribution of the pore throats within the sample can be determined. The capillary pressure curve obtained from the MICP analysis provides information

about the connectivity and geometry of the pore network, as well as the range of pore throat sizes present (Purcell, 1949; Swanson, 1981).

Understanding the pore throat size is crucial in reservoir characterization because it directly influences the flow of fluids through the rock. Pore throat size affects fluid flow rates, permeability, and the efficiency of hydrocarbon recovery from reservoirs.

Figure 5.7: Micromeritics Autopore IV

The tests were conducted using the high-pressure mercury injection method with Micromeritics Autopore IV (Figure 5.7). End trims of core plug samples were used for this purpose. Capillary pressure drainage curves were generated by calculating the volumes of the non-wetting phase (mercury) entering the pores of rock samples at various pressure increments ranging from 0.5 to 60,000 psia, and plotting the capillary pressure values against the saturations of the wetting phase (mercury vapor or air) obtained. With the help of this data, calculations were made to determine the pore throat size distribution for the samples.

The calculation of the distribution of pore throat sizes is done by measuring how much mercury enters the pore size corresponding to each pressure using the basic capillary pressure formula. The pore throat diameter corresponding to different pressures is calculated using the Washburn equation (Washburn, 1921) as stated in (4). With this formula, it is possible to determine theoretically which pore sizes larger than a certain diameter will allow mercury to enter at each applied pressure.

$$D_i = \frac{a*\gamma*(-4*cos\theta)}{P_i} \qquad (4)$$

D_i = pore throat diameter, micron

a = Washburn constant, 0.145

γ = interfacial tension, dyne/cm

θ = contact angle, rad

P_i = pressure, psi

Through this formula, the pore throat size corresponding to any given pressure can be calculated. The assumption in this formula is that the pore throat forms the same angle as the two pores that constitute it, which is spherical. Additionally, the temperature is assumed to be 20°C. Deviations from these two assumptions will naturally result in errors in the pore throat diameters. However, since the same values are used for each rock sample and the pore throat sizes are used to compare rocks rather than their numerical significance, these errors can be neglected.

Comprehensive information about pore sizes of the samples was obtained through MICP measurements. Based on the measurements, pore throat size distributions calculated during drainage have been determined for each sample. Additionally, the classification of pore throats has been performed. The classification, based on the total volume occupied by pore throat sizes, uses the following criteria (Nelson, 2009) in Table 5.8.

Table 5.8: Pore throat size classification (Nelson, 2009)

Micro Size	Pore Throat Diameter < 1 micron
Meso Size	1 micron < Pore Throat Diameter < 3 microns
Macro Size	Pore Throat Diameter > 3 microns

The data obtained based on these criteria have been used to generate pore throat size distribution curves for each sample. Figure 5.8 presents these curves collectively for comparison. The outcomes of the analysis concerning the distribution of pore throat sizes reveal that the core plug samples demonstrate uniform pore throat dimensions, falling within the range of 0.01 to 10 microns.

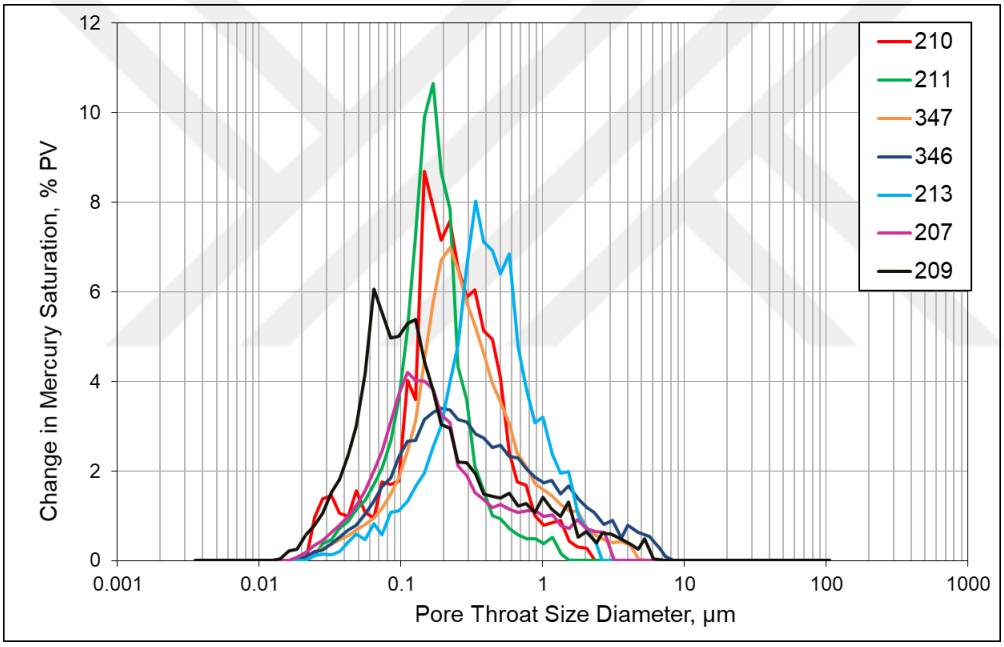

Figure 5.8: Pore throat size distribution curves of plug samples used in coreflood tests

5.2.4 Core Plug Saturation

Core plug samples are saturated with synthetic formation water prepared in the laboratory with 20,000 ppm NaCl solution by using vacuum pump (Figure 5.9). Core plugs are kept in a saturator for at least two days to ensure ionic balance.

Figure 5.9: Vacuum saturator (left), plug samples in formation water (right)

5.3 Coreflood Experimental Setup

The coreflood system enables researchers to simulate reservoir conditions and study the effects of chemicals as an enhanced oil recovery agent on core samples, providing valuable insights into their potential applications in the oil and gas industry.

As part of this investigation, flow tests were carried out using the core flood system. During the flow tests, nanocellulose solutions and other fluids were injected into the core samples at controlled flow rates, mimicking the injection process in actual reservoirs. These flow tests are essential to understand the interaction between the nanocellulose or other fluids and the reservoir rock, as well as to evaluate the efficiency of nanocellulose as an enhanced oil recovery agent. Parameters such as pressure, flow rates, and fluid properties are carefully monitored and recorded using pressure transducers and data acquisition systems.

Figure 5.10 illustrates the coreflood system used in laboratory experiments for investigating nanocellulose-enhanced oil recovery. Each number on the illustration corresponds to various components within the coreflood system:

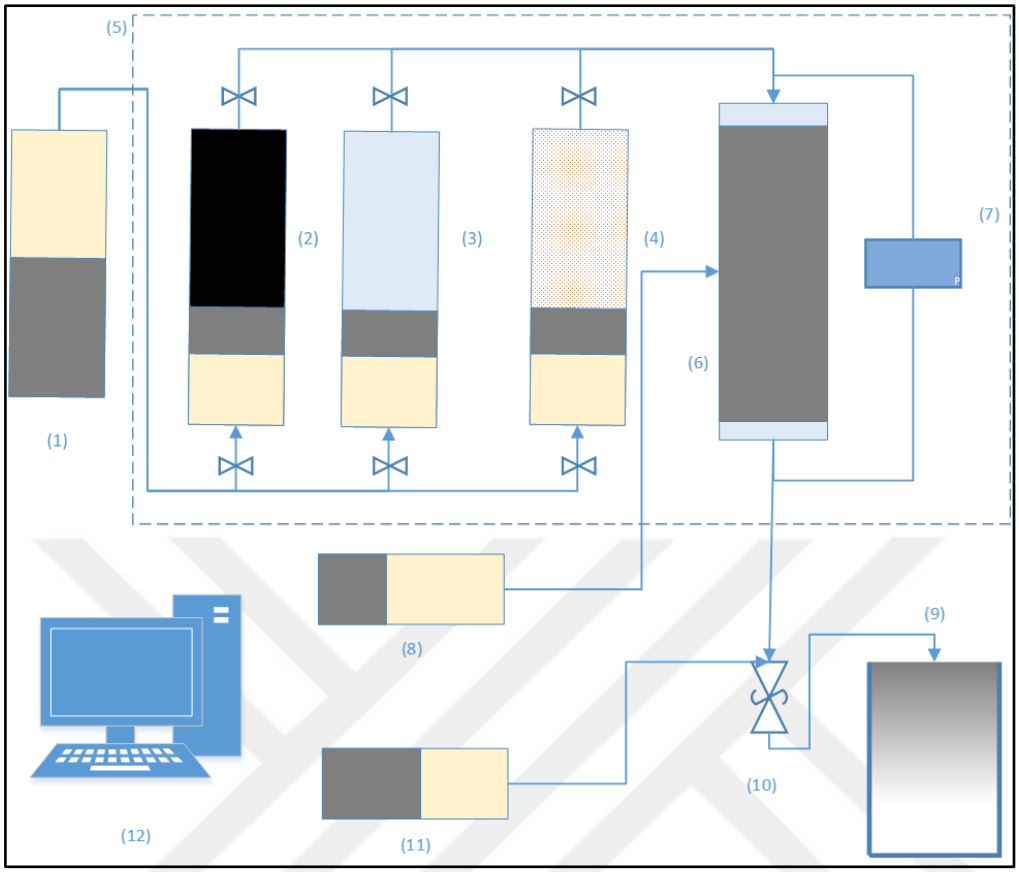

Figure 5.10: Schematic drawing of coreflood setup

1. Injection Pump: The injection pump is responsible for delivering nanocellulose solutions or other fluids into the core sample at a controlled flow rate.
2. Oil Accumulator: The oil accumulator stores the oil phase used in the coreflood experiment.
3. Formation Brine Accumulator: The formation brine accumulator holds the brine solution representing the reservoir formation water.
4. Nanocellulose Accumulator: The nanocellulose accumulator stores the nanocellulose solution used as an enhanced oil recovery agent.
5. Heating Cabinet/Oven: The heating cabinet or oven maintains the desired temperature of the coreflood experiment, ensuring it matches the reservoir conditions.

6. Core Holder: The core holder securely holds the core sample during the experiment, allowing fluid injection and flow through the sample.
7. Pressure Transducer: The pressure transducer measures the pressure changes within the core sample during fluid injection and flow.
8. Overburden Pump: The overburden pump applies confining pressure on the core sample to simulate reservoir conditions.
9. Outlet Collector: The outlet collector collects the effluent fluids that have passed through the core sample during the experiment.
10. Back Pressure Regulator: The back pressure regulator maintains a constant pressure at the outlet collector, controlling the flow rate of effluent fluids.
11. Hydraulic Pump: The hydraulic pump pressurizes the nanocellulose or other fluids for injection into the core sample.
12. Data Acquisition System: The data acquisition system records and stores the experimental data, such as pressure and flow rates for analysis and interpretation.

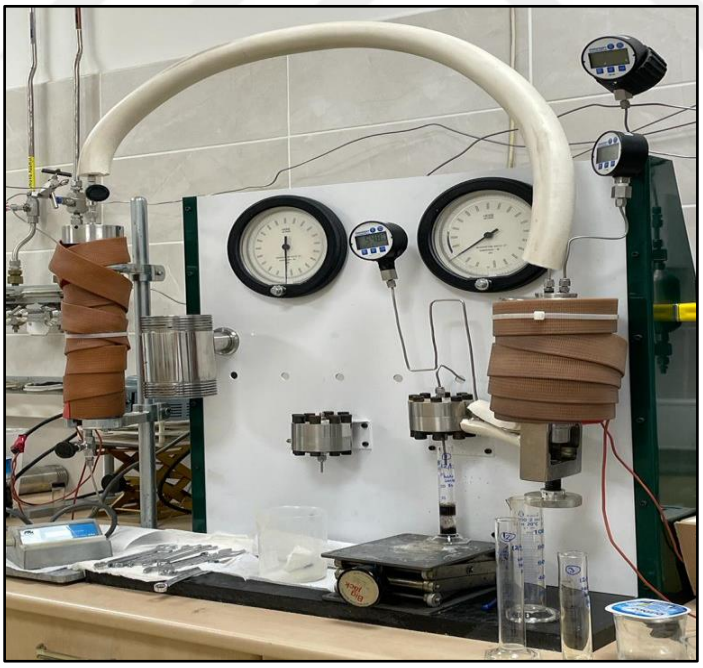

Figure 5.11: Coreflood System, CFS-1 Setup

Two separate core flood systems were used for the tests. Coreflood system-1 (CFS-1) in Figure 5.11 consists of heating belts to provide reservoir temperature of 65 °C for fluid accumulators (water and oil) and core holder. Furthermore, isolation belts were added into the system by covering flow lines in order to maintain reservoir temperature in the whole system and prevent heat losses.

Some of the coreflood tests were conducted using the CFS700 (Core Flooding System) from Vinci Technologies in Paris, France. This system consists of gas, water, and oil accumulators, as well as connecting lines, all housed in an oven. CFS700 (Figure 5.12) has 10,000 psi fluid and confining pressure and 150°C temperature limitations. Apart from CFS-1, this particular system includes a high temperature oven. Gas, liquid, and oil accumulators and a core holder (for 1.5-inch plugs) with the connected lines are placed in this oven system, which allows it to reach reservoir temperature.

The core sample used in the experiment had a diameter of 1.5 inches, and it was positioned vertically with the fluid inlets for oil and water at the top. Pressure sensors were used to measure the upstream, downstream, and differential pressures. A dual pump was employed for continuous oil or water flooding, and a separate pump automatically controlled the confining pressure. The fluid pressure at the outlet was regulated by a back-pressure regulator.

Figure 5.12: Coreflood System, CFS700 Setup

5.4 Coreflood Test Procedure

Flow tests were performed to analyze extra oil production after nanocellulose application and observe the effect of nanocellulose on additional oil recovery.

Within the scope of flow tests, saturated core plug is placed in the core holder and heated up to reservoir temperature. Overburden pressure and back pressure are set to a specific value. All the fluids (dead oil from the field and synthetic formation water) are placed into accumulators and heated up to the reservoir temperature. Flow test steps are summarized as follows:

- When the system reaches reservoir temperature, heated synthetic formation water is injected into the core plug and plug, and the plug sample is saturated for two days.

- Then, synthetic formation water is injected at steady-state conditions, using varying flow rates. The average permeability is then calculated by using Darcy's equation.

- Subsequently, dead oil is injected into the system with a constant flow rate, and the cumulative volume of water produced is recorded. Oil permeability (ko) at irreducible water saturation (Swi) is measured by injecting oil at varying flow rates.

- Then, the system is left for the aging process for at least four weeks at reservoir temperature and net confining stress. The aging process is the restoration of wettability with the original one under reservoir conditions to have more realistic results in terms of relative permeability values.

- After the aging process, dead oil injection is initiated at a constant flow rate. The pressure difference across the core plug is monitored to confirm the complete displacement of the post-aging crude.

- Then, synthetic formation water injection takes place to reach residual oil saturation (Sor) condition. Synthetic formation water is injected through the core plug with a constant flow rate. Once the pressure and saturation are stabilized at 100% water fractional flow, the injection rate is increased up to three or five times (ie. bump flood) to reduce any possible capillary end effect. During the test, the pressure difference (dP) across the plug is closely monitored for permeability calculations. Throughout these periods, oil recovery from the core is constantly monitored. Water injection is stopped when a water cut of 99.5% is attained.

- Nanocellulose solution is introduced into core plug with a flow rate of 1 cc/min. Nanocellulose solution is injected until the water cut of 99.5% is reached.

- Then, the system is left for a soaking process for 24 hours before water flood.

- After the completion of the nanocellulose flooding and soaking process, synthetic formation water injection is repeated to measure permeability and recover additional oil left in the core plug.
- Finally, synthetic formation water is injected with a constant flow rate and varying flow rates (bump flow) to recover the remaining oil in the plug sample. Water injection continues until a water cut of 99.5% is achieved.

The process involved injecting fluids in a series of injections until a stable condition is reached, except for nanocellulose injection. The steady-state conditions can be described as follows:

- Flow rates remain constant throughout the injections.
- The fractional flow of each phase remains constant.
- There should be a constant pressure drop.

5.5 Further Analysis on Core Plug Samples

After completing the injection process, the pressure in the system is released, and the core plug is removed from the core holder. Subsequently, the core plug sample is halved to facilitate additional analysis, which involves X-ray diffraction (XRD), scanning electron microscopy with energy-dispersive X-ray spectroscopy (SEM/EDS), and thin section analysis.

5.5.1 X-Ray Diffraction (XRD) Analysis

XRD (X-ray diffraction) is a technique used to determine the mineralogy of a sample, specifically identifying the different phases present. X-ray diffraction is commonly utilized not only for the qualitative identification of minerals in geological samples using a fingerprinting method; but has also demonstrated its efficacy in quantifying mineralogical data. Quantification relies on the principle that the intensities of X-ray

diffraction peaks from a specific mineral are proportionate to its concentration within the sample. Thus, by measuring peak intensities, valuable information about the relative abundance of the corresponding mineral phase can be obtained (Bish and Post, 1989).

The end trim of the core plug sample before conducting the coreflood test was analyzed by XRD, which represents the mineralogical composition of the core plug sample before any test. After completing coreflood test, one of the half slabs of the core plug was analyzed by XRD to see any change in mineralogical composition of the core plug after nanocellulose flood. The bulk powder and clay fraction XRD results are presented in this report later on.

5.5.2 SEM/EDS Analyses

Scanning Electron Microscope (SEM) imaging analysis and Energy Dispersive Spectroscopy (EDS) chemical analysis were performed for the plug samples before and after coreflood tests. The end trims of core plug samples were used for this purpose.

SEM-EDS analysis is an analytical technique that does not cause damage to the sample. However, unlike XRF (X-ray fluorescence) analysis, which can be conducted without removing the sample, SEM-EDS requires the removal of a sample. In SEM-EDS, the sample material is exposed to electrons, which results in the emission of characteristic x-rays from the elements present. The energy emissions are then translated into spectral peaks of varying intensity, creating a spectrum profile. This profile helps identify the different inorganic elements in the sample, such as lead, iron, copper, zinc, and others (The University of Melbourne, n.d.). It is important to note that SEM-EDS analysis is not quantitative. The intensity of the x-rays (size of spectrum peaks) is directly proportional to the concentration of elements in the sample.

Samples were prepared for SEM analysis by coating with gold-palladium (Au-Pd) alloy coating material. Without the alloy coating, non-conductive samples are mostly invisible to electron microscopes. Zeiss Evo-10 SEM device was used for SEM analysis, and Bruker Quantax-200 EDS detector was used for EDS analysis. 15 kV acceleration voltage and 30 μA beam current were selected. SEM images of some of the minerals that were detected in XRD analysis and their EDS spectrums are presented in this report later on.

General views of the samples are given in these figures at low magnification in order to understand the general features (such as visible porosity, differences in grain/crystal sizes, homogeneity of the coating process, etc.). Gold (Au) and Palladium (Pd) peaks in EDS spectrums are caused by the Au-Pd alloy coating material, which does not belonge to the original materials detected in the samples.

5.5.3 Thin Section Analysis

A thin section is a wafer-thin slice of rock or mineral sample that is prepared for microscopic examination. It is typically around 30 micrometers thick, allowing for detailed analysis of the sample's mineral composition, texture, and other geological features. Thin sections are commonly used in the field of geology and petrology to study rocks, minerals, and their properties.

To create a thin section, a small piece of rock or mineral sample is cut and mounted onto a glass slide. The sample is then ground and polished to achieve a smooth, flat surface. The prepared thin section is placed under a petrographic microscope, where it can be analyzed using various techniques such as polarized light microscopy and mineral identification methods.

Thin sections provide important insights into the mineralogy, texture, and structure of rocks. They allow geologists to identify different minerals present in a sample, observe their crystal forms and associations, study the rock's fabric and sedimentary structures, and interpret the rock's formation and history.

CHAPTER 6

RESULTS AND DISCUSSION

As part of this study, flow tests were carried out using core plug samples under reservoir conditions to evaluate the effectiveness of nanocellulose dispersion as an enhanced oil recovery agent. In summary, all the tests were conducted on carbonate rock samples at a temperature of 65 °C. Each coreflood experiment aimed to assess the performance of nanocellulose under different conditions.

6.1 Oil Recovery Coreflood Test Results

Test conditions of each coreflood experiment was given in this section. Additionally, pressure difference through core plug sample during each injection stage and oil recovery values were presented for each coreflood experiment test.

6.1.1 Coreflood Test #1

Saturated core plug #210 is placed in the core holder and heated up to reservoir temperature, 65 °C. Overburden pressure and back pressure are set to 1,250 psi and 550 psi, respectively. All the fluids (dead oil from the field and synthetic formation water) are placed into accumulators and heated to the reservoir temperature. Test conditions for coreflood test #1 are given in Table 6.1.

Table 6.1: Test conditions for test #1 with plug #210

Test No	Plug No	Overburden Pressure (psi)	Back Pressure (psi)	Test Temp (°C)	Salinity (ppm)	API Gravity of Oil
1	210	1,250	550	65	20,000	16

The below procedure was followed for testing enhanced oil recovery efficiency of nanocellulose through coreflooding test:

- Total 10 pore volumes (PV) of formation brine was injected into the core plug with varying flow rates (20 cc/min and 40 cc/min) and differential pressure (dP) in the core plug sample for each flow rate was recorded as seen in Table 6.2.

Table 6.2: Differential pressure values for water injection to plug #210

flow rate (cc/min)	differential pressure (dP)	injected fluid
20	14.1	Water
40	33	Water

- Subsequently, a total 4.3 PV of dead oil was injected into the system with a constant flow rate, and the cumulative volume of water produced was recorded. Oil permeability (ko) at irreducible water saturation (Swi) was measured by injecting oil at varying flow rates. Flow rates were applied as 1 cc/min and 0.5 cc/min, and differential pressure (dP) in the core plug sample vs. injected PV was recorded (Figure 6.1).
- Then, the system is left for the aging process for at least four weeks at reservoir temperature and net confining stress. The aging process is basically the restoration of wettability with the original one under reservoir conditions to have more realistic results in terms of relative permeability values.

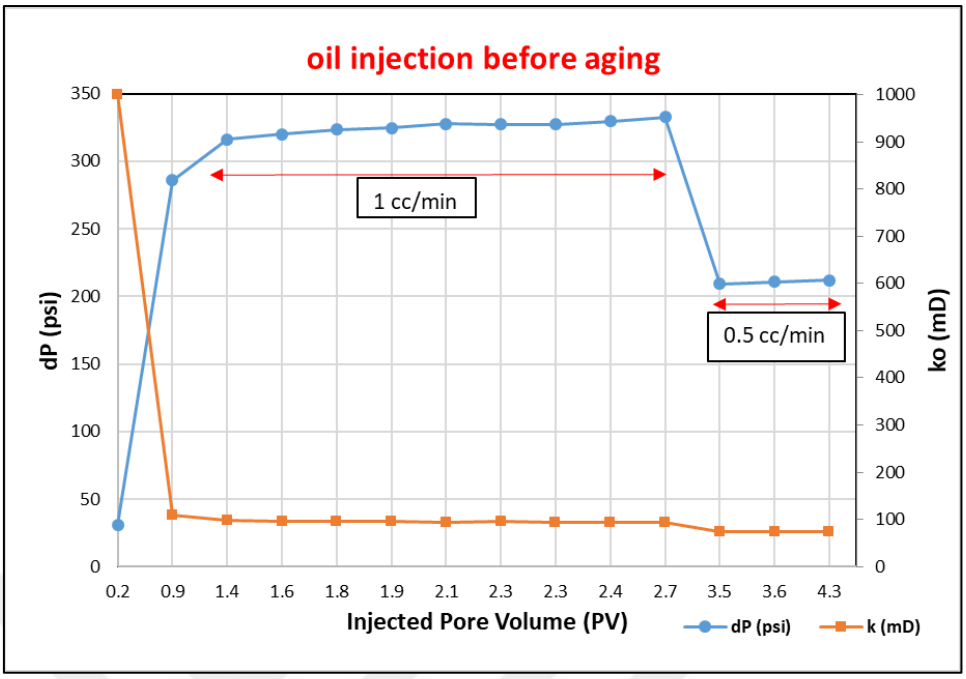

Figure 6.1: Oil injection before aging for plug #210

- Next, synthetic formation water injection took place in order to reach residual oil saturation (Sor) condition. 3.1 PV water was injected through the core plug with a flow rate of 1 cc/min. Once the pressure and saturation are stabilized at 100% water fractional flow, the injection rate is increased up to 5 times (bump flood) to reduce any possible capillary end effect. During the test, the pressure difference (dP) across the plug is closely monitored for permeability calculations (Figure 6.2). Throughout these periods, the recovery of oil from the core was constantly monitored. Water injection was stopped when a water cut of 99.5% was attained. During the waterflood, a total of 4.75 PV of brine was injected with a recovery of 64.3% OOIP.

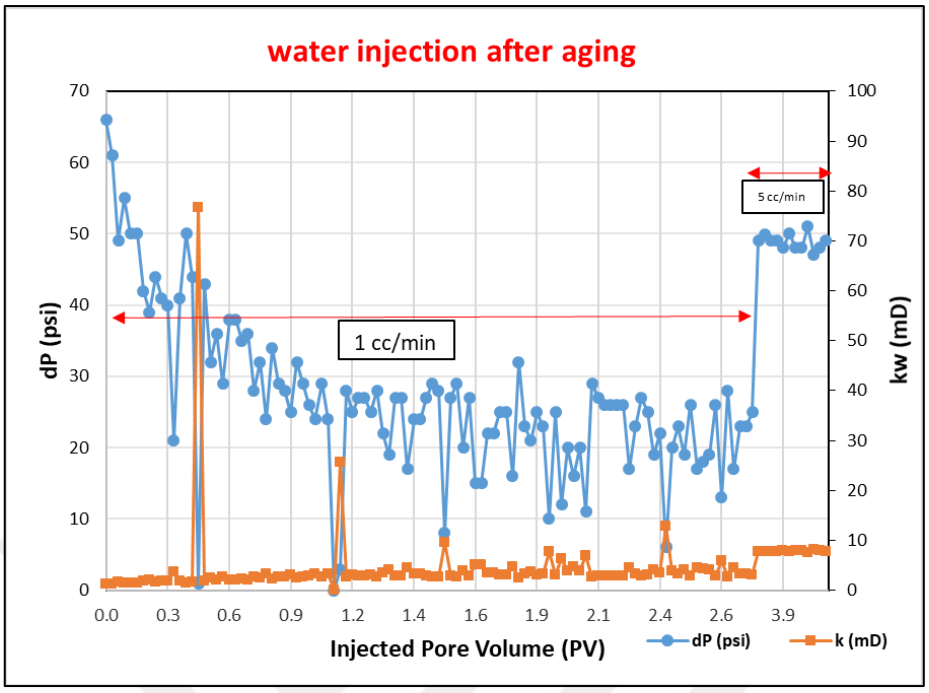

Figure 6.2: Water injection after aging of plug #210

- 2 wt% nanocellulose solution was introduced into core plug with a flow rate of 1 cc/min. A total of 2.3 PV of this solution was injected until a water cut of 99.5% was reached with a recovery of 14.6% OOIP (Figure 6.3). The steady-state conditions could not be achieved due to an increasing pressure difference while maintaining a constant flow rate. It is most probably due to the log jamming effect.
- Then, the system was left for a soaking process for 24 hours before water flood.
- After the completion of the nanocellulose flooding and soaking process, synthetic formation water injection was repeated to measure permeability and recover additional oil left in the core plug.
- Finally, a total of 5.1 PV synthetic formation water was injected with a flow rate of 1 cc/min and 5 cc/min (bump flow) to recover the remaining oil in the plug sample (Figure 6.4). Water injection continued until a water cut of 99.5% was achieved. The incremental oil recovery during the water flood was 2.9% OOIP and the total oil recovery reached 81.9%.

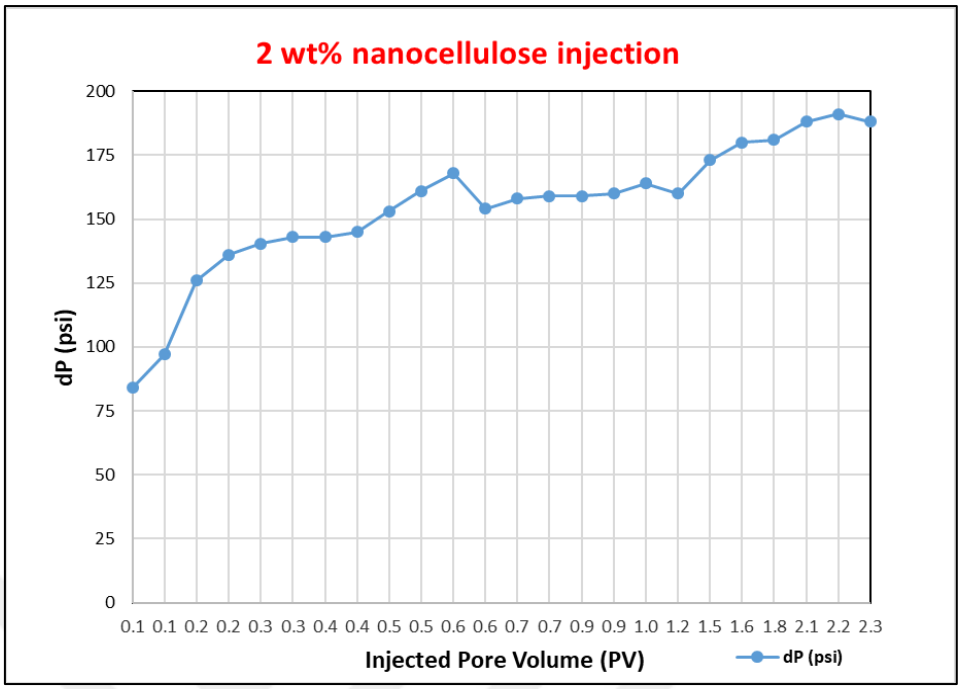

Figure 6.3: 2 wt% nanocellulose injection to plug #210

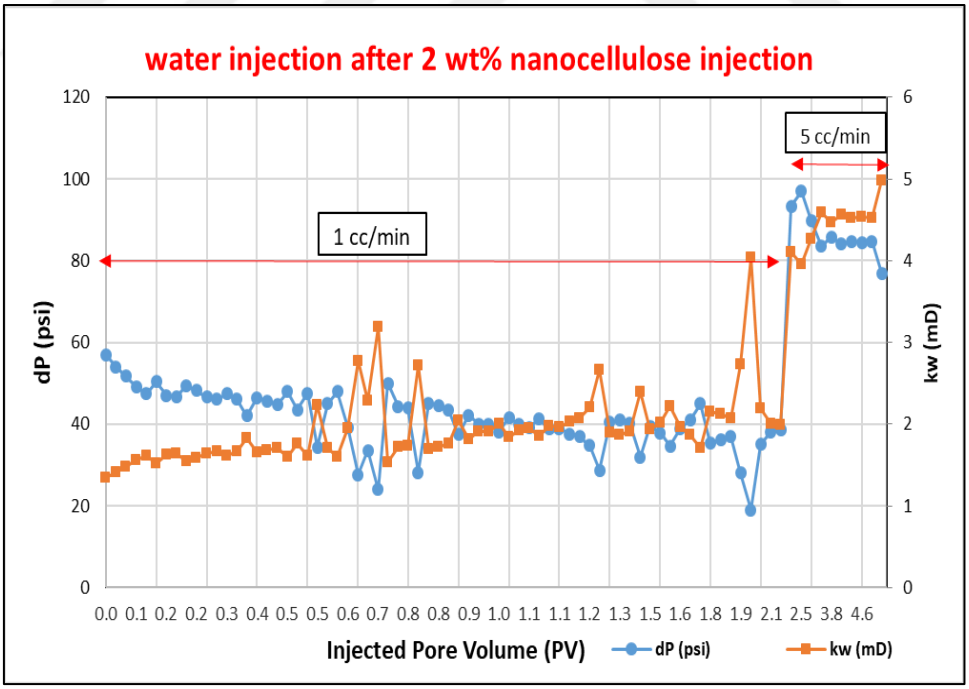

Figure 6.4: Water injection after 2 wt% nanocellulose soaking, plug #210

Table 6.3 displays the values of irreducible water saturation, residual oil saturation, and initial oil recovery obtained from test #1 performed on core plug #210.

Table 6.3: Saturation results for test #1

Test No	Plug No	Swi (%)	Sor (%)	Oil Recovery (%)
1	210	15.8	30.0%	64.3%

Additional oil recovery values by injection of nanocellulose and water injection to plug #210 are presented in Table 6.4.

Table 6.4: Oil recovery test results for plug #210

Initial Oil Recovery (%)	Additional Oil Recovery by Nanocellulose (% OOIP)	Additional Oil Recovery by Water Injection after Nanocellulose (% OOIP)	Incremental Oil Recovery by Nanocellulose+Water Injection (% OOIP)	Total Oil Recovery (% OOIP)
64.3%	14.6%	2.9%	17.5%	81.9%

6.1.2 Coreflood Test #2

Saturated core plug #211 is placed in the core holder and heated up to reservoir temperature, 65 °C. Overburden pressure and back pressure are set to 1,500 psi and 550 psi, respectively. All the fluids (dead oil from the field and synthetic formation water) are placed into accumulators and heated to the reservoir temperature. Test conditions for coreflood test #2 is given in Table 6.5.

Table 6.5: Test conditions for test #2 with plug #211

Test No	Plug No	Overburden Pressure (psi)	Back Pressure (psi)	Test Temp (°C)	Salinity (ppm)	API Gravity of Oil
2	211	1,500	550	65	20,000	16

The below procedure was followed for testing enhanced oil recovery efficiency of nanocellulose through coreflooding test:

- Total 12.5 pore volumes of formation brine was injected into the core plug with varying flow rates (10 cc/min and 20 cc/min), and differential pressure in the core plug sample for flow rate of 10 cc/min was recorded (Figure 6.5).

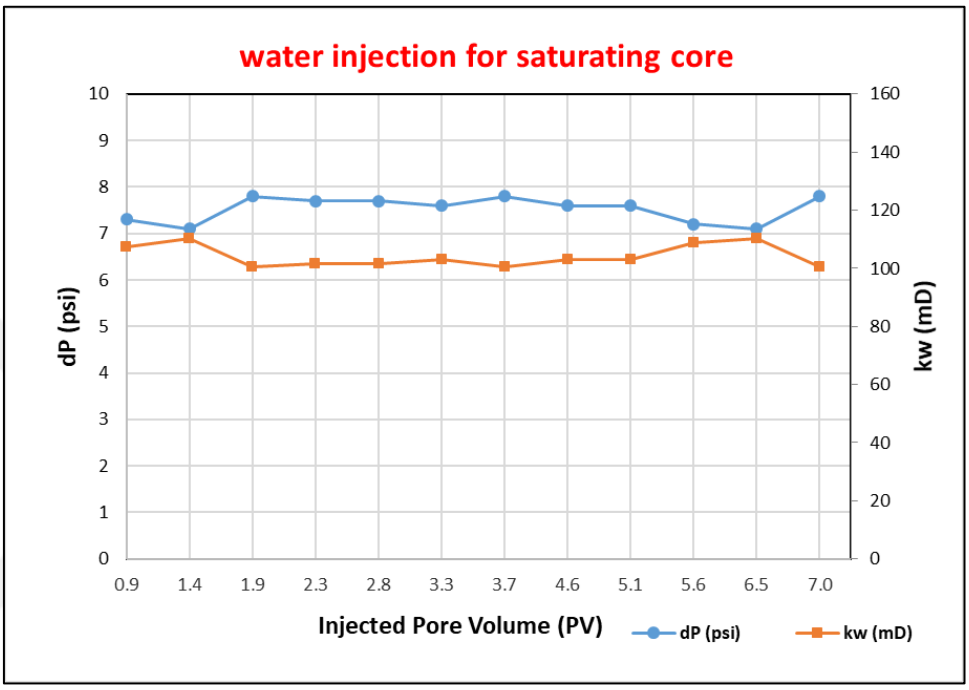

Figure 6.5: Water injection for saturating core plug #211

- Subsequently, a total 10.5 PV of dead oil was injected into the system with a constant flow rate, and the cumulative volume of water produced was recorded. Oil permeability (ko) at irreducible water saturation (Swi) was measured by injecting oil at varying flow rates. Flow rate of 1 cc/min was applied during injection and differential pressure in the core plug sample vs. injected PV was recorded (Figure 6.6).

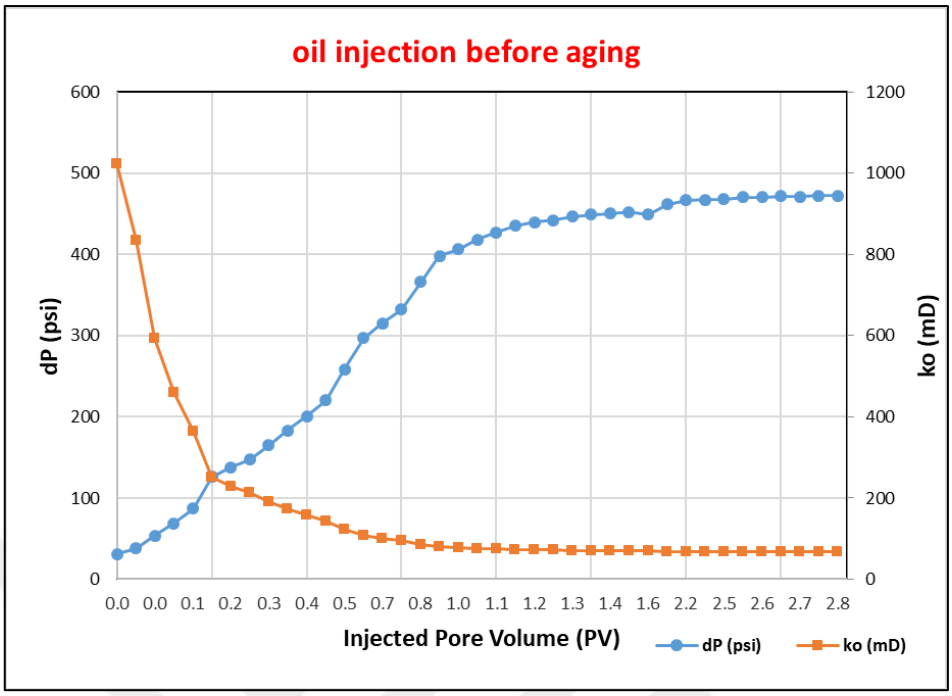

Figure 6.6: Oil injection before aging for plug #211

- Then, the system is left for the aging process for at least four weeks at reservoir temperature and net confining stress. The aging process is the restoration of wettability with the original one under reservoir conditions to have more realistic results in terms of relative permeability values.
- Next, synthetic formation water injection took place in order to reach residual oil saturation (Sor) condition. 18 PV water was injected through the core plug with a flow rate of 1 cc/min. Once the pressure and saturation are stabilized at 100% water fractional flow, the injection rate is increased up to 5 and 10 times (bump flood) to reduce any possible capillary end effect. During the test, the pressure difference (dP) across the plug is closely monitored for permeability calculations (Figure 6.7). Throughout these periods, the recovery of oil from the core was constantly monitored. Water injection was stopped when a water cut of 99.5% was attained. During waterflood, a total of 28 PV of brine was injected with a recovery of 52.7% OOIP.

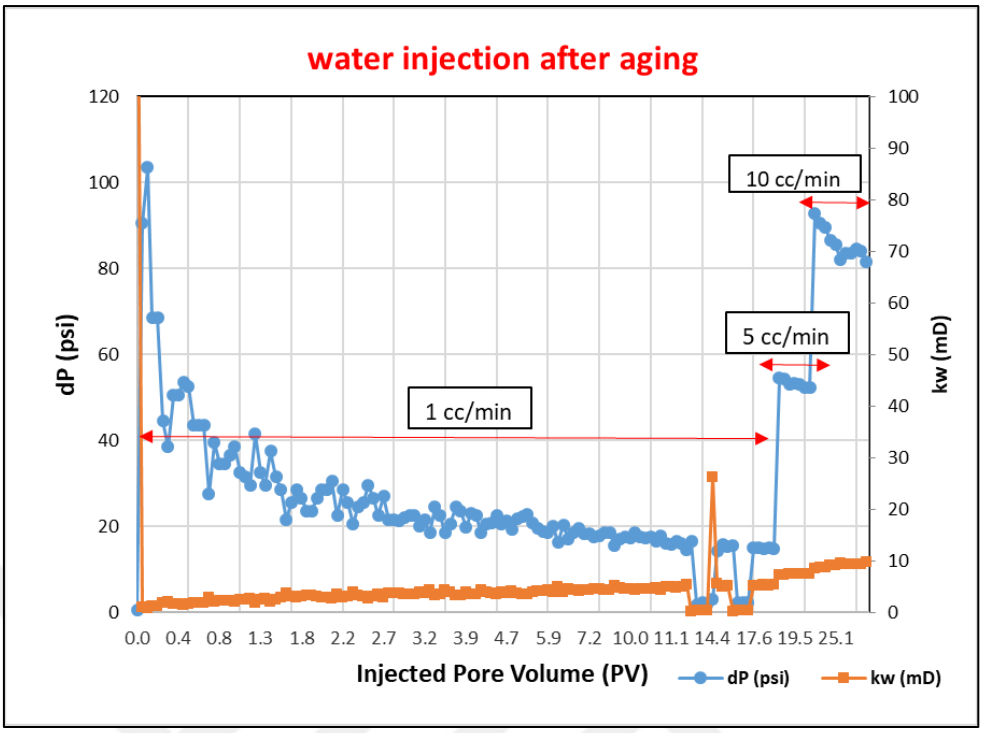

Figure 6.7: Water injection after aging of plug #211

- 2 wt% nanocellulose solution was introduced into core plug with a flow rate of 1 cc/min. A total of 4.4 PV of this solution was injected until a water cut of 99.5% was reached with a recovery of 13.4% OOIP (Figure 6.8). The steady-state conditions could not be achieved due to an increasing pressure difference while maintaining a constant flow rate.

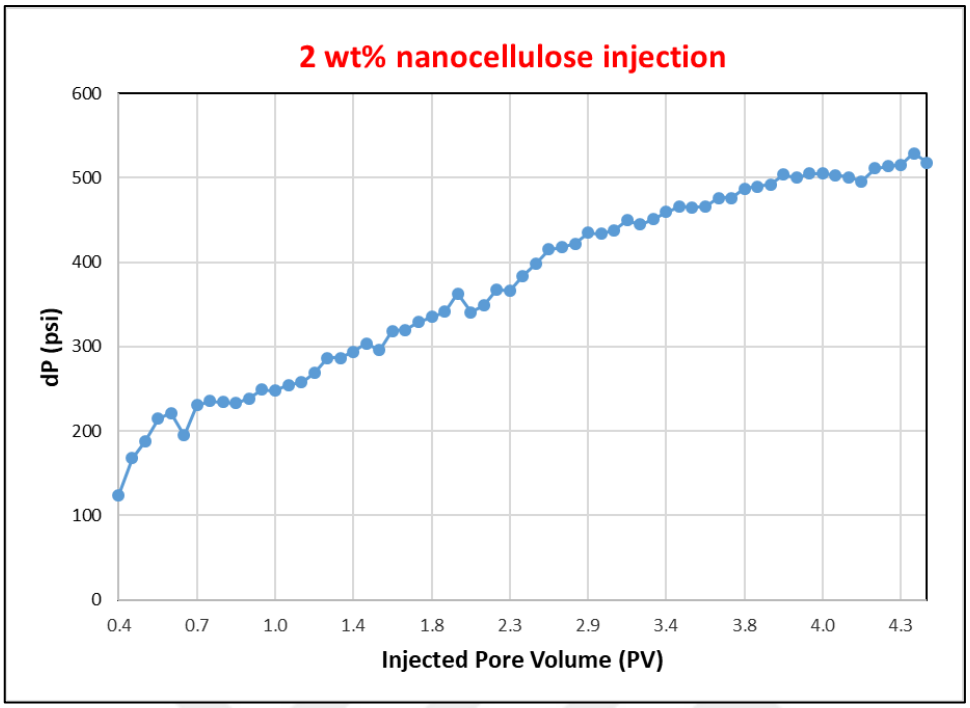

Figure 6.8: 2 wt% nanocellulose injection to plug #211

- Then, the system was left for a soaking process for 24 hours before the water flood.
- After the completion of the nanocellulose flooding and soaking process, synthetic formation water injection was repeated to measure permeability and recover additional oil left in the core plug.
- Finally, a total of 8.7 PV synthetic formation water was injected with a flow rate of 1 cc/min and 5 cc/min (bump flow) to recover the remaining oil in the plug sample (Figure 6.9). Water injection continued until a water cut of 99.5% was achieved. The incremental oil recovery during water flood was 2.9% OOIP and the total oil recovery reached 69.0%.

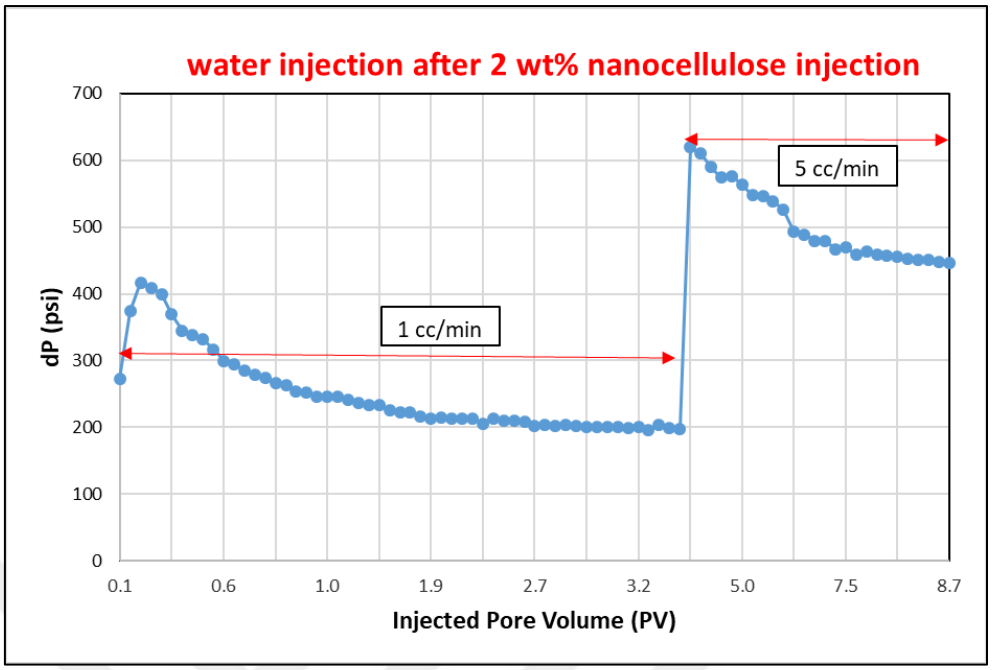

Figure 6.9: Water injection after 2 wt% nanocellulose soaking, plug #211

Table 6.6 displays the values of irreducible water saturation, residual oil saturation, and initial oil recovery obtained from test #2 performed on core plug #211.

Table 6.6: Saturation results for test #2

Test No	Plug No	Swi (%)	Sor (%)	Oil Recovery (%)
2	211	20.1	37.8%	52.7%

Additional oil recovery values by injection of nanocellulose and water injection to plug #211 is presented in Table 6.7.

Table 6.7: Oil recovery test results for plug #211

Initial Oil Recovery (%)	Additional Oil Recovery by Nanocellulose (% OOIP)	Additional Oil Recovery by Water Injection after Nanocellulose (% OOIP)	Incremental Oil Recovery by Nanocellulose+Water Injection (% OOIP)	Total Oil Recovery (% OOIP)
52.7%	13.4%	2.9%	16.3%	69.0%

6.1.3 Coreflood Test #3

Saturated core plug #347 is placed in core holder and heated up to reservoir temperature, 65 °C. Overburden pressure and back pressure are set to 1,500 psi and 550 psi, respectively. All the fluids (dead oil from the field and synthetic formation water) are placed into accumulators and heated to the reservoir temperature. Test conditions for coreflood test #3 are given in Table 6.8.

Table 6.8: Test conditions for test #3 with plug #347

Test No	Plug No	Overburden Pressure (psi)	Back Pressure (psi)	Test Temp (°C)	Salinity (ppm)	API Gravity of Oil
3	347	1,500	550	65	20,000	22

The below procedure was followed for testing enhanced oil recovery efficiency of nanocellulose through coreflooding test:

- Total of 15.8 pore volumes (PV) of formation brine was injected into the core plug with a flow rate of 20 cc/min and differential pressure (dP) in the core plug sample for mentioned flow rate was recorded as shown in Table 6.9.

  Table 6.9: Differential pressure value for water injection to plug #347

flow rate (cc/min)	differential pressure (psi)	injected fluid
20	30.9	Water

- Subsequently, total 12.1 PV of dead oil was injected into the system with a constant flow rate, and the cumulative volume of water produced was recorded. Oil permeability (ko) at irreducible water saturation (Swi) was measured by injecting oil at varying flow rates. Flow rates was applied as 1 cc/min and differential pressure (dP) in the core plug sample vs. injected PV was recorded (Figure 6.10).

- Then, the system is left for the aging process for at least four weeks at reservoir temperature and net confining stress.

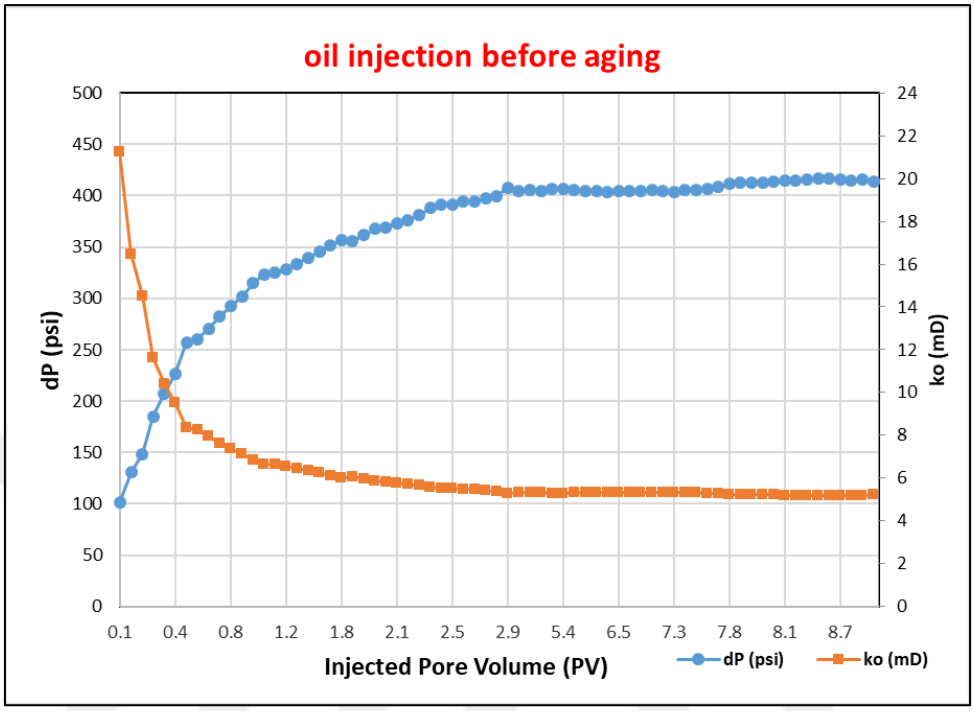

Figure 6.10: Oil injection before aging for plug #347

- Next, synthetic formation water injection took place in order to reach residual oil saturation (Sor) condition. 6.2 PV water was injected through the core plug with a flow rate of 1 cc/min. Once the pressure and saturation are stabilized at 100% water fractional flow, the injection rate is increased up to 5 times (bump flood) to reduce any possible capillary end effect. During the test, the pressure difference (dP) across the plug is closely monitored for permeability calculations (Figure 6.11). Throughout these periods, the recovery of oil from the core was constantly monitored. Water injection was stopped when a water cut of 99.5% was attained. During the waterflood, a total of 16.7 PV of brine was injected with a recovery of 67.1% OOIP.
- 2 wt% nanocellulose solution was introduced into core plug with a flow rate of 1 cc/min. A total of 3 PV of this solution was injected until a water cut of 99.5% was reached with a recovery of 16.7% OOIP (Figure 6.12). The

steady-state conditions could not be achieved due to an increasing pressure difference (dP) while maintaining a constant flow rate.

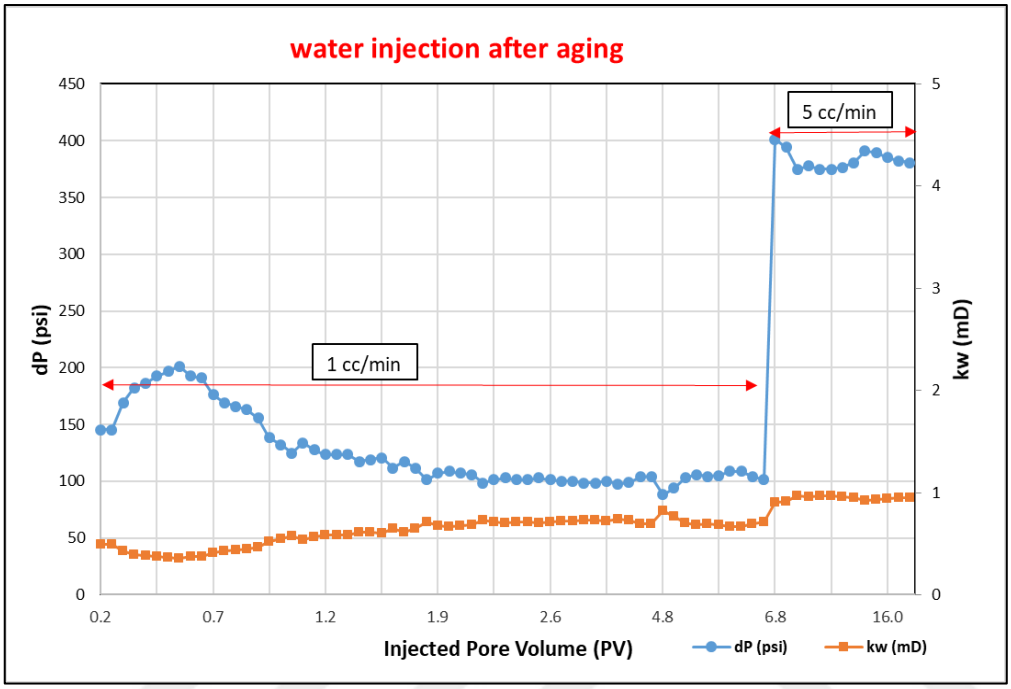

Figure 6.11: Water injection after aging of plug #347

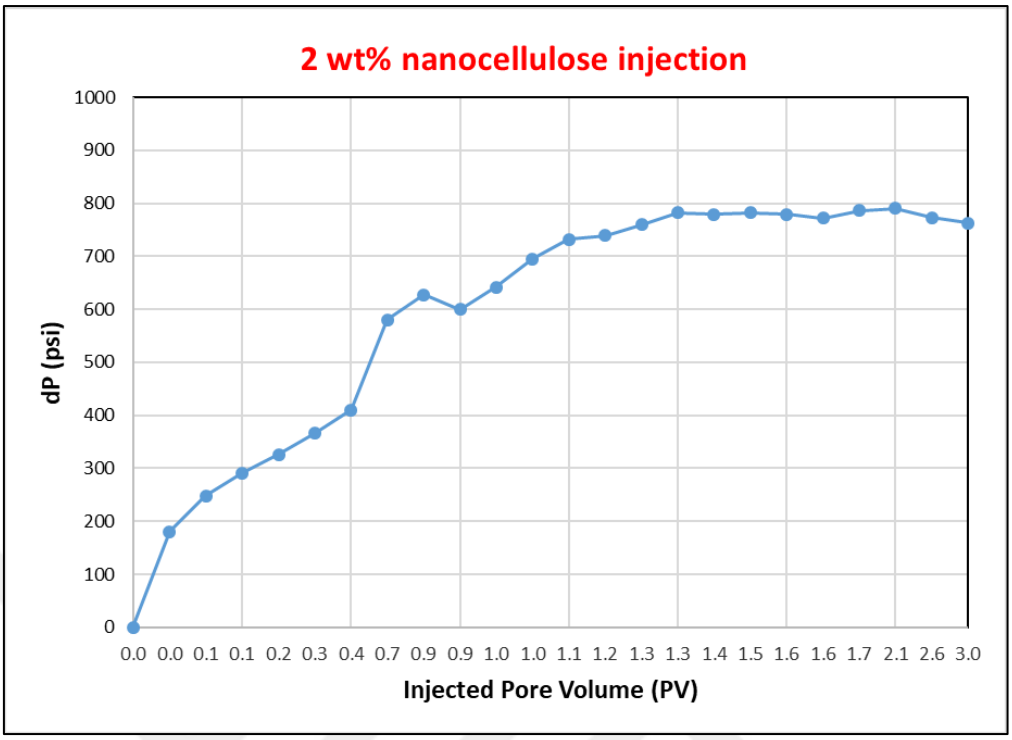

Figure 6.12: 2 wt% nanocellulose injection to plug #347

- Then, the system was left for a soaking process for 24 hours before water flood.
- After the completion of the nanocellulose flooding and soaking process, synthetic formation water injection was repeated to measure permeability and recover additional oil left in the core plug.
- Finally, a total of 26.7 PV synthetic formation water was injected with a flow rate of 1 cc/min and 3 cc/min (bump flow) to recover the remaining oil in the plug sample (Figure 6.13). Water injection continued until a water cut of 99.5% was achieved. The incremental oil recovery during the water flood was 5.0% OOIP and the total oil recovery reached 88.8%.

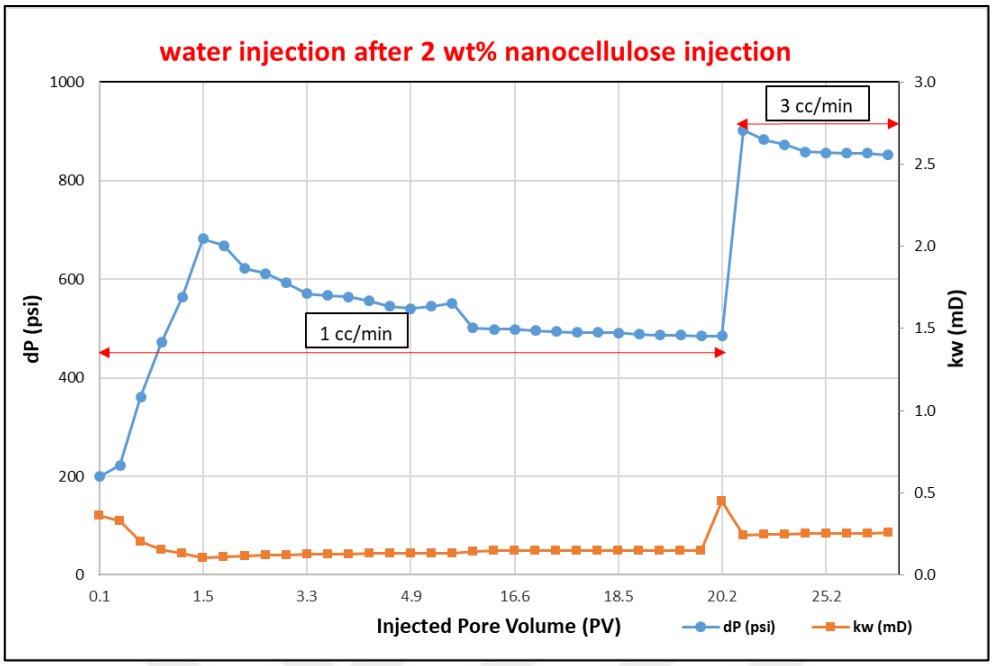

Figure 6.13: Water injection after 2 wt% nanocellulose soaking, plug #347

Table 6.10 displays the values of irreducible water saturation, residual oil saturation, and initial oil recovery obtained from test #3 performed on core plug #347.

Table 6.10: Saturation results for test #3

Test No	Plug No	Swi (%)	Sor (%)	Oil Recovery (%)
3	347	11.1	29.3%	67.1%

Additional oil recovery values by injection of nanocellulose and water injection to plug #347 are presented in Table 6.11.

Table 6.11: Oil recovery test results for plug #347

Initial Oil Recovery (%)	Additional Oil Recovery by Nanocellulose (% OOIP)	Additional Oil Recovery by Water Injection after Nanocellulose (% OOIP)	Incremental Oil Recovery by Nanocellulose+Water Injection (% OOIP)	Total Oil Recovery (% OOIP)
67.1%	16.7%	5.0%	21.7%	88.8%

6.1.4 Coreflood Test #4

Saturated core plug #346 is placed in the core holder and heated up to reservoir temperature, 65 °C. Overburden pressure and back pressure are set to 1,500 psi and 550 psi, respectively. All the fluids (dead oil from the field and synthetic formation water) are placed into accumulators and heated to the reservoir temperature. Test conditions for coreflood test #4 are given in Table 6.12.

Table 6.12: Test conditions for test #4 with plug #346

Test No	Plug No	Overburden Pressure (psi)	Back Pressure (psi)	Test Temp (°C)	Salinity (ppm)	API Gravity of Oil
4	346	1,500	550	65	20,000	22

The below procedure was followed for testing enhanced oil recovery efficiency of nanocellulose through coreflooding test:

- Total of 18.4 pore volumes (PV) of formation brine was injected into the core plug with varying flow rates (1 cc/min, 5 cc/min and 10 cc/min) and differential pressure (dP) in the core plug sample was recorded (Figure 6.14).
- Subsequently, total of 10.3 PV of dead oil was injected into the system with a constant flow rate, and the cumulative volume of water produced was recorded. Oil permeability (ko) at irreducible water saturation (Swi) was measured by injecting oil at varying flow rates. Flow rates was applied as 1 cc/min and differential pressure in the core plug sample vs. injected PV was recorded (Figure 6.15).
- Then, the system is left for the aging process for at least four weeks at reservoir temperature and net confining stress.

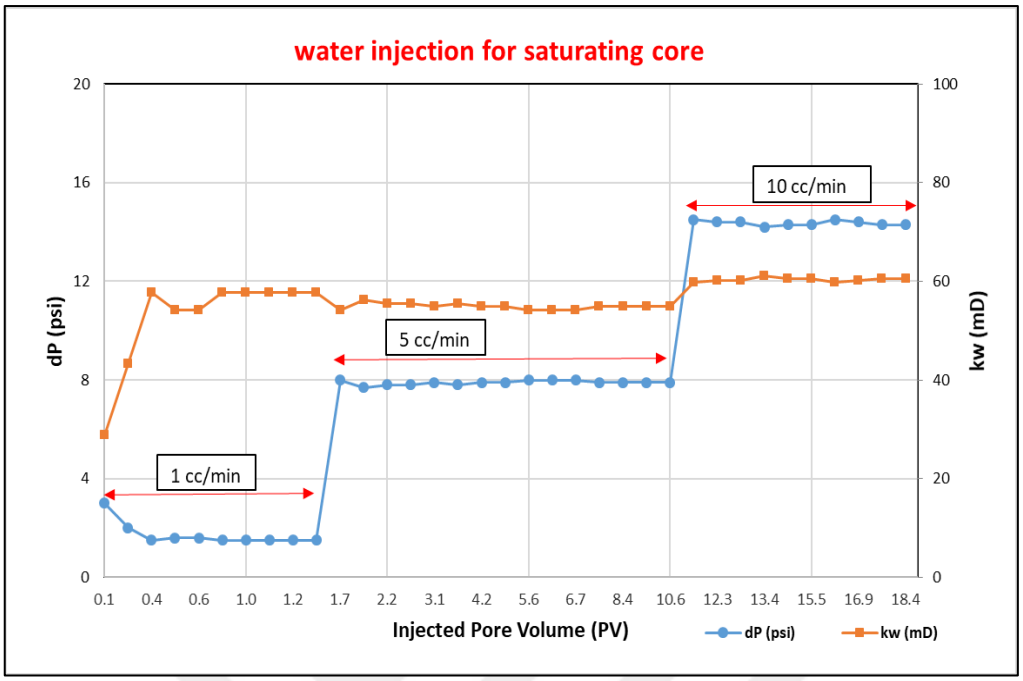

Figure 6.14: Water injection for saturating core plug #346

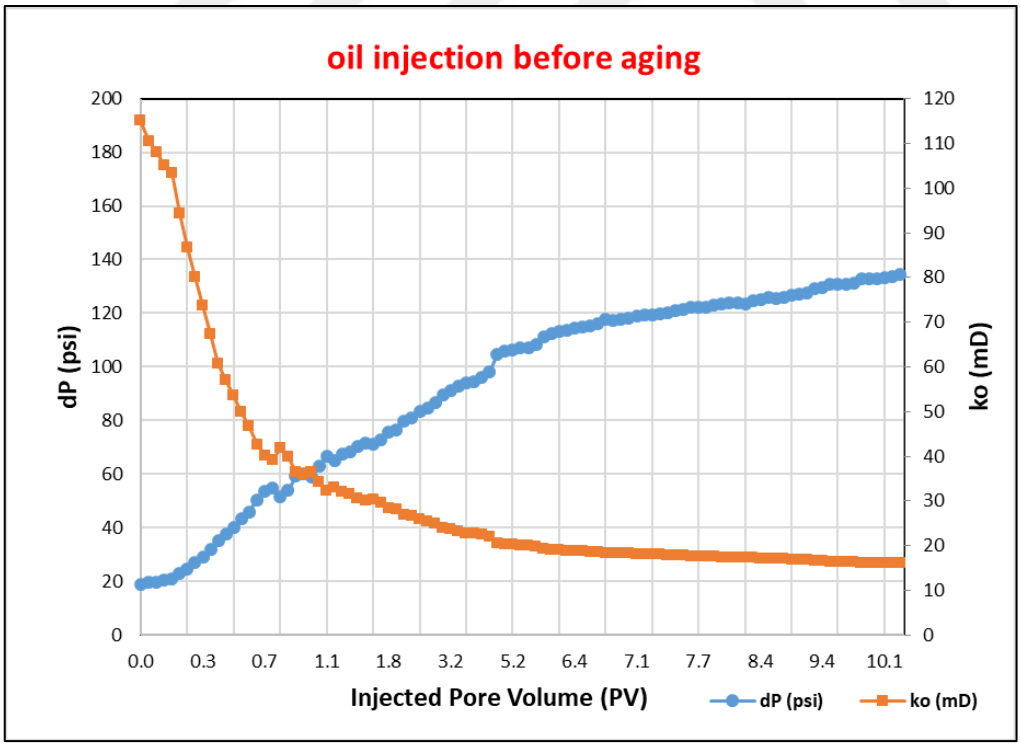

Figure 6.15: Oil injection before aging for plug #346

- After the aging process, dead oil injection was initiated at a constant flow rate of 1 cc/min. The pressure difference across the core plug is monitored to confirm the complete displacement of the post-aging crude as illustrated in Figure 6.16.

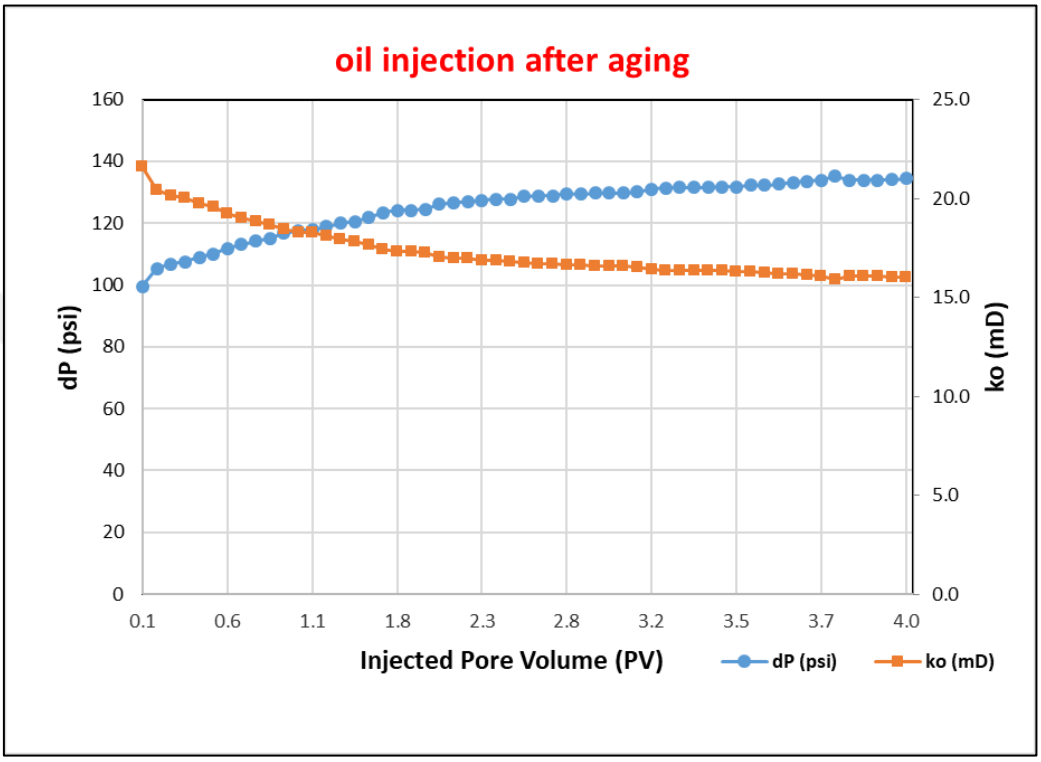

Figure 6.16: Oil injection after aging for plug #346

- Then, synthetic formation water injection took place in order to reach residual oil saturation (Sor) condition. 17.7 PV water was injected through the core plug with a flow rate of 1 cc/min. Once the pressure and saturation are stabilized at 100% water fractional flow, the injection rate is increased up to 5 times (ie. bump flood) to reduce any possible capillary end effect. During the test, the pressure difference (dP) across the plug is closely monitored for permeability calculations (Figure 6.17). Throughout these periods, the recovery of oil from the core was constantly monitored. Water injection was stopped when a water cut of 99.5% was attained. During the waterflood, a total of 35.4 PV of brine was injected with a recovery of 70.8% OOIP.

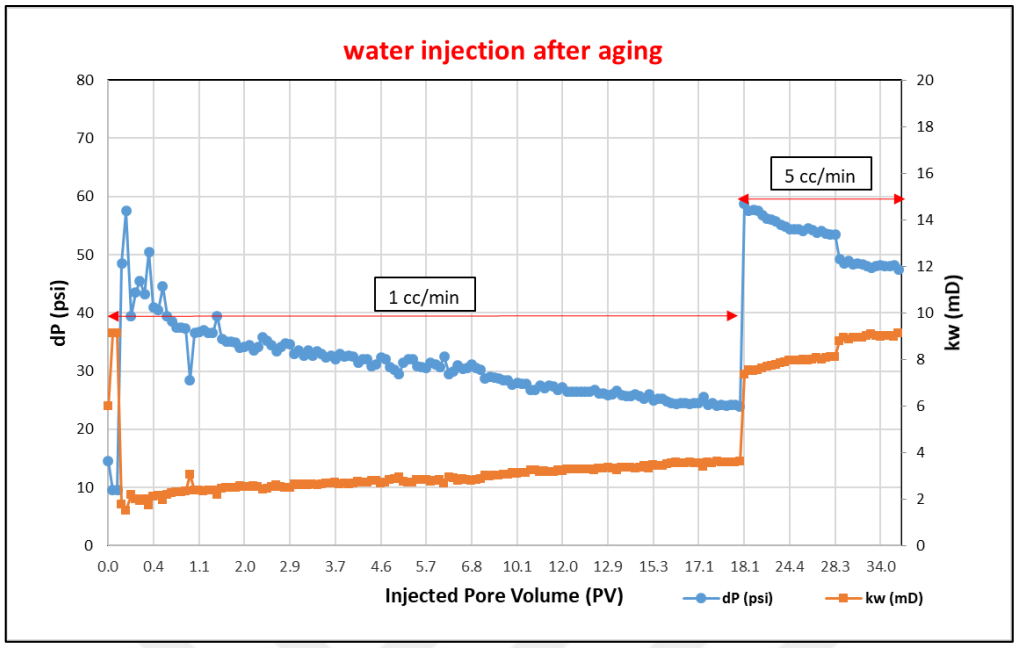

Figure 6.17: Water injection after aging of plug #346

- 1 wt% nanocellulose solution was introduced into core plug with a flow rate of 1 cc/min. A total of 4.4 PV of this solution was injected until a water cut of 99.5% was reached with a recovery of 19.2% OOIP (Figure 6.19). The steady-state conditions could not be achieved due to an increasing pressure difference (dP) while maintaining a constant flow rate.
- Then, the system was left for a soaking process for 24 hours before water flood.
- After the completion of the nanocellulose flooding and soaking process, synthetic formation water injection was repeated to measure permeability and recover additional oil left in the core plug.
- Finally, a total of 22 PV synthetic formation water was injected with a flow rate of 1 cc/min and 3 cc/min (bump flow) to recover the remaining oil in the plug sample (Figure 6.19). Water injection continued until a water cut of 99.5% was achieved. The incremental oil recovery during the water flood was 5.8% OOIP and the total oil recovery reached 95.8%.

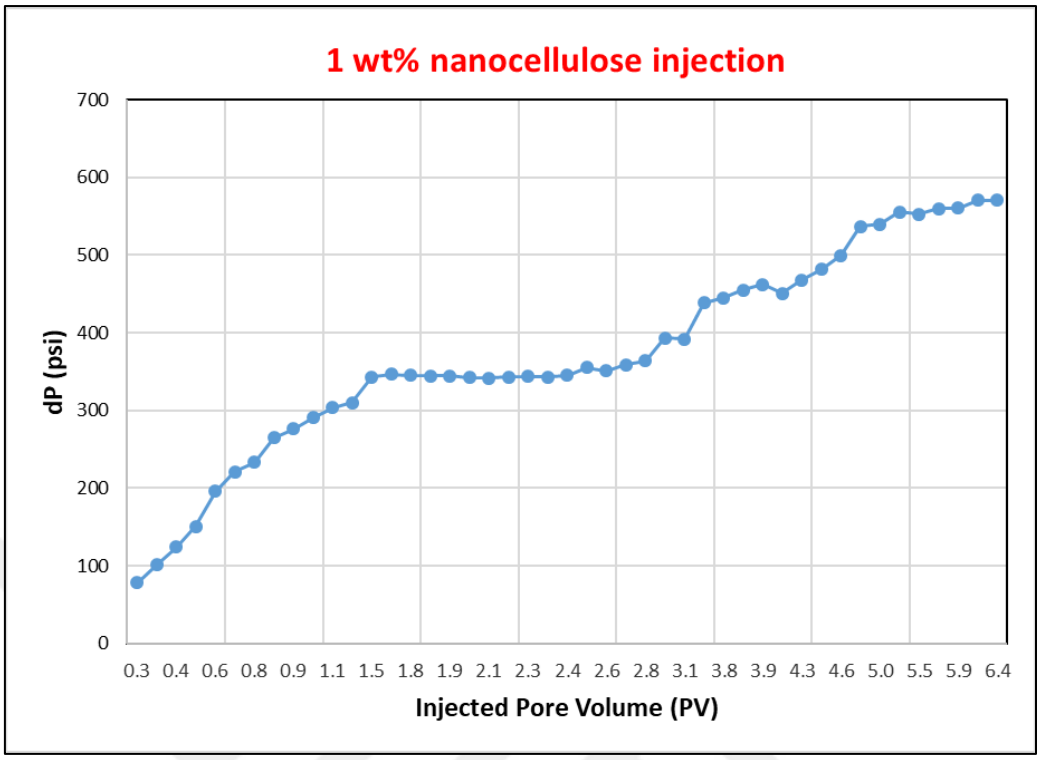

Figure 6.18: 1 wt% nanocellulose injection to plug #346

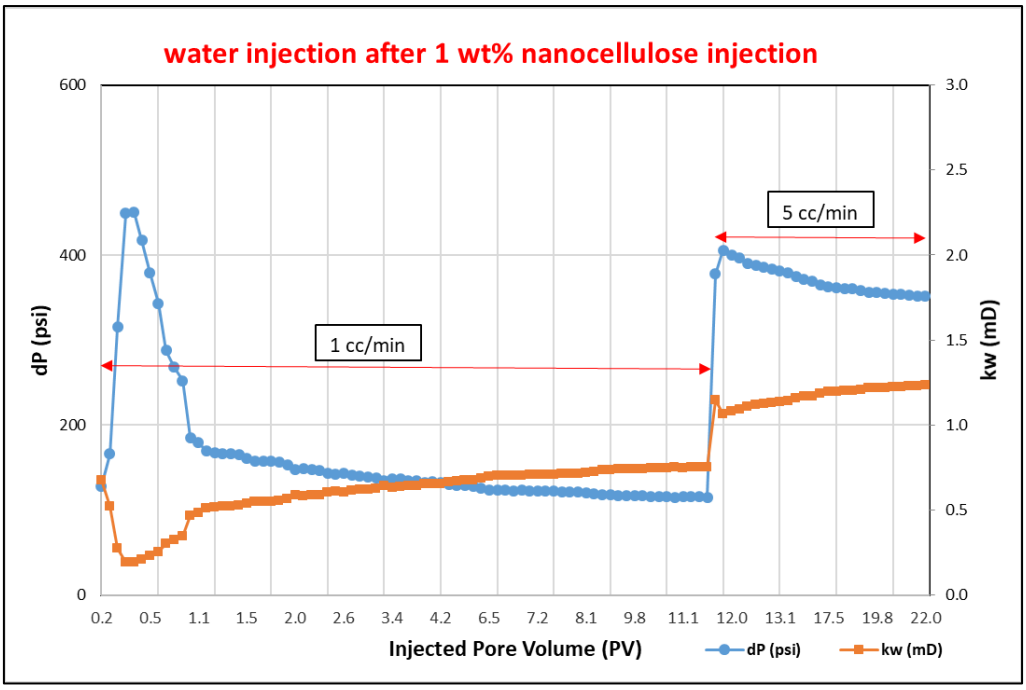

Figure 6.19: Water injection after 1 wt% nanocellulose soaking, plug #346

Table 6.13 displays the values of irreducible water saturation, residual oil saturation, and initial oil recovery obtained from test #4 performed on core plug #346.

Table 6.13: Saturation results for test #4

Test No	Plug No	Swi (%)	Sor (%)	Oil Recovery (%)
4	346	15.0	24.8%	70.8%

Additional oil recovery values by injection of nanocellulose and water injection to plug #346 is presented in Table 6.14.

Table 6.14: Oil recovery test results for plug #346

Initial Oil Recovery (%)	Additional Oil Recovery by Nanocellulose (% OOIP)	Additional Oil Recovery by Water Injection after Nanocellulose (% OOIP)	Incremental Oil Recovery by Nanocellulose+Water Injection (% OOIP)	Total Oil Recovery (% OOIP)
70.8%	19.2%	5.8%	25.0%	95.8%

6.1.5 Coreflood Test #5

Saturated core plug #213 is placed in the core holder and heated up to reservoir temperature, 65 °C. Overburden pressure and back pressure are set to 1,500 psi and 550 psi, respectively. All the fluids (dead oil from the field and synthetic formation water) are placed into accumulators and heated to the reservoir temperature. Test conditions for coreflood test #5 are given in Table 6.15.

Table 6.15: Test conditions for test #5 with plug #213

Test No	Plug No	Overburden Pressure (psi)	Back Pressure (psi)	Test Temp (°C)	Salinity (ppm)	API Gravity of Oil
5	213	1,500	550	65	20,000	36

The below procedure was followed for testing enhanced oil recovery efficiency of nanocellulose through coreflooding test:

- Total 8 pore volumes (PV) of formation brine was injected into the core plug with varying flow rates (5 cc/min and 10 cc/min) and differential pressure (dP) in the core plug sample was recorded as seen in Table 6.16.

Table 6.16: Differential pressure values for water injection to plug #213

flow rate (cc/min)	differential pressure (psi)	injected fluid
5	7.3	Water
10	13.1	Water

- Subsequently, a total of 10 PV of dead oil was injected into the system with a constant flow rate, and the cumulative volume of water produced was recorded. Oil permeability (ko) at irreducible water saturation (Swi) was measured by injecting oil at varying flow rates. Flow rates were applied as 1 cc/min and differential pressure (dP) in the core plug sample vs. injected PV was recorded (Figure 6.20).

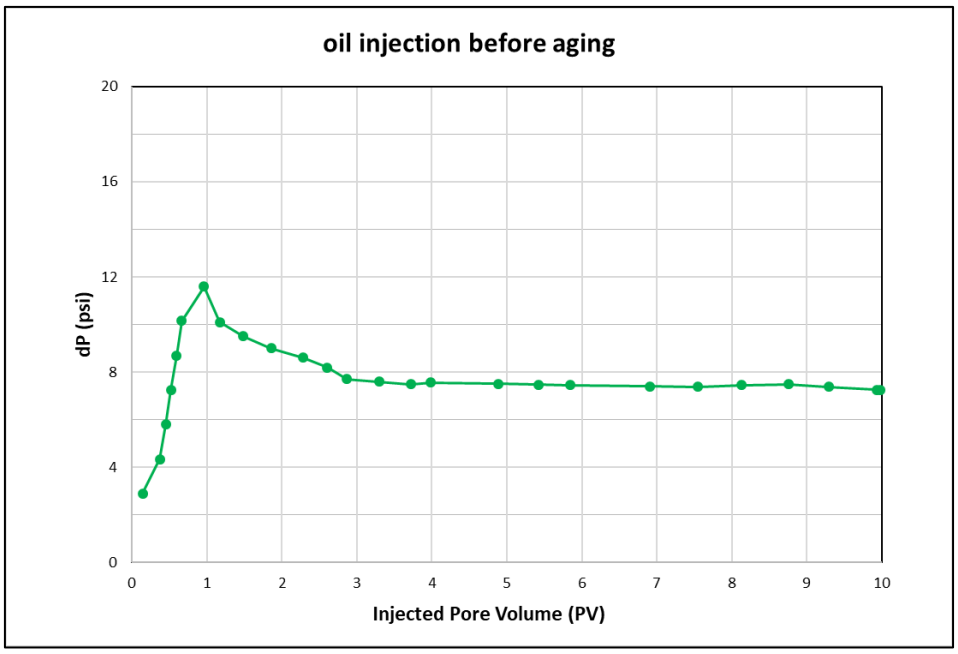

Figure 6.20: Oil injection before aging for plug #213

- Then, the system is left for the aging process for at least four weeks at reservoir temperature and net confining stress.
- Next, synthetic formation water injection took place in order to reach residual oil saturation (Sor) condition. 3.9 PV water was injected through the core plug with a flow rate of 1 cc/min. Once the pressure and saturation are stabilized at 100% water fractional flow, the injection rate is increased up to 3 times (bump flood) to reduce any possible capillary end effect. During the test, pressure difference (dP) across the plug is closely monitored for permeability calculations (Figure 6.21). Throughout these periods, the recovery of oil from the core was constantly monitored. Water injection was stopped when a water cut of 99.5% was attained. During the waterflood, a total of 10.1 PV of brine was injected with a recovery of 61.2% OOIP.

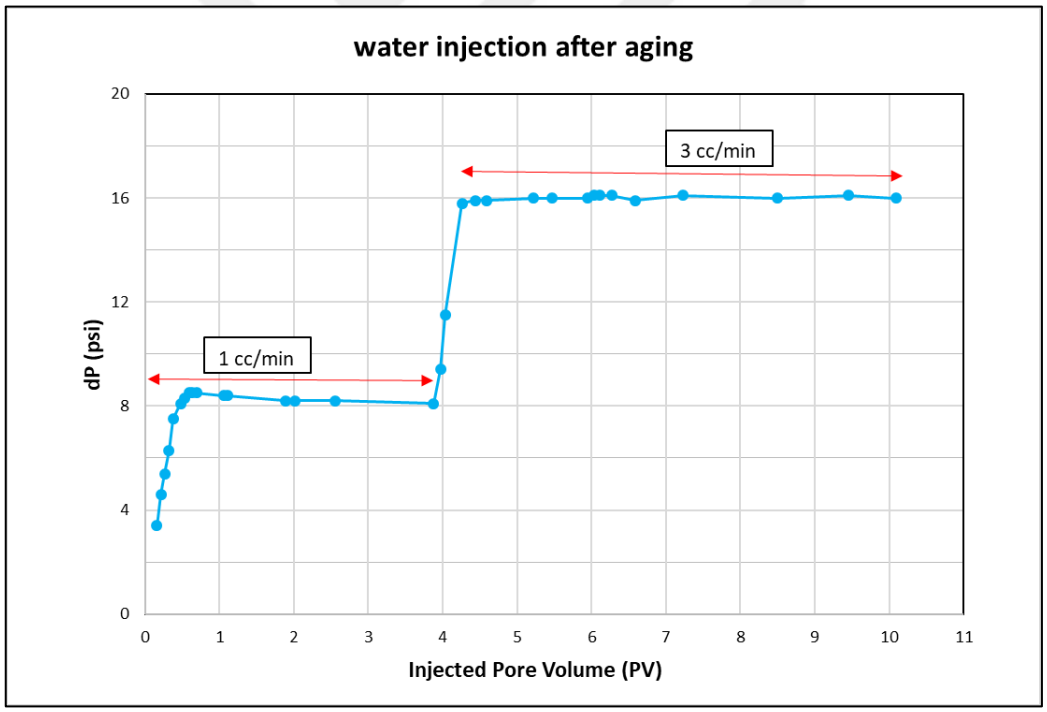

Figure 6.21: Water injection after aging for plug #213

- 1 wt% nanocellulose solution was introduced into core plug with a flow rate of 1 cc/min. A total of 4.4 PV of this solution was injected until a water cut

of 99.5% was reached with a recovery of 24.7% OOIP (Figure 6.22). The steady-state conditions could not be achieved due to an increasing pressure difference (dP) while maintaining a constant flow rate.

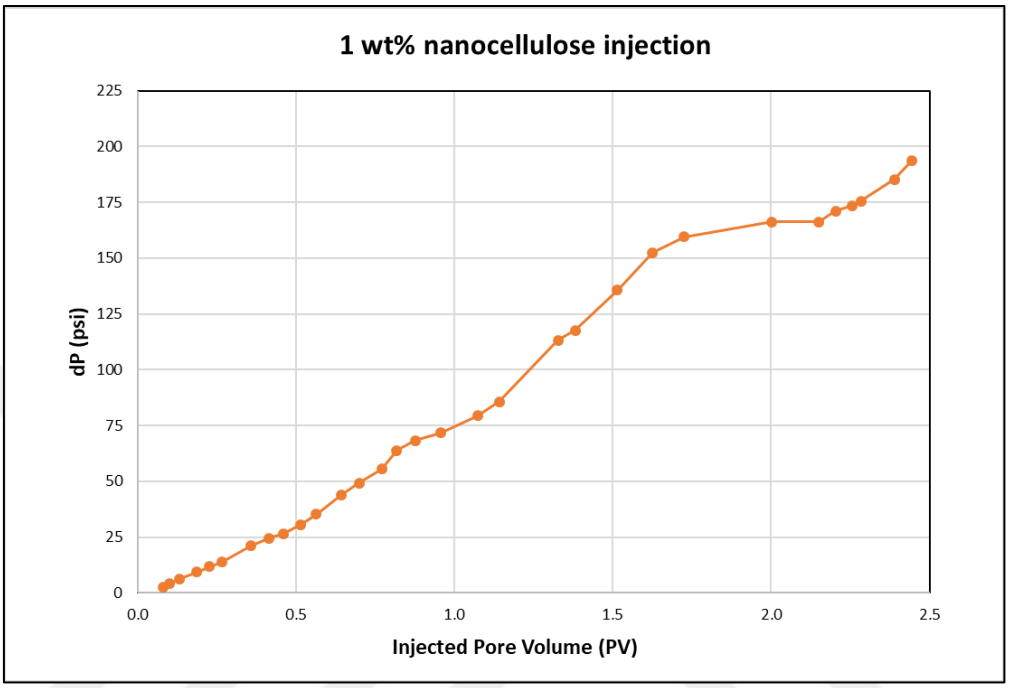

Figure 6.22: 1 wt% nanocellulose injection to plug #213

- Then, the system was left for a soaking process for 24 hours before the water flood.
- After the completion of the nanocellulose flooding and soaking process, synthetic formation water injection was repeated to measure permeability and recover additional oil left in the core plug.
- Finally, a total of 17 PV synthetic formation water was injected with a flow rate of 1 cc/min, 3 cc/min and 5 cc/min (bump flows) to recover the remaining oil in the plug sample (Table 6.17). Water injection continued until a water cut of 99.5% was achieved. The incremental oil recovery during water flood was 3.5% OOIP and the total oil recovery reached 89.4%.

Table 6.17: Differential pressure values for water injection to plug #213 after 1 wt% nanocellulose soaking

flow rate (cc/min)	differential pressure (psi)	injected fluid
1	200	Water
3	226	Water
5	255	Water

Table 6.18 displays the values of irreducible water saturation, residual oil saturation, and initial oil recovery obtained from test #5 performed on core plug #213.

Table 6.18: Saturation results for test #5

Test No	Plug No	Swi (%)	Sor (%)	Oil Recovery (%)
5	213	54.9	17.5%	61.2%

Additional oil recovery values by injection of nanocellulose and water injection to plug #213 are presented in Table 6.19.

Table 6.19: Oil recovery test results for plug #213

Initial Oil Recovery (%)	Additional Oil Recovery by Nanocellulose (% OOIP)	Additional Oil Recovery by Water Injection after Nanocellulose (% OOIP)	Incremental Oil Recovery by Nanocellulose+Water Injection (% OOIP)	Total Oil Recovery (% OOIP)
61.2%	24.7%	3.5%	28.2%	89.4%

6.1.6 Coreflood Test #6

Saturated core plug #207 is placed in the core holder and heated up to reservoir temperature, 65 °C. Overburden pressure and back pressure are set to 1,500 psi and

550 psi, respectively. All the fluids (dead oil from the field and synthetic formation water) are placed into accumulators and heated to the reservoir temperature. Test conditions for coreflood test #6 are given in Table 6.20.

Table 6.20: Test conditions for test #6 with plug #207

Test No	Plug No	Overburden Pressure (psi)	Back Pressure (psi)	Test Temp (°C)	Salinity (ppm)	API Gravity of Oil
6	207	1,500	550	65	20,000	36

The below procedure was followed for testing enhanced oil recovery efficiency of nanocellulose through the coreflooding test:

- Total of 7.7 pore volumes (PV) of formation brine was injected into the core plug with varying flow rates (5 cc/min and 10 cc/min) and differential pressure (dP) in the core plug sample was monitored (Figure 6.23).

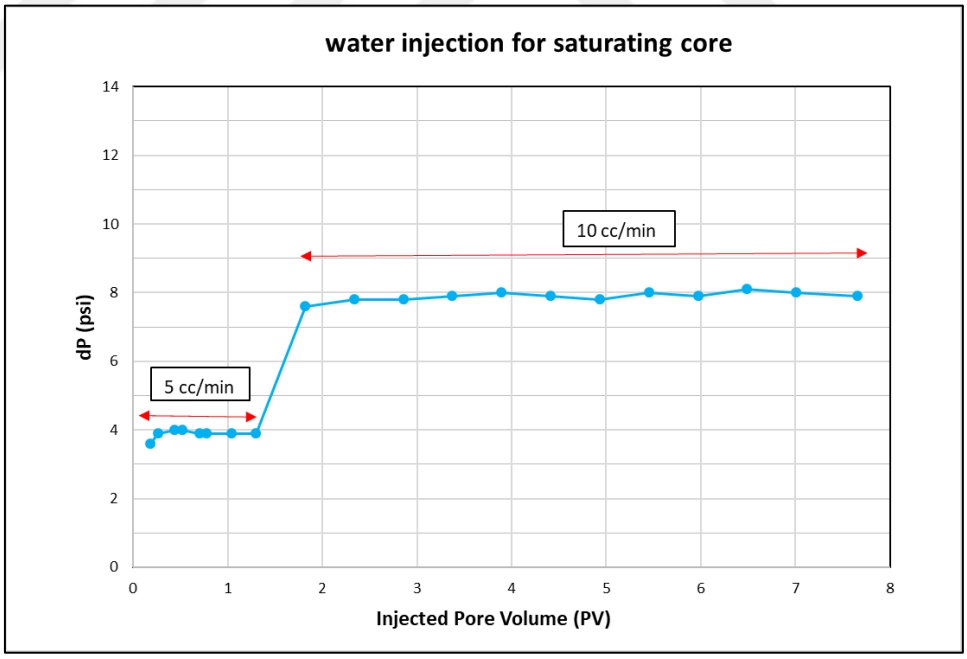

Figure 6.23: Water injection for saturating core plug #207

- Subsequently, total 8.7 PV of dead oil was injected into the system with a constant flow rate, and the cumulative volume of water produced was

recorded. Oil permeability (ko) at irreducible water saturation (Swi) was measured by injecting oil at varying flow rates. Flow rates was applied as 1 cc/min, 3cc/min and 5 cc/min and differential pressure (dP) in the core plug sample vs. injected PV was monitored as shown in Figure 6.24.

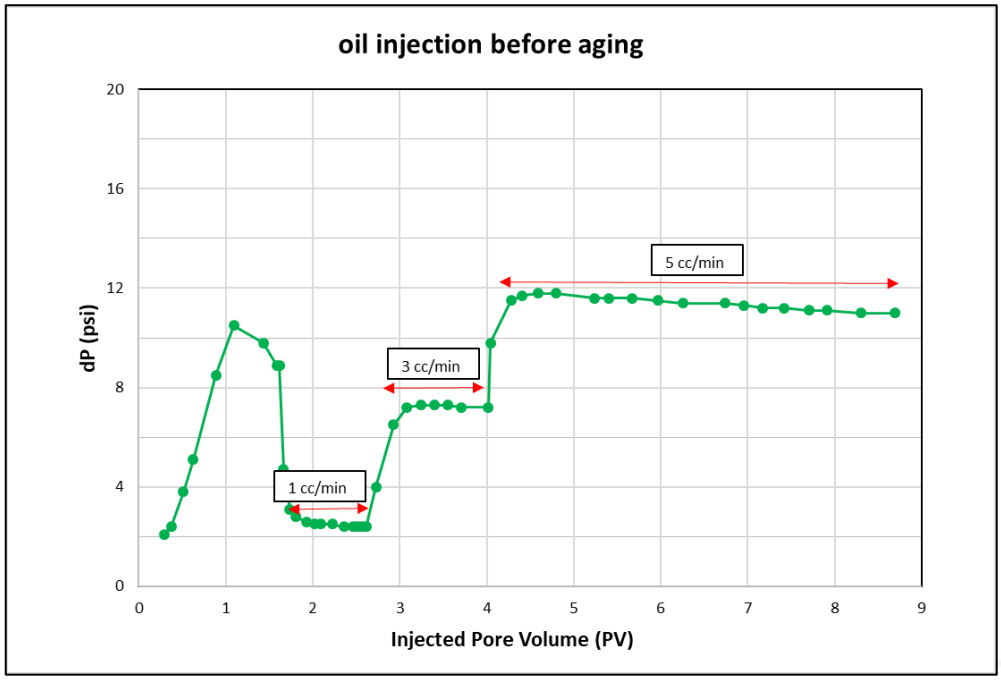

Figure 6.24: Oil injection before aging for plug #207

- Then, the system is left for the aging process for at least four weeks at reservoir temperature and net confining stress.
- Next, synthetic formation water injection took place in order to reach residual oil saturation (Sor) condition. 2.1 PV water was injected through the core plug with a flow rate of 1 cc/min. Once the pressure and saturation are stabilized at 100% water fractional flow, the injection rate is increased up to 3 and 5 times (bump flood) to reduce any possible capillary end effect. During the test, the pressure difference (dP) across the plug is closely monitored for permeability calculations (Figure 6.25). Throughout these periods, the recovery of oil from the core was constantly monitored. Water injection was stopped when a water cut of 99.5% was attained. During the

waterflood, a total of 6.1 PV of brine was injected with a recovery of 66.0% OOIP.

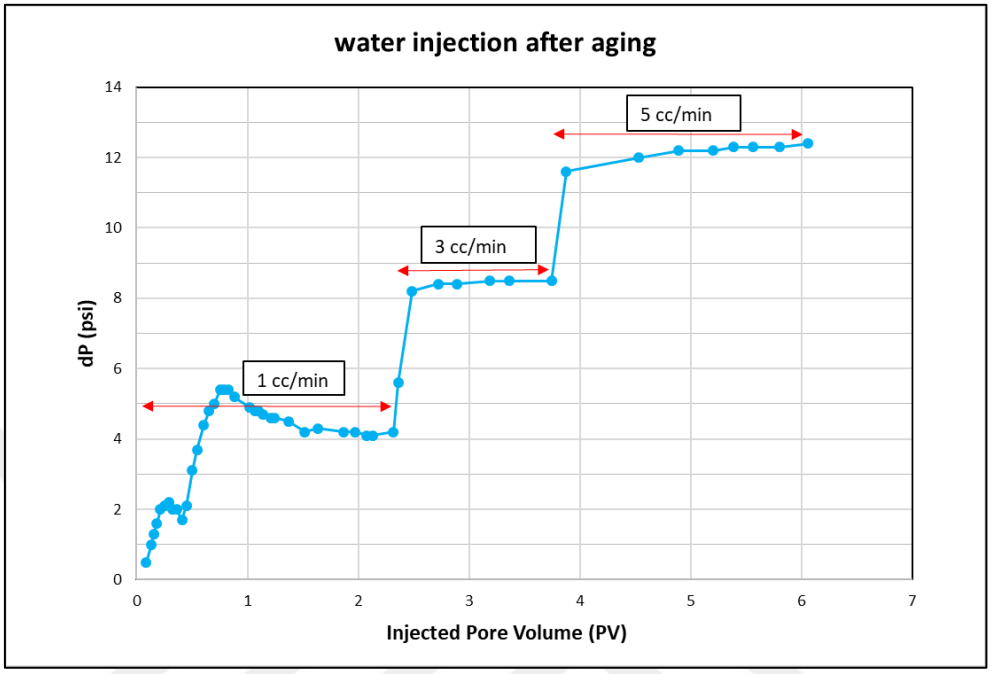

Figure 6.25: Oil injection after aging for plug #207

- 0.5 wt% nanocellulose solution was introduced into the core plug with a flow rate of 1 cc/min and 3 cc/min. A total of 4.7 PV of this solution was injected until a water cut of 99.5% was reached with a recovery of 11.3% OOIP (Figure 6.26). The steady-state conditions could not be achieved due to an increasing pressure difference (dP) while maintaining a constant flow rate.
- Then, the system was left for a soaking process for 24 hours before the water flood.
- After the completion of the nanocellulose flooding and soaking process, synthetic formation water injection was repeated to measure permeability and recover additional oil left in the core plug.
- Finally, a total of 11.2 PV synthetic formation water was injected with a flow rate of 1 cc/min and 3 cc/min (bump flow) to recover the remaining oil in the plug sample (Figure 6.27). Water injection continued until a water cut of

99.5% was achieved. The incremental oil recovery during the water flood was 4.3% OOIP and the total oil recovery reached 81.6%.

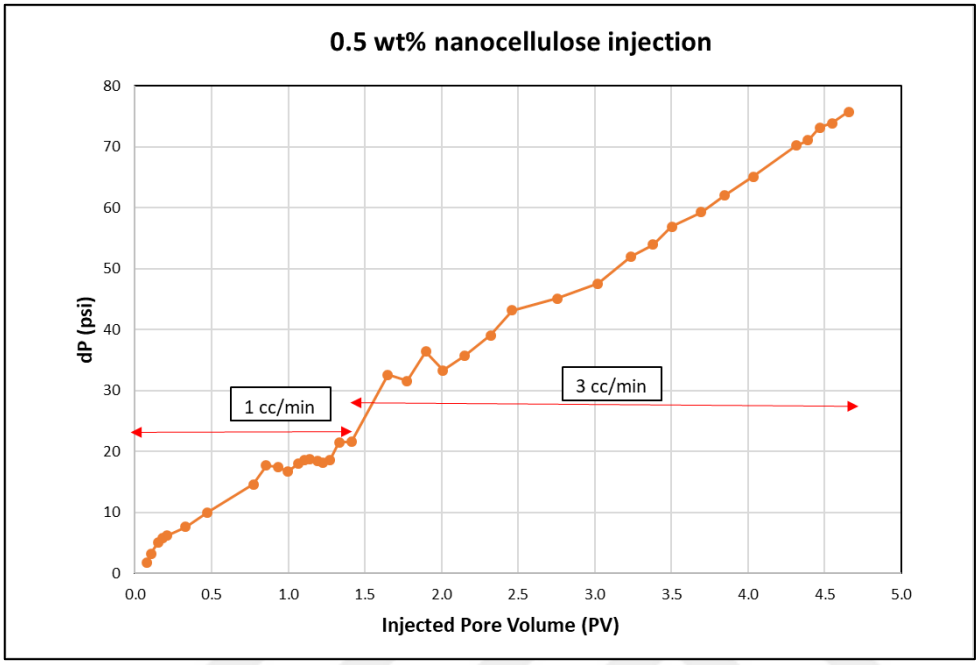

Figure 6.26: 0.5 wt% nanocellulose injection to plug #207

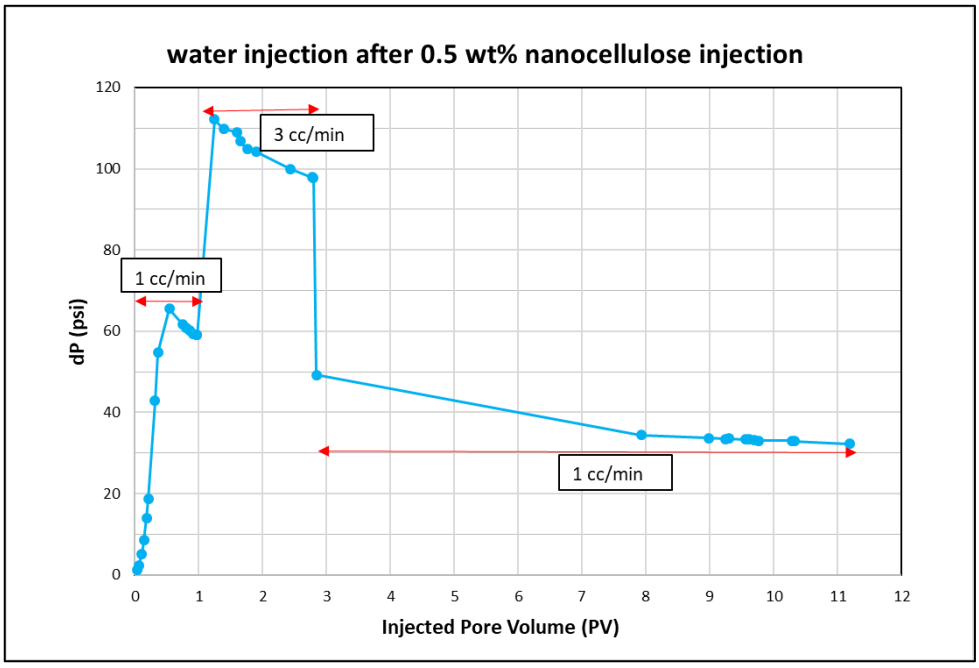

Figure 6.27: Water injection after 0.5 wt% nanocellulose soaking, plug #207

Table 6.21 displays the values of irreducible water saturation, residual oil saturation, and initial oil recovery obtained from test #6 performed on core plug #207.

Table 6.21: Saturation results for test #6

Test No	Plug No	Swi (%)	Sor (%)	Oil Recovery (%)
6	207	26.8	24.9%	66.0%

Additional oil recovery values by injection of nanocellulose and water injection to plug #207 is presented in Table 6.22.

Table 6.22: Oil recovery test results for plug #207

Initial Oil Recovery (%)	Additional Oil Recovery by Nanocellulose (% OOIP)	Additional Oil Recovery by Water Injection after Nanocellulose (% OOIP)	Incremental Oil Recovery by Nanocellulose+Water Injection (% OOIP)	Total Oil Recovery (% OOIP)
66.0%	11.3%	4.3%	15.6%	81.6%

6.1.7 Coreflood Test #7

Saturated core plug #209 is placed in the core holder and heated up to reservoir temperature, 65 °C. Overburden pressure and back pressure are set to 1,500 psi and 550 psi, respectively. All the fluids (dead oil from the field and synthetic formation water) are placed into accumulators and heated to the reservoir temperature. Test conditions for coreflood test #7 are given in Table 6.23.

Table 6.23: Test conditions for test #7 with plug #209

Test No	Plug No	Overburden Pressure (psi)	Back Pressure (psi)	Test Temp (°C)	Salinity (ppm)	API Gravity of Oil
7	209	1,500	550	65	20,000	36

The below procedure was followed for testing enhanced oil recovery efficiency of nanocellulose through coreflooding test:

- Total of 10 pore volumes (PV) of formation brine was injected into the core plug with varying flow rates (1 cc/min, 3 cc/min, and 5 cc/min) and differential pressure (dP) in the core plug sample for each flow rate was monitored as shown in Figure 6.28.

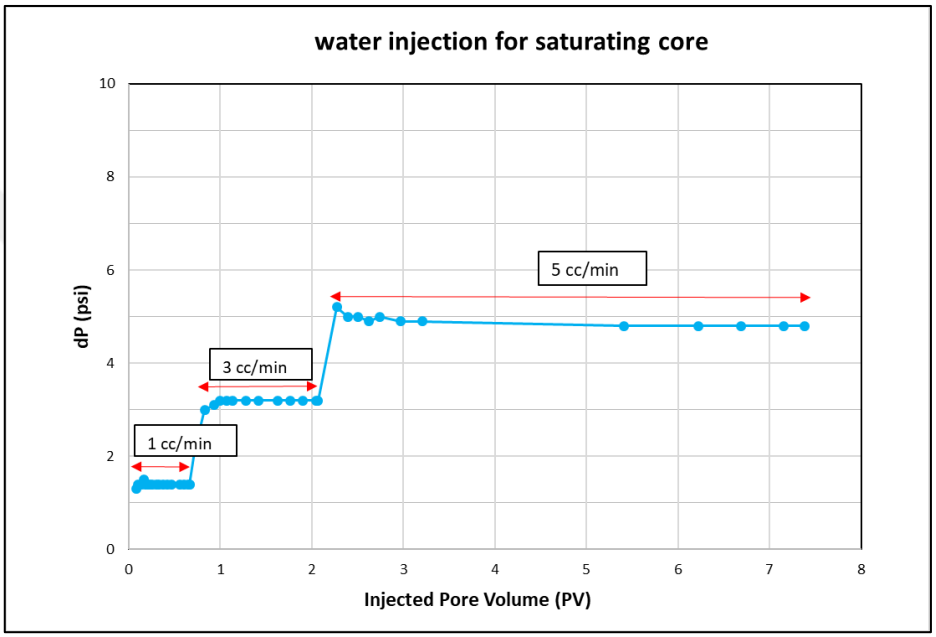

Figure 6.28: Water injection for saturating core plug #209

- Subsequently, total of 8.6 PV of dead oil was injected into the system with a constant flow rate, and the cumulative volume of water produced was recorded. Oil permeability (ko) at irreducible water saturation (Swi) was measured by injecting oil at varying flow rates. Flow rates was applied as 1 cc/min and 3cc/min and differential pressure (dP) in the core plug sample vs. injected PV was monitored as shown in Figure 6.29.

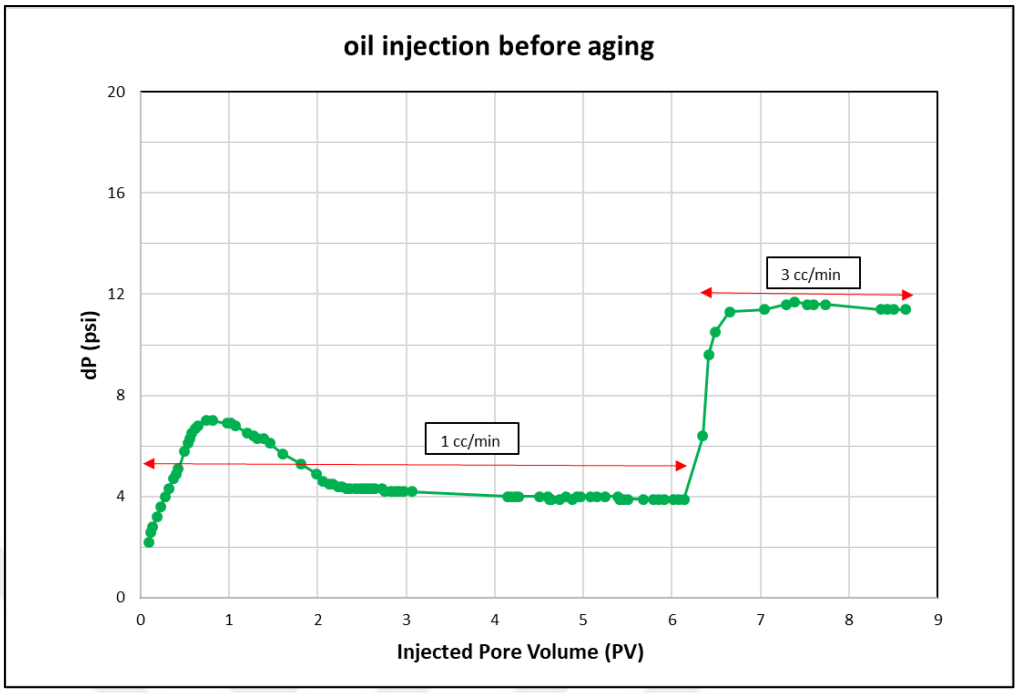

Figure 6.29: Oil injection before aging for plug #209

- Then, the system is left for the aging process for at least four weeks at reservoir temperature and net confining stress.
- Next, synthetic formation water injection took place in order to reach residual oil saturation (Sor) condition. A total of 6.2 PV water was injected through the core plug with a flow rate of 1 cc/min. During the test, the pressure difference (dP) across the plug is closely monitored for permeability calculations (Figure 6.30). Throughout these periods, the recovery of oil from the core was constantly monitored. Water injection was stopped when a water cut of 99.5% was attained. Brine was injected with a recovery of 59.6% OOIP.

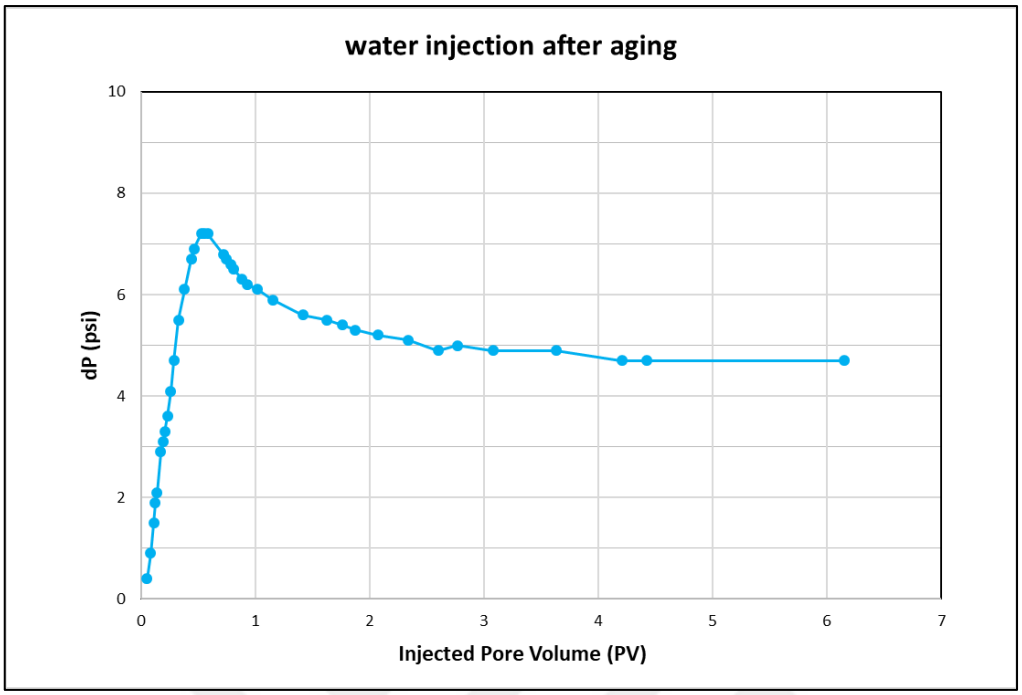

Figure 6.30: Water injection after aging of plug #209

- 0.5 wt% nanocellulose solution was introduced into core plug with a flow rate of 1 cc/min. A total of 3.3 PV of this solution was injected until a water cut of 99.5% was reached with a recovery of 9.6% OOIP (Figure 6.31). The steady-state conditions could not be achieved due to an increasing pressure difference (dP) while maintaining a constant flow rate.
- Then, the system was left for a soaking process for 24 hours before the water flood.
- After the completion of the nanocellulose flooding and soaking process, synthetic formation water injection was repeated to measure permeability and recover additional oil left in the core plug.
- Finally, a total of 6.4 PV synthetic formation water was injected with a flow rate of 1 cc/min and 2 cc/min (bump flow) to recover the remaining oil in the plug sample (Figure 6.32). Water injection continued until a water cut of 99.5% was achieved. The incremental oil recovery during water flood was 0.9% OOIP and the total oil recovery reached 70.2%.

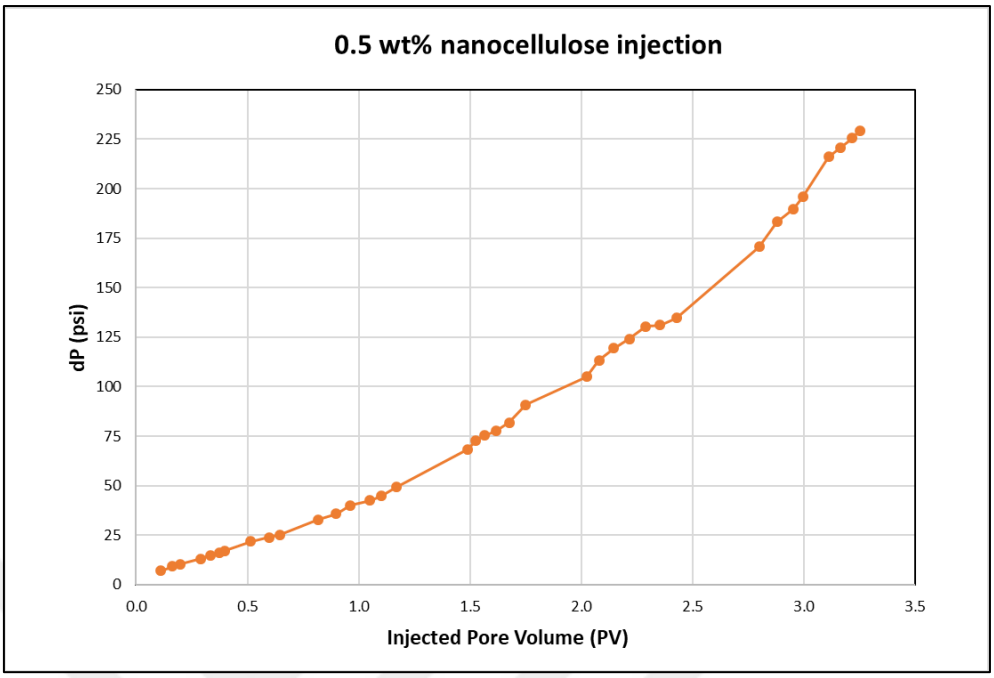

Figure 6.31: 0.5 wt% nanocellulose injection to plug #209

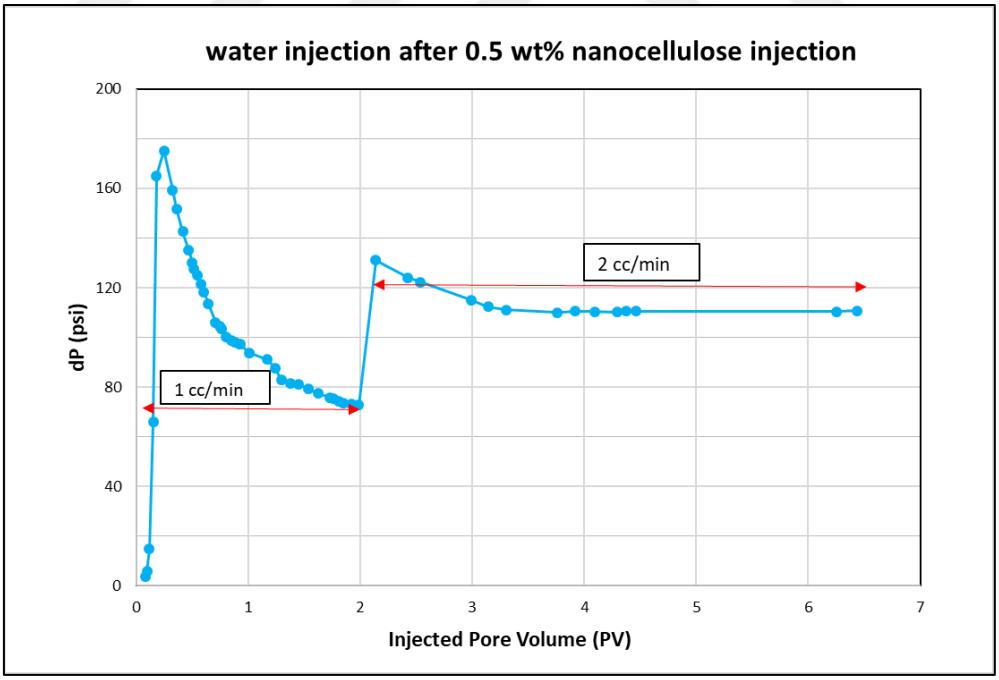

Figure 6.32: Water injection after 0.5 wt% nanocellulose soaking, plug #209

Table 6.24 displays the values of irreducible water saturation, residual oil saturation, and initial oil recovery obtained from test #7 performed on core plug #209.

Table 6.24: Saturation results for test #7

Test No	Plug No	Swi (%)	Sor (%)	Oil Recovery (%)
7	209	47.1	21.4%	59.6%

Additional oil recovery values by injection of nanocellulose and water injection to plug #209 are presented in Table 6.25.

Table 6.25: Oil recovery test results for plug #209

Initial Oil Recovery (%)	Additional Oil Recovery by Nanocellulose (% OOIP)	Additional Oil Recovery by Water Injection after Nanocellulose (% OOIP)	Incremental Oil Recovery by Nanocellulose+Water Injection (% OOIP)	Total Oil Recovery (% OOIP)
59.6%	9.6%	0.9%	10.5%	70.2%

6.2 XRD Analysis Results

Core plug samples #211, #347 and #346 were trimmed into smaller sections (Figure 6.33) before and after the coreflood tests to see the mineralogical content of each sample before and after introducing the nanocellulose into the core plug samples. These samples were chosen to perform XRD analysis before and after oil recovery coreflood tests, due to the fact that higher nanocellulose concentrations (2 wt% nanocellulose for core plug #211 and #347, and 1 wt% nanocellulose for core plug #346) were used during these core plug samples' coreflood tests. The core plugs, on which low concentration nanocellulose (0.5 wt%) was applied for oil recovery, were not chosen for comparison of the mineralogy of the rock before and after the test.

Figure 6.33: End trim samples of core plug 211, 347 and 346 before and after oil recovery coreflood tests

Table 6.26 presents the summarized results of X-ray diffraction (XRD) analysis conducted on core plug samples before and after the coreflood tests. The detailed XRD raw data can be found in the Appendix A.

According to Table 6.26, the mineralogical content of all the rock samples consists predominantly of calcite, typical for carbonate rocks, accounting for almost 100% of the composition. After the nanocellulose treatments at concentrations of 2 wt% and 1 wt%, the mineralogical content of the samples remained constant. This indicates that the application of nanocellulose, even at different concentrations, did not alter the rock's mineralogical composition. The constant mineralogical content observed is likely due to the preflush step conducted after nanocellulose soaking, which helped preserve the original mineralogical composition of the rock samples during the coreflood tests.

Table 6.26: XRD analysis results for core plug samples #211, #347, and #346

Sample Name	XRD Bulk Powder Mineralogy (wt%)							Total (%)
	Quartz	Feldspar		Calcite	Dolomite	Pyrite	Total Clay+ Mica	
		Plagioclase	Alkaline Feldspar					
211-Before	-	-	-	100	-	-	-	100
211-After	-	-	-	100	-	-	-	100
347-Before	1	-	-	99	-	-	-	100
347-After	1	-	-	99	-	-	-	100
346-Before	-	-	-	100	-	-	-	100
346-After	-	-	-	100	-	-	-	100

6.3 SEM/EDS Analysis Results

In addition to XRD analysis, SEM/EDS analysis was performed to analyze the surface of rock samples to check whether the rock samples contain any nanocellulose sample or not. These analyses were performed for core plug sample #347 both before and after oil recovery tests with nanocellulose. The end trim samples (Figure 6.33), trimmed for XRD analysis, were used for this purpose.

6.3.1 Results for Before Nanocellulose Oil Recovery Tests

Prior to conducting any flow tests, EDS/SEM analysis was carried out to assess the original condition of the sample. This analysis provides valuable insights into the composition and characteristics of the sample, allowing to understand its initial state before subjecting it to any experimental procedures. First of all, the sample in Figure 6.34 was used to analyze with SEM/EDS before conducting coreflood test.

First SEM image of core sample #347 before coreflood tests can be seen in Figure 6.35. The EDS analysis results of specific points indicated in this image (01, 02, and 03) is presented in Figure 6.36.

Figure 6.34: Sample used for before nanocellulose oil recovery test (core plug #347)

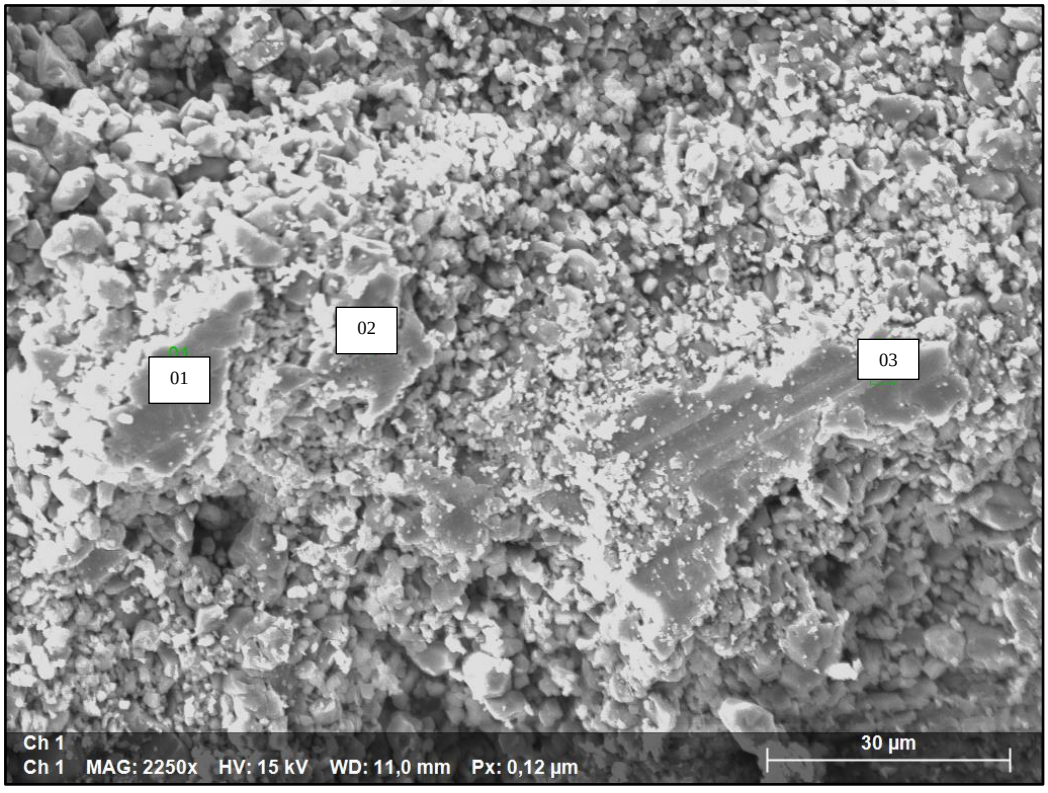

Figure 6.35: SEM image-1 of core sample #347 before coreflood tests

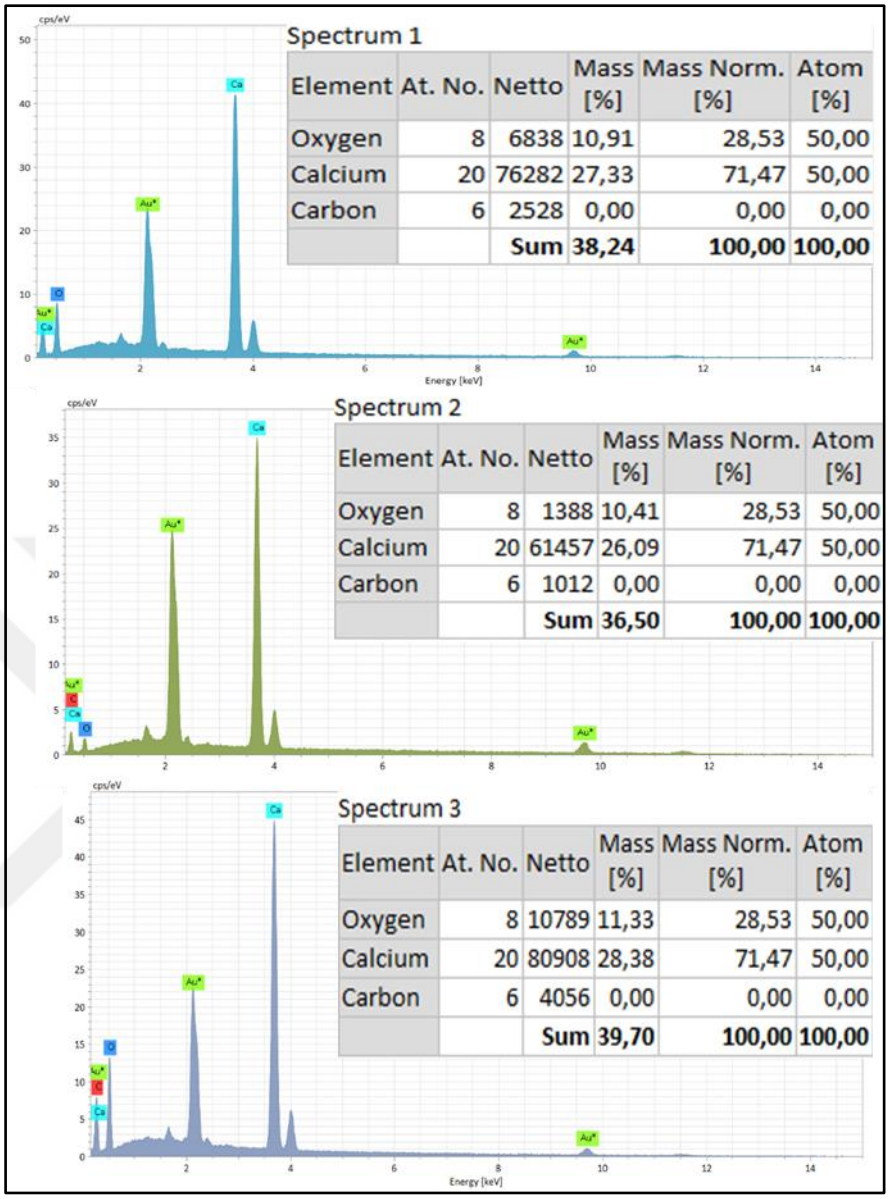

Figure 6.36: EDS results for the points (01, 02 and 03) mentioned in Figure 6.35

The EDS results obtained from each specific point in Figure 6.36 indicate that the sample is composed of carbon, calcium, and oxygen, which is consistent with the presence of calcium carbonate. These results align with the expectations based on the X-ray diffraction (XRD) analysis conducted earlier. The EDS analysis further confirms the mineralogical composition of the sample as calcium carbonate and provides additional evidence to support the XRD findings.

Second SEM image of core sample #347 before coreflood tests can be seen in Figure 6.37. The EDS analysis results of specific points indicated in this image (01, 02, and 03) is presented in Figure 6.38.

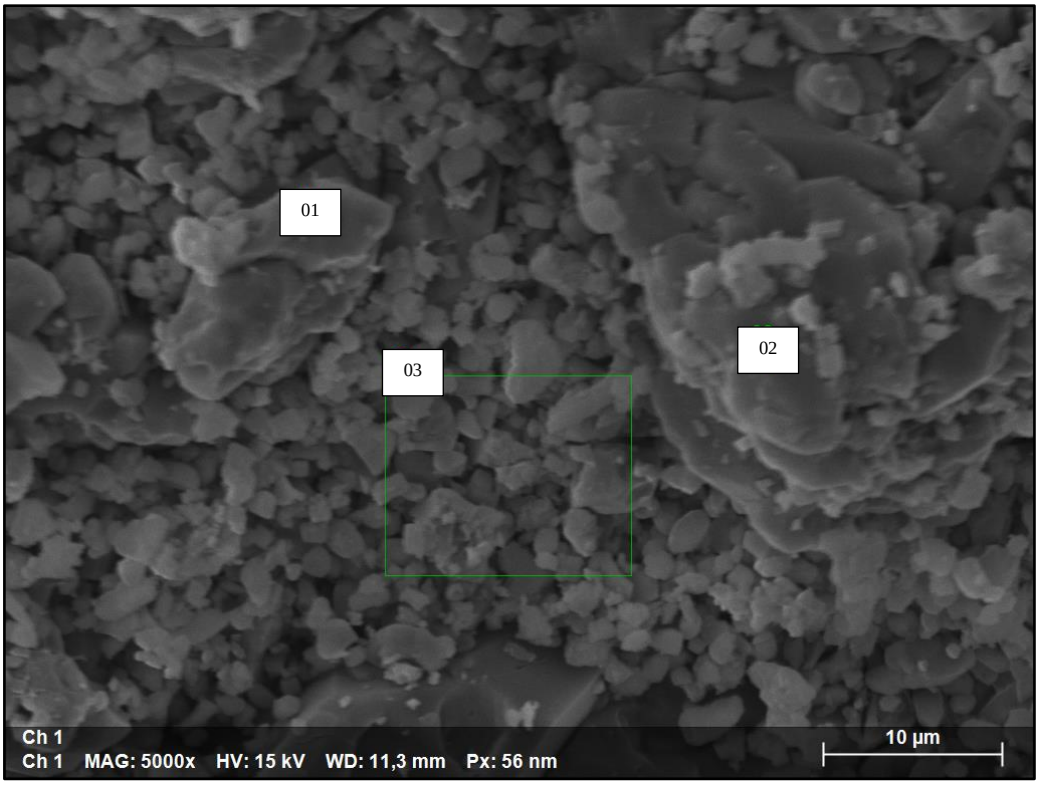

Figure 6.37: SEM image-2 of core sample #347 before coreflood tests

In the second image shown in Figure 6.37, different structures were analyzed using EDS, and the results were almost identical to the previous image, despite the differences in appearance between the structures. The EDS analysis revealed similar elemental compositions, with carbon, calcium, and oxygen being the dominant elements, confirming the presence of calcium carbonate in these structures. This consistency in results strengthens the conclusion that the samples consist mainly of calcium carbonate, even though the structures may appear visually distinct.

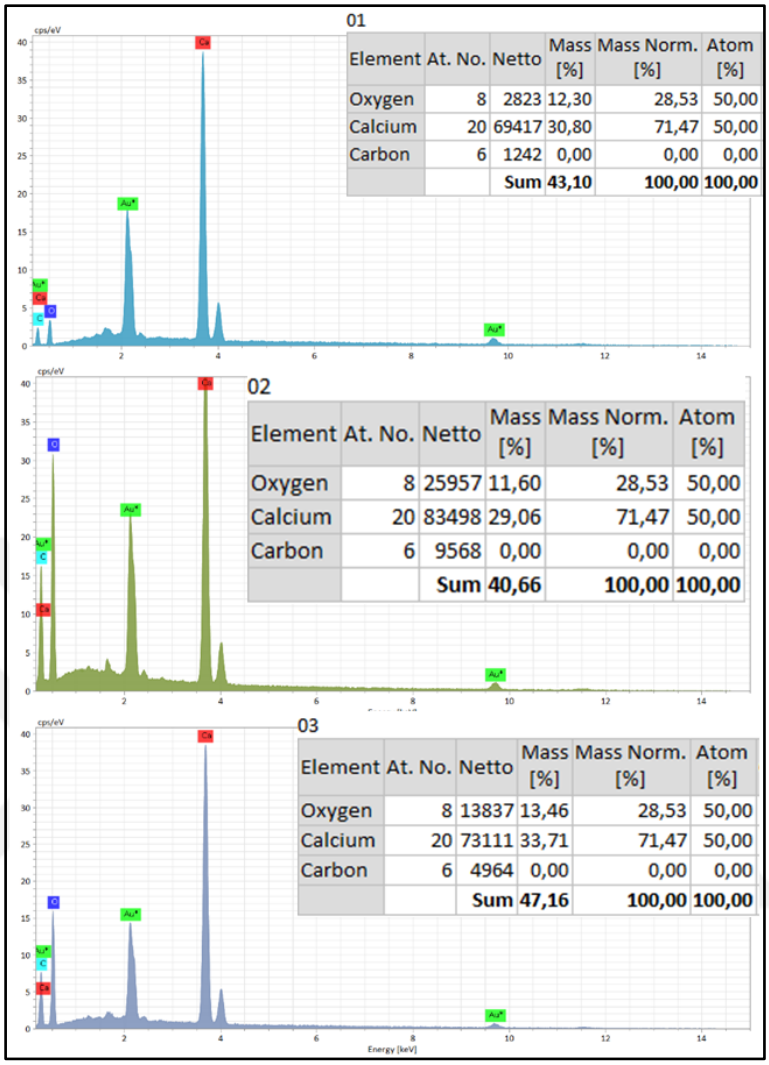

Figure 6.38: EDS results for the points (01, 02 and 03) mentioned in 6.37

6.3.2 Results for After Nanocellulose Oil Recovery Tests

The samples in Figure 6.39 were used to analyze with SEM/EDS after conducting coreflood test. First of all, the sample on the left was used for SEM/EDS analysis.

The first SEM image of core sample #347 (sample in the left in Figure 6.39) after the oil recovery test with 2 wt% nanocellulose can be seen in Figure 6.40. The EDS analysis results of specific points indicated in this image (01, 02, and 03) is presented in Figure 6.41.

Figure 6.39: Samples used for after oil recovery test with 2 wt% nanocellulose (core plug #347)

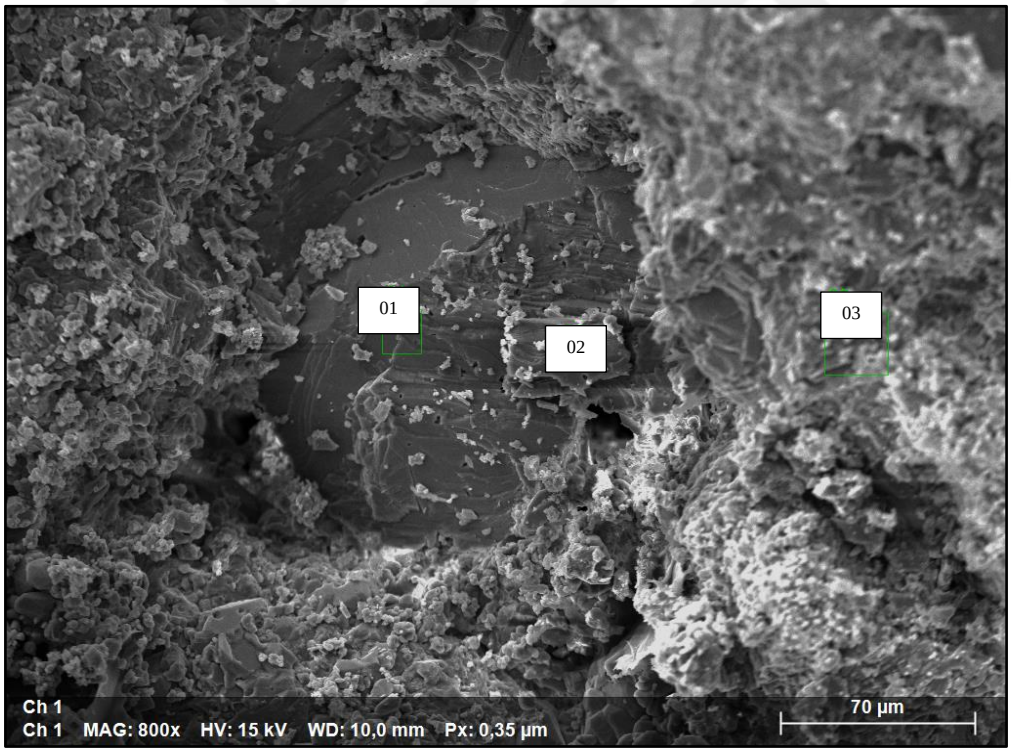

Figure 6.40: SEM image-1 of core sample #347 (sample in the left in Figure 6.39) after oil recovery test with 2 wt% nanocellulose

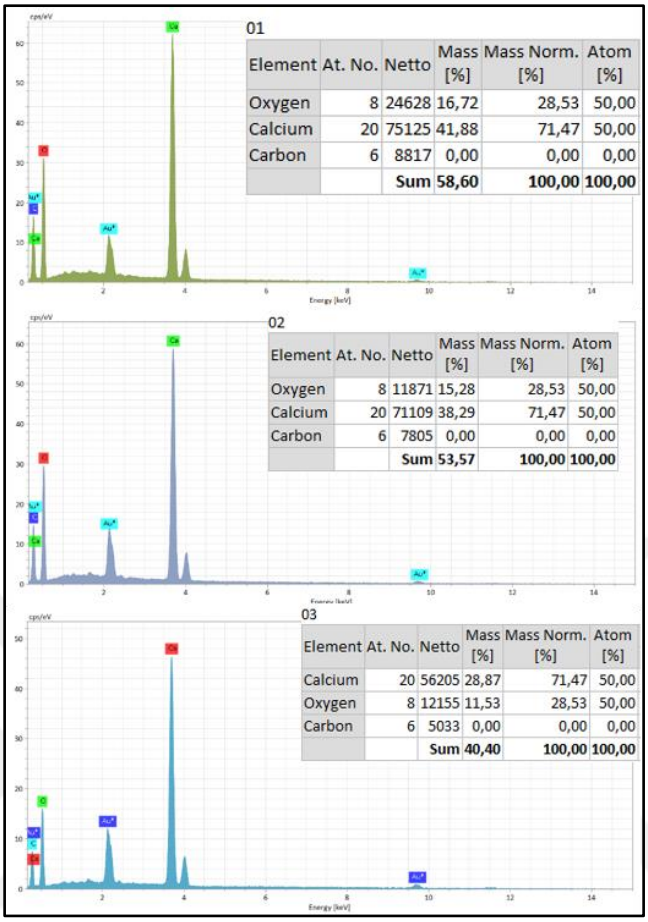

Figure 6.41: EDS results for the points (01, 02 and 03) mentioned in Figure 6.40

Second SEM image of core sample #347 (sample in the left in Figure 6.39) after the oil recovery test with 2 wt% nanocellulose can be seen in Figure 6.42. The EDS analysis results of specific points indicated in this image (01, 02, and 03) is presented in Figure 6.43.

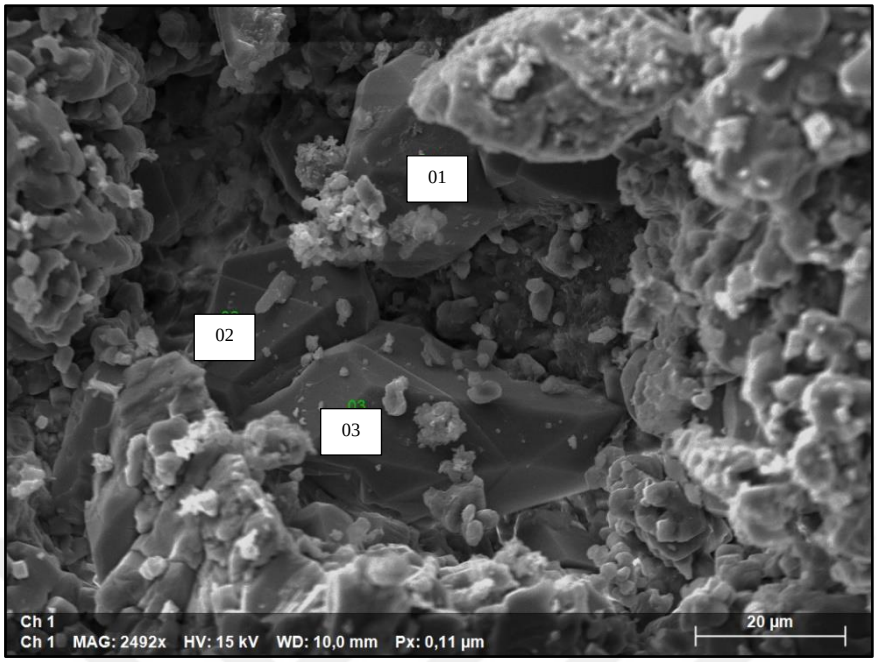

Figure 6.42: SEM image-2 of core sample #347 (sample in the left in Figure 6.39) after oil recovery test with 2 wt% nanocellulose

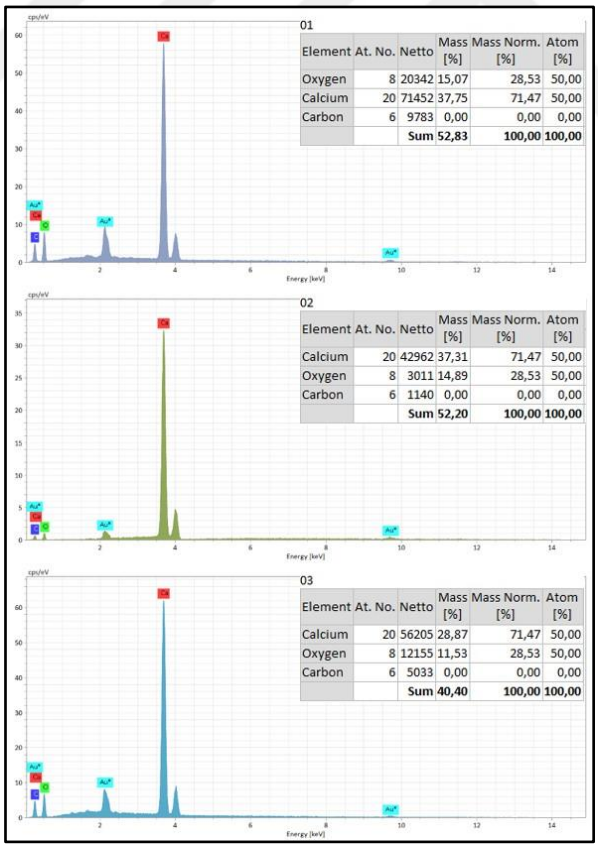

01

Element	At. No.	Netto	Mass [%]	Mass Norm. [%]	Atom [%]
Oxygen	8	20342	15,07	28,53	50,00
Calcium	20	71452	37,75	71,47	50,00
Carbon	6	9783	0,00	0,00	0,00
		Sum	**52,83**	**100,00**	**100,00**

02

Element	At. No.	Netto	Mass [%]	Mass Norm. [%]	Atom [%]
Calcium	20	42962	37,31	71,47	50,00
Oxygen	8	3011	14,89	28,53	50,00
Carbon	6	1140	0,00	0,00	0,00
		Sum	**52,20**	**100,00**	**100,00**

03

Element	At. No.	Netto	Mass [%]	Mass Norm. [%]	Atom [%]
Calcium	20	56205	28,87	71,47	50,00
Oxygen	8	12155	11,53	28,53	50,00
Carbon	6	5033	0,00	0,00	0,00
		Sum	**40,40**	**100,00**	**100,00**

Figure 6.43: EDS results for the points (01, 02 and 03) mentioned in Figure 6.42

First SEM image of core sample #347 (sample in the right in Figure 6.39) after oil recovery test with 2 wt% nanocellulose can be seen in Figure 6.44. The EDS analysis results of the specific point indicated in this image (01) is presented in Figure 6.45.

Figure 6.44: SEM image-1 of core sample #347 (sample in the right in Figure 6.39) after oil recovery test with 2 wt% nanocellulose

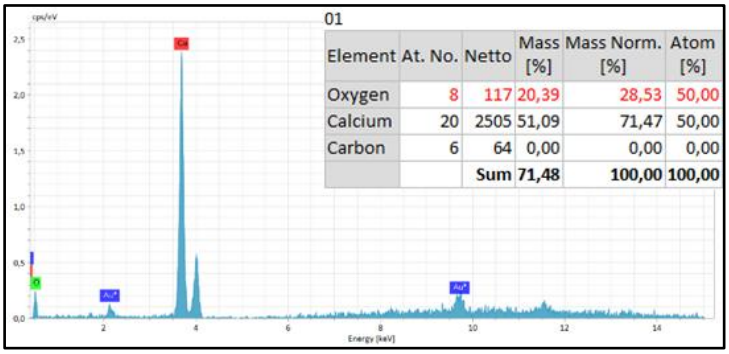

Figure 6.45: EDS results for the point (01) mentioned in Figure 6.44

The second SEM image of core sample #347 (sample in the right in Figure 6.39) after the oil recovery test with 2 wt% nanocellulose can be seen in Figure 6.46. The EDS analysis results of specific point indicated in this image (01) is presented in Figure 6.47.

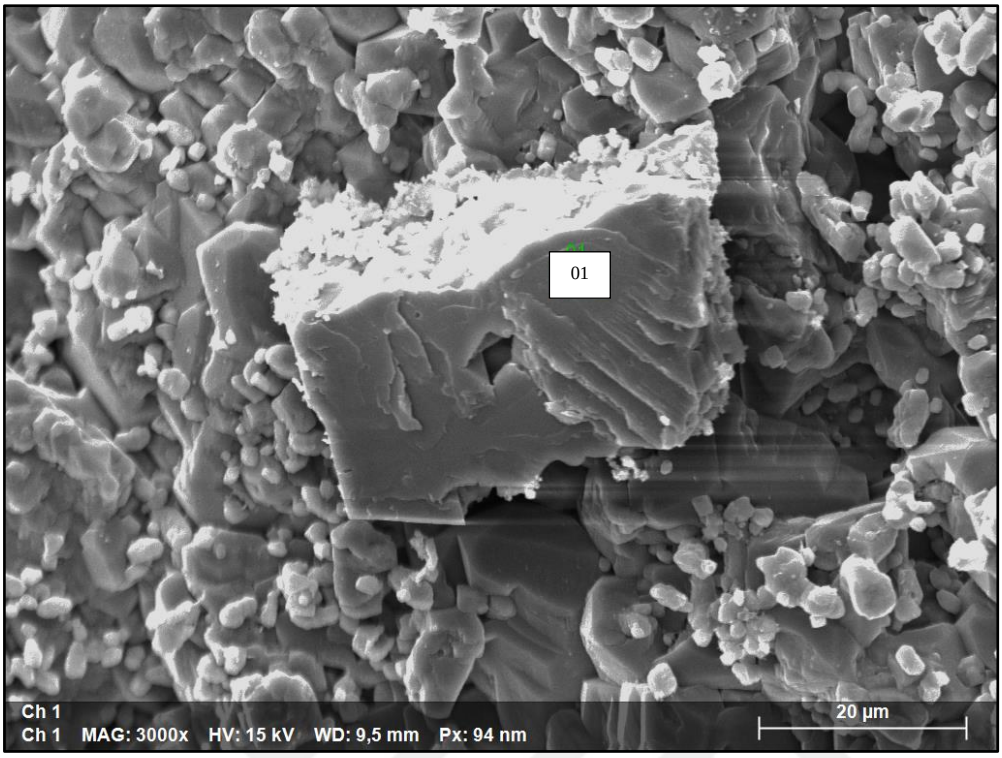

Figure 6.46: SEM image-2 of core sample #347 (sample in the right in Figure 6.39) after oil recovery test with 2 wt% nanocellulose

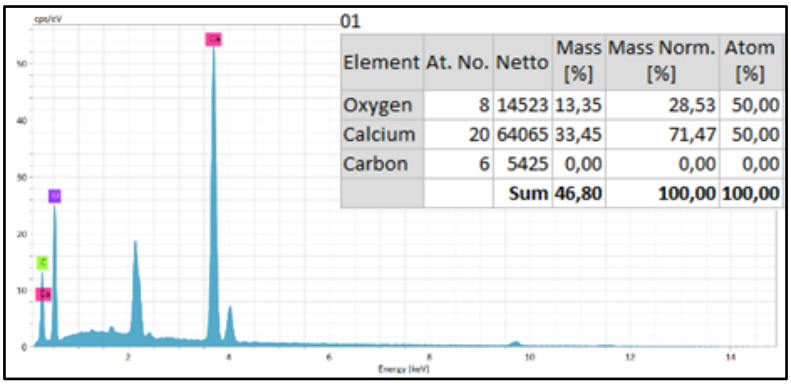

Figure 6.47: EDS results for the point (01) mentioned in Figure 6.46

The third SEM image of core sample #347 (sample in the right in Figure 6.39) after the oil recovery test with 2 wt% nanocellulose can be seen in Figure 6.48. The EDS analysis results of specific points indicated in this image (01, 02, and 03) is presented in Figure 6.49.

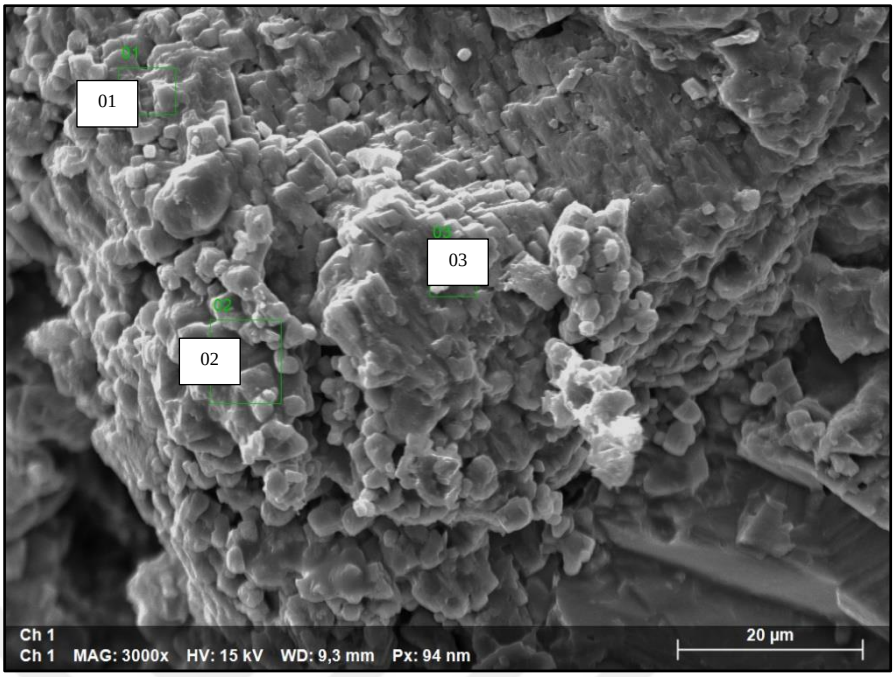

Figure 6.48: SEM image-3 of core sample #347 (sample in the right in Figure 6.39) after oil recovery test with 2 wt% nanocellulose

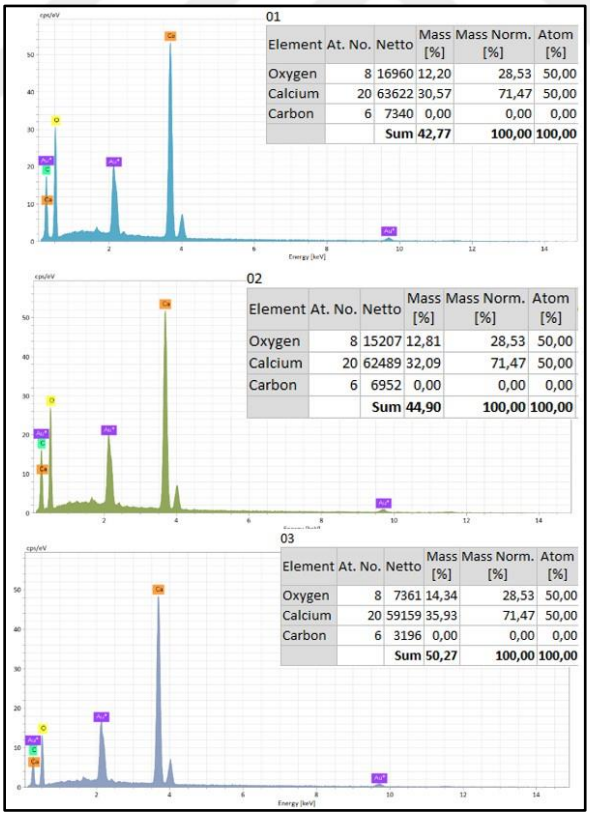

01

Element	At. No.	Netto	Mass [%]	Mass Norm. [%]	Atom [%]
Oxygen	8	16960	12,20	28,53	50,00
Calcium	20	63622	30,57	71,47	50,00
Carbon	6	7340	0,00	0,00	0,00
		Sum	42,77	100,00	100,00

02

Element	At. No.	Netto	Mass [%]	Mass Norm. [%]	Atom [%]
Oxygen	8	15207	12,81	28,53	50,00
Calcium	20	62489	32,09	71,47	50,00
Carbon	6	6952	0,00	0,00	0,00
		Sum	44,90	100,00	100,00

03

Element	At. No.	Netto	Mass [%]	Mass Norm. [%]	Atom [%]
Oxygen	8	7361	14,34	28,53	50,00
Calcium	20	59159	35,93	71,47	50,00
Carbon	6	3196	0,00	0,00	0,00
		Sum	50,27	100,00	100,00

Figure 6.49: EDS results for the points (01, 02 and 03) mentioned in Figure 6.48

The EDS results obtained from the samples after the coreflood tests with nanocellulose show similar outcomes to the ones observed before flow tests with nanocelllose. The elemental composition of carbon, calcium, and oxygen remains consistent, indicating that the presence of nanocellulose during the coreflood tests did not significantly alter the mineralogical composition of the sample. This finding reinforces the idea that nanocellulose treatment had no substantial impact on the original composition of the sample, and the mineralogical content remained relatively unchanged after the coreflood tests.

6.4 Thin Section Analysis

Core plug samples #211 and #347 were trimmed into smaller sections both before and after the coreflood tests to examine the mineralogical contents before and after introducing a 2 wt% nanocellulose solution into the core plug samples. These trimmed sections were subsequently ground and polished to achieve a smooth and flat surface. The prepared thin sections were placed under a petrographic microscope, allowing for analysis using polarized light microscopy. This microscopic analysis technique enables the examination and study of the mineralogical composition of the core plug samples, providing valuable insights into any changes that may have occurred as a result of the nanocellulose injection and subsequent coreflood tests.

6.4.1 Thin Section Analysis for Plug #211

Thin section core plug #211 was analyzed by polarized microscope before performing any coreflood experiment. As a general reference, in the thin section of a rock sample, the blue areas typically correspond to the pores within the rock, indicating void spaces. On the other hand, the light-brown areas represent skeletal fragments or solid components of the rock. The contrast between blue (pores) and

light-brown (skeletal fragments) helps visually identifying and understanding the rock's porosity and texture under microscope.

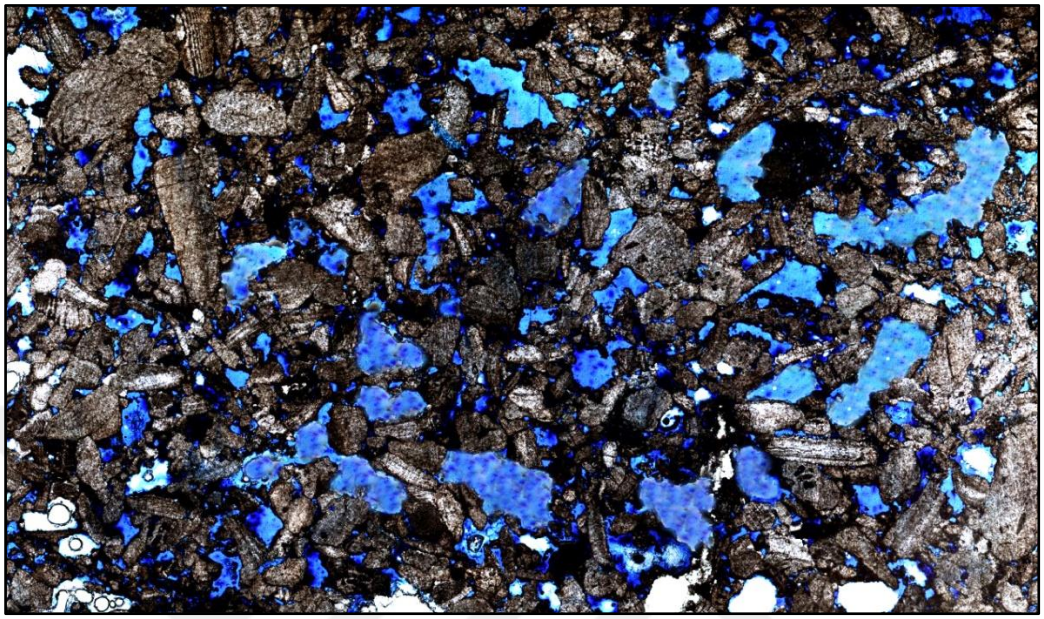

Figure 6.50: Skeletal packstone with porosity, plug #211 before coreflood tests

Based on Figure 6.50, the thin section analysis performed prior to injecting any fluids into the system reveals that the blue parts in the image represent the pores within the sample. On the other hand, the brown parts indicate the presence of skeletal fragments. The analysis helps to distinguish and visualize the pore spaces and skeletal components within the examined system.

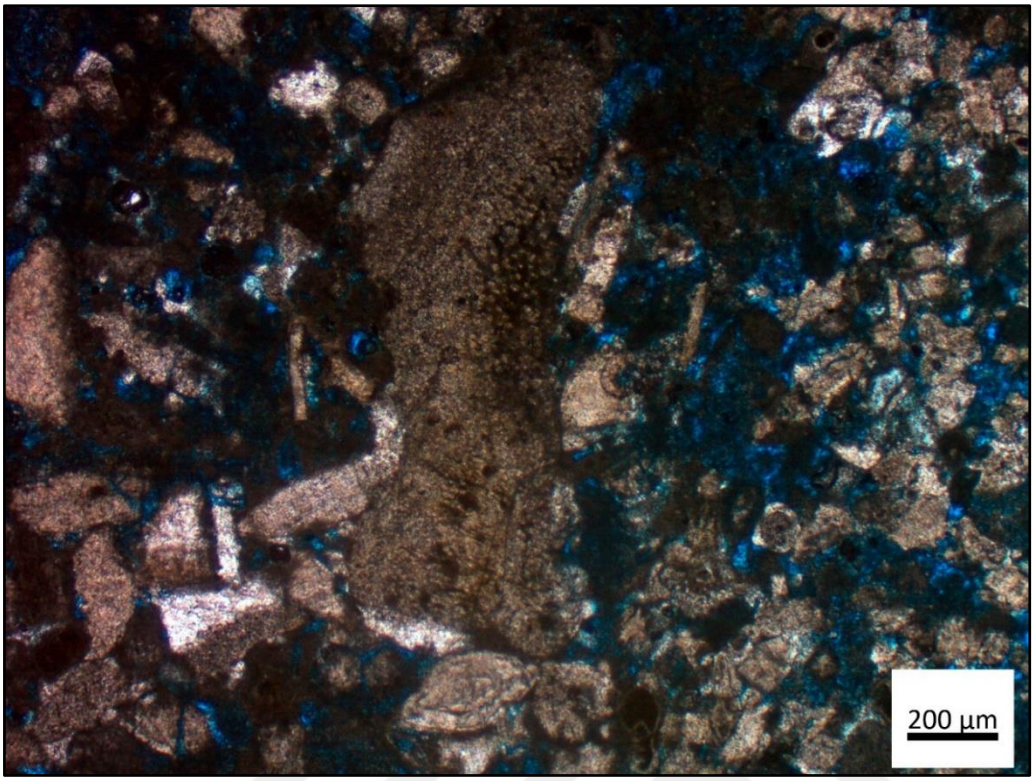

Figure 6.51: Microscope image for plug #211 after coreflood tests with nanocellulose followed by waterflood

Figure 6.51 shows that the thin section analysis of the core plug sample after nanocellulose injection followed by waterflooding reveals certain observations. The blue parts in the thin section represent pores that contain no additional fluid. Some pores still exhibit traces of oil. Notably, there is no evidence of nanocellulose present in the system, indicating that the nanocellulose has likely been displaced by the waterflooding process completely.

6.4.2 Thin Section Analysis for Plug #347

Figure 6.52, Figure 6.53 and Figure 6.54 represent the thin section views of core plug #347 prior to any experimental procedure. Skeletal packstone/rudstone type facies are commonly observed. Echinoid fragments are mostly seen as fragmented due to compaction. In addition to skeletal fragment, calcispherulids and benthic fragments can also be defined.

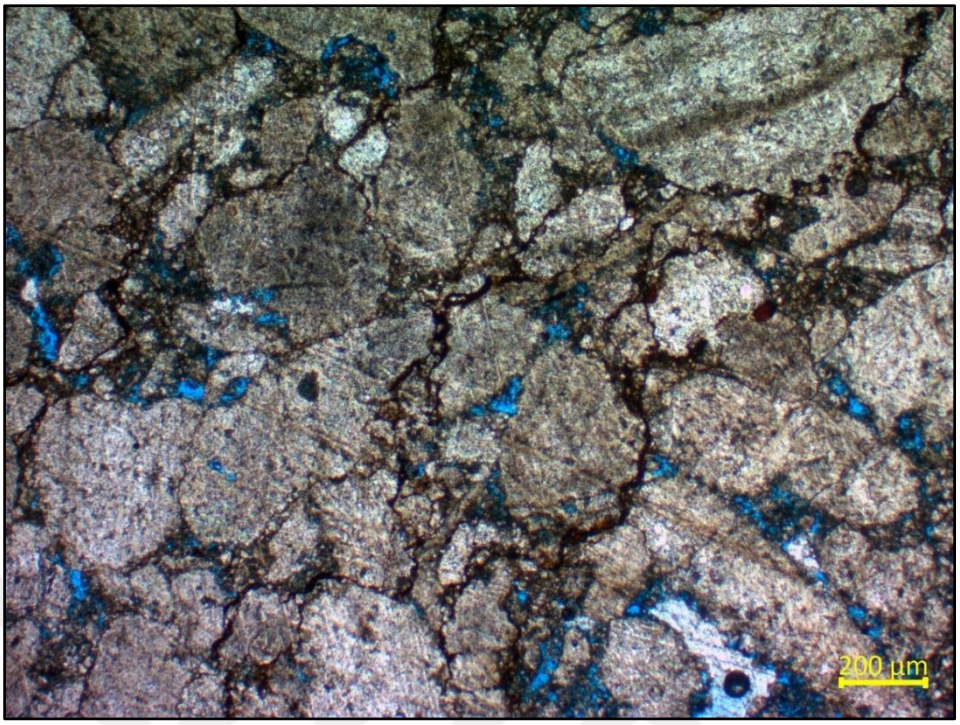

Figure 6.52: Image-1-Skeletal packstone with stylolites and vuggy porosity, plug #347 before coreflood tests

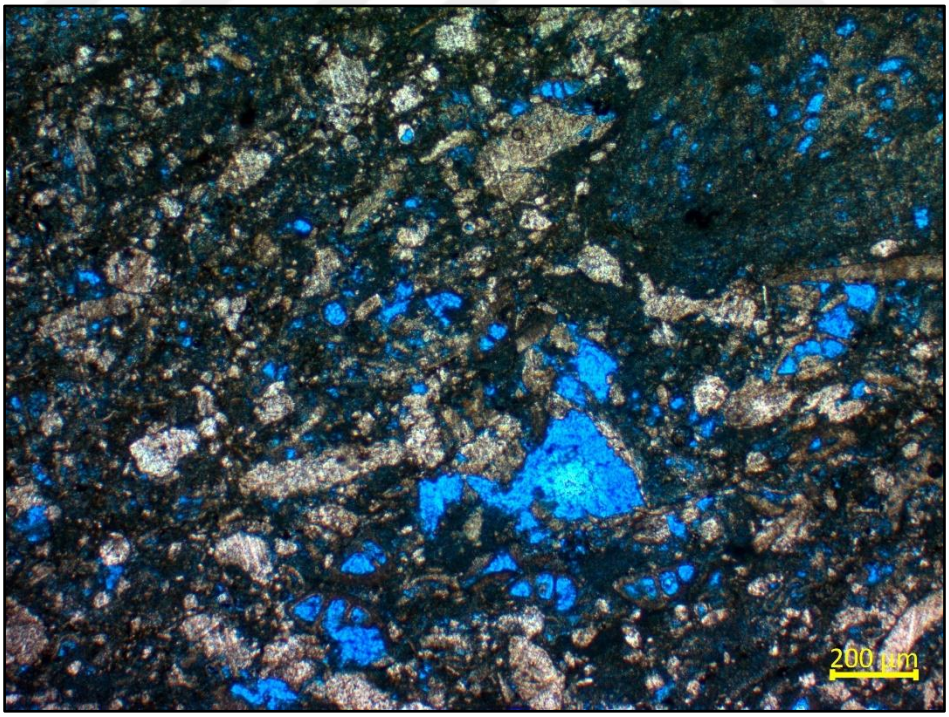

Figure 6.53: Image-2- Calcispherulid-bearing benthic foraminiferal skeletal pacsktone with moldic and vuggy porosity, plug #347 before coreflood tests

Due to the dissolution of the benthic foraminifers and calcispherulids, moldic porosity is formed (Figure 6.53 and Figure 6.54). The most common porosity type is vuggy porosity, which enhances permeability in this carbonate formation. Fracture porosity and stylolites can also increase permeability. In some other cases, stylolites can behave as barriers in the rocks.

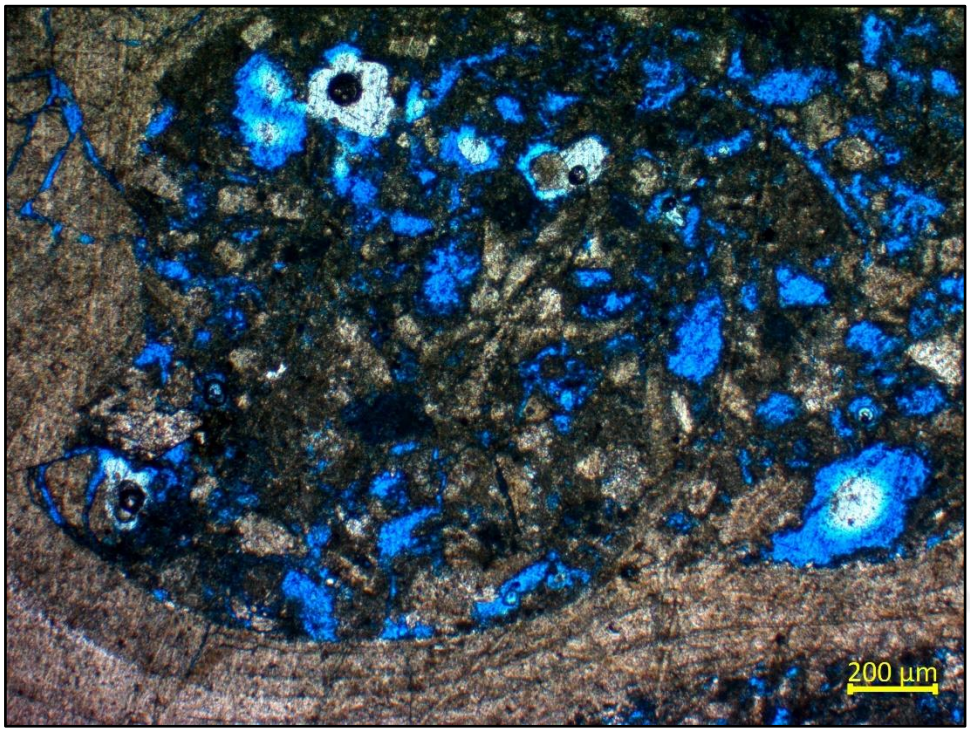

Figure 6.54: Image-3- Skeletal rudstone with fracture porosity and vuggy porosity, plug #347 before coreflood tests

Figure 6.55 displays thin section images of plug 347 after undergoing nanocellulose treatment. The blue regions seen in the thin section correspond to pores that do not contain any additional fluid. Some pores still display remnants of oil. Importantly, there is no indication of nanocellulose presence in the system, suggesting that the nanocellulose has been entirely displaced by the waterflooding process. This observation suggests that the nanocellulose has been effectively flushed out of the system during the waterflooding phase.

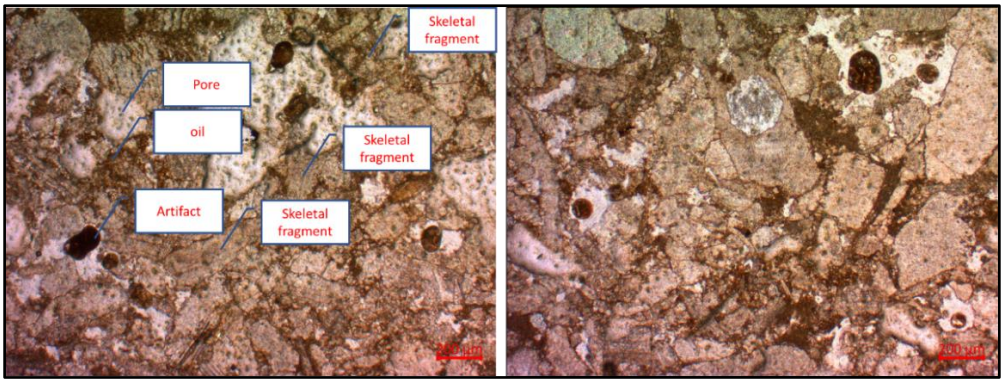

Figure 6.55: Plug #347 after coreflood tests with nanocellulose flood followed by waterflood

6.5 Discussion

To summarize, seven sets of coreflood oil recovery tests were conducted within this study to analyze the utilization of nanocellulose as an eco-friendly EOR agent. The test procedure was applied to each test as follows: core plug selection, core cleaning, routine core analysis, core saturation with synthetic formation brine, injection of oil into the system, wettability restoration by aging, steady state injection of synthetic formation brine to reach Sor, additional oil recovery by nanocellulose injection, soaking of nanocellulose in the core plug, and additional oil recovery by synthetic formation brine.

Test conditions, including overburden pressure, back pressure and test temperature and detailed information regarding formation water salinity, API gravity and viscosity of oil used for each plug sample are presented in Table 6.27. Additionally, the basic core properties of each core plug sample are also tabulated in Table 6.28.

Table 6.27: Test conditions and fluid properties for oil recovery coreflood tests

Test No	Plug No	Overburden Pressure (psi)	Back Pressure (psi)	Test Temperature (°C)	Salinity (ppm)	API Gravity of Oil	Oil Viscosity (cp)	Injected Nanocellulose Concentration wt (%)
1	210	1,250	550	65	20,000	16	202.4	2
2	211	1,500	550	65	20,000	16	202.4	2
3	347	1,500	550	65	20,000	22	14.9	2
4	346	1,500	550	65	20,000	22	14.9	1
5	213	1,500	550	65	20,000	36	2.3	1
6	207	1,500	550	65	20,000	36	2.3	0.5
7	209	1,500	550	65	20,000	36	2.3	0.5

Table 6.28: Basic core properties of each core plug

Plug Name	Depth (m)	Length (mm)	Diameter (mm)	Pore Volume (cc)	Porosity (%)	ka (md)	kL(md)	Grain Density (g/cc)
210	1217.5	69.75	37.67	20.3	26.1	218.7	198.7	2.70
211	1217.8	71.3	37.67	21.8	27.1	211.7	191.7	2.70
347	2036.2	65.9	37.7	13.5	18.2	55.6	49.0	2.69
346	2035.9	65.8	37.7	14.1	19.3	101.4	80.0	2.69
213	1219.6	70.65	37.6	18.8	24.0	136.1	124.2	2.70
207	1186.1	65.38	37.31	19.3	26.9	244.5	224.5	2.69
209	1216.9	68.67	37.8	22.7	29.0	151.7	139.4	2.70

Basically, continuous increase in pressure difference in core plug was observable for each coreflood tests during introducing nanocellulose into the system. It is most probably due to an increase in viscosity of nanocellulose at high temperature values.

According to Table 6.29, it is obvious that nanocellulose can be utilized as an enhanced oil recovery agent. In each oil recovery tests, nanocellulose was able to produce additional oil. The process of enhancing oil recovery through the introduction of nanocellulose into water involves intricate mechanisms that could involve various factors. It is better to understand the mechanisms behind this EOR process before going through results. These factors may include modifying the wettability of the rock surface, changing it from oil-wet to more water-wet, creating a log-jamming effect, and increasing the viscosity of the water phase during the flooding process. The change in wettability and other properties could potentially be driven by structural disjoining pressure.

Table 6.29: Summary of oil recovery coreflood tests

Test No	Plug No	Swi (%)	Sor (%)	Oil Recovery (%)	Additional Oil Recovery by Nanocellulose (% OOIP)	Additional Oil Recovery by Water Injection after Nanocellulose Soaking (% OOIP)	Incremental Oil Recovery by Nanocellulose+Water Injection (% OOIP)	Total Oil Recovery (% OOIP)
1	210	15.8	30.0%	64.3%	14.6%	2.9%	17.5%	81.9%
2	211	20.1	37.8%	52.7%	13.4%	2.9%	16.3%	69.0%
3	347	11.1	29.3%	67.1%	16.7%	5.0%	21.7%	88.8%
4	346	15.0	24.8%	70.8%	19.2%	5.8%	25.0%	95.8%
5	213	54.9	17.5%	61.2%	24.7%	3.5%	28.2%	89.4%
6	207	26.8	24.9%	66.0%	11.3%	4.3%	15.6%	81.6%
7	209	47.1	21.4%	59.6%	9.6%	0.9%	10.5%	70.2%

Possible oil recovery mechanism for nanocellulose particles in this study might be due to the structural disjoining pressure mechanism as mentioned previously. Studies have demonstrated that during nanoflooding, the arrangement and layering of nanoparticles create an additional pressure within the wedge film, known as structural disjoining pressure.

McElfresh et al. (2012) conducted an analysis of the disjoining pressure mechanism, focusing on electrostatic repulsion forces. As nanoparticles decrease in size, the electrostatic repulsion force between them intensifies. Moreover, an increase in the number of nanoparticles leads to a corresponding increase in this repulsive force. These particles, when present in the region where three phases converge, tend to create a wedge-like film structure. This results from the imbalanced forces at the interface among the solid, oil phase, and aqueous phase, where nanocellulose is involved in our scenario. As a consequence, the contact angle (θ) of the aqueous phase decreases nearly to zero, forming a wedge film. This wedge film acts as a barrier, effectively separating formation fluids like oil, water, and gas from the surface.

Wasan and Nikolov (2003) observed that the primary force driving the spreading of nanofluids is the gradient of the structural disjoining pressure, often referred to as film tension. This force guides nanofluids from the bulk solution toward the wedge. The film tension is most pronounced near the vertex of the wedge, owing to the arrangement of nanoparticles within the confined space, as depicted Figure 6.56. This tension prompts the nanofluids to spread at the tip of the wedge, a phenomenon amplified by the increasing film tension toward the vertex. Their study also unveiled that the spreading coefficient experiences exponential growth as the film thickness diminishes or the number of particle layers within the film reduces. As the film thickness decreases closer to the vertex of the wedge, the structural disjoining pressure intensifies.

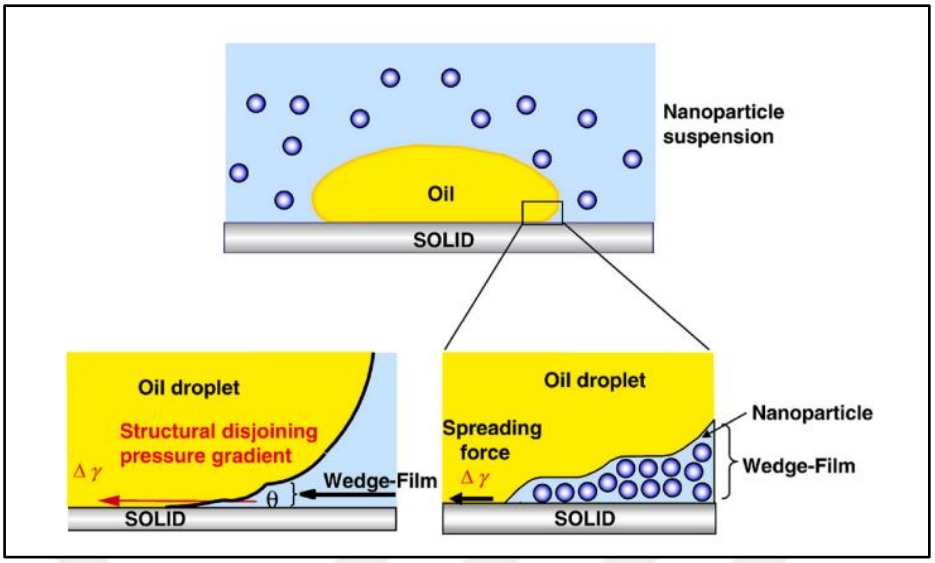

Figure 6.56: Nanoparticles organized within wedge-shaped films, resulting in a gradient of structural disjoining pressure at the wedge vertex (Wasan et al., 2011)

The interface between the nanofluid and oil cuts through the oil-solid contact, facilitating the detachment of oil droplets from the pore throat in order to extract them (Zhang et al., 2016). This process is crucial for the transportation of the nanofluid-oil interface and subsequent oil recovery. The arrangement of nanoparticles in the wedge film was proposed as the main factor responsible for changing the wettability.

Altering the wettability of a reservoir from a water-wetting system to a strongly water-wet condition plays a crucial role in enhancing oil production and is considered an important mechanism for enhanced oil recovery. Various active agents and techniques are available to modify the wettability of rock surfaces to a more favorable state (Khalil et al., 2017). Understanding the concept of disjoining pressure during nanofluid flooding is essential for comprehending the mechanism behind reducing the contact angle and changing the reservoir's wettability from oil-wet to water-wet.

The alteration of wettability can significantly enhance the effectiveness of displacing crude oil within porous media. This effect is predominantly attributed to to changes in wettability rather than alterations in interfacial tension. As noted by Chengara et

al. in 2004, under the influence of injection pressure, nanoparticles create a slim film on the rock surface and tend to organize into structured layers. This, in turn, results in an additional disjoining pressure at the interface, exceeding that in the bulk liquid phase.

Furthermore, as reported by McElfresh et al. in 2012, the developed nanofluid film on the rock surface possesses the capacity to separate and release trapped hydrocarbons within the reservoir, facilitating the shift from an oil-wet to a water-wet system. However, it is important to note, as pointed out by Aveyard et al. (2003) that several factors can influence the characteristics of this film, including nanoparticle concentrations and sizes, salinity, temperature, and the properties of the rock surface.

According to McElfresh et al. (2012), nanoparticles have a tendency to arrange themselves in a wedge-like form. This observation is supported by a previous study by Wasan and Nikolov (2003), which discussed the mechanism of oil removal from soil using nanofluids. The wedge-like structure of nanoparticles enhances their ability to displace the oil phase from the surface of rocks.

In our case, when hydrophilic nanocellulose adhere to the rock surface, it creates a thin nano texture that coats the surface. Consequently, the wettability of the surface shifts towards becoming more water-wet. This phenomenon of wettability alteration was also confirmed by a contact angle study for nanocellulose in the scope of material characterization of nanocellulose (Figure 6.57).

Another mechanism in nanoparticles EOR process is log jamming. Log jamming refers to the situation where nanofluids injected into the reservoir cause the formation's pores or rock matrix to become clogged or plugged. This phenomenon can obstruct the flow of fluids, including the injected nanofluids, oil, or water, thereby reducing the effectiveness of the EOR process. Log jamming is a potential challenge that researchers and engineers need to address during EOR tests.

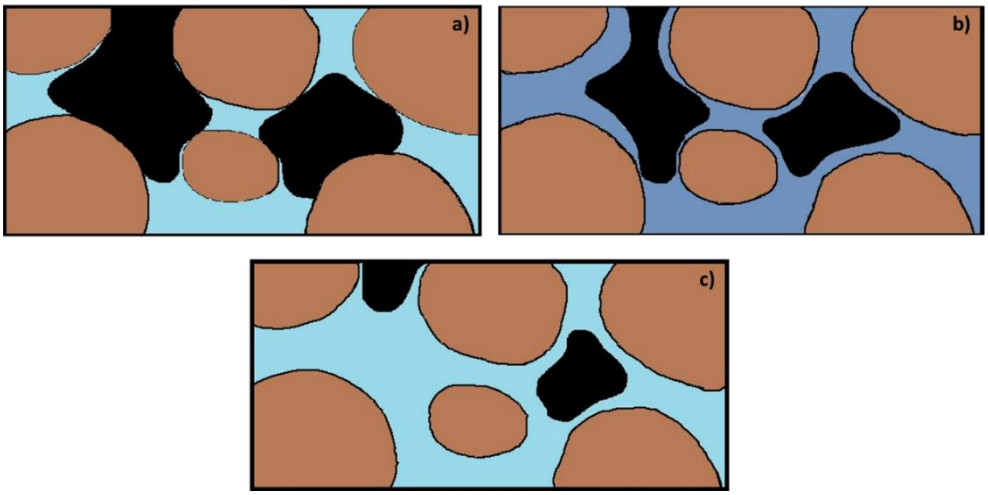

Figure 6.57: Wettability alteration mechanism by disjoining pressure (a-first oil-wet condition of the pore system, b-injection of nanocellulose into system, c-subsequent injection of water after nanocellulose)

It was also observable in our study that there was a log-jamming effect during nanocellulose injection at each coreflood test. The steady increase in differential pressure while injecting nanocellulose is a crucial sign for the log-jamming effect. Despite log jamming, there is additional oil recovery at each core flood during nanocellulose injection. In extremely narrow pore throats, the disparity in density between the nanoparticles and the water hinders the movement of particles, leading to their accumulation. This accumulation results in increased pressure in the surrounding pores, which in turn displaces the oil. Once the oil is released, the pressure in the vicinity decreases, allowing the blockage to dissolve gradually and the particles to flow along with the water. This phenomenon can be described as a transient log-jamming process (El-Diasty and Ragab, 2013), as depicted in Figure 6.58.

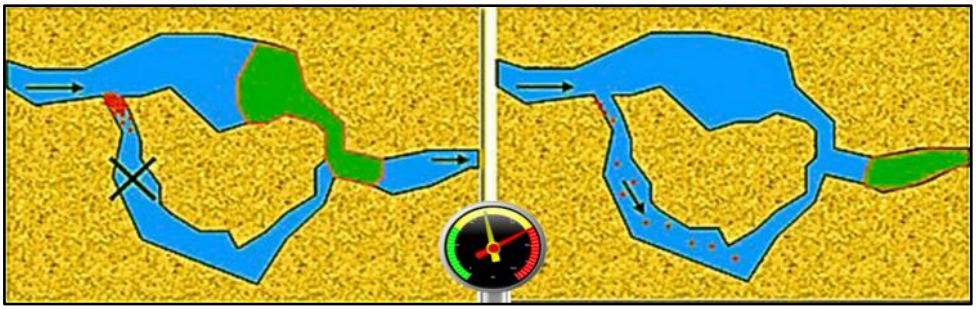

Figure 6.58:Transient log-jamming process (El-Diasty and Ragab, 2013)

The factors contributing to log jamming can vary depending on the specific conditions, including the type of nanofluid, reservoir characteristics, and injection parameters. Some possible causes of log jamming include particle aggregation, filter cake formation, and rock wettability alteration.

In coreflood tests 1 and 2, the same oil sample with an API gravity of 16 was used. Enhanced oil recovery tests were performed with 2 wt% nanocellulose solution for both tests. The core plug samples #210 and #211 also have similar basic core properties, including porosity and permeability. The major concern for performing coreflood tests with similar properties is to confirm the repeatability of the test. When the oil recovery results were compared for coreflood tests 1 and 2, 2 wt% nanocellulose injection resulted in similar improved recovery values for both tests, which are 17.5% and 16.3%, respectively (Figure 6.59).

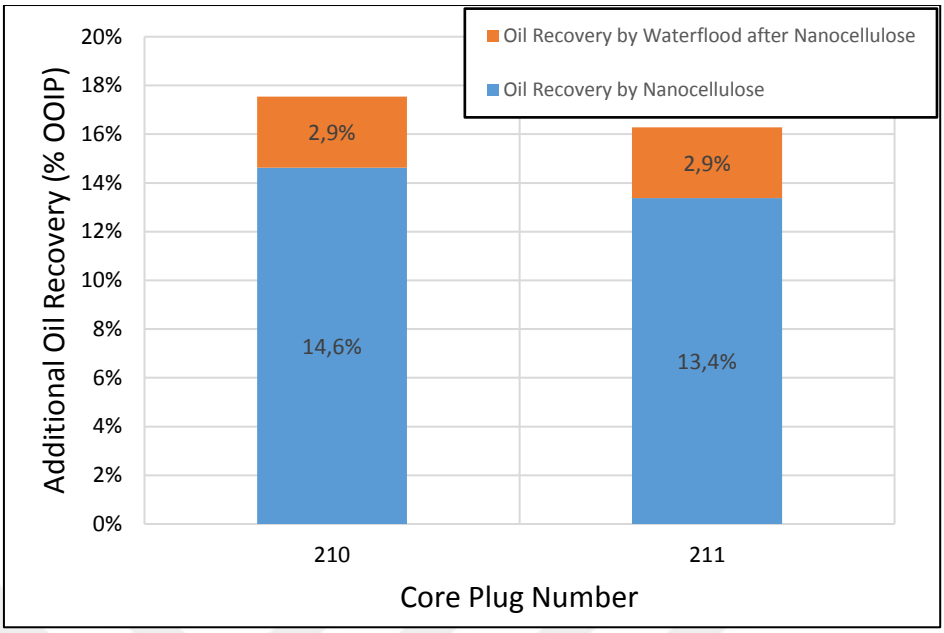

Figure 6.59: Additional oil recovery comparison for coreflood tests 1 and 2

In coreflood tests 1, 2 and 3, enhanced oil recovery tests were performed with 2 wt% nanocellulose solution for both tests. However, with an oil API gravity of 22, the oil used in coreflood test 3 is lighter than the oil used coreflood tests 1 and 2. The primary purpose of coreflood test 3 is to see the effect of oil API gravity for the same nanocellulose concentration. Although; the permeability value of core plug sample #347 is one fourth of the other two samples (#210 and #211), individual improved oil recovery and overall improved oil recovery (16.7% and 5.0%, respectively) by nanocellulose for coreflood test #3 is higher than those for coreflood tests 1 and 2 (Figure 6.60). It might be due to the oil API gravity and, consequently, the viscosity of oil used in coreflood test 3. Structural disjoining pressure might be more effective on systems with lighter oil to move oil through the system.

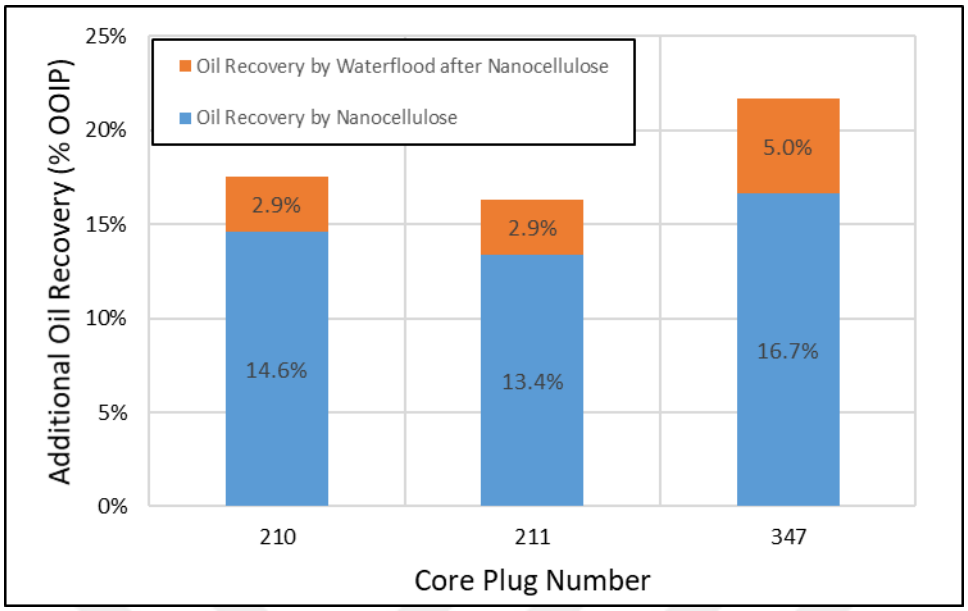

Figure 6.60: Additional oil recovery comparison for coreflood tests 1, 2 and 3

In coreflood tests 3 and 4, enhanced oil recovery tests were performed with 2 and 1 wt% nanocellulose solutions, respectively. The same oil sample with an API gravity of 22 was used for both core plug samples #347 and #346. Coreflood test 4 primarily aims to examine the impact of nanocellulose concentration on improved oil recovery. Both tests demonstrate similar findings, with slight deviations of approximately 2-3% in additional oil recovery after the application of nanocellulose (Figure 6.61). Total improved oil recovery by nanocellulose and waterflooding is more in coreflood test 4 than the one in coreflood test 3, with additional oil recovery values of 21.7% and 25.0%, respectively.

In the case of oil recovery tests with 2 wt% nanocellulose in coreflood tests 1, 2 and 3, overall additional oil recovery is less than the one in coreflood tests 4 conducted with 1 wt% nanocellulose. It is clear that decrease in nanocellulose concentration enhances the oil recovery slightly more. There is a specific threshold for the concentration of injected nanoparticles, as exceeding this limit can result in pore throat blockage and a decrease in the overall oil recovery. If the concentration becomes too high, the nanoparticles tend to aggregate and accumulate around the inlet, thereby diminishing the displacement efficiency (Hendraningrat et al., 2014).

Opting for a lower nanocellulose concentration would be advisable for economic reasons, given that these results indicate similarity.

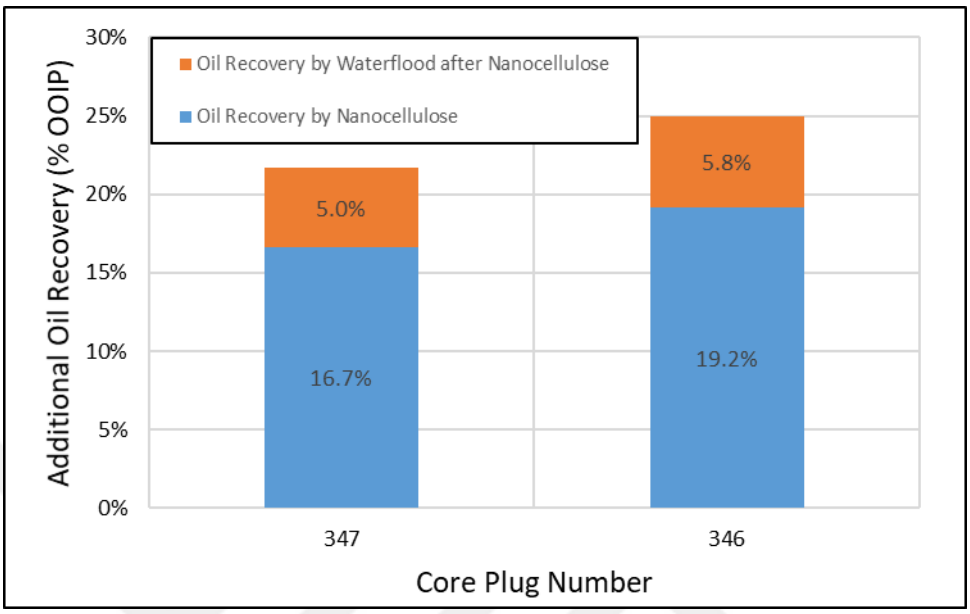

Figure 6.61: Additional oil recovery comparison for coreflood tests 3 and 4

In coreflood tests 4 and 5, the experiments aimed to enhance oil recovery using a 1 wt% nanocellulose solution. However, there is a difference in the oil API gravity between the two tests, with the oil used in coreflood test 5 being lighter compared to coreflood test 4. The core plug samples, #346 and #213, share similar basic core properties including porosity and permeability. Coreflood test 5 specifically focuses on observing the impact of oil API gravity on a consistent nanocellulose concentration.

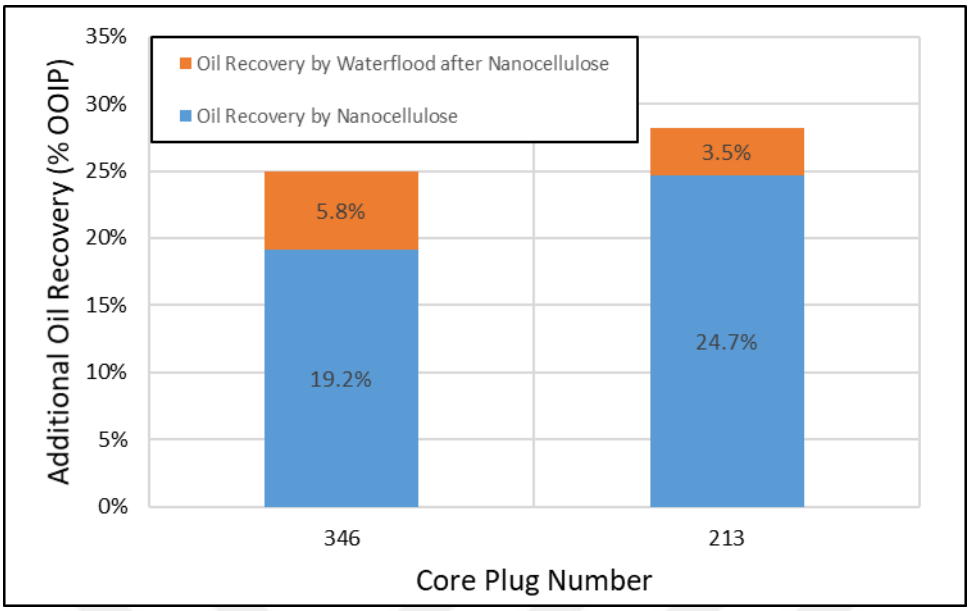

Figure 6.62: Additional oil recovery comparison for coreflood tests 4 and 5

The overall improved oil recovery achieved by nanocellulose in coreflood test 5 is higher (28.2%) compared to coreflood test 4 (25.0%) (Figure 6.62). This trend is consistent with the observations made in coreflood tests 1 and 2 compared to coreflood test 3. It can be concluded that systems with lighter oil have a tendency to generate more additional oil when nanocellulose is applied. Furthermore, when comparing coreflood test 5 to other coreflood tests, it exhibits the highest additional oil recovery through nanocellulose flooding and waterflooding following nanocellulose injection. This holds true regardless of the nanocellulose concentration and oil API gravity.

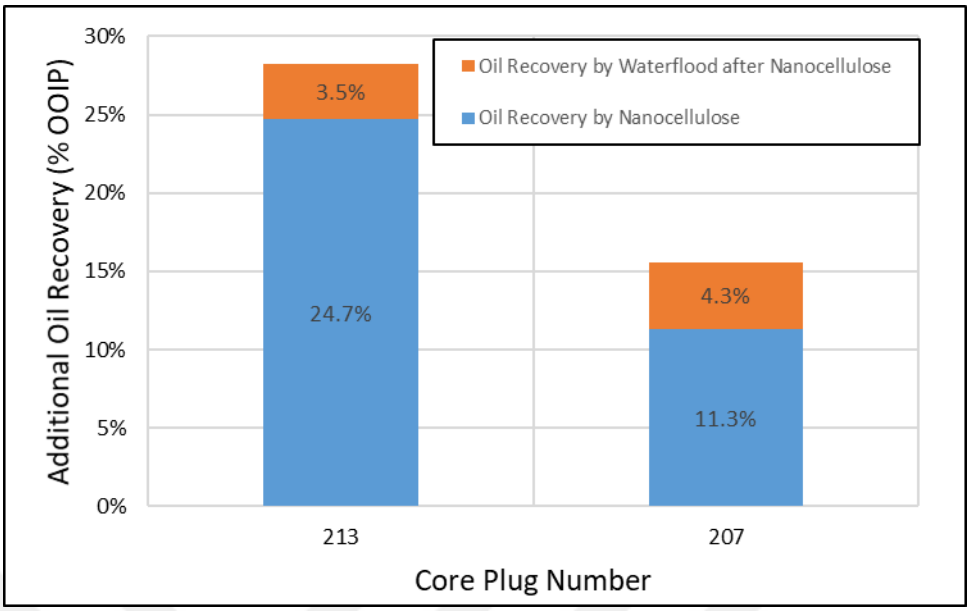

Figure 6.63: Additional oil recovery comparison for coreflood tests 5 and 6

In coreflood tests 5 and 6, enhanced oil recovery tests were performed with 1 and 0.5 wt% nanocellulose solution, respectively. The same oil sample with an API gravity of 36 was used for both core plug samples #213 and #207. The primary objective of coreflood test 4 is to investigate how different nanocellulose concentrations can enhance oil recovery, specifically in lighter oil reservoir systems. It is evident that reducing the nanocellulose concentration significantly improves the oil recovery process (Figure 6.63). In coreflood test 6, the combined application of nanocellulose and waterflooding results in a greater overall improvement in oil recovery compared to coreflood test 5. Specifically, coreflood test 6 achieves additional oil recovery values of 28.2%, while coreflood test 5 demonstrates a lower increase of 15.6%. This indicates that the specific nanocellulose concentration used in coreflood test 6 is more effective in generating a greater improvement in oil recovery compared to the concentration used in coreflood test 5.

The concentration of injected nanoparticles is a crucial factor that influences the enhanced oil recovery process. As noted by Chengara et al. (2014), higher nanoparticle concentrations lead to an increase in disjoining pressure and Brownian motion, which in turn results in stronger repulsion forces. The increase in

concentration also enhances the displacement efficiency due to the improved viscosity of the nanofluid and the spreading of nanoparticles on the surface of the grains. Based on the results, it can be concluded that selecting the optimal nanocellulose concentration is crucial for achieving the maximum additional oil recovery. The findings suggest that there is an optimal range of nanocellulose concentration that yields the highest increase in oil recovery, emphasizing the importance of careful consideration and optimization in this parameter.

In coreflood tests 6 and 7, the same oil sample with an API gravity of 36 was used, and enhanced oil recovery tests were conducted using a 0.5 wt% nanocellulose solution for both tests. The core plug samples, #207 and #209, also share similar basic properties such as porosity and permeability. The primary objective of performing coreflood tests with similar properties is to ensure the repeatability of the test, particularly in cases involving lower nanocellulose concentration and lighter oil. Comparing the oil recovery results of coreflood tests 6 and 7, it is observed that the injection of a 0.5 wt% nanocellulose solution led to a higher overall improved oil recovery in coreflood test 6 compared to coreflood test 7. The respective oil recovery values were 15.6% and 10.5%, as indicated in Figure 6.64. The slight difference in oil recovery values could be attributed to the lower permeability of core plug sample #209, accepted as an outlier according to FZI values.

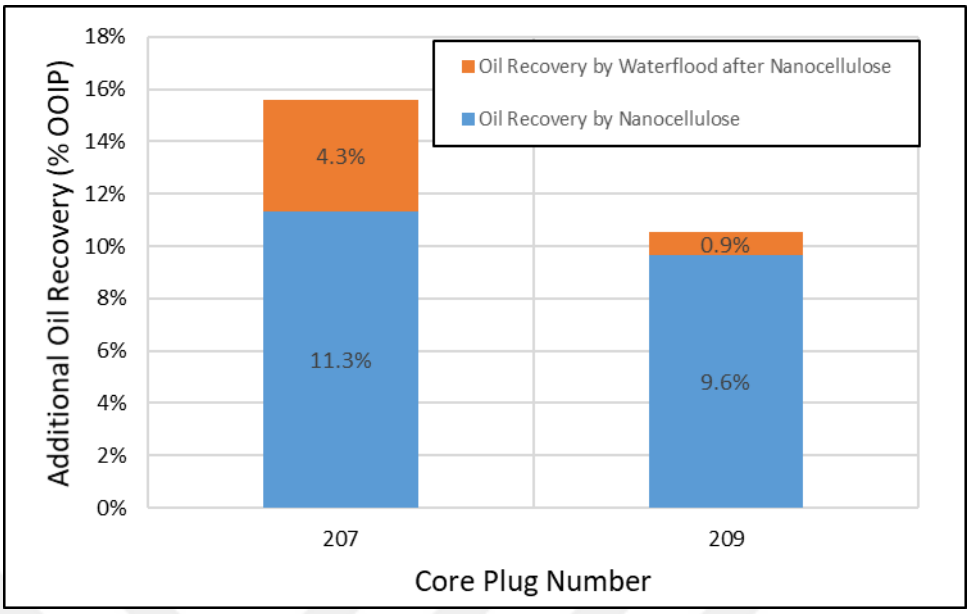

Figure 6.64: Additional oil recovery comparison for coreflood tests 6 and 7

In addition to coreflood oil recovery test results, XRD, SEM/EDS, and thin section analyses provide specific findings. The XRD and SEM/EDS results obtained before and after nanocellulose injection followed by waterflooding indicate that the core plug samples are primarily composed of calcite, accounting for nearly 100% of the composition in all cases. These analytical techniques have revealed that the mineralogical composition of the core plug samples remains predominantly calcite before and after the nanocellulose injection and subsequent waterflood.

The thin section analyses performed on the core plug sample before and after nanocellulose injection followed by waterflooding have provided detailed observations. Although traces of oil are still present in some pores, the most significant finding is the absence of detectable nanocellulose in the system. In addition to XRD and SEM/EDS data, this strongly suggests that the nanocellulose has been effectively displaced by the waterflooding process, leading to its almost complete removal from the analyzed sample.

CHAPTER 7

CONCLUSIONS AND RECOMMENDATIONS

The study conducted seven core flood experiments to investigate the potential of nanocellulose as a chemical enhanced oil recovery additive. Three different concentrations of nanocellulose were tested using oil samples with varying API gravities. The study assessed nanocellulose stability under solubility tests, considering factors such as salinity, nanocellulose concentration, and temperature. Additionally, particle size distribution and zeta potential measurements were conducted to understand the physical properties of nanocellulose in solution. The viscosity bottle test was employed to evaluate the stability of nanocellulose solutions over time and under shear. Furthermore, interfacial tension, wettability studies, and contact angle measurements were performed to gain insights into the impact of nanocellulose on wettability properties and oil recovery mechanisms. The study yields several key findings that can be inferred as follows:

- Nanocellulose functions as an environmentally friendly agent to foster the development of an alternative EOR technique, with particular emphasis on carbonate reservoirs. It recovered additional oil up to 24.7% by itself. Additional waterflooding after nanocellulose soaking helped recovering additonal oil up to 5.8%.
- The possible oil recovery mechanism for nanocellulose particles in this study might be due to the structural disjoining pressure mechanism. The primary factor responsible for the spreading of nanofluids is the variation in structural disjoining pressure (film tension) across the fluid, causing the nanofluids to move from the bulk solution towards the wedge region.
- The arrangement of nanoparticles within the wedge film plays a crucial role in altering the wettability characteristics. Wettability alteration is identified

as one of the primary mechanisms of enhanced oil recovery (EOR) for nanocellulose, owing to its hydrophilic nature as an organic polymer. This proposition is substantiated by the results obtained from wettability studies and contact angle measurements. The experimental findings support the notion that nanocellulose can effectively modify the wettability of the reservoir, decreasing contact angle between rock surface and oil droplet from 135.1° to 67.3°. These observations highlight the significance of wettability alteration as a key mechanism by which nanocellulose enhances the recovery of oil during the EOR process.

- The concentration of injected nanoparticles is critical in influencing the enhanced oil recovery process. Higher concentrations of nanoparticles have several effects on the process. Firstly, they lead to an increase in disjoining pressure and Brownian motion, resulting in stronger repulsion forces between the nanoparticles. This enhanced repulsion aids in the displacement of oil. Secondly, higher concentrations improve the viscosity of the nanofluid, leading to better flow characteristics and increased displacement efficiency. Additionally, the nanoparticles spread more effectively on the surface of the reservoir grains, facilitating the displacement of oil. The study reveals that there exists a specific concentration threshold for injected nanoparticles. Among different nanocelluse concentrations (0.5 wt%, 1 wt%, and 2 wt%), it appears that an application concentration of around 1 wt% nanocellulose is the optimal choice for this study. It is important to note that exceeding this threshold can lead to undesirable consequences such as pore throat blockage, which can hinder the flow of fluids and ultimately decrease the overall oil recovery. Therefore, careful consideration and monitoring of nanoparticle concentration are crucial to avoid potential adverse effects and ensure optimal oil recovery during the enhanced oil recovery process.
- The tests conducted indicate that nanocellulose exhibits higher stability in low salinity water. This finding is significant as it suggests that nanocellulose is particularly well-suited for application in areas where fresh water sources

are readily available for nanocellulose preparation. The abundance of fresh water resources can provide a favorable environment for the preparation and utilization of nanocellulose as an organic material in enhanced oil recovery. This information can help guide decision-making regarding the feasibility and practicality of implementing nanocellulose-based EOR applications in regions with accessible fresh water sources.

- Water flooding conducted immediately after nanocellulose flooding proved successful in terms of recovering additional oil (up to 5.8% additional oil recovery) and removing any residual nanocellulose by additional analyses. These findings collectively suggest that nanocellulose application does not substantially alter the mineralogical or elemental composition of the reservoir plugs and can be effectively removed through subsequent water flooding, enabling successful oil recovery.
- The absence of studies highlights a gap in the research regarding the potential application and effectiveness of nanocellulose for EOR in carbonate reservoirs, specifically in the context of Turkey's Southeastern Region. It would be valuable for future research efforts to explore the feasibility and performance of nanocellulose as an EOR agent specifically for carbonate formations in this region with further research and investigation.
- It is important to emphasize that this study is focused on assessing the impact of nanocellulose on carbonate rocks. The analysis has shown that micro and meso pore throats were the predominant features in the plug samples, demonstrating that nanocellulose was investigated as a means to improve oil recovery from the matrix. This research is specifically concentrated on matrix-based production. Furthermore, it is possible to conduct additional research to explore how natural fractures affect the performance of nanocellulose as an EOR agent.
- Indeed, further investigation into the effects of different nanocellulose soaking times and oil aging times on oil recovery is essential, as they can directly influence wettability and potentially impact the overall recovery

process. To study the influence of nanocellulose soaking time, different experiments can be conducted by subjecting the nanocellulose to varying soaking durations before the waterflooding process. The oil recovery efficiency can then be assessed and compared to determine the optimal soaking time that yields the highest recovery. Similarly, investigating the effects of different oil aging times is also important. The aging process involves exposing the oil to reservoir conditions for varying periods before subjecting it to waterflooding. This aging can lead to changes in the oil's composition and properties, which can subsequently impact its interaction with the reservoir rock. By studying different oil aging times in conjunction with nanocellulose treatments, researchers can gain insights into how oil characteristics evolve over time and its subsequent effect on recovery efficiency. By systematically exploring the effects of nanocellulose soaking time and oil aging time, researchers can better understand their influence on wettability and optimize the waterflooding process for enhanced oil recovery.

- Overall, this study concludes that nanocellulose exhibits promise as a green chemical EOR additive (with an additional oil recovery up to 28.2%), with its stability, physical properties, and interactions with oil supporting its effectiveness in enhancing oil recovery. Further research and optimization of nanocellulose concentrations and application conditions are recommended to maximize its EOR potential.

REFERENCES

Aadland, R.C., Jakobsen, T.D., Heggset, E.B., Long-Sanouiller, H., Simon, S., Paso, K.G., Syverud, K. 2019. High Temperature Core Flood Investigation of Nanocellulose as a Green Additive for Enhanced Oil Recovery. Nanomaterials 9, 665−691.

Abdallah W., Buckley J., Carnegie A. et al. 2007. Fundamentals of wettability. Oilfield Review.44-61.

Abdulkadir, U., Hashim, J., Alkali, M., Kumar, A. 2017. Application of Thermal Methods for Heavy Oil Recovery: Phase One. International Journal of Advance Research, Ideas and Innovations in Technology, 2(5) www.IJARnD.com.

Abidina, A.Z., Puspasaria, T., Nugroho, W.A. 2012. Polymers for Enhanced Oil Recovery Technology. Procedia Chemistry, 4, 11–16.

Abitbol, T., Rivkin, A., Cao, Y., Nevo, Y., Abraham, E., Ben-Shalom,T., Lapidot, S., Shoseyov, O. 2016. Nanocellulose, a Tiny Fiber with Huge Applications, Curr. Opin. Biotechnol. 39, 76–88.

Agbalaka, C. C., Dandekar, A. Y., Patil, S. L. 2008. The Effect of Wettability on Oil Recovery: A Review. In SPE Asia Pacific Oil and Gas Conference and Exhibition. Society of Petroleum Engineers.

Alajmi, A.F.F., Algharaib, M.K., Gharbi, R.C. 2009. Experimental Evaluation of Heavy Oil Recovery by Hot Water Injection in a Middle Eastern Reservoir. SPE Middle East Oil and Gas Show and Conference. Society of Petroleum Engineers.

Aldhaheri, M.N., Wei, M., Bai, B. 2016. Comprehensive Guidelines for the Application of in situ Polymer Gels for Injection Well Conformance Improvement Based on Field Projects. In: SPE IOR Conference.

Al-Mashrafi, A., Fani, M., Asfand, F. 2021. Downhole Steam Generation for Green Heavy Oil Recovery. 10.2118/207597-MS.

Al-Shahrani, F. F., Baluch, Z. A., Al-Otaibi, N. M., Sarfraz, T. 2007. Successful Water Shut-off in Open Hole Horizontal Well Using Inflatables. Society of Petroleum Engineers. doi:10.2118/110968-MS.

Alvarez, J., Han, S. 2013. Current Overview of Cyclic Steam Injection Process. J. Pet. Sci. Res. 2 (3), 116.

Amaefule, J. O., Altunbay, M., Tiab, D., Kersey, D. G., Dare K. K. 1993. Enhanced Reservoir Description: Using Core and Log Data to Identify Hydraulic (Flow) Units and Predict Permeability in Uncored Intervals/Wells. Paper presented at the SPE Annual Technical Conference and Exhibition, Houston, Texas. doi: https://doi.org/10.2118/26436-MS.

Anderson, W.G. 1986. Wettability Literature Survey - Part 2: Wettability Measurement, J. Petroleum Technol. 38 (11) 1246e1262.

Ardanuy, M., Claramunt, J., Arévalo, R., Parés, F., Aracri, E., Vidal, T. 2012. Nanofibrillated Cellulose (NFC) as Potential Reinforcement for High Performance Cement Moretar Composites. BioResources 7 (3), 3883–3894.

Aveyard, R., Binks, B.P., Clint, J.H. 2003. Emulsions Stabilized Solely by Colloidal Particles. Adv. Colloid Interface Sci. 100, 503–546.

Ayatollahi, S., Zerafat, M.M. 2012. Nanotechnology-assisted EOR techniques: new solutions to old challenges. In: SPE international oilfield nanotechnology conference and exhibition, Noordwijk, The Netherlands, 12–14 June.

Babu, K., Pal, N., Bera, A., Saxena, V.K., Mandal, A. 2015. Studies on Interfacial Tension and Contact Angle of Synthesized Surfactant and Polymeric from Castor Oil for Enhanced Oil Recovery. Appl. Surf. Sci. 353, 1126–1136.

Bailey, B., Crabtree, M., Tyrie, J. 2000. Water Control. Oilfield Review 12 (1): 30—51.

Barry, M.M., Jung, Y., Lee, J.K., Phuoc, T.X., Chyu, M.K. 2015. Fluid Filtration and Rheological Properties of Nanoparticle Additive and Intercalated Clay Hybrid Bentonite Drilling Fluids. J. Pet. Sci. Eng. 127, 338–346. http://dx.doi.org/10.1016/j.petrol.2015.01.012.

Benmekki, E.H., Mansoori, G.A. 1986. Accurate Vaporizing Gas-Drive Minimum Miscibility Pressure Prediction. SPE Reprint Series. SPE Paper # 15677. 10.2118/15677-PA.

Bera, A., Babadagli, T. 2015. Status of Electromagnetic Heating for Enhanced Heavy Oil/Bitumen Recovery and Future Prospects: A Review. Appl. Energy 151, 206–226.

Bera, A., Belhaj, H. 2016. Application of Nanotechnology by Means of Nanoparticles and Nanodispersions in Oil Recovery - A Comprehensive Review. Journal of Natural Gas Science and Engineering. 34. 10.1016/j.jngse.2016.08.023.

Betancur, S., Franco, C.A., Cortés, F.B., 2016. Magnetite-Silica Nanoparticles with a Core-Shell Structure for Inhibiting the Formation Damage Caused by the Precipitation/ Deposition of Asphaltene. J. Magnetohydrodyn. Plasma Res. 21 (3), 289–322.

Bhatia, K., Chacko, L. 2011. Ni-Fe Nanoparticle: An Innovative Approach for Recovery of Hydrates (SPE 143088). In: SPE EUROPEC/EAGE Annual Conference and Exhibition, Vienna, Austria, 23–26 May, http://dx.doi.org/10.2118/143159-ms.

Bish, D.L., Post, J.E. 1989. Modern Powder Diffraction. Mineralogical Society of America, Reviews in Mineralogy, vol. 20, p. 369.

Brinchi, L., Cotana, F., Fortunati, E., Kenny, J. M. 2013. Production of Nanocrystalline Cellulose from Lignocellulosic Biomass: Technology and Applications. Carbohydrate Polymers, 94(1), 154–169.

Bortolotti, V., Gottardi, G., Macini, P., Srisuriyachai, F. 2009. Intermittent Alkali Flooding in Vertical Carbonate Reservoirs. Europec/EAGE Conference and Exhibition. Society of Petroleum Engineers.

Butler, R. 1985. A New Approach to the Modeling of Steam-Assisted Gravity Drainage, J. Can. Petrol. Technol., 42-50.

Butler, R., 1991. Thermal Recovery of Oil and Bitumen, 1st ed. Prentice Hall, Dallas, TX.

Cervin, N.T., Johansson, E., Benjamins, J.W., Wågberg, L. 2015. Mechanisms behind the Stabilizing Action of Cellulose Nanofibrils in Wet-Stable Cellulose Foams. Biomacromolecules 16 (3), 822–831. https://doi.org/10.1021/bm5017173.

Chang, H.L. 1978. Polymer Flooding Technology –Yesterday, Today and Tomorrow, SPE 7043, J. Petrol. Technol. 30, 8, 1113-1128.

Chen, F., Jiang, H., Bai, X., Zheng, W., 2013. Evaluation the Performance of Sodium Metaborate as a Novel Alkali in Alkali/Surfactant/Polymer Flooding. J. Ind. Eng. Chem. 19 (2), 450–457.

Chengara, A., Nikolov, A.D., Wasan, D.T., Trokhymchuk, A., Henderson, D. 2004. Spreading of Nanofluids Driven by The Structural Disjoining Pressure Gradient, Adv. Colloid Interface Sci. 280, 192–201.

Chu, C. 1977. A Study of Fireflood Field Projects, SPE 5821, J. Petrol. Technol., 111-120.

Chu, C. 1982. State-of-the-Art Review of Fireflood Field Projects, SPE 9772, J. Petrol. Technol., 19-32.

Clarke, A., Howe, A.M., Mitchell, J., Staniland, J., Hawkes, L.A. 2016. How Viscoelasticpolymer Flooding Enhances Displacement Efficiency. Soc. Petrol. Eng. J. 21 (3), 675–687, 0.

Cotter, W.H. 1962. Twenty-Three Years of Gas Injection into a Highly Undersaturated Crude Reservoir. J Pet Technol 14 (4): 361-365. SPE-82-PA. http://dx.doi.org/10.2118/82-PA.

Dai, H.J., Wu, J.H., Zhang, H., Chen, Y. 2020. Recent Advances On Cellulose Nanocrystals For Pickering Emulsions: Development and challenge. Trends Food Sci. Technol. 102, 16−29.

Danaei M., Dehghankhold M., Ataei S. 2018. Impact of Particle Size and Polydispersity Index on the Clinical Applications of Lipidic Nanocarrier Systems. Pharmaceutics. May 18; 10(2):57. doi: 10.3390/pharmaceutics10020057. PMID: 29783687; PMCID: PMC6027495.

De Farias, M. L., de Souza, A. L., da Silveira Carvalho, M., Hirasaki, G. 2012. A Comparative Study of Emulsion Flooding and other IOR Methods for Heavy Oil. Paper presented at the SPE Latin America and Caribbean Petroleum Engineering Conference, Mexico City, Mexico, April 2012. doi: https://doi.org/10.2118/152290-MS.

Demir, M., Topguder, N., Karabakal, U., Gould, J. 2008. Water Shutoff Gels Improved Oil Recovery in Naturally Fractured Raman Heavy Oilfield. 10.2118/116878-MS.

Dino, R., Rocha, P.S., Sanches, C., Le Thiez, P. 2007. EOR and Storage Activities Driven by CO2 in Brazil—Experience from the Buracica and Miranga Oil Fields Performance: Planned Operations. Presented at the 2nd International Symposium: Capture and Geological Storage of CO2, Paris, France.

Donaldson, E.C., Chilingarian, G.V., Yen, T.F. 1989. Enhanced Oil Recovery, II: Processes and Operations. Elsevier.

Dong, X.M., Revol, J.F., Gray, D.G. 1998. Effect of Microcrystallite Preparation conditions on the Formation of Colloid Crystals of Cellulose. Cellulose, 5(1), 19–32.

Dufresne, A. 2012. Nanocellulose: Potential Reinforcement in Composites, Nat. Polym., Vol. 2: Nanocompos. 2, 1–32.

Edmondson, T. 1965. Effect of temperature on waterflooding. J. Can. Petrol. Technol. 4 (4), 236–242.

Ehtesabi, H., Ahadian, M.M., Taghikhani, V., Ghazanfari, M.H. 2013. Enhanced Heavy Oil Recovery in Sandstone Cores Using TiO2 Nanofluids. Energy Fuels; 28(1):423–30.

El-Diasty, A.I., Ragab, A.M.S. 2013. Applications of Nanotechnology in the Oil & Gas Industry: Latest Trends Worldwide & Future Challenges in Egypt. In North Africa Technical Conference and Exhibition; Society of Petroleum Engineers: Cairo, Egypt, 2013.

Fan, T., Buckley, T. 2002. Rapid and Accurate SARA Analysis of Medium Gravity Crude Oils. Energy & Fuels 2002 16 (6), 1571-1575. DOI: 10.1021/ef0201228.

Farouq Ali, S.M., Meldau R.F. 1979. Current Steamflood Technology, J. Petrol. Technol., 1332-1342.

Farouq Ali, S.M. 1982. Steam Injection Theory – A Unified Approach, paper SPE 10746, California Regional Meeting of the Society of Petroleum Engineers, San Francisco, March 24-26, 1982.

Farouq Ali, S.M., Thomas, S. 1986. Tertiary Oil Recovery of Two Alberta Oils by Micellar Flooding, Proceedings of the 37th Annual Technical Meeting of the Petroleum Society of CIM, Calgary, Alberta, June 8-11, 1986, pp. 159-184.

Fath A. F., Pouranfard A. R. 2014. Evaluation of Miscible and Immiscible CO2 Injection in One of the Iranian Oil Fields. Egyptian Journal of Petroleum, 23(3), 255–270.

Fleury, M., Sissmann, O., Brosse, E. 2017. A Silicate Based Process for Plugging the Near Well Bore Formation. Energy Procedia 114: 4172—4187. http://dx.doi.org/https://doi.org/10.1016/j.egypro.2017.03.1558.

Foroozesh, J., Kumar, S. 2020. Nanoparticles Behaviors in Porous Media: Application to Enhanced Oil Recovery. Journal of Molecular Liquids. 316. 113876. 10.1016/j.molliq.2020.113876.

Froning, H.R., Leach, R.O. 1967. Determination of Chemical Requirement and Applicability of Wettability Alteration Flooding, J. Petrol. Technol., 839-843.

Jalalalhosseini, S. 2015. Microwave Heating as an Enhanced Oil Recovery Method—Potentials and Effective Parameters. Energy Sources Part A Recovery Utilization and Environmental Effects. 37. 742-749. 10.1080/15567036.2011.592906.

Giraldo J., Benjumea, P., Lopera, S., Corteüs, F.B., Ruiz, M.A. 2013. Wettability Alteration of Sandstone Cores by Alumina-Based Nanofluids. Energy Fuels 2013;27(7):3659–65.

Gogarty, W.B., Tosch, W.C. 1968. Miscible-type Waterflooding: Oil Recovery with Micellar Solutions, J. Petrol. Technol., 1407-1414.

Grattoni, C.A., Jing, X.D., Zimmerman, R.W. 2001. Disproportionate Permeability Reduction When a Silicate Gel is Formed In-Situ to Control Water Production. Society of Petroleum Engineers. doi:10.2118/69534-MS.

Gurgel, A., Moura, M.C.P.A., Dantas, T.N.C., Barror Neto, E.L., Dantas Neto, A.A., 2008. A Review on Chemical Flooding Methods Applied in Enhanced Oil Recovery. Braz. J. Pet. Gas 2 (2), 83–95.

Habibi, Y., Lucia, L.A., Rojas, O.J. 2010. Cellulose Nanocrystals: Chemistry, Self-Assembly, and Applications, Chem. Rev. 110 3479–3500, https://doi.org/10.1021/cr900339w.

Hall, L.J., Deville, J.P., Araujo, C.S., Li, S., Rojas, O.J. 2017. Nanocellulose and Its Derivatives for High-Performance Water-Based Fluids. In SPE International Conference on Oilfield Chemistry. OnePetro.

Hall, L.J., Deville, J.P., Santos, C.M., Rojas, O.J., Araujo, C.S. 2018. Nanocellulose and Biopolymer Blends for High-Performance Water-Based Drilling Fluids. Paper presented at the IADC/SPE Drilling Conference and Exhibition, Fort Worth, Texas, USA, March 2018. doi: https://doi.org/10.2118/189577-MS.

Hendraningrat, L., Li, S., Torster, O. 2013. A Coreflood Investigation of Nanofluid Enhanced Oil Recovery. J Petrol Sci Eng; 111:128–38.

Hendraningrat, L. and O. Torsaeter. 2014. Unlocking the Potential of Metal Oxides Nanoparticles to Enhance the Oil Recovery. Offshore Technology Conference-Asia. 2014. Offshore Technology Conference.

Hoelscher, K.P., De Stefano, G., Riley, M., Young, S., 2012. Application of Nanotechnology in Drilling Fluids. Paper SPE-157031eMS. In: Presented at the SPE International Oilfield Nanotechnology Conference and Exhibition, Noordwijk, The Netherlands, 12-14 June.

Holm, L.W. 1959. Carbon dioxide Solvent Flooding for Increased Oil Recovery, Trans. AIME 216, 225-231.

Holtz, M.H. 2008. Summary of Sandstone Gulf Coast CO2 EOR Flooding Application and Response (SPE-113368). In Proceedings of SPE/DOE Symposium on Improved Oil Recovery, Tulsa, OK, USA.

Husein, M. 2017. Preparation of Nanoscale Organosols and Hydrosols via the Phase Transfer Route. J Nanopart Res; 19(12):405.

Isogai, A. 2013. Wood Nanocelluloses: Fundamentals and Applications as New Bio-based Nanomaterials, J. Wood Sci. 59 449–459, https://doi.org/10.1007/s10086-013-1365-z.

Jozala, A.F., de Lencastre-Novaes, L.C., Lopes, A.M. 2016. Bacterial nanocellulose production and application: a 10-year overview. Appl Microbiol Biotechnol 100, 2063–2072 (2016). https://doi.org/10.1007/s00253-015-7243-4.

Kalashnikova, I., Bizot, H., Cathala, B., Capron, I. 2011. New Pickering Emulsions Stabilized by Bacterial Cellulose Nanocrystals. Langmuir 2011, 27, 7471−7479.

Kamel, S. 2007. Nanotechnology and Its Applications in Lignocellulosic Composites, a Mini Review. eXPRESS Polymer Letters. 1:546–575. DOI: 10.3144/expresspolymlett.78.

Khalil, M., Jan, B.M., Tong, C.W., Berawi, M.A. 2017. Advanced Nanomaterials in Oil and Gas Industry: Design, Application and Challenges. App. Energy 191, 287–310.

Khalilinezhad, S.S., Cheraghian, G., Karambeigi, M.S., Tabatabaee, H, Roayaei, E. 2016. Characterizing the Role of Clay and Silica Nanoparticles in Enhanced Heavy Oil Recovery During Polymer Flooding, Arabian.J. Sci. Eng. 41:2731–2750.

Khazraji, A.C., Robert, S. 2013. Self-assembly and Intermolecular Forces When Cellulose and Water Interact Using Molecular Modeling, J. Nanomater. https://doi.org/10.1155/2013/745979.

Kogler, F., Dopffel, N., Mahler, E., Alkan, H. 2017. Dynamic screening for microbial enhanced oil recovery (MEOR). In: IOR 2017-19th European Symposium on Improved Oil Recovery, vol. 1. European Association of Geoscientists & Engineers, pp. 1–14.

Kovscek, A.R., Radke, C.J. 1994. Fundamentals of From Transport in Porous Media. In: Schramm LL, editor. Foam: Fundamentals and Applications in the Petroleum Industry. Washington, D.C.: American Chemical Society.

Kovscek, A.R. 2012. Emerging Challenges and Potential Futures for Thermally Enhanced Oil Recovery. Journal of Petroleum Science and Engineering, Volumes 98–99, Pages 130-143, ISSN 0920-4105, https://doi.org/10.1016/j.petrol.2012.08.004.

Kusanagi, K., Murata, S., Goi, Y., Sabi, M., Zinno, K., Kato, Y., Togashi, N. 2015. In Application of Cellulose Nanofiber as Environment-Friendly Polymer for Oil Development, Paper Presented at the SPE/IATMI Asia Pacific Oil & Gas Conference and Exhibition, Nusa Dua, Bali, Indonesia, October 2015. Paper Number: SPE-176456-MS.

Lake, L.W., Walsh, M.P. 2008. Enhanced Oil Recovery (EOR) Field Data Literature Search. Department of Petroleum and Geosystems Engineering University of Texas at Austin, Austin, Texas.

Lavoine, N., Desloges, I., Dufresne, A., Bras, J. 2012. Micro fibrillated Cellulose – Its Barrier Properties and Applications in Cellulosic Materials: A Review, Carbohydr. Polym. 90 735–764.

Li, W., Zhu, J., Qi, J. 2007. Application of Nano-Nickel Catalyst in the Viscosity Reduction of Liaohe Extra-Heavy Oil by Aqua-Thermolysis, J. Fuel Chem. Technol. 35 (2) 176e180.

Li, M.C., Wu, Q., Song, K., Yan, Q., Wu, Y.Q. 2015. Cellulose Nanoparticles as Modifiers for Rheology and Fluid Loss in Bentonite Water-Based Fluids. ACS Appl. Mater. Interfaces 2015, 7, 5006−5016.

Li, Q.Z., Wei, B., Lu, L.M., Li, Y.B., Wen, Y.B., Pu, W.F., Li, H. 2017. Investigation of Physical Properties and Displacement Mechanisms of Surface-Grafted Nano-Cellulose Fluids for Enhanced Oil Recovery. Fuel, 207, 352−364.

Liu, J., Korpinen, R., Mikkonen, K.S., Willför, S., Xu, C. 2014. Nanofibrillated Cellulose Originated from Birch Sawdust after Sequential Extractions: A Promising Polymeric Material from Waste to Films, Cellulose 21 (2014) 2587–2598, https://doi.org/10.1007/s10570-014-0321-4.

Liu, X.L., Qu, J.L., Wang, A., Wang, C.P., Chen, B., Wang, Z.G., Wu, B.B. 2019a. Hydrogels Prepared from Cellulose Nanofibrils Via Ferric Iron-Mediated Crosslinking Reaction for Protecting Drilling Fluid. Carbohydr. Polym. 2019, 212, 67−74.

Liu, X.L., Wang, A., Wang, C.P., Qu, J.L., Wen, Y.B., Chen, B., Wang, Z.G. 2019b. Preparation and Performance of Salt Tolerance and Thermal Stability Cellulose Nanofibril Hydrogels and Their Application in Drilling Engineering. Biomaterials 2019, 4, 10−22.

Liu, L., Fan, H.F., Sun, J. H., Zhao, J. 2019. Research Progress of Nanoparticles-stabilized Foam for EOR. Oilfield Chem. 2019, 36, 748−754.

Lu, T., Li, Z., Zhou, Y., Zhang, C. 2017. Enhanced Oil Recovery of Low-Permeability Cores by SiO2 Nanofluid. Energy Fuels;31(5):5612–21.

Luo D., Wang F., Alam M.K., Yu F., Mishra I.K., Bao J., Willson R.C., Ren Z. 2017 Colloidal Stability of Graphene-Based Amphiphilic Janus Nanosheet Fluid, Chem. Mater. 29, 3454–3460.

Mahmoud, O., Nasr-El-Din, H.A., Vryzas, Z., Kelessidis, V.C. 2017. Characterization of Filter Cake Generated by Nanoparticle-Based Drilling Fluid for HP/HT Applications (SPE 184572). In: SPE International Conference on Oilfield Chemistry, Montgomery, Texas, USA, 3–5 April, http://dx.doi.org/10.2118/184572-ms.

Mahmoud, O., Nasr-El-Din, H. 2018. Formation Damage Assessment and Filter Cake Characterization of NPs/Ca-Bentonite Fluids for Drilling Harsh Environments Using Computed-Tomography Scan (SPE 191155). In: SPE Trinidad and Tobago Section Energy Resources Conference, Port of Spain, Trinidad and Tobago, 25–26 June, http://dx.doi.org/10.2118/191155-ms.

Malkin, A.Y. 2013. Non-Newtonian Viscosity in Steady-State Shear Flows. J Nonnewtonian Fluid Mech 2013; 192:48–65.

Mandal, A., Bera, A., Ojha, K., Kumar, T. 2012. Characterization of Surfactant Stabilized Nanoemulsion and its Use in Enhanced Oil Recovery. In Proceedings of the SPE International Oilfield Nanotechnology Conference and Exhibition, Noordwijk, the Netherlands, 12–14 June 2012.

Mandal, A., Bera, A. 2015. Modeling of Flow of Oil-In-Water Emulsions through Porous Media. Petrol. Sci. 12 (2), 273–281.

Manshad, A.K., Rezaei, M., Moradi, S., Nowrouzi, I., Mohammadi, A.H. 2017. Wettability Alteration and Interfacial Tension (IFT) Reduction in Enhanced Oil Recovery (EOR) Process by Ionic Liquid Flooding, J. Molecular Liquids 248, 153–162.

Martin, A.J., Solomon, S.T., Hartmann, D.J. 1997. Characterization of Petrophysical Flow Units in Carbonate Reservoirs. AAPG Bulletin, 81, 734-759. https://doi.org/10.1306/522B482F-1727-11D7-8645000102C1865D.

Mc.Elfresh, P., Holcomb, D., Ector, D. 2012. Application of Nanofluid Technology to Improve Recovery in Oil and Gas Wells. Paper SPE 154827-MS Presented at SPE International Oilfield Technology Conference, Noordwijk, The Netherlands, 12–14 June.

McElfresh, P., Wood, M., Ector, D. 2012. Stabilizing Nanoparticle Dispersions in High Salinity, High Temperature Downhole Environments. In: SPE international oilfield nanotechnology conference and exhibition, Noordwijk, The Netherlands, 12–14.

McGlade, C., Sondak, G., Han, M. 2018. Whatever Happened to Enhanced Oil Recovery?. International Energy Agency. https://www.iea.org/commentaries/whatever-happened-to-enhanced-oil-recovery.

Medronho, B., Lindman, B. 2014. Competing Forces During Cellulose Dissolution: From Solvents to Mechanisms. Curr. Opin. Colloid Interface Sci. 2014, 19, 32−40.

Meldrum, N. 1988. Hydrocyclones: A Solution to Produced-Water Treatment. Society of Petroleum Engineers. doi:10.2118/16642-PA.

Metin, C.O., Lake, L.W., Miranda, C.R. 2011. Stability of Aqueous Silica Nanoparticle Dispersions. J Nanopart Res 13, 839–850. https://doi.org/10.1007/s11051-010-0085-1.

Mishra, R. 2018. Materials Chemistry and the Futurist Eco-friendly Applications of Nanocellulose: Status and prospect. Journal of Saudi Chemical Society. 22. 10.1016/j.jscs.2018.02.005.

Mohammadi, M., Dadvar, M., Dabir, B., 2017. TiO2/SiO2 Nanofluids as Novel Inhibitors for the Stability of Asphaltene Particles in Crude Oil: Mechanistic Understanding, Screening, Modeling, and Optimization. J. Mol. Liq. 238, 326–340.

Molnes, S.N., Torrijos, I.P., Strand, S., Paso, K.G., Syverud, K. 2016. Sandstone Injectivity and Salt Stability of Cellulose Nanocrystals (CNC) Dispersions-Premises for Use of CNC in Enhanced Oil Recovery. Ind. Crops Prod., 93, 152−160.

Molnes, S.N., Mamonov, A., Paso, K.G., Strand, S., Syverud, K. 2018. Investigation of a New Application for Cellulose Nanocrystals: A Study of the Enhanced Oil Recovery Potential by Use of a Green Additive. Cellulose, 25, 2289−2301.

Moon, R.J., Martini, A., Nairn, J., Simonsen,J., Youngblood, J. 2011. Cellulose Nanomaterials Review: Structure, Properties and Nanocomposites, Chem. Soc. Rev. 40, 3941–3994.

Moritis, G. 2008. Worldwide EOR Survey. Oil Gas J. 2008, 106, 41–42, 44–59.

Murshed, S.M.S., Tan, S., Nguyen, N. 2008. Temperature Dependence of Interfacial Properties and Viscosity of Nanofluids for Droplet-based Microfluidics. J Phys D Appl Phys ;41(8):085502.

Muskat, M. 1949. Physical Principles of Oil Production, 470-502. New York City: McGraw-Hill Book Co. Inc.

Nanocellulose (n.d.). Retrieved on June 15th 2023, from https://nanografi.com/nanoparticles/nanocellulose/.

Nassar, N.N., Hassan, A., Carbognani, L., Lopez-Linares, F., Pereira-Almao, P., 2012. Iron Oxide Nanoparticles for Rapid Adsorption and Enhanced Catalytic

Oxidation of Thermally Cracked Asphaltenes. Fuel 95, 257–262. http://dx.doi.org/10.1016/j.fuel. 2011.09.022.

Needham, R.B., Threlkeld, C.B., Gall, J.W. 1974. Control of Water Mobility Using Polymers and Multivalent Cations. Society of Petroleum Engineers. doi:10.2118/4747-MS.

Nelson, P. H. 2009. Pore Throat Sizes in Sandstones, Tight Sandstones, and Shales. AAPG Bulletin, Volume 93, No.3, pages 329-340.

Nikfarjam, N., Qazvini, N.T., Deng, Y. 2015. Surfactant Free Pickering Emulsion Polymerization of Styrene In W/O/W System Using Cellulose Nanofibrils. Eur. Polym. J. 2015, 64, 179−188.

Nowrouzi, I., Manshad, A., Mohammadi, A. 2020. Effects of TiO2, MgO and γ-Al2O3 Nano-Particles on Wettability Alteration and Oil Production under Carbonated Nano-Fluid Imbibition in Carbonate Oil Reservoirs. Fuel. 259. 116110. 10.1016/j.fuel.2019.116110.

Nwidee, L., Theophilus, S., Barifcani, A., Sarmadivaleh, M., Iglauer, S. 2016. EOR Processes, Opportunities and Technological Advancements, In L. Romero-Zeron (ed.), Chemical Enhanced Oil Recovery (cEOR) - a Practical Overview, 2-52. Croatia: InTech.

Nwidee, L., Barifcani, A., Sarmadivaleh, M., Iglauer, S. 2018. Nanofluids as Novel Alternative Smart Fluids for Reservoir Wettability Alteration. 10.5772/intechopen.72267.

Oren, P. E., Billiote, J., Pinczewski, W.V. 1992. Mobilization of Waterflood Residual Oil by Gas Injection for Water- Wet Conditions. SPE Formal Evaluation, 7, 70–78.

Orodu, O.D., Tang, Z., Fei, Q. 2009. Hydraulic (Flow) Unit Determination and Permeability Prediction: A Case Study of Block Shen-95, Liaohe Oilfield, North-East China. Journal of Applied Sciences, 9: 1801-1816.

Owens, W.D., Suter, V. 1965. Steam Simulation for Secondary Recovery. J Can Pet Technol 4: 227–235. doi: https://doi.org/10.2118/65-04-08.

Pandey, A., Derakhshandeh, M., Kedzior, S.A., Pilapil, B., Shomrat, N., Segal-Peretz,T. Bryant, S.L. 2018. Role of Interparticle Interactions on Microstructural and Rheological Properties of Cellulose Nanocrystal Stabilized Emulsions, J. Colloid Interface Sci. 532 808–818.

Particle Size and Zeta Potential Measurement Laboratory (PZL) | Central Laboratory. (n.d.). Retrieved on June 3rd, 2023 from https://merlab.metu.edu.tr/en/particle-size-and-zeta-potential-measurement-laboratory-pzl.

Peng, B.L., Dhar, N., Liu, H.L., Tam, K.C. 2011. Chemistry and Applications of Nanocrystalline Cellulose and Its Derivatives: A Nanotechnology Perspective, Can. J. Chem. Eng. 89, 1191–1206.

Petrus, G. 2015. Plant Derived Cellulose Compositions for Use as Drilling Muds, US Patent 20150203737 A1.

Phanthong, P., Reubroycharoen, P., Hao, X., Abudula, A., Guan, G. 2018. Nanocellulose: Extraction and application. Carbon Resources Conversion. 1. 10.1016/j.crcon.2018.05.004.

Poletto, M., Pistor, V., Zattera, A.J. 2013. Structural Characteristics and Thermal Properties of Native Cellulose, Cellul. – Fundam. Asp. 45–68. doi:10.5772/50452.

Pramana, A.A., Abdassah, D., Rachmat, S., Mikrajuddin, A. 2010. Electromagnetic Induction Heat Generation of Nano-Ferrofluid and Other Stimulants for Heavy Oil Recovery. In: The Third Nanoscience and Nanotechnology Symposium, Bandung, Indonesia, 16–16 June, http://dx.doi.org/10.1063/1.3515543.

Purcell, W. R. 1949. Capillary Pressures - Their Measurement Using Mercury and the Calculation of Permeability Therefrom. Society of Petroleum Engineers. doi:10.2118/949039-G.

Ramasamy, J., Amanullah, M. 2020. Nanocellulose for Oil and Gas Field Drilling and Cementing Applications. J. Pet. Sci. Eng. 2020, 184, No. 106292.

Rangel-German, E.R., Schembre, J., Sandberg, C., Kovscek, A. 2004. Electrical Heating-Assisted Recovery for Heavy Oil. J. Petrol. Sci. Eng. 45 (3–4), 213–231.

Raval N., Maheshwari R., Kalyane D. 2019. Chapter 10 - Importance of Physicochemical Characterization of Nanoparticles in Pharmaceutical Product Development, Editor(s): Rakesh K. Tekade, In Advances in Pharmaceutical Product Development and Research, Basic Fundamentals of Drug Delivery, Academic Press, 2019, Pages 369-400, ISBN 9780128179093, https://doi.org/10.1016/B978-0-12-817909-3.00010-8.

Ravera, F., Santini, E., Loglio, G., Ferrari, M., Liggieri, L. 2006. Effect of Nanoparticles on the Interfacial Properties of Liquid/Liquid and Liquid/Air Surface Layers. J Phys Chem; 110(39):19543–51.

Raza, S., Gates, I.D. 2021. Effect of Cellulose Nanocrystal Nanofluid on Displacement of Oil in a Hele-Shaw Cell. J. Pet. Sci. Eng., 196, No. 108068.

Rezvani, H., Khalilnezhad, A., Ganji, P., Kazemzadeh, Y. 2018. How ZrO2 Nanoparticles Improve The Oil Recovery By Affecting The Interfacial Phenomena In The Reservoir Conditions? . Journal of Molecular Liquids. 252. 158-168. 10.1016/j.molliq.2017.12.138.

Roustaei, A., Moghadasi, J., Iran, A., Bagherzadeh, H., Shahrabadi, A. 2012. An Experimental Investigation of Polysilicon Nanoparticles' Recovery Efficiencies through Changes in Interfacial Tension and Wettability Alteration. Paper presented at the SPE International Oilfield Nanotechnology Conference and Exhibition, Noordwijk, The Netherlands. doi: https://doi.org/10.2118/156976-MS.

Sagala, F., Hethnawi, A., Nassar, N. N. 2020. Hydroxyl-Functionalized Silicate-Based Nanofluids for Enhanced Oil Recovery, Fuel, vol. 269, no. January, p. 117462, Jun. 2020, doi: 10.1016/j.fuel.2020.117462.

Sahni, A., Kumar, M., Knapp, R. 2000. Electromagnetic Heating Methods for Heavy Oil Reservoirs, SPE 62550. SPE/AAPG Western Regional Meeting, 19–23 June, Long Beach, CA.

Samanta, A., Bera, A., Ojha, K., Mandal, A. 2012. Comparative Studies on Enhanced Oil Recovery by Alkali–Surfactant and Polymer Flooding. J. Pet. Explor. Prod. Technol. 2 (2), 67–74.

Sanchez L., Astudillo A., Rodriguez F., Morales J., Rodriguez A. 2005. Nitrogen Injection in the Cantarell Complex: Results after Four Years of Operation, SPE 97385, Proceedings of the Latin American and Caribbean Petroleum Engineering Conference, Rio de Janeiro, Brazil, June 20-23, 2005.

Sanchez, F., Sobolev, K. 2010. Nanotechnology in Concrete: a Review. Constr. Build. Mater. 24 (11), 2060–2071.

Sarapardeh H. A., Ayatollahi S., Ghazanfari M.H., Masihi M. 2014. Experimental Determination of Interfacial Tension and Miscibility of the CO2–Crude Oil System; Temperature, Pressure, and Composition Effects. Journal of Chemical Engineering Data, 59(1), 61–69.

Sharma, T., Velmurugan, N., Patel, P., Chon, B. H., Sangwai, J. 2015. Use of Oil-in-water Pickering Emulsion Stabilized by Nanoparticles in Combination with Polymer Flood for Enhanced Oil Recovery. Petroleum Science and Technology. 33. 1595-1604. 10.1080/10916466.2015.1079534.

Sebastian, H.M., and D.D. Lawrence. 1992. Nitrogen Minimum Miscibility Pressures. Paper presented at the SPE/DOE Enhanced Oil Recovery Symposium, Tulsa, Oklahoma. doi: https://doi.org/10.2118/24134-MS.

Seright, R. S., Lane, R. H., Sydansk, R. D. 2001. A Strategy for Attacking Excess Water Production. Society of Petroleum Engineers. doi:10.2118/70067-MS.

Seright, R. S., Lane, R. H., Sydansk, R. D. 2003. A Strategy for Attacking Excess Water Production. Society of Petroleum Engineers. doi:10.2118/84966-PA.

Seright R., Lindquist W., Cai R. 2008. Understanding the rate of clean up for oil zones after a gel treatment. Presented at the SPE Improved oil recovery symposium, Tulsa, 19-23 April. SPE 112976-MS. http://dx.doi.org/10.2118/112976-MS.

Shehabi, J.A.N. 1979. Effective Displacement of Oil by Gas Injection in a Preferentially Oil-Wet, Low-Dip Reservoir. J Pet Technol 31 (12): 1605-1613. SPE-7652-PA. http://dx.doi.org/10.2118/7652-PA.

Sheng, J. 2013. Foams and Their Applications in Enhancing Oil Recovery. Enhanced Oil Recovery Field Case Studies. 251-280. 10.1016/B978-0-12-386545-8.00011-7.

Shirman E., Wojtanowicz A. 2000. More Oil using Downhole Water-Sink Technology: A Feasibility Study. SPE Production and Facilities 15(4):234-240. SPE 66532-PA. http://dx.doi.org/10.2118/66532-PA.

Shokrlu, Y.H., Babadagli, T. 2010. In-Situ Upgrading of Heavy Oil/Bitumen during Steam Injection by Use of Metal Nanoparticles: A Study on In-Situ Catalysis and Catalyst Transportation, SPE Reserv. Eval. Eng. 16 (03) (2013) 333e344.

Srinivasan, A., Shah, S.N. 2014. Surfactant-Based Fluids Containing Copper-Oxide Nanoparticles for Heavy Oil Viscosity Reduction, SPE Annual Technical Conference and Exhibition.

Stalkup, F.I. 1987. Displacement Behavior of the Condensing/Vaporizing Gas Drive Process. Paper presented at the SPE Annual Technical Conference and Exhibition, Dallas, Texas. doi: https://doi.org/10.2118/16715-MS.

Sun, X., Wu, Q., Lee, S., Qing, Y., Wu, Y. 2016. Cellulose Nanofibers as a Modifier for Rheology, Curing and Mechanical Performance of Oil Well Cement. Sci. Rep. https://doi.org/10.1038/srep31654.

Sun, X., Bai, B. 2017. Comprehensive Review of Water Shutoff Methods for Horizontal Wells. Petroleum Exploration and Development 44 (6): 1022—1029. http://dx.doi.org/https://doi.org/10.1016/S1876-3804(17)30115-5.

Sunmonu, R., Onyekonwu, M.O. 2013. Enhanced Oil Recovery Using Foam Injection; a Mechanistic Approach. SPE. 10.2118/167589-MS.

Sydansk, R. D. 1990. A Newly Developed Chromium (III) Gel Technology. Society of Petroleum Engineers. doi:10.2118/19308-PA.

Sydansk, R.D. 2007. Polymers, Gels, Foams, and Resins. In Petroleum Engineering Handbook, second edition, ed. L. W. Lake, Chap. 13, 1149–1260. Richardson, Texas: Society of Petroleum Engineers.

Swanson, B.F. 1981. A Simple Correlation between Permeabilities and Mercury Capillary Pressures. JPT, Dec., 2488–2504.

Swisher, M. D., Wojtanowicz, A. K. 1995. New Dual Completion Method Eliminates Bottom Water Coning. Society of Petroleum Engineers. doi:10.2118/30697-MS.

Taborda, E. A., Franco, C. A., Ruiz, M. A., Alvarado, V., Cortes, F. B. 2017. Experimental and Theoretical Study of Viscosity Reduction in Heavy Crude Oils by Addition of Nanoparticles. Energy Fuels, 31, 1329–1338. DOI: 10.1021/acs.energyfuels. 6b02686.

Taheri, A., Høier, L., Ole T. 2013. Miscible and Immiscible Gas Injection for Enhancing of Condensate Recovery in Fractured Gas Condensate Reservoirs. Paper presented at the EAGE Annual Conference & Exhibition incorporating SPE Europec, London, UK. doi: https://doi.org/10.2118/164934-MS.

Tang, G., Morrow, N. 1997. Salinity, Temperature, Oil Composition, and Oil Recovery by Waterflooding. SPE Reserv. Eng. 12 (NOV (4)), 269–276 1996 Annual Technical Conference and Exhibition of Society-of-Petroleum-Engineers, Denver, Co, Oct 06-09, 1996.

The University of Melbourne. (n.d.). Scanning Electron Microscopy / Energy Dispersive Spectroscopy. Retrieved on 13rd June, 2023 from https://arts.unimelb.edu.au/grimwade-centre-for-cultural-materials-conservation/conservation-services/services-support/technical-analysis.

The US Department of Energy. (n.d.). Enhanced Oil Recovery. Retrieved on 15th January, 2023 from https://www.energy.gov/fecm/science-innovation/oil-gas-research/enhanced-oil-recovery.

Thomas, S. 2008. Enhanced Oil Recovery - An Overview. Oil & Gas Science and Technology – Rev. IFP, Vol. 63. 9-19. 10.2516/ogst: 2007060.

Thomas, P., Duolikun, T., Rumjit, N.P., Moosavi, S., Lai, C.W., Johan, M.R.B., Fen, L.B. 2020. Comprehensive Review on Nanocellulose: Recent Developments, Challenges and Future Prospects. J. Mech. Behav. Biomed. Mater. 110, 103884. https://doi.org/10.1016/j.jmbbm.2020.103884.

Torsater, O., Engeset, B., Hendraningrat, L., Suwanro, S. 2012. Improved Oil Recovery by Nanofluids Flooding: An Experimental Study. In Proceedings of the SPE Kuwait International Petroleum Conference and Exhibition, Kuwait City, Kuwait.

Turbak, A.F., Snyder, F.W., Sandberg, K.R. 1982. Food Products Containing Microfibrillated Cellulose. (Vol. US Patent no. 4341807).

Turbak, A. F., Snyder, F. W., Sandberg, K. R. 1983. Microfibrillated Cellulose, Anew Cellulose Product: Properties, Uses, and Commercial Potential. Journal of Applied Polymer Science, 37, 815–827.

Turkenburg, D.H., Chin, P.T.K., Fischer, H.R. 2012. Use of Modified Nanoparticles in Oil and Gas Reservoir Management. Paper SPE-157120eMS. In: Presented at the SPE International Oilfield Nanotechnology Conference, Noordwijk, The Netherlands, 12-14 June.

Vafaei, S., Borca-Tasciuc, T., Podowski, M., Purkayastha, A., Ramanath, G., Ajayan, P. 2006. Effect of Nanoparticles on Sessile Droplet Contact Angle. Nanotechnology; 17(10):2523.

Villard, J.M., Buckley, J.S., Morrow, N.R., Gauchet, R. 1993. Wetting and Waterflood Oil Recovery of a Moderately Viscous Crude Oil, SCA1993-23, Society of Core Analysts.

Yousefi, S.H., Rashidi, F., Sharifi, M. 2019. Prediction of Immiscible Gas Flooding Performance: A Modified Capacitance–Resistance Model and Sensitivity Analysis. Pet. Sci. 16, 1086–1104 (2019). https://doi.org/10.1007/s12182-019-0342-6.

Wang, H.W., Gong, Y., Lu, W.C., Chen, B.L. 2008. Influence of Nano-SiO2 on Dilational Viscoelasticity of Liquid/Air Interface of Cetyltrimethyl Annonium Bromide. Appl. Surf. Sci. 254 (11), 3380–3384.

Wang, X., Lei, Q., Luo, J., Wang, P., Xiao, P., Ye, Y., Wu, X. 2021. Application of Nanocellulose in Oilfield Chemistry. ACS Omega. 2021 Aug 9;6(32):20833-20845. doi: 10.1021/acsomega.1c02095. Erratum in: ACS Omega. 2021 Aug 25;6 (35):23007. PMID: 34423191; PMCID: PMC8374909.

Wasan, D.T., Nikolov, A. 2003. Spreading of Nanofluids on Solids.J.Nat.423,156–159.

Wasan, D., Nikolov, A., Kondiparty, K. 2011. The Wetting and Spreading of Nanofluids on Solids: Role of the Structural Disjoining Pressure. Curr Opin Colloid Interface Sci, 16(4):344–9.

Washburn, E.W. 1921. The Dynamics of Capillary Flow. Physical Review, 17, 273-283. http://dx.doi.org/10.1103/PhysRev.17.273.

Wei, B., Li, H., Li, Q.Z., Wen, Y.B., Sun, L., Wei, P., Pu, W.F., Li, Y.B. 2017. Stabilization of Foam Lamella Using Novel Surface-Grafted Nanocellulose-Based Nanofluids. Langmuir 33 (21), 5127–5139. https://doi.org/10.1021/acs.langmuir.7b00387.

Wei, B., Li, Q.Z., Ning, J., Wang, Y.Y., Sun, L., Pu, W.F. 2019a. Macro-and Micro-Scale Observations of a Surface-Functionalized Nanocellulose Based Aqueous Nanofluids in Chemical Enhanced Oil Recovery (C-EOR). Fuel 236, 1321–1333. https://doi.org/10.1021/10.1016/j.fuel.2018.09.105.

Wei, B., Wang, Y.Y., Mao, R.X., Xu, X.G. 2019b. Design of Nanocellulose Fibrils Containing Lignin Segment (L-NCF) for Producing Stable Liquid Foams as “Green”

Flooding Agents for Oil Recovery. ACS Sustainable Chem. Eng. 2019, 7, 11426−11437.

Wei, B., Ning, J., Mao, R., Wang, Y., Xu, X., Bai, M. 2019c. Rational Design and Fabrication of an Alkali-Induced O/W Emulsion Stabilized with Cellulose Nanofibrils (CNFs): Implication for Eco-Friendly and Economic Oil Recovery Application. Soft Matter, 15 (19), 4026−4034.

Wei, B., Tian, Q. T., Mao, R. X., Xue, Y., Wen, Y. B., Pu, W. F. 2020. Application and Prospect of Nano-Cellulosic Materials in the Development of Oil and Gas Field. Pet. Geol. Recovery Effic. 2020, 27, 98−104.

Wever, D.A.Z., Picchioni, F., Broekhuis, A.A. 2011. Polymers for Enhanced Oil Recovery: A Paradigm for Structure–Property Relationship in Aqueous Solution. Progress in Polymer Science, 36(11), 1558–1628.

Yu, J., Mo, D., Liu, N., Robert, L. 2013. The Application of Nanoparticle-Stabilized CO2 Foam for Oil Recovery. Paper presented at the SPE International Symposium on Oilfield Chemistry, The Woodlands, Texas, USA. doi: https://doi.org/10.2118/164074-MS.

Zallaghi, M., Kharrat, R., Hashemi, A. 2018. Improving the Microscopic Sweep Efficiency of Water Flooding Using Silica Nanoparticles. J Pet Explor Prod Technol; 8(1):259–69.

Zeyghami, M., Kharrat, R., Ghazanfari, M.H. 2014. Investigation of the Applicability of Nano Silica Nanoparticles as A Thickening Additive for Polymer Solutions Applied in EOR Processes. Energy. Res., Part A. 36:1315–1324.

Zhang, T., Davidson, D., Bryant, S.L., Huh, C. 2010. Nanoparticle-Stabilized Emulsions for Applications in Enhanced Oil Recovery. In Proceedings of the SPE Improved Oil Recovery Symposium, Tulsa, OK, USA, 24–28 April 2010.

Zhang, H., Ramakrishnan, T. S., Nikolov, A., Wasan, D. 2016. Enhanced Oil Recovery Driven by Nanofilm Structural Disjoining Pressure: Flooding Experiments and Microvisualization. Energy Fuels 2016, 30, 2771–2779.

Zhou, K., Zhou, X., Liu, J., Huang, Z. 2020. Application of magnetic nanoparticles in petroleum industry: A review, Journal of Petroleum Science and Engineering, Volume 188, 2020, 106943, ISSN 0920-4105, https://doi.org/10.1016/j.petrol.2020.106943.

Zhu, H., Xia, J.H., Sun, Z.G., Zhan, J., Zhan, Y.M., Wang, F.H. 2006. Application of Nanometer-Silicon Dioxide in Tertiary Oil Recovery. Acta Petrol. Sin. 27 (6), 96–99.

Zhu, J., Xie, S., Yang, Z., Li, X., Chen, J., Zhang, X., Zheng, N. 2021. A Review of Recent Advances and Prospects on Nanocellulose Properties and Its Applications in Oil and Gas Production. Journal of Natural Gas Science and Engineering. 96. 104253. 10.1016/j.jngse.2021.104253.

Zoppe, J.O., Venditti, R.A., Rojas, O.J., 2021. Pickering Emulsions Stabilized by Cellulose Nanocrystals Grafted with Thermo-Responsive Polymer Brushes. J. Colloid Interface Sci. 369 (1), 202–209. https://doi.org/10.1016/j.jcis.2011.12.011.

APPENDICES

A. XRD Results of End Trim Samples

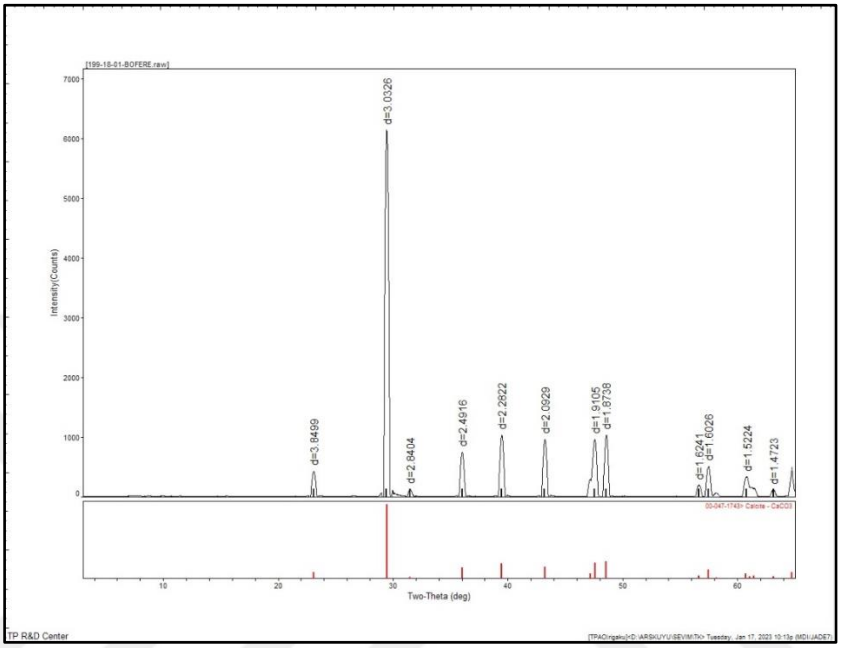

Appendix A-1: XRD analysis result for core plug #211 before coreflood tests

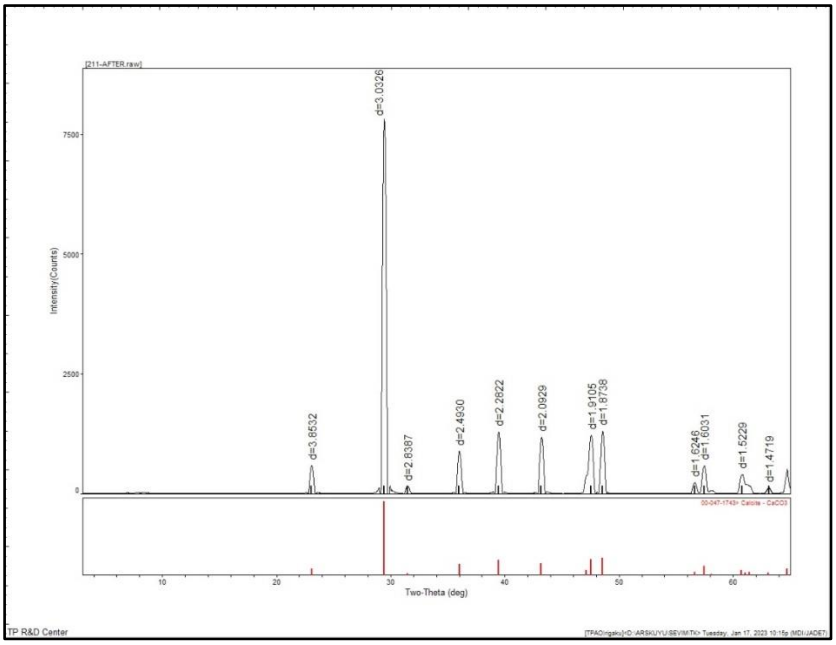

Appendix A-2: XRD analysis result for core plug #211 after coreflood tests

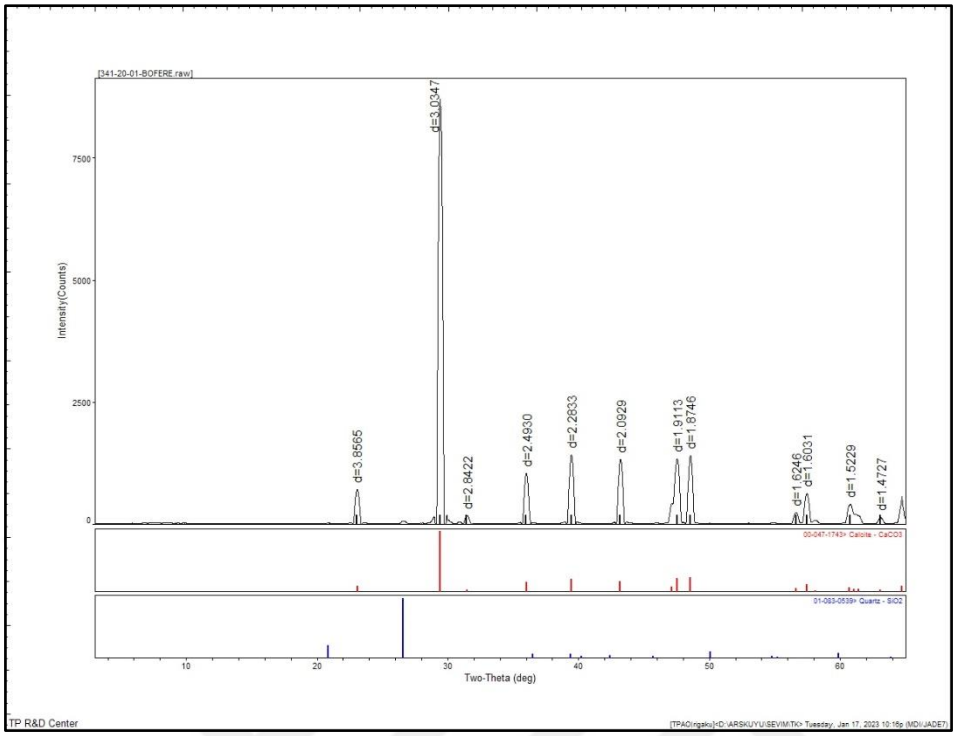

Appendix A-3: XRD analysis result for core plug #347 before coreflood tests

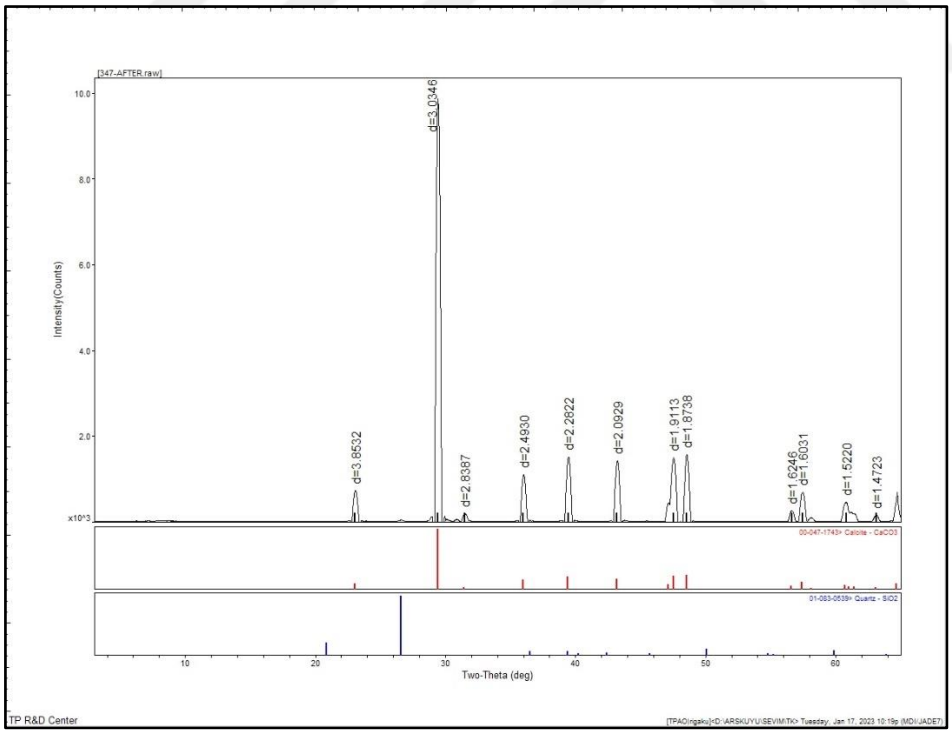

Appendix A-4: XRD analysis result for core plug #347 after coreflood tests

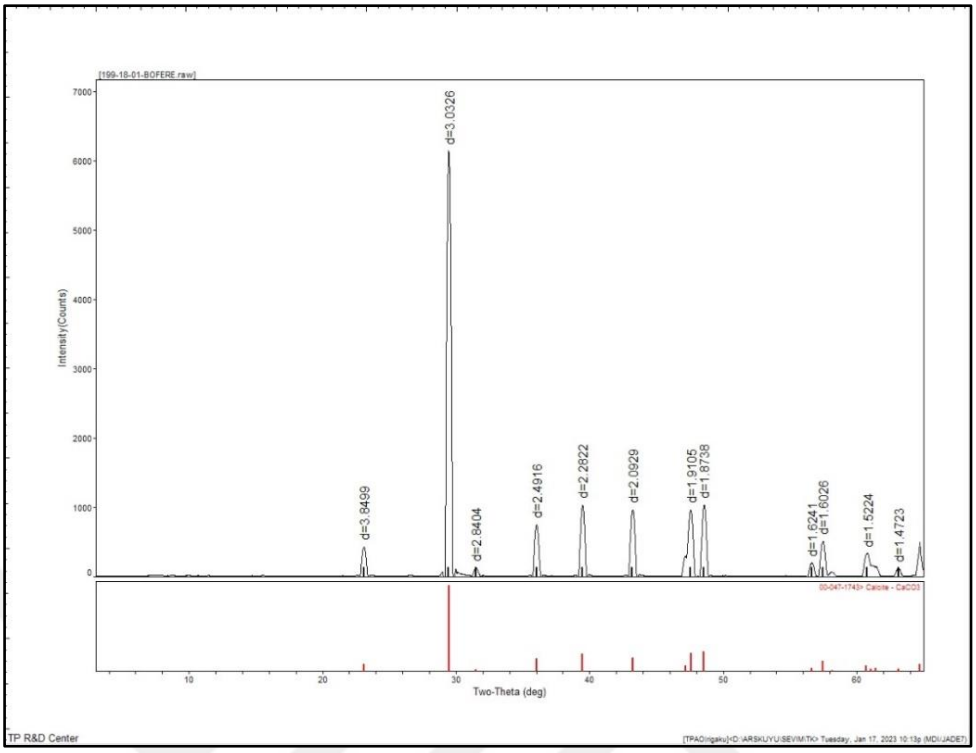

Appendix A-5: XRD analysis result for core plug #346 before coreflood tests

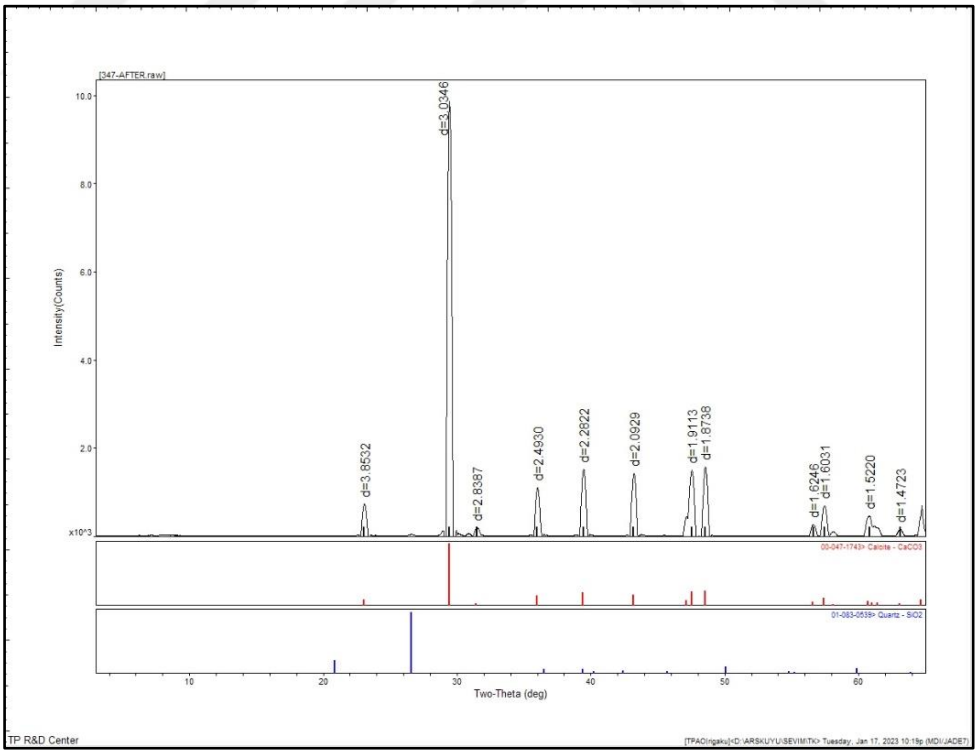

Appendix A-6: XRD analysis result for core plug #346 after coreflood tests

CURRICULUM VITAE

Surname, Name: Ünal Kızılırmak, Candan

EDUCATION

Degree	Institution	Year of Graduation
MS	Texas A&M University Petroleum Engineering	2016
BS	METU Petroleum and Natural Gas Engineering	2013
High School	Atatürk Anadolu High School, Ankara	2008

WORK EXPERIENCE

Year	Company	Enrollment
2016-Present	Turkish Petroleum Corporation (TPAO)/ R&D Center	Senior Petroleum Engineer
2016	Texas A&M University Petroleum Engineering	Teaching Assistant
2013-2014	NV Turkse PERENCO	Petroleum Engineer

FOREIGN LANGUAGES

Advanced English, Intermediate German